Vapor Intrusion at a Site with an Alternative Pathway and a Fluctuating Groundwater Table

by

Yuanming Guo

A Dissertation Presented in Partial Fulfillment
of the Requirements for the Degree
Doctor of Philosophy

Approved November 2015 by the
Graduate Supervisory Committee:

Paul C. Johnson, Chair
Matthew Fraser
Paul Westerhoff

ARIZONA STATE UNIVERSITY

December 2015

ABSTRACT

Vapor intrusion (VI), can pose health risks to building occupants. Assessment and mitigation at VI impacted sites have been guided by a site conceptual model (SCM) in which vapors originate from subsurface sources, diffuse through soil matrix and enter into a building by gas flow across foundation cracks. Alternative VI pathways and groundwater table fluctuations are not often considered.

Alternative VI pathways, involving vapor transport along sewer lines and other subsurface infrastructure, have recently been found to be significant contributors to VI impacts at some sites. This study evaluated approaches for identifying and characterizing the significance of alternative VI pathways and assessed the effectiveness of conventional mitigation at a site with an alternative VI pathway that can be manipulated to be on or off. The alternative pathway could not be identified using conventional pathway assessment procedures and can only be discovered under controlled pressure method (CPM) conditions. Measured emission rates were two orders of magnitude greater than screening model estimates and sub-foundation vertical soil gas profiles changed and were no longer consistent with the conventional VI conceptual model when the CPM test was conducted. The pipe flow VI pathway reduced the vacuum performance of the sub-slab depressurization (SSD) VI mitigation system, but the SSD system still provided sufficient protection to the house.

The relationship between groundwater table fluctuations and subsurface vapor emissions and transport is examined using multi-year data from the field site, and is studied in the laboratory. In addition, a broader range of conditions is examined through use of modeling validated with the experimental data. The results indicate that fluctuating

groundwater tables will lead to amplified volatile organic chemical (VOC) emissions from groundwater to soil surface relative to steady water table elevation, however, the magnitude of this amplification is less concerned when long-term water fluctuation present. No clear correlations were found between VOC emissions and water table changes at the study site where annual water table fluctuations of about 0.3 m existed. Significant VOC emission amplifications by water table fluctuation would be expected under shallow groundwater conditions according to model analysis results.

ACKNOWLEDGEMENTS

I would like to thank my advisor Dr. Paul Johnson for providing me such great opportunities to be a graduate student and researcher in Arizona State University. I learned a lot from his guidance, support, and contributions to this work.

I would like to thank the members of my committee, Dr. Matt Fraser and Dr. Paul Westerhoff for their comments, questions, and support in the latter part of this research.

Additionally, I would like say thank you to Dr. Paul Dahlen and Dr. Hong Luo. Without their professional guidance and effort, this project would never would have been accomplished.

Mr. Kyle Gorder and Dr. Erik Dettenmaier from Hill Air Force Base kindly invested their time in this project. I thank them for their patience, support and friendship.

I would also like to acknowledge the Strategic Environmental Research and Development Program (SERDP) for funding this research.

I appreciate all of the past students from my research group, Dr. Chase Holton, Dr. Bridget Cavanagh, Mr. Sean Wilson, Dr. Ryan Ekre, and Dr. Elsy Escobar. Their help in the laboratory, edits and suggestions, and friendship encouraged me throughout my study in US.

Finally I would like to thank my beloved families for their unconditional support.

TABLE OF CONTENTS

Page

CHAPTER Page

LIST OF TABLES

LIST OF FIGURES

Figure Page

Figure Page

Figure Page

Figure Page

Figure Page

CHAPTER 1

LITERATURE REVIEW AND RESEARCH OBJECTIVES

This chapter provides an overview of vapor intrusion, including vapor intrusion guidance, assessment and remediation, a review of research studies, and a summary of challenges and opportunities for furthering the understanding of vapor intrusion and vapor intrusion assessment. The chapter closes with a discussion of the objectives of this research work and the organization of this dissertation.

1.1 INTRODUCTION

1.1.1 Background. The health risks brought by vapor intrusion have become an increasing concern in the past two decades, since exposure to contaminant vapors can impose short-term (acute) and/or long-term (chronic) human health risks to the occupants of affected structures (Little et al., 1992; ITRC, 2007). The U.S. Environment Protection Agency (USEPA) defines vapor intrusion (VI) as "*the … migration of hazardous vapors from any subsurface contaminant source, such as contaminated soil or groundwater or contaminated conduits(s), into overlying buildings or unoccupied structure via any opening of conduit*" in its latest guidance (USEPA, 2015a). Figure 1.1 shows a typical conceptual model of the VI pathway. Volatile chemical contaminant sources result from leaking chemical/waste storage tanks (and/or leaking chemical distribution infrastructure and/or spills). Volatile organic compounds (VOCs) from the resultant contaminated sediments and/or groundwater volatize into soil gas and can migrate through the vadose zone and ultimately into overlying structures through foundation cracks by diffusion and advection. Diffusion is driven by molecular random motion from high to low

concentrations, whereas advective flow is driven by pressure gradients. While advective and diffusive forces are at play along the full transport pathway, advective flow is generally expected to be predominant in the vicinity of the building foundation where building pressure disturbance is likely to be created naturally or mechanically (Johnson and Ettinger, 1991; USEPA, 2013). The VI pathway is considered "complete" at a site when entry routes and driving forces for vapor transport from a subsurface source to indoor air exist and when these are known or projected to result in indoor concentrations that exceed threshold levels deemed to be protective of human health (ITRC, 2007; USEPA, 2013).

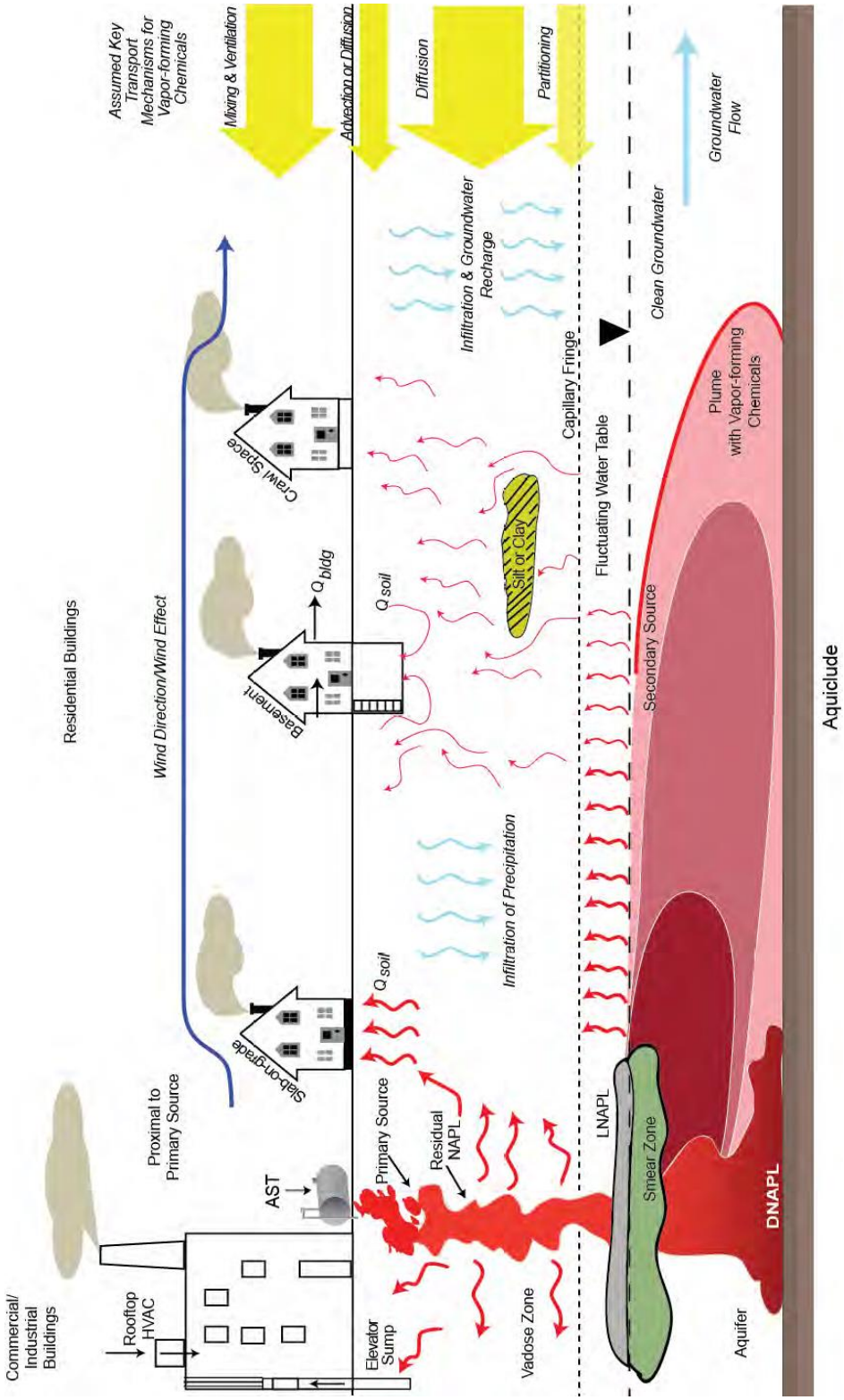

Figure 1.1. Illustration of Conceptual Model of Vapor Intrusion (USEPA, 2013).

Vapor intrusion was first identified as a concern in the early 1980's by a series of studies on radon migration from the subsurface to indoor air (Nazaroff et al., 1985; Nazaroff and Doyle, 1985; Nazaroff et al., 1987; Nazaroff, 1992; Loureiro et al., 1990; Riley et al., 1999). In the late 1980's and early 1990's, the potential risks brought by volatile anthropogenic chemicals were realized and transport of those chemical vapors was believed to have similar transport mechanisms as radon (Garbesi and Sextro, 1989; Johnson and Ettinger, 1991; Little et al., 1992; Moseley and Meyer, 1993). In addition, the chemicals of concern (COC) in VI investigations were both volatile and toxic. In 2013, the USEPA recommended a list of chemicals to be routinely evaluated during VI assessment (USEPA, 2013). That chemical inventory included petroleum hydrocarbons (PHCs) including but not limited to gasoline and diesel fuel constituency, and chlorinated solvents/hydrocarbons (CHCs) such as tetrachloroethene (PCE), 1, 1, 1-trichloroehtane (1,1,1-TCA) and trichloroethylene (TCE). A major difference between PHCs and CHCs regarding VI impact is that PHCs are biodegradable under aerobic conditions at rates that are significant relative to diffusion, whereas, the biodegradation of chlorinated solvents is a much slower process (USEPA, 2012a; Howard, 1991). Also, the degradation by-products of CHCs can also be compounds of concern due to their toxicity (i.e.1,1-dichloroethene (1,1-DCE) and vinyl chloride).

1.1.2 Vapor Intrusion Guidance, Assessment and Mitigation. The first vapor intrusion daft guidance issued by the USEPA was released in 2001. In this draft guidance, recommendations were provided to help determine if the subsurface vapor intrusion into indoor air pathway was complete and might present unacceptable risks (USEPA, 2001). Since then, regulators and other industry groups have developed alternate and

complementary guidance for assessing the VI pathway (API, 2005; NYSDOH, 2006; ITRC, 2007; DOD, 2009; CDTSC, 2011; MDEP, 2011; NJDEP 2013). The USEPA also released a series of updates and research reports regarding the subject over the past decade (USEPA, 2008; USEPA, 2010; USEPA, 2011; USEPA, 2012a; USEPA, 2012b; USEPA, 2012c; USEPA, 2012d; USEPA, 2012e; USEPA, 2013; USEPA, 2015a; USEPA, 2015b, USEPA, 2015c).

For most guidance documents, risk-based screening approaches are recommended to evaluate the VI pathway at potentially impacted sites. The primary objective of risk-based screening is to identify sites or buildings unlikely to pose a health concern through the vapor intrusion pathway. If the concentrations for chemicals of concern fall below risk-based screening levels, no further action is required (USEPA, 2015a). For example, the indoor air risk-based concentration estimates for the 10^{-6} excess cancer risk level are 0.60 ppb_v (4 $\mu g/m^3$) for PCE and 0.04 ppb_v (0.2 $\mu g/m^3$) for TCE (USEPA, 2011; USEPA, 2012e).

Due to the uncertainty associated with temporal and spatial variability of both indoor air and subsurface contaminant concentrations, a multiple-lines-of-evidence (MLE) approach was suggested by most guidance documents for VI investigation and decision-making. The MLE approach is based on the use of multiple types of site data in conjunction with professional judgment to assess current and future impacts of VI to indoor air. Site-specific data commonly used as lines of evidence include point-in-time and/or composite indoor air, point-in-time sub-slab or deeper soil gas, groundwater, and soil sampling, along with screening-level or more complex transport modeling results.

The awareness of factors that can impact VI investigations has been increasing after years of practice. For example, background sources, seasonal indoor air concentration changes, and building conditions and operation are considered of great importance when assessing a site (ITRC, 2007; USEPA, 2015a). In addition, in its most recent guidance, the USEPA (2015a) indicated that preferential VI pathways and groundwater table fluctuations would also potentially confound VI investigations. Preferential VI pathways, such as a utility corridor or more porous zones of soil or rock, could alter the conceptual site model (CSM) and consequently the remediation approach. On the other hand, groundwater table fluctuations could lead to elevated vapor concentrations in the vadose zone. Although a few recommendations are given in concerning these factors, there are still questions that need to be clearly answered, such as how to identify significant VI pathways and how water table fluctuations can affect VI impacts.

Once further action is required at a VI impacted site, remediation/mitigation is needed to reduce the VI risks. Remediation normally refers to an action(s) that eliminates or reduces the contaminant level in the subsurface source zone and is considered a long-term solution. Remediation may include technologies targeting subsurface contaminants, such as groundwater pump-and-treat and soil excavation. However, in cases where subsurface vapor sources cannot be remediated quickly, interim actions or mitigation strategies will be necessary that provide effective protections from health-risk exposure (USEPA, 2008; USEPA, 2015a; ITRC, 2007). The commonly used mitigation technologies are summarized in Table 1.1.

In the past decade, much has been learned about VI through site investigations, applied research, and numerical modeling. In addition, vapor intrusion guidance has evolved. However, vapor intrusion mechanisms are complex and site-specific, and improvements are still needed to better conduct VI pathway investigations and mitigations.

Table 1.1

Comparison of VI mitigation methods (ITRC, 2007)

Technology	Typical applications	Challenges	Range of installed costs
Passive barrier	• New construction • Crawl spaces • Often combined with passive or active venting, sealing openings in the slab, drains, etc.	•Preventing tears, holes • May not suffice as a stand-alone technology • Some states do not accept • Ensuring caulking seals cracks in floors, etc.	• \$0.50–\$5/ft^2 • Thinner, less-expensive barriers likely to be inadequate
Passive venting	• New construction • Low soil gas flux sites • Should be convertible to active system if necessary	• Relies on advective flow of air due to wind and heat stack effects • Air flows and suction typically far less than achieved by fans	• \$0.75–\$5/ft^2
Subslab depressurization (SSD)	• New and existing structures • Sumps, drain tiles, and block wall foundations may also be depressurized if present	• Low permeability and wet soils may limit performance • Otherwise, highly effective systems	• \$1–\$5/ft^2 • Residential systems typically in the \$1–2/ft^2 range
Sub-membrane depressurization	• Existing structures • Crawl spaces	• Sealing to foundation wall, pipe penetrations • Membranes may be damaged by occupants or trades people accessing crawl space	• \$1–\$6/ft^2 • Residential systems typically in the \$1.50–2/ft^2 range
Subslab pressurization	• Similar to SSD • Most applicable to highly permeable soils	• Higher energy costs and less effective than SSD • Potential for short-circuiting through cracks	• \$1–\$5/ft^2

Technology	Typical applications	Challenges	Range of installed costs
Building pressurization	• Large commercial structures, new or existing • Sensitive receptors	• Requires regular air balancing and maintenance • May not maintain positive pressure when building is unoccupied	• $1–$15/ft^2 • Heavily dependent on size and complexity of structure
Indoor air treatment	• Specialized cases only	• Typically generates a waste disposal stream • Effective capture of air contaminants may be difficult • Energy-intensive, with significant operation, maintenance, and monitoring burden	• $15K–$25K per application not atypical • Actual costs heavily dependent upon type of technology employed
Sealing the building envelope	• Cracks and holes in existing buildings	• Access to perforations • Permanence	• Highly dependent on the extent of sealing required

1.1.3 Overview of Past Vapor Intrusion Studies. Over the past few decades, VI pathway-related studies have spanned radon intrusion to VI from groundwater and soil contaminated with either PHCs or CHCs. The following sections emphasize knowledge relevant to VI temporal and spatial temporal variability in both indoor air and subsurface concentrations, as well as mechanisms causing it. An alternate VI assessment approach - the controlled pressure method (CPM) is also discussed, as it offers potential advantages over sampling under natural conditions.

1.1.3.1 Temporal and Spatial Variability. Multiple-lines-of-evidence (MLE) approaches are recommended in most VI investigation guidance documents. These generally require sampling of indoor air, groundwater and soil gas at low-density and low-frequency. For example, four indoor air samples collected quarterly might be a typical monitoring plan. There is evidence of VI temporal and spatial variability in the literature (Hubbard et al., 1995; McHugh et al., 2007; Luo, 2009; Folkes et al., 2009;

EPA, 2012b; EPA, 2012c; Holton et al., 2013) and this leads to questions about the reliability of sparse sampling schemes.

Temporal variation in indoor air concentrations has been observed in long-term radon intrusion studies. For example, in 1995, in an attempt to develop a method to predict long-term indoor air radon concentrations with short-term measurements, Hubbard et al. (1995) collected and analyzed over three years of indoor air radon measurements in a single-family house in the U.S. and 1 year of monthly measurements in 158 houses in Sweden. The data show about one order-of-magnitude variation in 24-h averaged indoor air radon concentrations. The authors concluded that radon concentrations correlated with outdoor temperature, with increasing indoor radon concentrations associated with decreases in outdoor temperatures.

Additional studies performed at VOC-impacted VI sites in the past decade observed both temporal and spatial variability in indoor air as well as sub-slab and subsurface contaminant concentrations. McHugh et al. (2007) reported groundwater, subsurface, and indoor air concentrations from three chlorinated solvent-impacted buildings (two at Hill AFB site and one at Altus AFB) to illustrate spatial and temporal variability. Two complete sampling events were conducted at the Hill AFB sites and four events were conducted at Altus AFB. Spatial variability in subsurface samples (groundwater and soil gas samples) was higher than the spatial variability in indoor air samples. Evaluation of both short and long term temporal variability indicated the relative percent difference (RPD) between subsurface VOC samples was about 30% and 30-100%, respectively. Variations in indoor air concentrations could not be observed due to concentrations at about the detection limit. Folkes et al. (2009) reviewed decade-long

groundwater and indoor air VOC monitoring results from the Redfield site in Colorado and over 19 months of monthly monitoring data from structures in New York State. 1,1-DCE concentrations in each of the 45 homes in Colorado ranged from 0.023 to 0.27 µg/m3. In general, 1,1-DCE concentrations were about 20% higher in summer and 50 % lower in winter than the average annual concentrations. In New York, sub-slab PCE soil gas concentrations at two adjacent houses were found to vary less than one order-of-magnitude, but one was consistently four to five times higher than the other. Luo et al. (2009), in a study of a warehouse at a decommissioned refinery site, found significant spatial variability in sub-slab soil gas concentrations ranging from <0.01 to 200 mg/L. Johnson (2013) conducted two 12-day studies of indoor air concentrations for PCE, one in 20 homes during summer and the other in 9 homes in the winter. Spatial variability and short-term and seasonal variability in PCE concentrations were observed. The author concluded that a single point-in-time indoor air sample is not adequate for characterizing time-varying concentrations.

Recently, two high-frequency long-term indoor air monitoring studies have been reported. The USEPA released results from monitoring of radon and VOCs for one year at a VI-impacted duplex in Indianapolis (USEPA, 2012b). Indoor air was sampled at multiple locations in the building on a weekly basis and radon was measured real-time and on a daily-to-weekly basis. Significant temporal variability was observed for both radon and VOCs. Indoor air concentrations of PCE varied by over two orders-of-magnitude from 0.1 to >10 $\mu g/m^3$, chloroform varied by over one order-of-magnitude from 0.1 to >5 $\mu g/m^3$, and radon ranged from 0.15 pCi/L to 12.22 pCi/L. In addition,

lower indoor air VOC concentrations were observed in summer and peak PCE concentrations occurred in winter.

Holton et al. (2013) performed intensive indoor air VOC and radon monitoring at 2-4 h intervals for over 2 years in a slab-on-grade residential house located at a chlorinated solvent groundwater plume site in Utah. TCE indoor air concentrations varied by over three orders-of-magnitude within periods of days and weeks. Elevated TCE indoor air concentrations were found mainly in late fall through the early spring followed by long periods of low TCE concentrations with only sporadic increases during the summer. The authors evaluated simple hypothetical sampling schemes (sparse and infrequent sampling) using a synthetic 24-h average concentration data set generated from the actual indoor air data set. The outcomes included relatively high probabilities of false-negative and false-positive decisions and poor characterization of long-term mean concentrations.

Numerical modeling studies have also addressed VI temporal and spatial variability. Luo (2009) used a modified version of the Abreu and Johnson 3-D numerical model (2005) to study the effects of transient wind load and barometric pressure on soil gas concentration distribution and indoor air concentration. Over two orders-of-magnitude variation in indoor air concentration were obtained using barometric pressure and wind speed data collected during a one-year VI study at a site in Wyoming as inputs.

A USEPA (2012d) report presents comprehensive VI simulation results for both non-biodegradable and biodegradable chemicals and for a range of scenarios that were selected to illustrate how site-specific conditions might influence both VOC subsurface distribution and indoor air quality. The simulation results suggested source zone-building

separation is a significant factor in determining VI impacts, for example, indoor air impacts decreased over 10X when the source zone to foundation separation increased from 1m to 16 m under homogeneous soil scenarios. Similar results were obtained by Yao et. al. (2012) using a finite element simulation approach. They examined VI transient effects using a sinusoidal pressure differential input. Their results showed that cycling building pressure between 0 to -5 Pa will lead to contaminant mass flow that varies by a factor of 2-20, and they concluded that temporal changes in indoor air concentrations are strongly related to building pressure fluctuations.

Together, these studies raise questions about the validity of current sparse VI assessment sampling plans. Though recommendations such as the collection of multiple time-integrated samples are suggested in studies and guidance documents, research is still needed to show that those recommendations can improve the accuracy and confidence in VI pathway assessment.

1.1.3.2 Factors affecting VI impacts. Realizing that both temporal and spatial variability exist and understanding the consequences of it in regard to VI assessments, attempts have been made to identify causative factors between VI impacts and site features. Source zone characteristics (e.g. source type, source strength, chemical properties, source-building separation), building characteristics (e.g. foundation type, HVAC operation, pressure fluctuation) as well as soil characteristics (e.g. permeability, stratigraphy, moisture content) are either known or suspected to be important factors that need to be considered (Loureiro, 1987; Nazaroff et al., 1987; Johnson and Ettinger, 1991; Riley et al., 1999; Abreu, 2005; Abreu et al., 2005; Abreu et al., 2006; Bozkurt et al., 2009; Gossett et al., 2010; USEPA, 2012d; Yao et al., 2012; Holton et al., 2015).

Groundwater table fluctuations could also influence VI impacts (USEPA, 2002; ITRC, 2007; NJDEP, 2013; USEPA, 2015a).; however, there has been limited lab based and modeling research focused on determining the significance of groundwater table movement on VOC emissions from groundwater and subsequent VI impacts

Groundwater table fluctuations occur at all sites, although the frequency and magnitude of the fluctuations can vary significantly from one site to the next. For example, diurnal fluctuations can be found ranging from 0.5-1.0 cm to meters per day due to temperature and atmosphere pressure change or tides (Gribovszki et al., 2010; Li and Jiao, 2007); and semiannual or seasonal fluctuations are also seen (Leduc et al, 1997).

McCarthy and Johnson (1993) studied TCE transport across the capillary fringe between groundwater and unsaturated soil using a lab-scale, two-dimensional, physical model. As part of that study, soil gas TCE concentrations were collected as the water table was lowered. In response, TCE concentrations increased by a factor of three throughout most of the unsaturated zone and then quickly declined to their original values after the water table was returned to its initial level. The authors conclude that molecular diffusion was the dominant vertical transport mechanism, but contaminant flux was not quantified during the event.

Werner and Hohener (2001) evaluated the influence of water table fluctuations on the transport of halogenated compounds from groundwater to soil gas in a glass column filled with wet sand. Water table fluctuations between 85 and 107 cm were generated for 2.5 cycles within a 600 h period. Over an order-of-magnitude increase in soil gas was observed for a retreating water table. Vertical diffusive flux was quantified based on soil

gas concentration profiles and Fick's Law; the cis-dichloroethene diffusive flux increased by about 2X and the 1,2-dichlorotetrafluoroethane diffusive flux increased by over one order of magnitude during declining water levels.

Picone et al. (2012) performed a sensitivity analysis on parameters and processes affecting vapor intrusion risks using a one-dimensional numerical model. Crawl space air benzene concentrations were simulated under the scenario with groundwater level fluctuating at 20 cm per semi-annual cycle for over 10 years. The maximum crawl space concentration was 2.3 times lower than the stationary groundwater level condition during water table rising, and it increased over two orders of magnitude during water table decreases.

Though there are some inconsistencies conclusions between the conclusions from these studies, they all suggest that groundwater fluctuation will lead to temporal changes in subsurface vapor concentrations and emission rates. To date, field-based studies have yet to be conducted to support their conclusions.

Another evolving but poorly-understood topic is that of alternative VI pathways. VI pathway assessment strategies and data interpretation are guided by conceptual site models and assume that vapors diffuse upward from source and enter the overlying building through foundation cracks; however, there are alternative VI pathways that can also contribute to VI impacts. Alternative VI pathways can include, but are not limited to, subsurface pipe networks (e.g., sewer mains and land drains). These subsurface conduits may contain contaminants of concern either from chemical discharge to those systems or from inflow of contaminated groundwater or vapors originating from subsurface contamination. Figure 2 shows the conventional soil VI pathway and alternative VI

pathways, which in this case are sewer and conduit pipelines. These neighborhood sewers, land drains, and other major underground piping can also distribute contaminant (vapors or dissolved phase) from one structure to another, or beyond the delineated footprints of regional dissolved groundwater plumes.

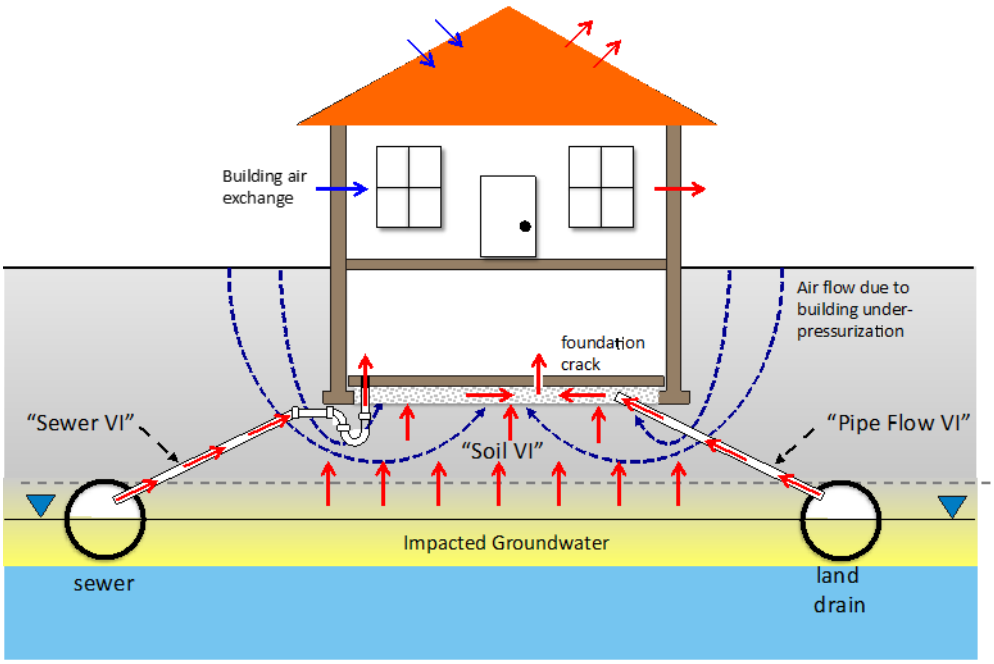

Figure 1.2. Vapor intrusion pathway conceptualization showing the conventional and alternative VI pathways.

In recent years, a few studies have concluded that alternative VI pathways can be significant contributors to VI impacts. Hawkins (2008) reported significant benzene migration through sewer lines at a gasoline-impacted site in Hazleton, PA. Riis et al. (2010) found that contaminated groundwater was entering the sewer system through cracks in the sewer lines and served as the primary vapor intrusion pathway at a site in Skuldelev, Denmark. VI impacted buildings were also found beyond the footprint of the groundwater plume. A recently published study by Pennell et al. (2013) showed how a

sewer line could be the primary pathway for PCE to indoor air at a residential house. At this site, the observation that unexpected high PCE indoor air measurements always occurred with sewer odors raised the suspicion of transport through the sewer. This was confirmed by a sequence of tests, including direct sewer head space gas samples and first floor indoor air comparison before and after sealing the bathroom.

There are no guidelines for identifying the presence and significance of alternative VI pathways and they might not readily identified by conventional VI pathway assessment approaches. Alternative VI pathways were discovered by Riis et al.(2010) and Pennell et al. (2013) only because they had more temporally and spatially extensive data sets than is typical. Moreover, the conventional VI mitigation approaches might be insufficient for alternative VI pathways. Passive sub-slab ventilation was ineffective for the buildings reported by Riis et al. (2010), but no other information can be found in well-controlled studies.

1.1.3.4 Controlled pressure method (CPM). Natural fluctuations in subsurface to indoor air pressure differentials is believed to be one of the factors that leads to indoor air concentration variability with time (Hintenlang et al., 1992; Robinson, 1996; Robinson et al., 1997; Luo, 2009). To account for this, the controlled pressure method (CPM) has been proposed as a method of assessment. This technique involves controlling the indoor-outdoor pressure differential over short period time to eliminate any impact of natural fluctuations.

A tracer test under depressurized building conditions conducted by Nazaroff et al. (1987) demonstrated that depressurization could lead to increased soil vapor migration. McHugh et al. (2012) manipulated pressures at five of six buildings using a box fan

blowing air directly in/out of buildings. The building pressure differential relative to atmospheric pressure was 1-5 Pa for both building depressurization and building pressurization. During these tests, tracer gas (sulfur hexafluoride, SF_6) was released in each building to measure building air exchange rates; contaminant mass discharge rates were then calculated for baseline (natural pressure conditions), negative (depressurized) and positive (over-pressurized) conditions. The results suggested that building pressure manipulation can control the movement of soil gas across the building foundation and that contaminant mass discharge would increase substantially when the building was under-pressurized relative to the atmosphere. They also concluded that CPM tests could also identify if indoor air sources were significant contributors to indoor air quality.

The first long-term and high-frequency monitoring CPM test was reported by Holton et al. (2015). Real-time TCE and radon indoor air concentrations were monitored under both natural and under-pressurized conditions in a residential house overlying a chlorinated solvent plume. The purpose was to examine the long-term temporal variability of CPM results and to evaluate the utility of CPM test results for VI risk assessment. The in-building pressure was maintained about 11 Pa lower than atmospheric and 5 Pa lower than sub-slab pressures for over 300 days using a blower installed in the ceiling into the attic. Both TCE and radon indoor air concentrations significantly increased under CPM conditions. Both TCE and radon indoor air concentrations varied much less under CPM testing than during 2-year indoor air monitoring under natural conditions in the same house,.

Holton et al. (2015) developed a relationship to project concentrations under natural conditions from CPM test results:

$$C(natural\ condition) = \frac{C(CPM\ condition) \times Q_b(CPM\ condition)}{Q_b(natural\ condition\ estimate\ )}$$

where *C(natural condition)* and *C(CPM condition)* are indoor air contaminant concentrations [M/L^3] under natural and CPM conditions, and Q_b *(CPM condition)* and Q_b *(natural condition estimate)* are building flow rates [L^3/T] under natural and CPM conditions. They concluded that this approach reasonably predicts maximum indoor air concentrations for natural conditions, but will likely overestimate long-term exposure levels.

Though many questions still exist (e.g. CPM test results may not provide representative VI risk for natural pressure conditions), VI assessment using CPM appears promising as a quick screening tool since it provides a rapid response and minimizes temporal variability created by building pressure fluctuations. Furthermore, CPM has the potential to be a useful diagnostic tool to better characterize VI pathways because the sensitivities of different VI pathways or sources to pressure fluctuation are different. For example, Patterson et al. (2009) identified the diffusion of vapors as the dominant vapor intrusion pathway when the building interior was under ambient pressure, while advective transport was the major VI contributor when the building was depressurized to 12 Pa lower than ambient.

1.1.4 Challenges and Opportunities for Research. As discussed above, vapor intrusion is a key topic of interest at soil and groundwater contaminated sites. Although our knowledge of VI and VI assessment has improved through studies discussed above, there are still important questions that need to be answered if we are to be able to confidently assess VI impacts quickly and cost-effectively.

First, while groundwater table movement has been recognized as one environmental factor that may result in temporal changes in subsurface contaminant transport, only limited modeling studies can be found discussing its impact on vapor intrusion investigation, and neither field data sets nor well-controlled physical lab tests were found in the literature.

Second, subsurface conduits and other alternative VI pathways are present at sites, but protocols for conventional VI investigations may not effectively identify them. Consequently, for those buildings that require VI mitigation, presumptive remedies may not be protective. For example, sub-slab depressurization (SSD) is known to be effective where soil VI is the dominant pathway (USEPA, 2008), but it is uncertain for homes where pipe flow and sewer VI pathways are significant.

For VI assessment, CPM testing seems a promising tool. However, there are still questions that need to be answered, the most important of which might be how to interpret and use CPM test results effectively and comprehensively. Combining CPM testing and MLE results might provide a much higher level of information that can be used for VI investigation.

Finally, there are no known field data sets of sites that include significant alternative VI pathway impact.

1.2 RESEARCH OBJECTIVES

This research aims to gain better understanding of groundwater table movement impact on vapor intrusion as well as to improve our understanding of alternative vapor intrusion pathway identification and mitigation.

The groundwater table fluctuation-related research was focused on answering the following questions:

a) Should practitioners assessing VI impacts be concerned with groundwater table elevation changes? Under most natural scenarios, are groundwater table elevation fluctuations likely to change vapor emissions and VI impacts relative to static water table conditions?
b) Are there scenarios under which the effects of groundwater table elevation changes are significant and should be considered in VI pathway assessment?
c) If groundwater table elevation changes are of significance, how should those scenarios be considered in VI pathway assessment?

To answer these questions, this work involved long-term field monitoring of vapor emissions, lab-scale physical model experiments, and modeling analyses.

The specific objectives of the alternate VI pathway-related work were to:

- develop and demonstrate an alternative VI pathway identification paradigm using CPM testing, soil gas monitoring, and screening model calculations.
- assess the effectiveness of SSD mitigation system(s) when alternative pathways are present.

The alternative VI pathway related research was conducted at a well-instrumented study house with a sub-slab depressurization mitigation system. A significant alternative VI pathway providing a direct conduit to the sub-slab region of the study house was

discovered and modified to enable researchers to connect/disconnect the conduit from the sub-slab region.

1.3 DISSERTATION ORGANIZATION

The chapters of this dissertation are organized as follows:

- Chapter 2 describes an integrated study focused on evaluating the impact of groundwater fluctuations on vapor emissions and VI impacts.
- Chapter 3 focuses on identifying alternative VI pathways using controlled pressure method (CPM) testing, soil gas monitoring, and screening model calculations.
- Chapter 4 evaluates the effectiveness of a sub-slab depressurization system at a VI site with and without an active alternative VI pathway.
- Chapter 5 summarizes conclusions from previous chapters and provides recommendations for future research work.
- Appendix I provides a description of the study site, including site history, monitoring and sampling network details, and other relevant information.
- Appendix II presents details of the experimental methods used.
- Appendix C presents the supporting information for impact of groundwater table fluctuations on chlorinated volatile organic compound (VOC) emissions.
- Appendix IV presents the supplemental information to Chapter 3.
- Appendix V presents the supplemental information to Chapter 4.

- Appendix VI presents the VOC concentrations in the land drain system in the vicinity of the study house.

1.4 REFERENCES

Abreu, L. (2009). A transient three dimensional numerical model to simulate vapor intrusion into buildings. (Dissertation), Arizona State University, Tempe, AZ, 2005.

Abreu, L., Johnson, P. C. (2005). Effect of vapor source-building separation and building construction on soil vapor intrusion as studied with a three-dimensional numerical model. *Environmental Science and Technology*, *39* (12), 4550-4561.

Abreu, L., Johnson, P. C. (2006). Simulating the Effect of Aerobic Biodegradation on Soil Vapor Intrusion into Buildings: Influence of Degradation Rate. Source Concentration, and Depth. *Environmental Science and Technology, 40*, 2304-2315.

American Petroleum Institute. (2005). *A practical strategy for assessing the subsurface vapor-to-indoor air migration pathway at petroleum hydrocarbon sites*. Washington, DC: American Petroleum Institute.

Bozkurt, O., Pennell, K. G., Suuberg, E. M. (2009). Simulation of the vapor intrusion process for nonhomogeneous soils using a three-dimensional numerical model. *Groundwater Monitoring and Remediation*, *29* (1), 92-104.

California Department of Toxic Substances Control. (2011). *Guidance for the evaluation and mitigation of subsurface vapor intrusion to indoor air (Vapor intrusion guidance).*

Department of Defense. (2009). *Vapor intrusion handbook*. Washington, DC: Department of Defense.

Folkes, D., Wertz, W., Kurtz, J., Kuehster, T. (2009). Observed spatial and temporal distributions of CVOCs at Colorado and New York vapor intrusion sites. *Ground Water Monitoring and Remediation, 29*, 70-80.

Garbesi, K., Sextro, R. G. (1989). Modeling and field evidence of pressure-driven entry of soil gas into a house through permeable below grade walls. *Environmental Science and Technology*, *23* (12), 1481-1487.

Gribovszki, Z., Szilagyi, J., Kalicz, P. (2010). Diurnal fluctuation in shallow groundwater levels and streamflow rates and their interpretation – A review. *Journal of Hydrology, 385*, 371-383.

Hawkins, J. (2008). Vapor Intrusion in Texas- Evaluating the Indoor Air Pathway. Presentation at Society of Texas Environmental Professionals (STEP). Texas.

Hintenlane, D.E., Al-Ahmady, K.K. (1992). Pressure Differentials for Radon Entry Coupled to Periodic Atmospheric Pressure Variations. *Indoor Air, 2* (12), 208-215.

Holton, C., Luo, H., Dahlen, P., Gorder, K. A., Dettenmaier, E. M., Johnson, P. C. (2013). Temporal variability of indoor air concentrations under natural conditions in a house overlying a dilute chlorinated solvent groundwater plume. *Environmental Science and Technology, 47*, 13347-13354.

Holton, C., Guo, Y., Luo, H., Dahlen, P., Gorder, K. A.; Dettenmaier, E. M.; Johnson, P. C. (2015). Long-Term Evaluation of the Controlled Pressure Method for Assessment of the Vapor Intrusion Pathway. *Environmental Science and Technology, 49*, 2091-2098.

Howard, P.H. (1991). *Handbook of Environmental Degradation Rates*. Lewis Publishers, Chelsea, MI.

Hubbard, L. M., Mellander, H., Swedejemark, G. A. (1995). Studies on temporal variations of radon in Swedish single-family houses. *Environment International*, *22*, S715-S722.

Interstate Technology & Regulatory Council. (2007). *Vapor intrusion pathway: A practical guideline*. Washington, DC: Interstate Technology & Regulatory Council.

Johnson, J. E. (2013). Assessing Exposure to Chlorinated Solvents from the Subsurface to Indoor Air Pathway. Ph.D. Dissertation, University of North Carolina, Chapel Hill, NC.

Johnson, P. C., Ettinger, R. A. (1991). Heuristic model for predicting the intrusion rate of contaminant vapors into buildings. *Environmental Science and Technology*, *25* (8), 1445-1452.

Leduc, C., Bromley, J., Schroeter, P. (1997). Water table fluctuation and recharge in semi-arid climate: some results of HAPEX-Sahel hydrodynamic survey (Niger). *Journal of Hydrology*, *188-189*, 123-138.

Li, H., Jiao, J. J. (2005). One-dimensional airflow in unsaturated zone induced by periodic water table fluctuation. *Water resources research, 41*(4).

Little, J. C., Daisey, J. M., Nazaroff, W. W. (1992). Transport of subsurface contaminants into buildings: An exposure pathway for volatile organics. *Environmental Science and Technology*, *26* (11), 2058-2066.

Loureiro, C. O. (1987). Simulation of Steady-state transport of radon from soil into houses with basement under constant negative pressure (Dissertation). Lawrence Berkeley Laboratory, Berkeley, CA.

Loureiro, C. O., Abriola, L. M., Martin, J. E., Sextro, R. G. (1990). Three-dimensional simulation of radon transport into houses with basements under constant negative pressure. *Environmental Science and Technology*, *24*, 1338-1348.

Luo, H. (2009). Field and modeling studies of soil gas migration into buildings at petroleum hydrocarbon impacted sites (Dissertation). Arizona State University, Tempe, AZ.

Luo, H., Dahlen, P., Johnson, P. C., Peargin, T., Creamer, T. (2009). Spatial variability of soil-gas concentrations near and beneath a building overlying shallow petroleum hydrocarbon-impacted soils. *Ground Water Monitoring and Remediation*, *29*, 81-91.

Massachusetts Department of Environmental Protection. (2011). *Interim final vapor Intrusion guidance*. Boston, MA: Massachusetts Department of Environmental Protection.

McCarthy, K. A.; Johnson, R. L. (1993). Transport of volatile organic compound across the capillary fringe. *Water Resources Research, 29* (6), 1675-1683.

McHugh, T. E., Nickels, T. N., Brock, S. (2007). Evaluation of spatial and temporal variability in VOC concentrations at vapor intrusion investigation sites. Proceedings of Air and Waste Management Association's *Vapor intrusion: Learning from the challenges*, Providence, RI, 129-142.

McHugh, T. E., Beckley, L., Bailey, D., Gorder, K., Dettenmaier, E., Rivera-Duarte, I., Brock, S., MacGregor, I. C. (2012). Evaluation of vapor intrusion using controlled building pressure. *Environmental Science & Technology*, *46*, 4792-4799.

Moseley, C. L., Meyer, M. R. (1993). Petroleum contamination of an elementary school: A case history involving indoor air, soil-gas, and groundwater monitoring. *Environmental Science and Technology, 26*, 185-192.

Nazaroff, W. W., Fuestel, H., Nero, A. V. Revzan, K. L., Grimsruf, D. T. (1985). Radon transport into a detached one-story house with a basement. *Environmental Science and Technology, 19* (1), 31-46.

Nazaroff, W. W., Doyle, S. M. (1985). Radon entry into house having a crawl space. *Health Physics*, *48* (3), 265-281.

Nazaroff, W. W., Lewis, S. R., Doyle, S. M., Moed, B. A., Nero, A. V. (1987). Experiments on pollutant transport from soil into residential basements by pressure-driven airflow. *Environmental Science and Technology, 21* (5), 459-466.

Nazaroff, W. W. (1992). Radon transport from soil to air. *Reviews of Geophysics, 30* (2), 137-160.

New Jersey Department of Environmental Protection. (2013). *Vapor intrusion technical guidance.* Trenton, NJ: New Jersey Department of Environmental Protection.

New York State Department of Health. (2006). *Guidance for Evaluating Soil Vapor Intrusion in the State of New York.* Troy, NY: New York State Department of Health.

Patterson, B. M. and Davis, G. B. (2009). Qualification of Vapor Intrusion Pathways into a Slab-on-Ground Building under Varying Environmental Conditions. *Environmental Science and Technology, 43*, 650-656.

Pennell, K. G., Scammell, M. K., McClean, M. D.; Ames, J.; Weldon, B., Friguglietti, L., Suuberg, E. M.; Shen, R., Indeglia, P. A., Heiger-Bernays, W. J. (2013). Sewer gas: An indoor air source of PCE to consider during vapor intrusion investigations. *Groundwater Monitoring and Remediation, 33* (3), 119-126.

Picone, S., Valstar, J., van Gaans, P., Grotenhuis, T., Rijnaarts, H. (2012). Sensitivity analysis on parameters and processes affecting vapor intrusion risk. *Environmental Toxicology and Chemistry, 31* (5), 1042-1052.

Riley, W. J., Robinson, A. L., Gadgil, A. J., Nazaroff, W. W. (1999). Effects of variable wind speed and direction on radon transport from soil into buildings: Model development and exploratory results. *Atmospheric Environment, 33*, 2157-2168.

Riis, C. E., Christensen, A. G., Hansen, M. H., Husum, H., Terkelsen, M. (2010). Vapor Intrusion through Sewer Systems: Migration Pathways of Chlorinated Solvents from Groundwater to Indoor Air. Presentation at the 7th Battelle International Conference on Remediation of Chlorinated and Recalcitrant Compounds, Monterey.

Robinson, A. L. (1993). Radon Entry into Buildings: Effects of Atmospheric Pressure Fluctuations and Building Structural Factors (Dissertation). University of California, Berkeley.

Robinson, A. L., Sextro, R. G., Fisk, W. (1997). Soil-gas entry into an experimental basement driven by atmospheric pressure fluctuations – measurements spectral analysis, and model comparison. *Atmospheric Environment, 31* (10), 1477-1485.

U.S. Environmental Protection Agency. (2001). *RCRA Draft Supplemental Guidance for Evaluating the Vapor Intrusion to Indoor Air Pathway (Vapor Intrusion Guidance).* Washington, DC: U.S. Environmental Protection Agency.

U.S. Environmental Protection Agency. (2002). *OSWER draft guidance for evaluation the vapor intrusion to indoor air pathway from groundwater and soils (Subsurface vapor intrusion guidance).*Washington, DC: U.S. Environmental Protection Agency.

U.S. Environmental Protection Agency. (2008). *Engineering Issue: Indoor Air Vapor Intrusion Mitigation Approaches*. Washington, DC: U.S. Environmental Protection Agency.

U.S. Environmental Protection Agency. (2010). *Review of the draft 2002 subsurface vapor intrusion guidance*. Washington, DC: U.S. Environmental Protection Agency.

U.S. Environmental Protection Agency. (2011). Toxicological review of trichloroethylene: In support of summary information on the integrated risk information system (IRIS). Washington, DC: U.S. Environmental Protection Agency.

U.S. Environmental Protection Agency. (2012). *Petroleum hydrocarbons and chlorinated hydrocarbons differ in their potential for vapor intrusion*. Washington, DC: U.S. Environmental Protection Agency.

U.S. Environmental Protection Agency. (2012). *Fluctuation of indoor radon and VOC concentrations due to seasonal variations*. Washington, DC: U.S. Environmental Protection Agency.

U.S. Environmental Protection Agency. (2012). *EPA's vapor intrusion database: Evaluation and characterization of attenuation factors for chlorinated volatile organic compounds and residential buildings*. Washington, DC: U.S. Environmental Protection Agency.

U.S. Environmental Protection Agency. (2012). *Conceptual model scenarios for the vapor intrusion pathway*. Washington, DC: U.S. Environmental Protection Agency.

U.S. Environmental Protection Agency. (2012). *Toxicological review of tetrachloroethylene (perchloroethylene): In support of summary information on the integrated risk information system (IRIS)*. Washington, DC: U.S. Environmental Protection Agency.

U.S. Environmental Protection Agency. (2013). *OSWER FINAL GUIDANCE FOR ASSESSING AND MITIGATING THE VAPOR INTRUSION PATHWAY FROM SUBSURFACE SOURCES TO INDOOR AIR (EXTERNAL REVIEW DRAFT)*. Washington, DC: U.S. Environmental Protection Agency.

U.S. Environmental Protection Agency. (2015). *OSWER TECHNICAL GUIDE FOR ASSESSING AND MITIGATING THE VAPOR INTRUSION PATHWAY FROM SUBSURFACE VAPOR SOURCES TO INDOOR AIR*. Washington, DC: U.S. Environmental Protection Agency.

U.S. Environmental Protection Agency. (2015). *Technical Guide for Addressing Petroleum Vapor Intrusion At Leaking Underground Storage Tank Sites*. Washington, DC: U.S. Environmental Protection Agency.

U.S. Environmental Protection Agency. (2014) *Vapor Intrusion Screening Level (VISL) Calculator, User's Guide*. Washington, DC: U.S. Environmental Protection Agency.

Wener, D., Hohener, P. (2002). The influence of water table fluctuations on the volatilization of contamination from groundwater. *IAHS PUBLICATION*, 213-218.

Yao, Y., Pennell, K. G., Suuberg, E. M. The influence of transient processes on vapor intrusion processes. Paper for the AWMA Vapor Intrusion Conference, September 2010.

Yao, Y., Shen, R.; Suuberg, E. M. (2012). Estimation of Contaminant Subslab Concentration in Vapor Intrusion Including Lateral Source-Building Separation. *Vadose Zone Journal*, doi:10.2136/vzj2012.0157.

CHAPTER 2

IMPACT OF WATER TABLE ELEVATION FLUCTUATION ON CHLORINATED HYDROCARBON (CHC) EMISSION FROM GROUNDWATER

2.0 ABSTRACT

The temporal fluctuation of groundwater table elevation can influence the release and transport of volatile organic chemicals (VOCs) from groundwater to soil gas. Recent vapor intrusion (VI) guidance documents have recognized that water table fluctuations may impact the assessment of a VI-impacted site, but the significance is not well understood. This study collected and analyzed long-term monitoring data from a site with groundwater impacted by dissolved chlorinated hydrocarbons (CHCs). Lab-scale two-dimensional physical models were also used to examine how groundwater table fluctuations affect vapor emission rates from groundwater. Those data were used to validate numerical modeling analyses conducted using HYDRUS 1-D (Simunek, 2013) to investigate behavior beyond the field and lab conditions. VOC emissions did not vary by more than about 50% about the average with time at the field study site where the groundwater table elevation typically declined by about 0.3 m from winter to summer and then increased from summer to winter, with shorter term fluctuations of about 0.05-0.2 m. This was consistent with the modeling analysis results for a similar depth to groundwater and soil type. The modeling analyses did identify some situations for which emissions could change significantly with time. For example, with monthly water table

fluctuations and shallow groundwater (0.5 m depth to groundwater), emissions were two orders of magnitude greater than the base static water table condition.

2.1 INTRODUCTION

The migration of vapor-phase contaminants from impacted soil or groundwater to indoor air, a process known as vapor intrusion (VI), can pose risks to human health. Current assessment of the pathway follows a multiple-lines-of-evidence (MLE) approach involving infrequent indoor air, sub-surface soil gas, groundwater, and soil sampling as well as screening-level modeling (ITRC, 2007; NJDEP, 2013; USEPA, 2015). However, temporal variations in both indoor air and subsurface contaminant concentrations have been reported (Folkes et. al, 2009; Luo, 2009; USEPA, 2012; Holton et. al, 2013) and factors influencing the temporal variability are not well understood. In general, indoor air temporal variability can reflect changes in building pressure, changes in resistance and attenuation along the transport pathway, and changes in the source emission rate. Building dynamics and indoor air pressure can be influenced by temporal patterns in the indoor-outdoor temperature difference, wind speed, and HVAC operation (Hubbard, 1996; Luo, 2009; Yao et al., 2010; Holton, 2015). Changes in resistance and attenuation along the subsurface transport pathway can be induced by precipitation patterns, moisture content changes and vapor source-building separation (Abreu and Johnson, 2005; Bozkurt et al., 2009; USEPA, 2012). Emission rates can be influenced by the above changes in resistance and attenuation along the subsurface transport pathway, but can also reflect changes in groundwater table elevation. Diurnal, seasonal, and semiannual

fluctuations (Turk, 1975; Leduc et al, 1997; Li and Jiao, 2005) are possible, the frequency and amplitude of which can vary from site to site.

Changes in groundwater table elevation can affect source emission rates in a number of ways. For soil-impacted source zones, raising and lowering of the water table can result in variable exposure and submersion of the source zone, which can effectively turn on and off emission from the source zone. In addition, it creates advective movement of soil gas through the impacted zone. For dissolved sources, raising and lowering of the water table can shorten and lengthen the transport pathway. A rising water table can also distribute dissolved contaminants upward into soils that then become unsaturated and exposed for emission when the water table lowers. Conclusions regarding the significance of these processes in the literature vary (McCarthy and Johnson 1993, Parker 2002, Werner and Hoehener 2002, Picone et al. 2012); however, there appears to be general agreement that emissions from impacted groundwater can increase during periods of declining water table elevation. Expected increases, based on lab experiments and modeling studies, range from factors of about two to more than an order of magnitude, with the magnitude being impacted by amplitude and frequency of groundwater elevation changes as well as soil and chemical properties. Some results also suggest decreasing emissions with increasing groundwater table elevation (Werner and Hoehener, 2002; Picone et al., 2012).

VI guidance documents recognize that VI impacts can be influenced by groundwater table elevation changes, but the significance is not well understood (USEPA, 2002; ITRC, 2007; NJDEP, 2013; USEPA, 2015). For example, USEPA (2015) suggests taking near source soil gas samples in different seasons that coincide with

groundwater table elevation changes to account for this. However, given that the significance is not well-understood and has not been studied in detail, practical questions such as "what dynamic groundwater scenarios will result in significant temporal changes in vapor emissions?" are unanswered.

This study focuses on the impact of groundwater table elevation changes on vapor emissions from dissolved groundwater sources, which is the most commonly seen vapor intrusion scenario for chlorinated hydrocarbon (CHC)-impacted sites. It looks at two issues: a) identifying conditions for which temporal variations in emissions will and will not be significant, and b) identifying scenarios where fluctuating groundwater tables produce emissions that are significantly different from the base-case static water table scenario. These are important from a practical standpoint; the former is important when selecting sampling density and frequency for pathway assessment plans implemented at suspected VI sites, and the latter is important when considering emissions and VI impacts predicted using models that assume a static groundwater table. This complements the analyses, observations, and conclusions of previous studies, by providing answers to the following practical questions of interest:

This study involved long-term field monitoring of vapor emissions, lab-scale physical model experiment results, and numerical modeling analyses. The impact of groundwater table fluctuations on subsurface vapor transport and emissions to a home was examined using long-term monitoring data from a dissolved chlorinated solvent impacted site. Results from two-dimensional lab-scale physical models, using three chlorinated chemicals and two different soil types, were used to guide and validate

mathematical modeling that examined a broader range of conditions using the HYDRUS 1-D model (Simunek, 2013).

2.2 THE INFLUENCE OF GROUNDWATER TABLE ELEVATION FLUCTUATION ON CHC TRANSPORT AND EMISSION AT A FIELD STUDY SITE

2.2.1 Experimental methods. *Site description*. The study site is a two-story, split-level house built into a slope with a 2.5 m elevation drop from the back to front yard. There is a living space and attached garage on the lower level. Multi-level soil gas and groundwater sampling points were installed inside through the foundation and outside of the building, with soil gas points installed to the following depths: sub-slab (SS), 0.9 m below slab (BS) and 1.8 m BS. Figure 2.1 presents a schematic view of the study house with groundwater and soil gas sampling locations. A detailed site description and information on sampling locations can be found in Appendix I. There is a land drain lateral pipe connecting the sub-foundation region to a neighborhood land drain system containing CHC-impacted groundwater and vapors. A valve was installed in the lateral pipe mid-way when it was discovered as described in Chapter 3. The land drain system is a VI pathway when the valve is open and does not contribute to VI impacts when it is closed.

The depth to groundwater at this site is approximately 2.5 m BS, and groundwater contains dilute concentrations of dissolved chlorinated hydrocarbons (CHCs). Trichloroethene (TCE) concentrations in groundwater samples collected below the

building foundation ranged spatially and temporally from 10 - 50 µg/L-H_2O over four years.

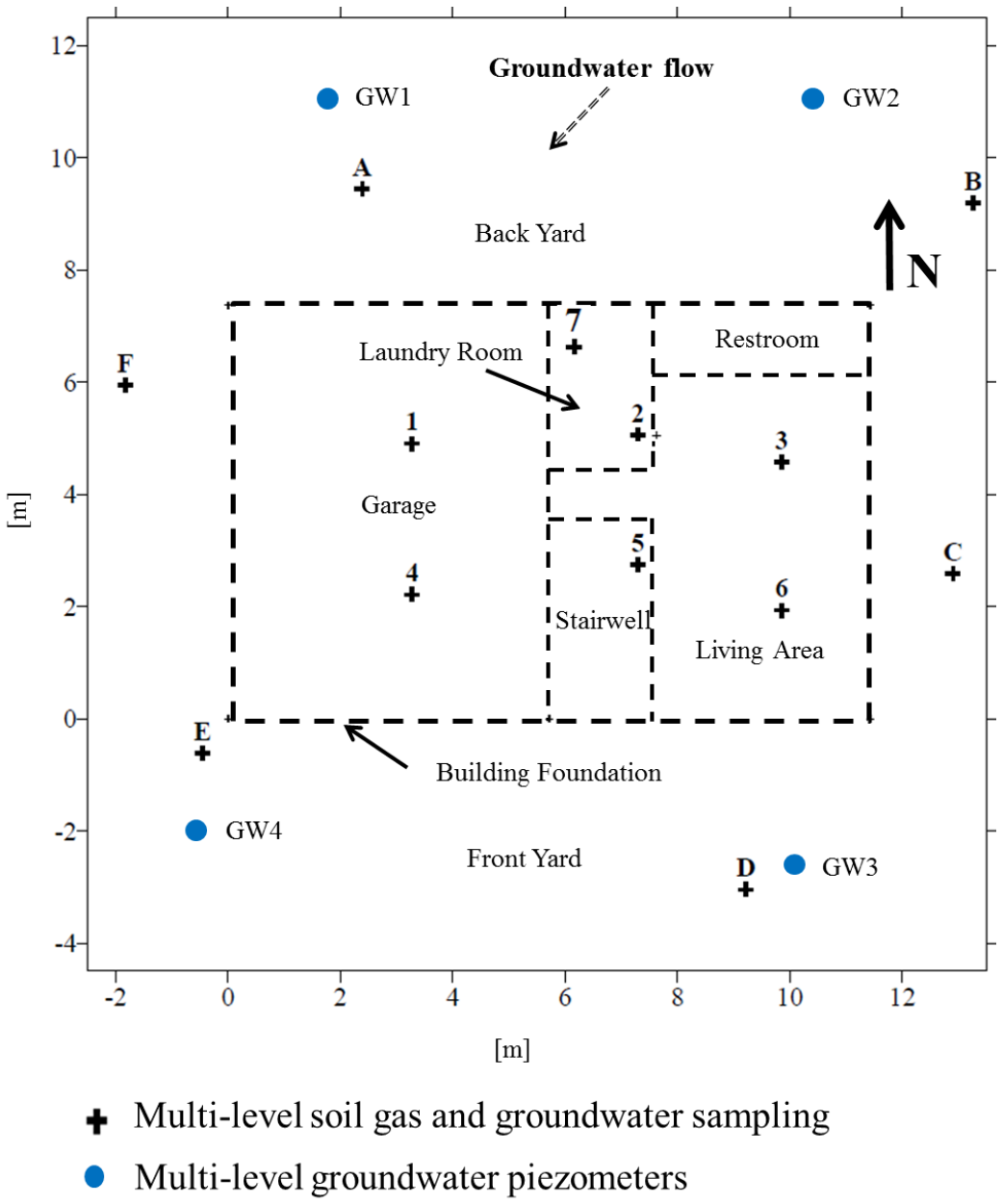

Figure 2.1. Schematic of the lower level of the study house showing interior and exterior subsurface monitoring locations.

The soil beneath and adjacent to the house is predominantly fine sandy silt with fine sand stringers. Grain size distribution tests on soil samples collected at 30 cm intervals along a soil core collected at location D indicated that the silt to clay size fraction (<0.0063 mm) dominated (>70%). Figure 2.2 shows the gravimetric soil moisture content profile below ground surface during early summer at locations C, D and F. The results were relatively consistent to 2.5 m above water table at the three sampling locations.

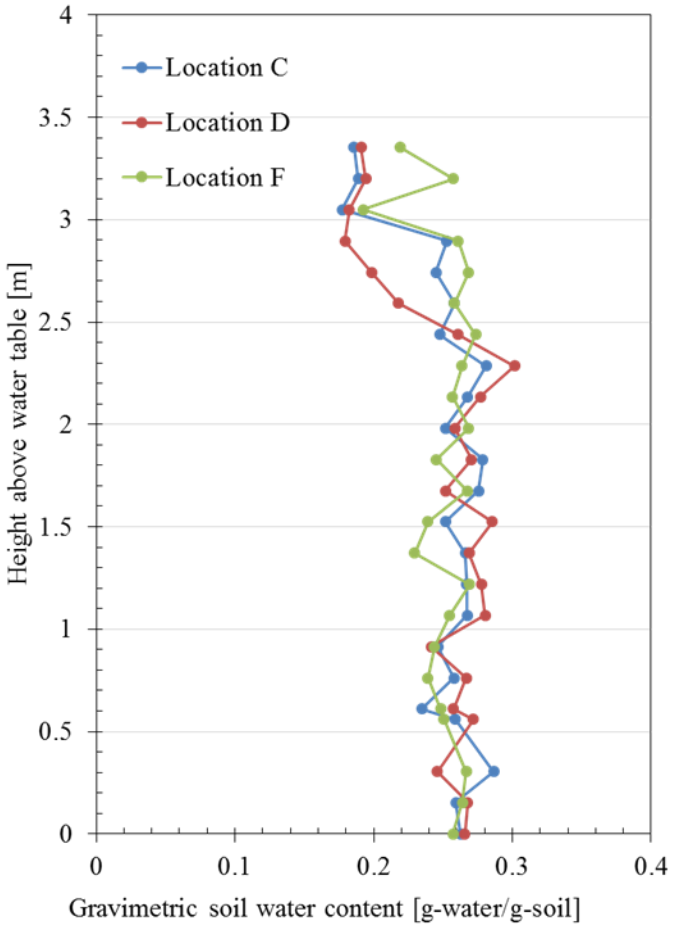

Figure 2.2. Soil moisture content results from three soil cores collected on May 2011.

Beginning on August 15, 2010 (t= 0 day), high-frequency and high spatial density monitoring was performed at this study site, including quantification of CHC concentrations in indoor air, soil gas and groundwater as well as other environmental factors. Results collected under natural and controlled building pressure conditions have been published by Holton et al (2013, 2015) and Guo et al. (2015). Of interest here are data collected from $1072 < t < 1157$ d during a controlled pressure method (CPM) test and when the lateral pipe valve was closed to eliminate any VI contributions from the land drain system and ensure that emissions to the building were coming from transport through the soil (the "soil VI pathway" defined in Chapter 3). The indoor air pressure was maintained at 11 ± 4 Pa lower than atmosphere by two dual-speed blowers installed in the attic. CHC entry rates into the building were calculated using measured building ventilation rates and indoor air concentrations as discussed below.

Data collection and analyses. CHC concentrations in both groundwater and soil gas were monitored. Groundwater samples were collected in 40 mL glass VOA vials using peristaltic pumps and were analyzed using a heated headspace method with on-column injection and an SRI® (SRI Instruments, Torrance, CA) gas chromatograph (GC) equipped with a dry electrolytic conductivity detector (DELCD) and a 60 m Restek MXT-1 column (Restek Corporation, Bellefonte, PA). Temperature programming for the GC oven was 66°C to 220°C at 12°C/min with a 3 min hold at 220°C. The DELCD was set at 1000 °C. The linear calibration range for TCE was between 5 and 100 µg/L-H_2O. GC calibrations were conducted before the analysis of every sample set.

Soil gas samples were collected and analyzed during synoptic, multi-depth soil gas surveys every 1-3 months. Samples were collected at sub-slab, 0.9 m below-slab

(BS), and 1.8 m BS depths at the locations shown in Figure 2.1. Samples were collected in 1-liter Tedlar bags (SKC 232-01) using a custom-built vacuum chamber sampler. Analyses were conducted within 3 hours of sample collection using the SRI 8610C GC equipped with a DELCD. Direct injection and sorbent trap pre-concentration were used as needed based on the soil gas concentration. The method detection limit (MDL) was 4.9 ppb_v (26 $\mu g/m^3$) for direct injection and 0.019 ppb_v (0.1 $\mu g/m^3$) for the pre-concentration method. Calibration for gas sample analysis was performed prior to every sampling event.

The depth to groundwater was monitored in real-time and synoptically throughout the field study. Real-time measurements used water level transducers (Solinst Level-Logger) installed at three depth-discrete and independent screened intervals (4.2 m, 6.9 m and 9.3 m below ground surface (BGS)) at groundwater monitoring location GW3. Data were logged every 12 h. Synoptic water table elevations were measured every 1-3 months at all groundwater elevation monitoring locations (GW1-4 in Figure 2.1) using a water level meter (Solinst Model 102).

Indoor air samples were collected every 8-12 h in the lower level of the house using sorbent tubes. For each sample, 12 L indoor air was pulled through a sorbent tube using two customized SRI Instruments (SRI Instruments, Torrance, CA) 20-stream gas sampling valves, a vacuum pump (Rena 301 series, model BE-3012 vacuum/pressure pump), and a vacuum-configured, 0-100 mL/min mass flow controller (Alicat Scientific, Tucson, AZ) run at 50 mL/min. Sorbent tubes were analyzed using a Markes Ultra auto-sampler and Markes Unity thermal desorber (Markes International, UK) connected to an HP5890 gas chromatograph equipped with a Restek 60 m Rxi-5 capillary column and an

HP5972 mass spectrometer. Samples were analyzed using selective ion mode (SIM) with an MDL of 0.008 ppb_v.

Real-time indoor air exchange rates were determined by releasing SF_6 tracer gas to indoor air at 5 mL/min and measuring the resulting indoor air concentration. Indoor air SF_6 concentrations were monitored on 30 minute intervals using an SRI GC equipped with a VICI pulsed-discharge detector (PDD; Valco Instrument Co. Inc.).

Data reduction. TCE emissions from groundwater, expressed as flux rates (mass/time per unit area) were calculated using two approaches. The first approach (F_1) was based on the assumption that diffusion was the dominant vapor transport mechanism in deep soil (Johnson et al., 1991), and utilized synoptic soil gas concentrations, effective diffusion coefficients, and Fick's Law:

$$F_1 = D_i^{eff} \frac{\Delta C_{g,i}}{L_i} \quad (1)$$

where subscript i denotes different locations, $\Delta C_{g,i}$ is the soil gas concentration difference $[M/L^3]$ over the vertical distance L_i [m], and D_i^{eff} $[L^2/T]$ is the effective diffusion coefficient. D_i^{eff} values were obtained using the Johnson et al. (1998) push-pull tracer method, and results from five field surveys were averaged for use in Equation (1).

The uncertainty associated with this calculation is primarily due to concentration measurement errors and the compounding of those errors associated with the subtraction of two concentration values in equation (1). The average percentage difference between duplicate samples was 25.5% and D_i^{eff} and L_i were fixed values for all calculations at each sampling location i. The uncertainty in F_1 values due to concentration measurement errors is then (Harris, 2009):

$$e_i = D_i^{eff} \frac{\sqrt{(0.255 \times C_{g,i,0.9\,m\,BS})^2 + (0.255 \times C_{g,i,1.8\,m\,BS})^2}}{L_i} \quad (2)$$

The second approach (F_2) utilized indoor data collected during controlled pressure method (CPM) test conditions. As mentioned previously, from t= 1071 d to t= 1157 d, the study house was constantly under-pressurized and isolated from the land drain network. Assuming no CHC degradation during transport, then TCE emissions from groundwater are equivalent to emissions to indoor air above the groundwater, and so F_2 can be calculated:

$$F_2 = C_{indoor} \times (C^o_{tracer}/C_{tracer}) \times Q_{tracer}/A \quad (3)$$

where C_{indoor} is the TCE indoor air concentration [M/L^3], Q_{tracer} is SF_6 tracer release rate [L^3/T], C^o_{tracer} and C_{tracer} are release and resulting indoor SF_6 concentrations, respectively [M/L^3], and A is the building footprint area of 84.4 m^2.

Two measurements are involved in F_2 calculations. The indoor air TCE and tracer concentrations, C_{indoor} and C_{tracer}, are measured using TD GC/MS and GC/PDD respectively. These two quantities are not measured at the same time; C_{tracer} was collected approximately every 30 min and C_{indoor} was collected every 4 h and a time-averaged C_{tracer} (±4 hours about the C_{indoor} measurement) was used in Equation (3). Therefore, the uncertainty for C_{tracer} was estimated using the percent standard deviation ($\%S_{ctracer}$) within that averaging time. The measurement error for TD GC/MS analyses was estimated to be <10 % based on the holding test described in Appendix B (Table B.3). The uncertainty in each F_2 value was calculated as:

$$e_{F2} = F_2 \sqrt{(10\%)^2 + (\%S_{Ctracer})^2} \quad (4)$$

2.2.2 Results and discussion. *Groundwater and soil gas TCE concentrations vs. groundwater elevation.* Figure 2.3 presents the groundwater table elevation at GW3 relative to the base of the building slab vs. spatially-averaged groundwater TCE concentrations beneath the building for about four years at the study site. Error bars represent standard deviations for each sampling event. On average, the groundwater table was positioned 3.3 ± 0.1 m below the building slab. A seasonal pattern in groundwater table elevations is evident; the groundwater table elevation typically increased from late winter to spring and declined during late summer to fall, with the magnitude of changes being about 0.3 m and the difference between the minimum and maximum elevations was about 0.4 m. Groundwater concentration patterns roughly mimic groundwater elevations. Increased TCE concentrations in groundwater were commonly seen when groundwater elevation was highest; with seasonal variations of about ±50% about the average concentrations. In interpreting these data, it is important to note that that samples are collected from a fixed vertical position, so apparent changes in concentration with time might reflect a non-uniform vertical concentration profile (i.e., a concentration profile that increases in concentration with depth) instead of any real concentration changes with time in the groundwater plume.

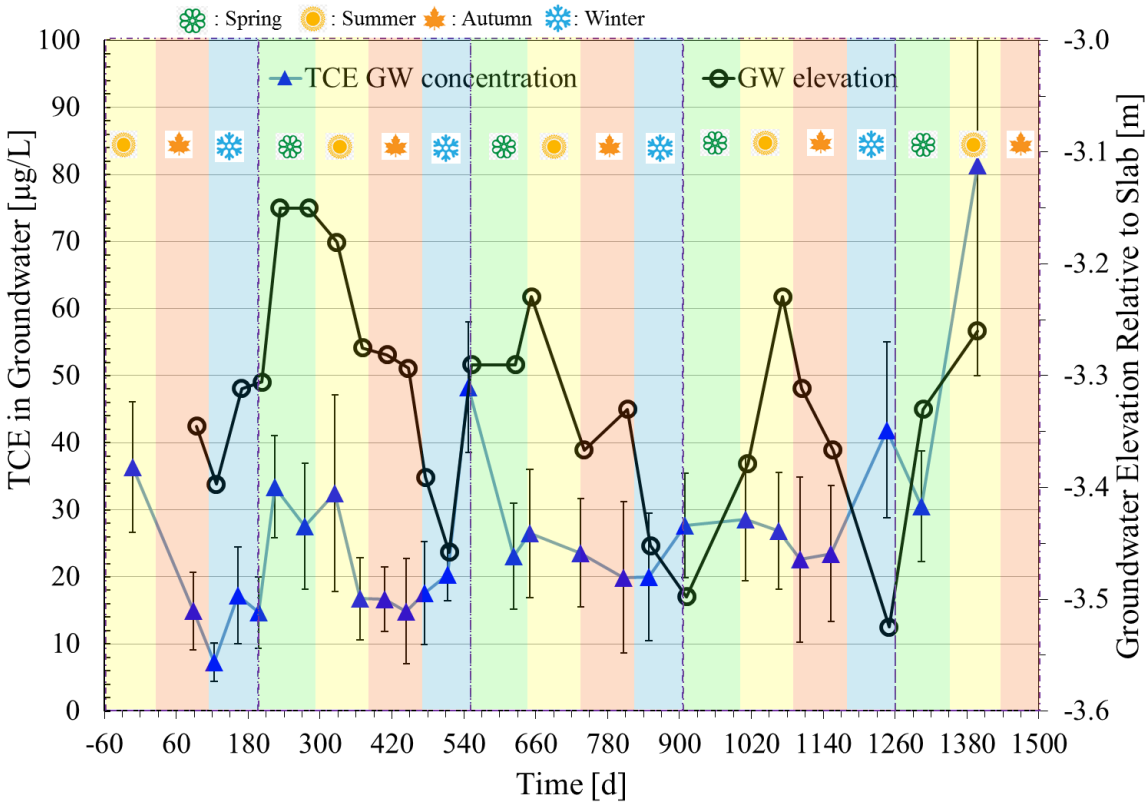

Figure 2.3. Groundwater elevation and spatially-averaged TCE groundwater concentrations. Error bars denote the maximum and minimum values for each event. Shaded color areas in background represent seasons.

Figures 2.4 a-k present TCE soil gas concentrations at 0.9 m BS and 1.8 m BS and water table elevation measurements from groundwater monitoring well GW3. At location A and B, vapor sampling was only possible at 0.9 m BS due to water saturation of the soil matrix at 1.8 m BS in those locations.

It is important to note that all soil gas sampling port elevations are referenced to the house slab and that the ground surface elevation rises from the front yard to back yard. Diffusion dominated transport theory anticipates higher soil gas concentrations for back yard sampling locations vs. front yard sampling points at similar depths.

Unlike groundwater concentrations, a correlation between soil gas TCE concentration and groundwater elevation is not visually evident. TCE concentrations at 1.8 m BS are elevated at some locations after declines in water table elevation, while others are depressed. For example, from t= 203 d to t= 447 d, 1.8 m BS TCE concentrations increased about 3X at location 1 as the groundwater elevation dropped about 0.3 m. At location 2, on the other hand, the concentration at 1.8 m TCE decreased from 281 ppb_v to 88 ppb_v in the same period. The increase in soil gas concentrations expected with a depleting water table (McCarthy and Johnson 1993, Parker 2002, Werner and Hoehener 2002) were observed over some time periods at some locations, but that was not consistent with time at all locations. Increasing temporal and spatial variations in soil gas concentration were also found as the sampling location and depth moved closer to the building foundation and ground surface.

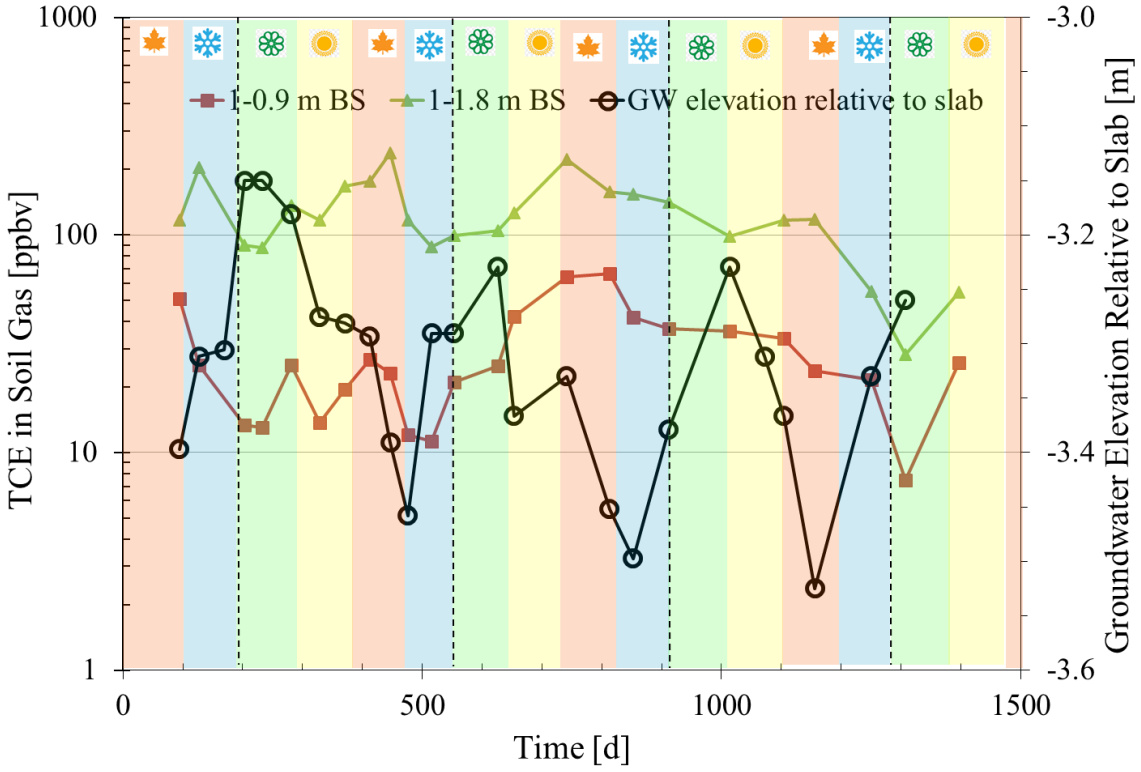

(a) TCE soil gas concentrations at location 1

: Spring : Summer : Autumn : Winter

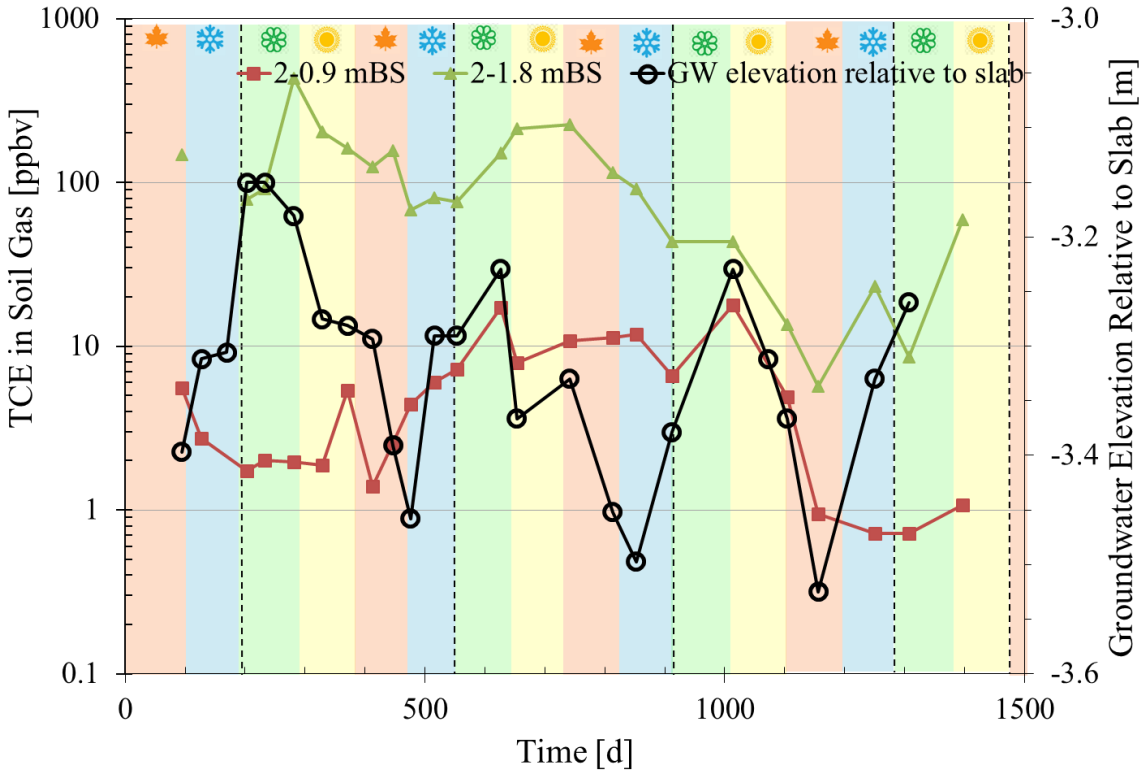

(b) TCE soil gas concentrations at location 2

: Spring : Summer : Autumn : Winter

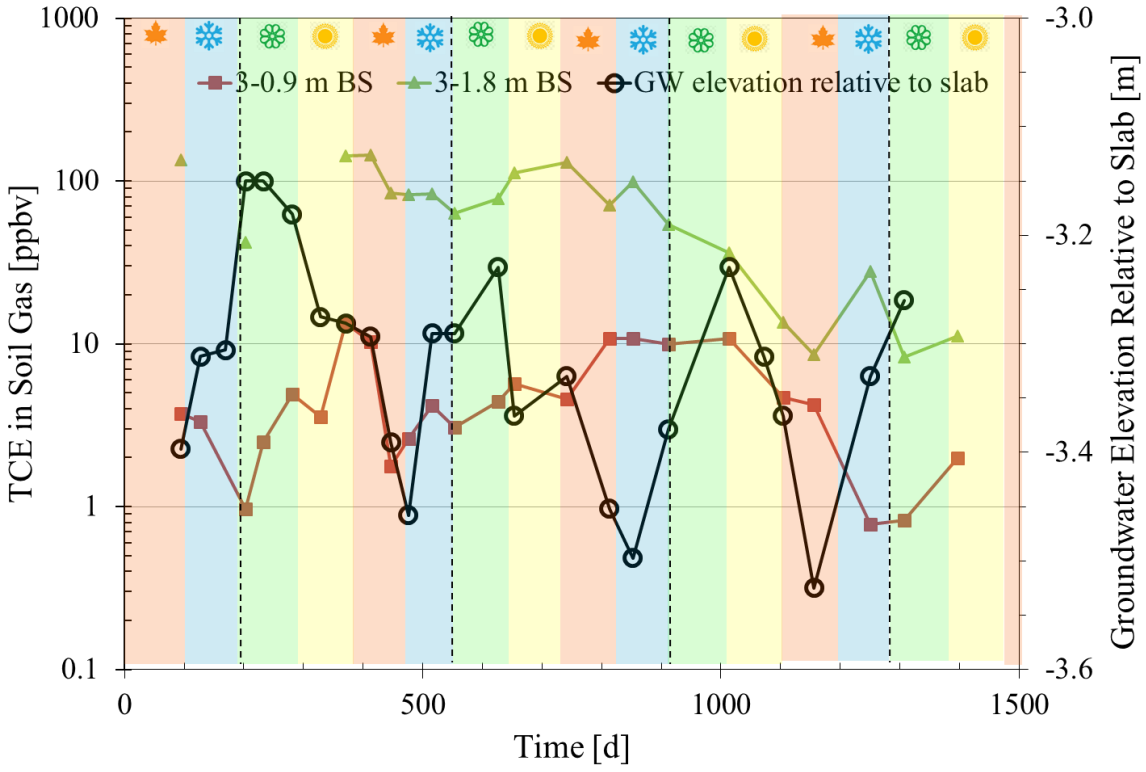

(c) TCE soil gas concentrations at location 3

: Spring : Summer : Autumn : Winter

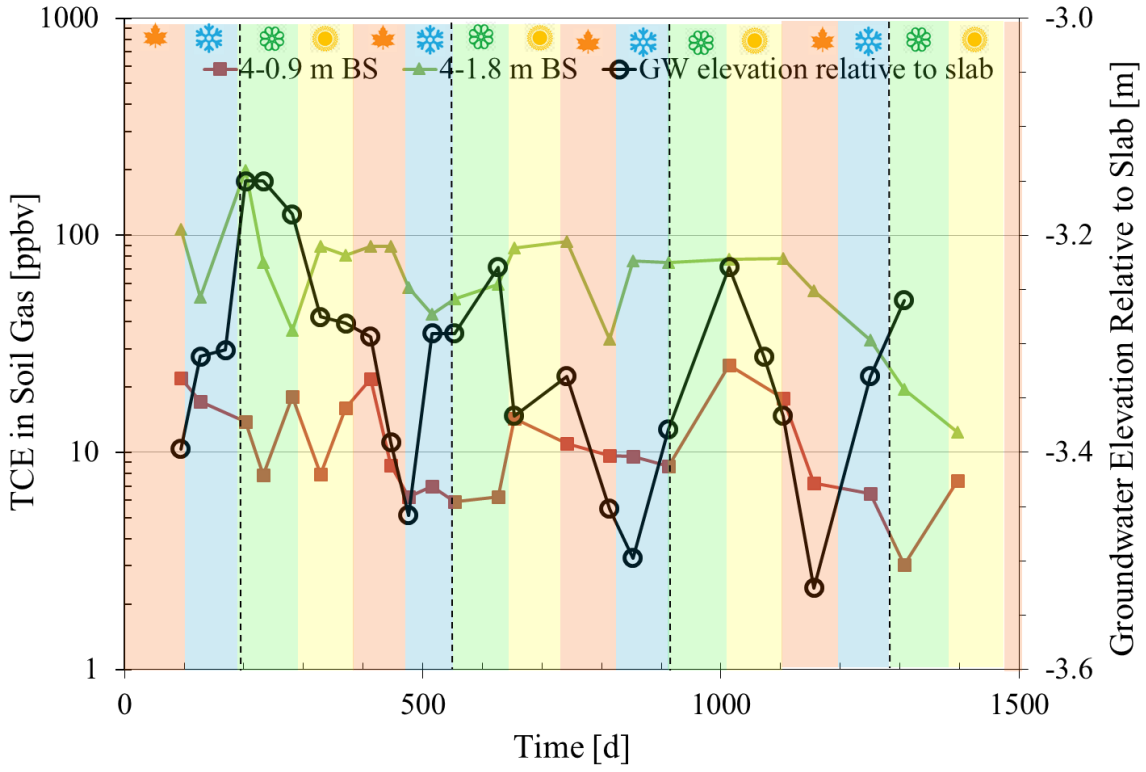

(d) TCE soil gas concentrations at location 4

: Spring : Summer : Autumn : Winter

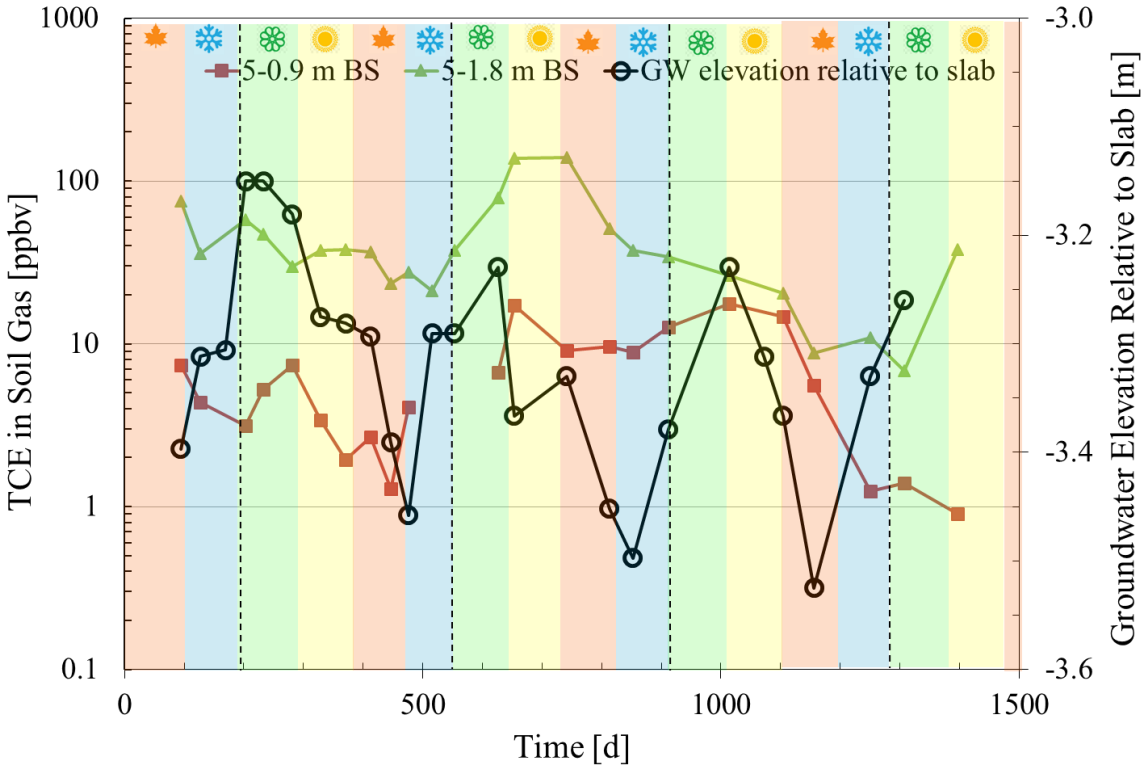

(e) TCE soil gas concentrations at location 5

: Spring : Summer : Autumn : Winter

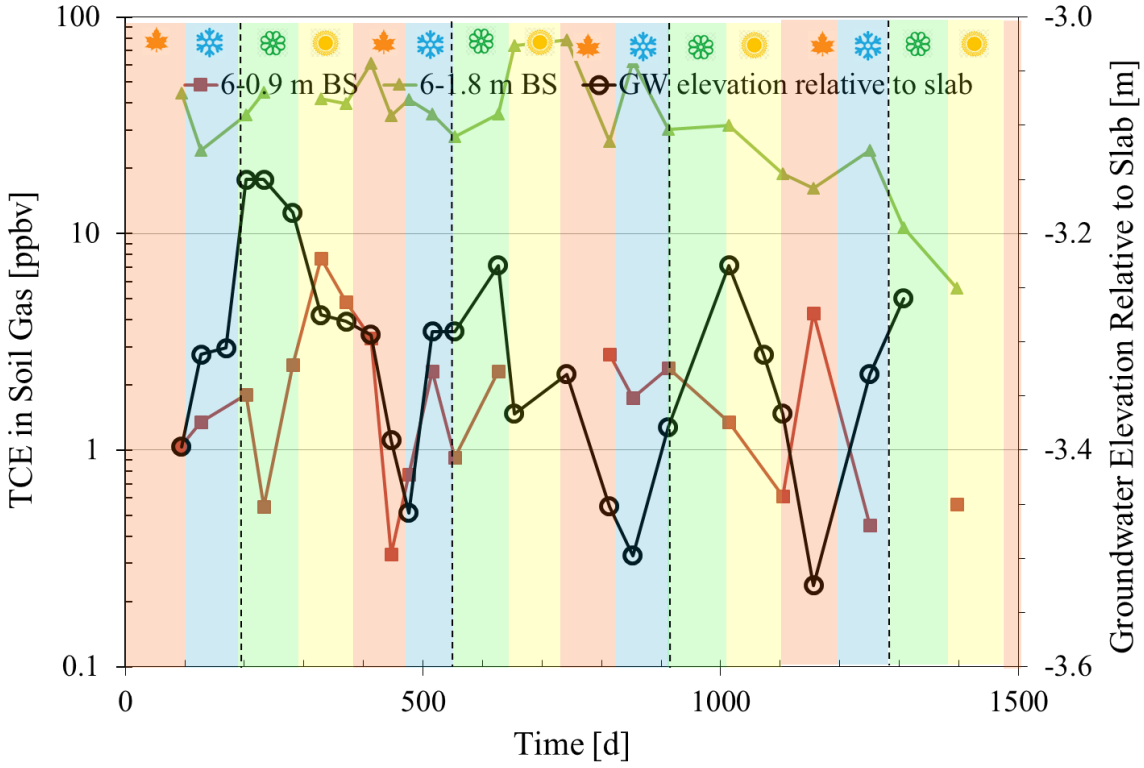

(f) TCE soil gas concentrations at location 6

: Spring : Summer : Autumn : Winter

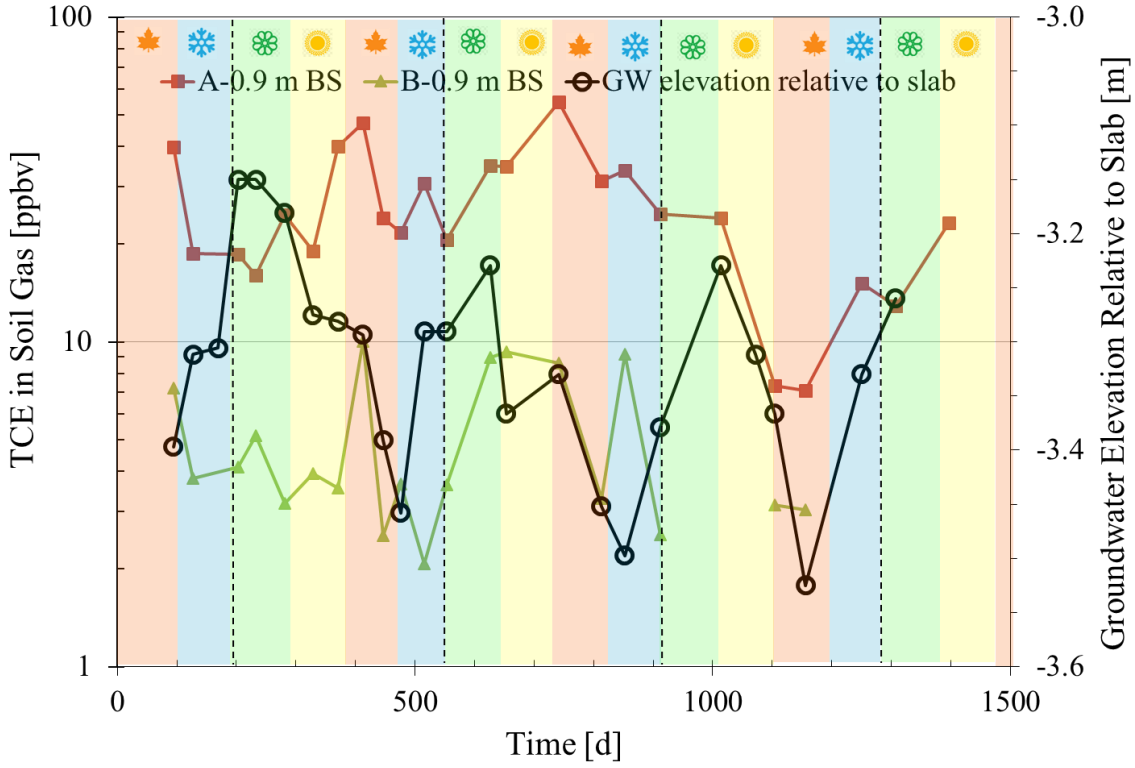

(g) TCE soil gas concentrations at location A and B

: Spring : Summer : Autumn : Winter

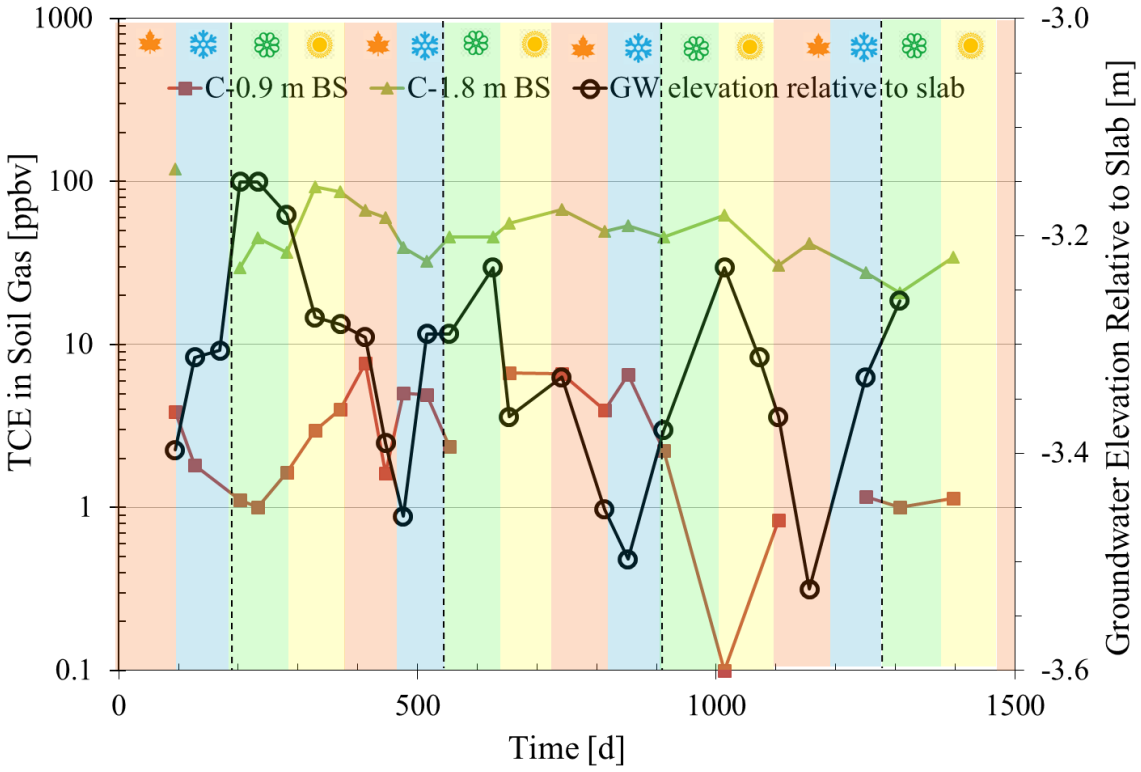

(h) TCE soil gas concentrations at location C

: Spring : Summer : Autumn : Winter

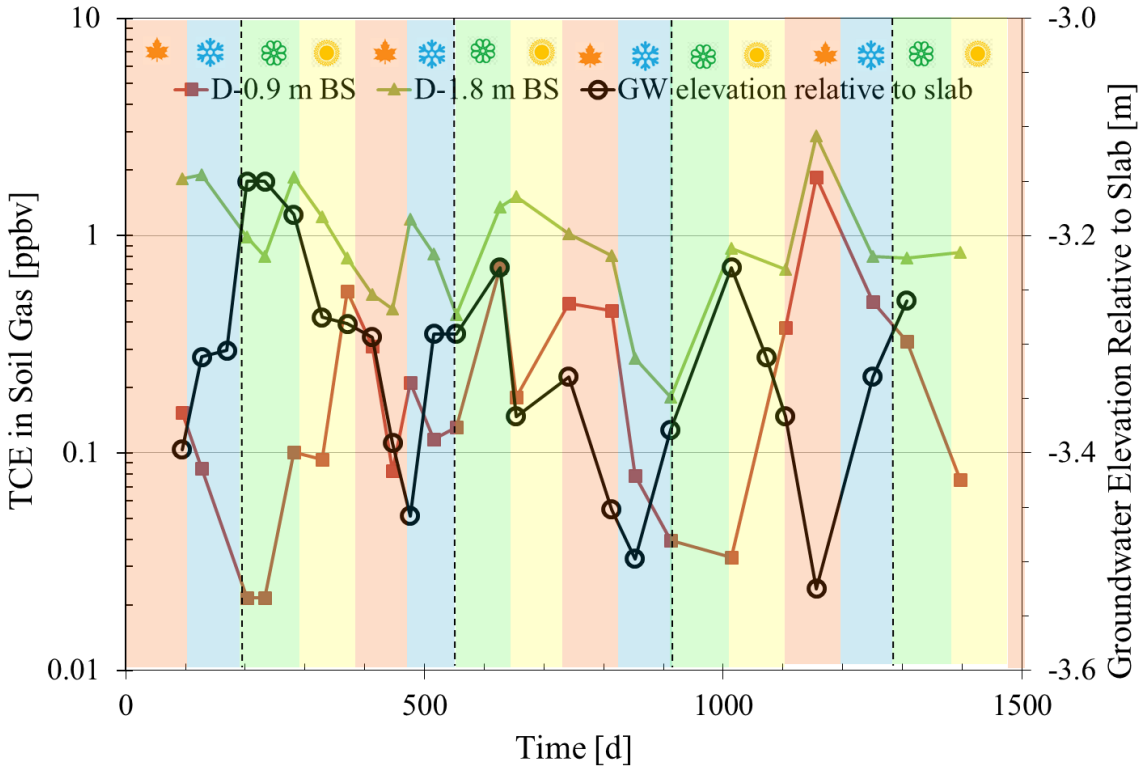

(i) TCE soil gas concentrations at location D

: Spring : Summer : Autumn : Winter

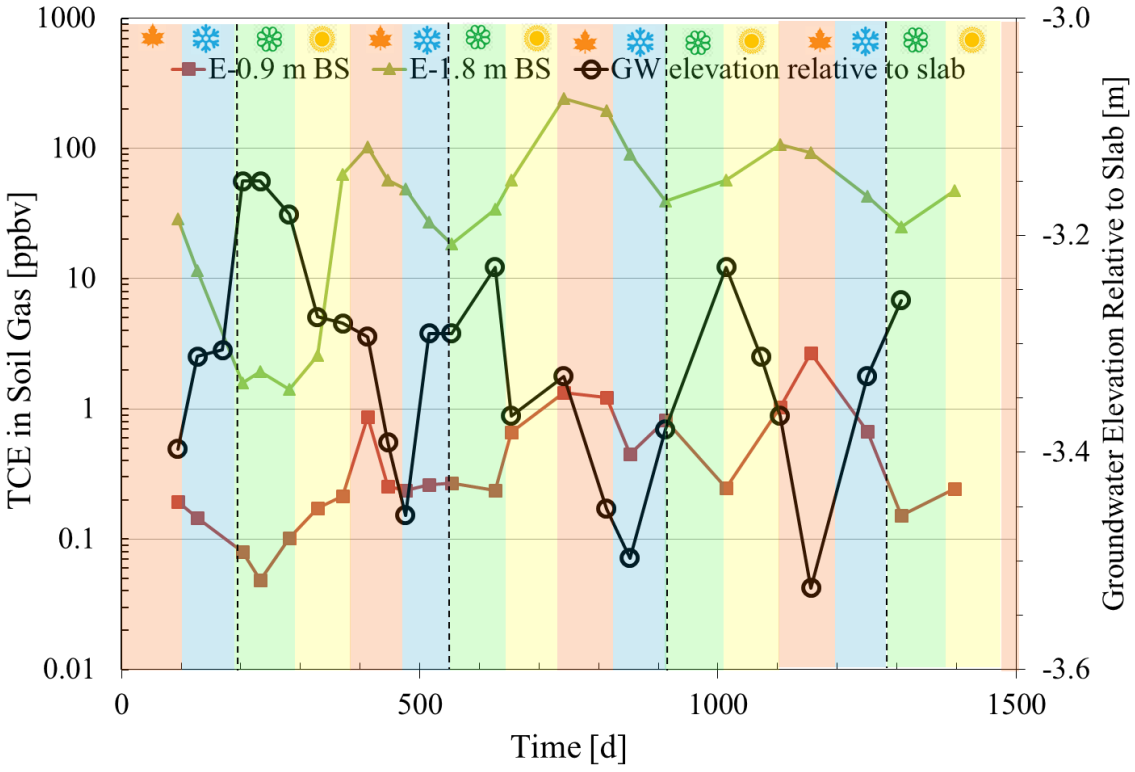

(j) TCE soil gas concentrations at location E

: Spring : Summer : Autumn : Winter

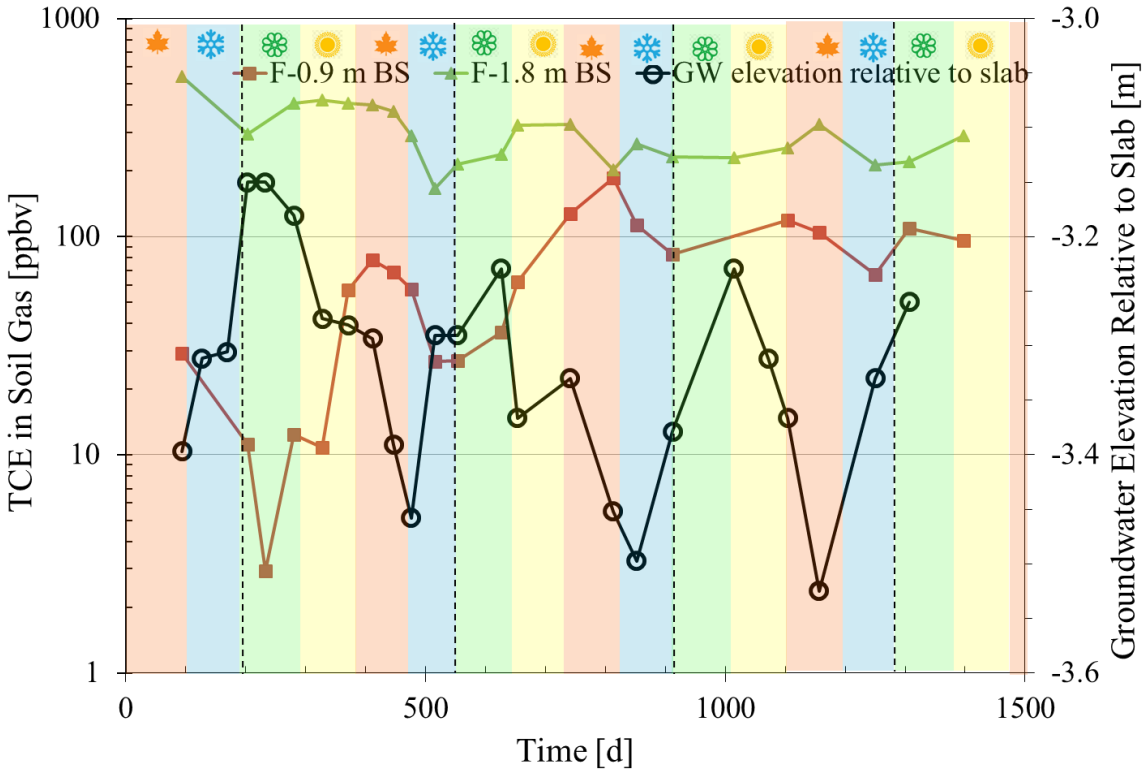

(k) TCE soil gas concentrations at location F

Figure 2.4. TCE soil gas concentrations at 0.9 m BS and 1.8 m BS and groundwater table elevation for interior (locations 1-6) and exterior (locations A-F) locations. Shaded background color areas indicate seasons. Conditions: 0 – 740 d, natural conditions with land drain lateral connected; 780 - 1045 d, CPM conditions with land drain lateral connected; 1071 - 1157 d, CPM conditions with land drain lateral disconnected.

TCE emission rates vs. groundwater elevation. Figures 2.5 a-j present TCE emission rates per unit area calculated using the results from synoptic soil gas and groundwater table elevation sampling (method F_1), with error bars spanning the uncertainty for each calculation. Average F_1 values and the standard deviation of the average within the building footprint are shown in Figure 2.6. A statistical summary of F_1

values and uncertainties is presented in Table 2.1. The following can be concluded from a review of these figures and table:

- The temporal variation in F_1 values spans from about one to two orders-of-magnitude across all locations. For example the temporal variability is about an order of magnitude at location 1 and about two orders-of-magnitude at location 2. In reviewing the results, it is important to note that there are three different sets of operational conditions represented across the time frame presented: 0 – 740 d involved natural conditions with the land drain lateral connected; 780 - 1045 d involved CPM conditions with the land drain lateral connected; 1071 - 1157 d involved CPM conditions with land drain lateral disconnected; and after 1157 d involved natural conditions with the land drain lateral valve closed.
- The uncertainty in each F1 value is about 40% and the standard deviation of all F1 values at each location ranges from 34% - 131% of the average F1 value at that location.
- The effect of closing the land drain lateral valve is evident in F1 values vs. time for interior locations and is not evident in F1 values vs. time for exterior locations.
- Figure 2.6 presents average interior F_1 values and their standard deviations. If this plot is divided into regions with and without the land drain lateral connection, it can be seen that any temporal variations, if they exist, are smaller than the standard deviation of the averages. Thus, at this site, changes

in emission rates are at most about 50% of the time-averaged value for groundwater table elevation changes of about 0.3 m.

Figure 2.7 presents the spatial distribution of F_1 values, 1.8 m BS TCE soil gas concentrations, and TCE shallow groundwater concentrations collected under natural conditions with the land drain lateral connected for the sampling conducted 368 d < t < 370 d. With the exception of one location, all F_1 emission values are within an order of magnitude and beneath the house they are within about 50% of the average value. The spatial distribution of F_1 values is similar to that of the 0.9 m BS and 1.8 m BS soil gas concentrations. While not highly spatially variable, the spatial trend in F_1 values is different than what would be expected from a relatively uniform groundwater concentration distribution and the sloped ground surface at this site; diffusion-dominated transport theory anticipates increasing emission rates with shorter distances to ground surface and the opposite is observed in this data set.

Table 2.1

Characteristics of TCE F_1 calculations under natural conditions (0<t<740 d).

	F_1 under natural pressure condition [µg/d-m^2]									
Location	1	2	3	4	5	6	C	D	E	F
Maximum	60.2	228.7	75.0	53.5	70.7	55.1	14.4	0.4	43.7	103.2
Minimum	5.8	2.5	2.4	1.4	1.8	3.6	2.5	0.03	0.2	3.5
Average	31.9	81.0	52.9	19.7	27.0	29.8	6.9	0.2	8.4	58.9
% Standard Deviation	40.3	62.4	33.9	55.6	69.1	39.1	46.1	61.1	131.9	36.1
	Uncertainty of F_1 calculation [µg/d/m^2]									
Maximum	17.1	32.4	32.1	14.7	29.2	14.1	3.8	0.2	11.2	27.9
Minimum	2.1	3.8	1.2	1.1	1.0	1.01	0.7	0.01	0.1	8.6
Average	10.0	18.7	14.2	6.0	7.6	8.0	1.9	0.06	2.2	17.7

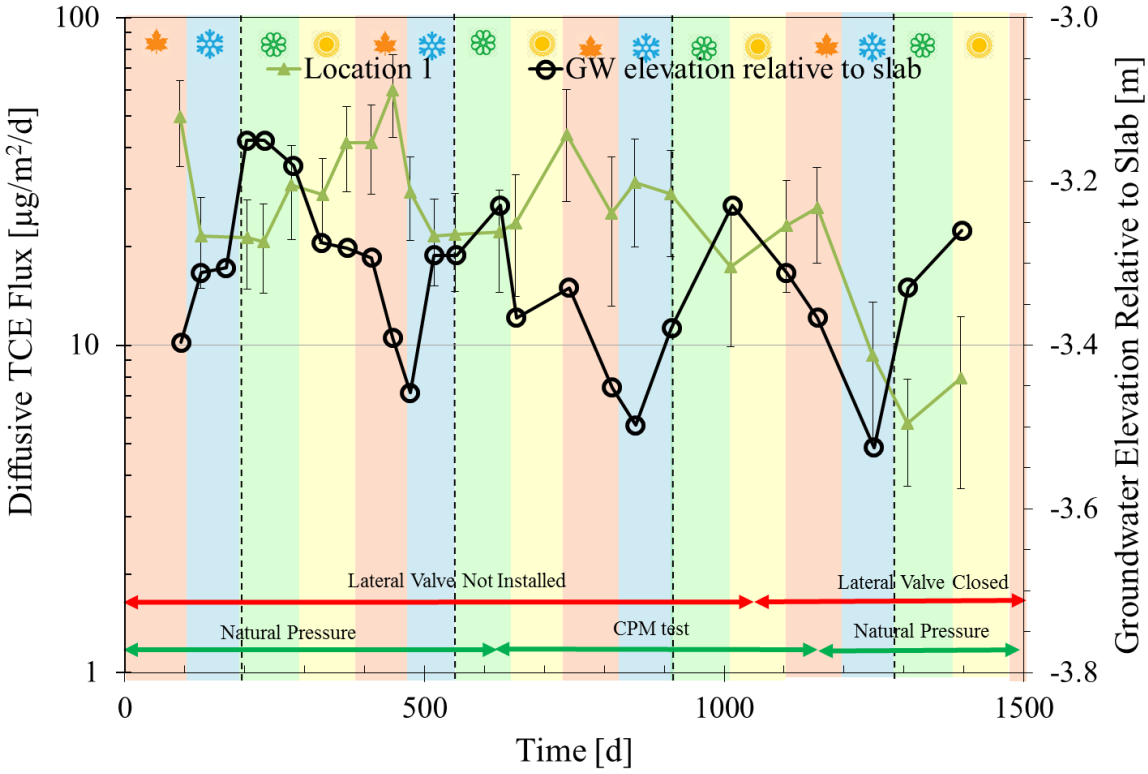

(a) TCE emissions per unit area at location1

: Spring : Summer : Autumn : Winter

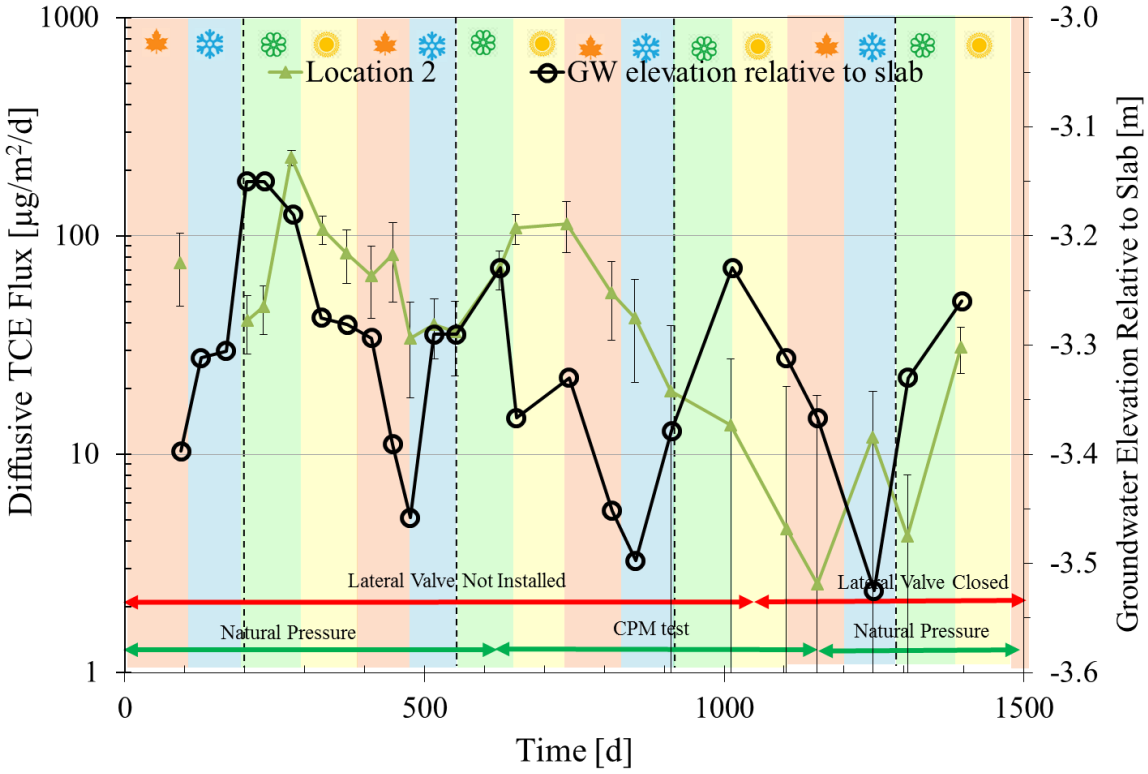

(b) TCE emissions per unit area at location 2

: Spring : Summer : Autumn : Winter

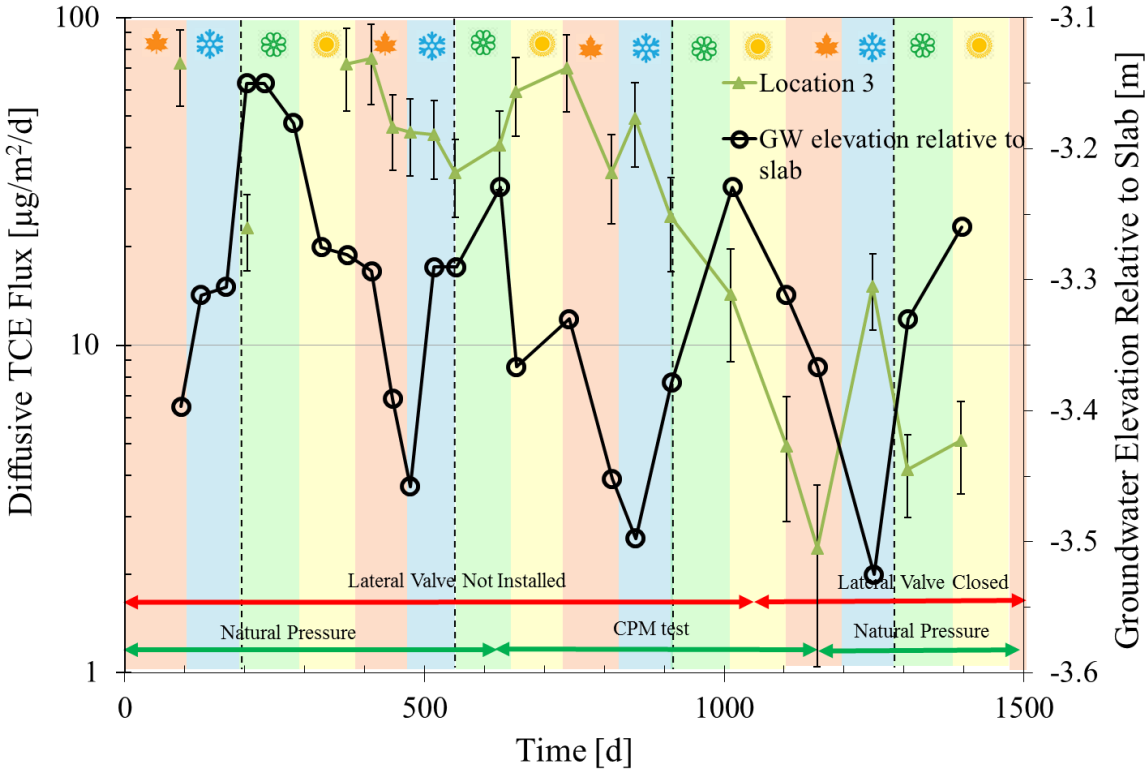

(c) TCE emissions per unit area at location 3

: Spring : Summer : Autumn : Winter

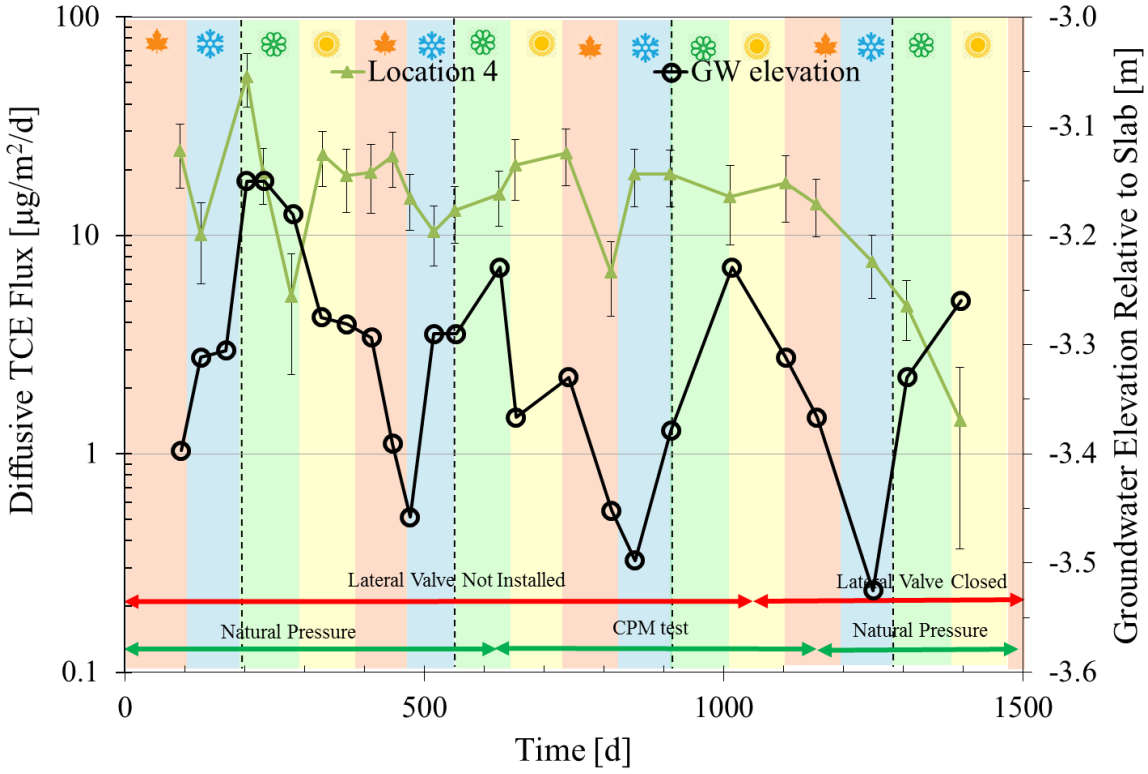

(d) TCE emissions per unit area at location 4

: Spring : Summer : Autumn : Winter

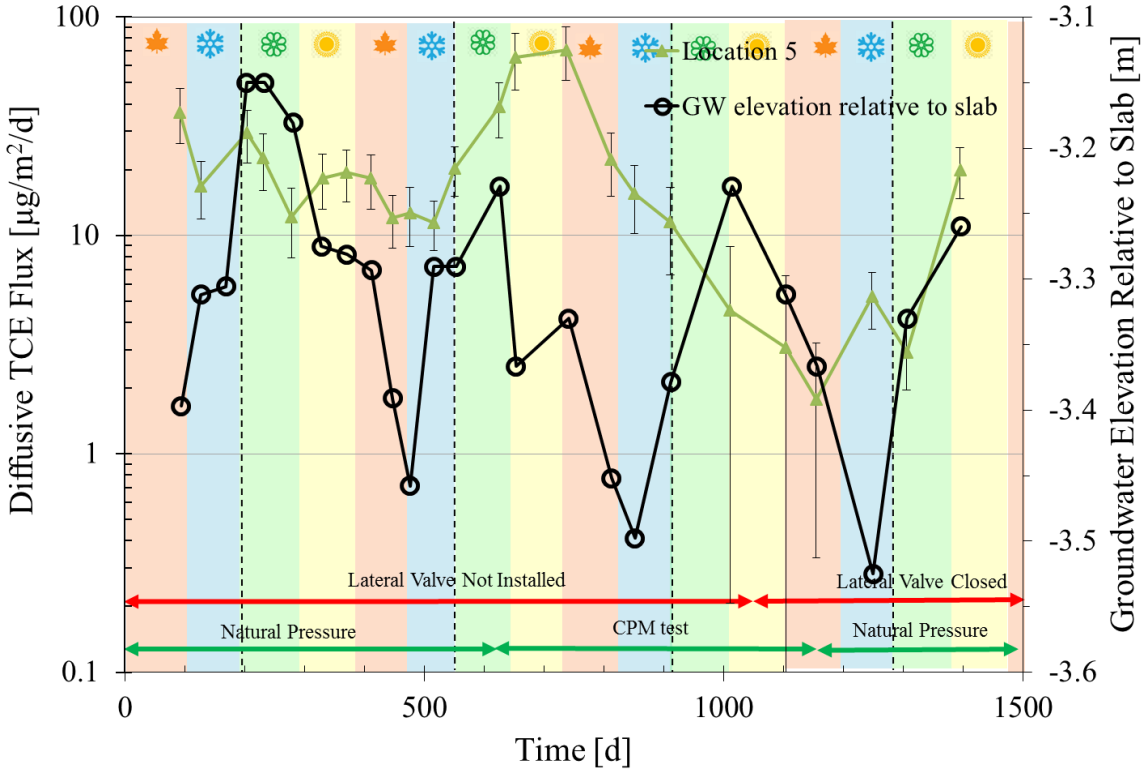

(e) TCE emissions per unit area at location 5

: Spring : Summer : Autumn : Winter

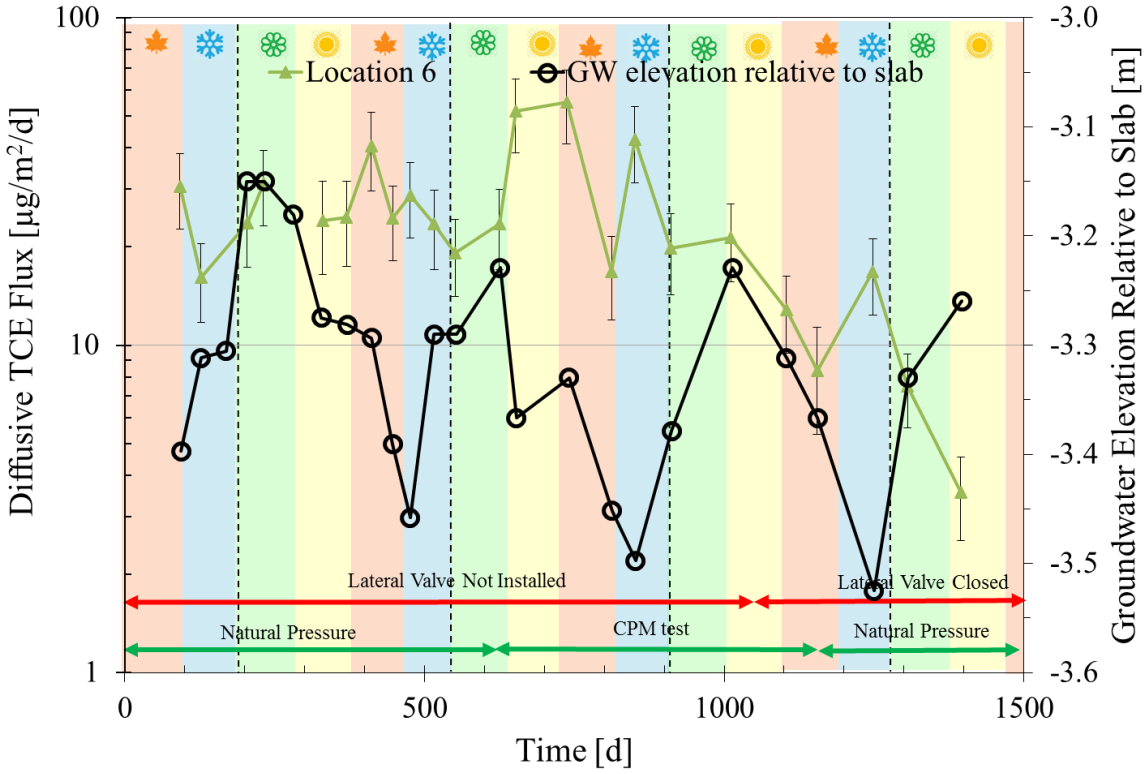

(f) TCE emissions per unit area at location 6

: Spring : Summer : Autumn : Winter

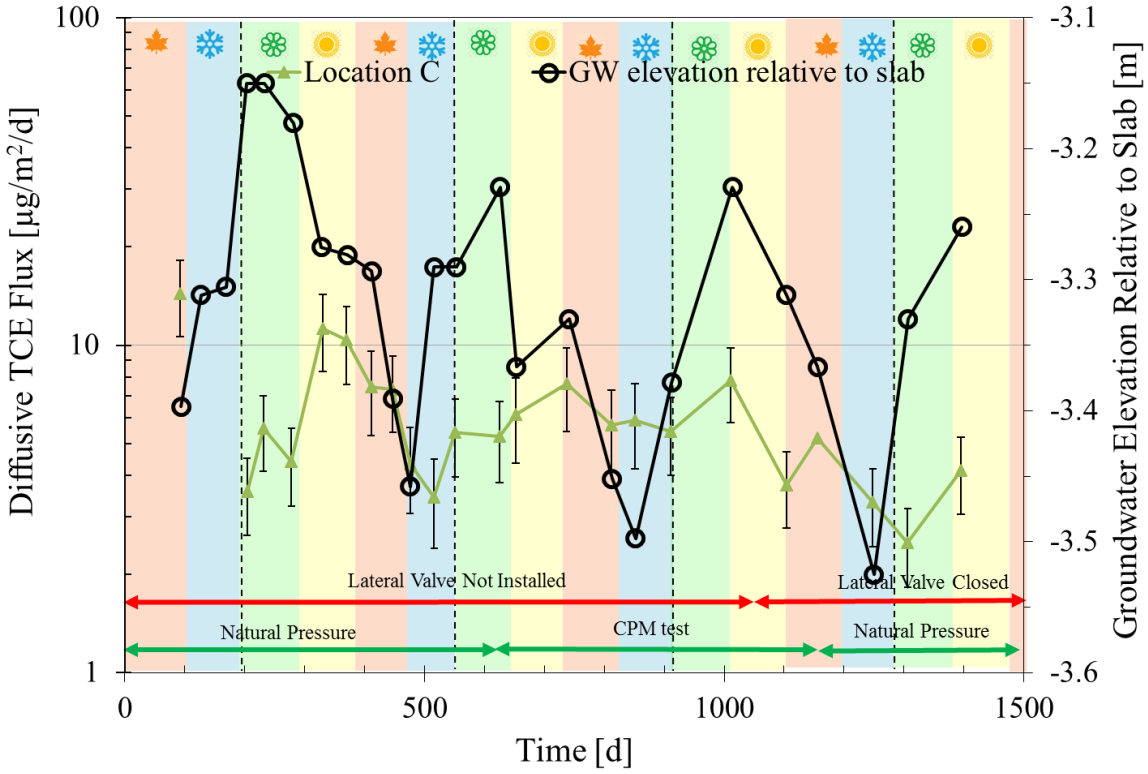

(g) TCE emissions per unit area at location C

: Spring : Summer : Autumn : Winter

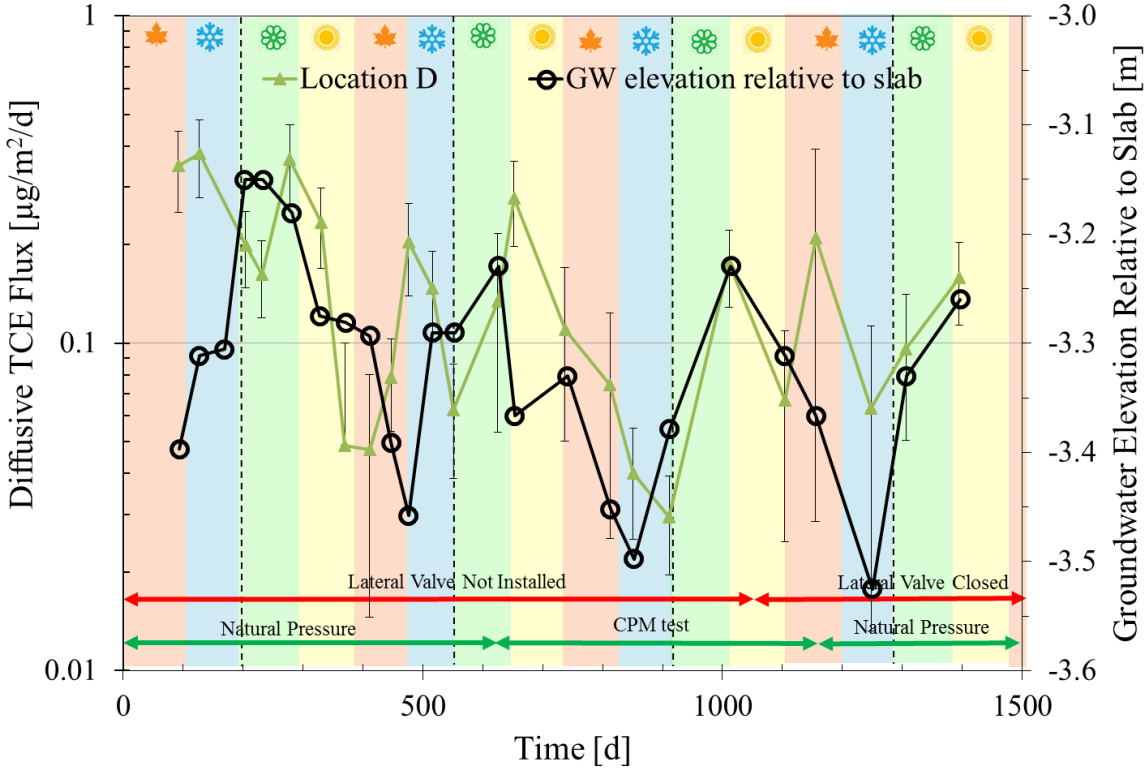

(h) TCE emissions per unit area at location D

: Spring : Summer : Autumn : Winter

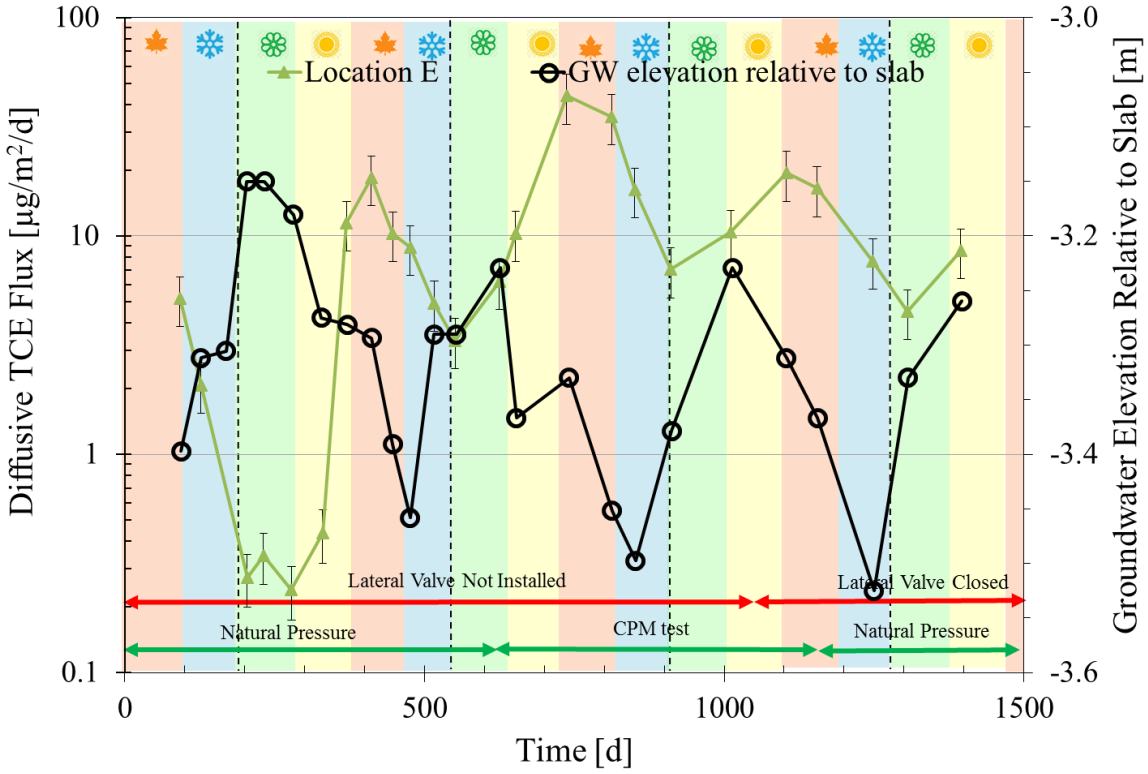

(i) TCE emissions per unit area at location E

: Spring : Summer : Autumn : Winter

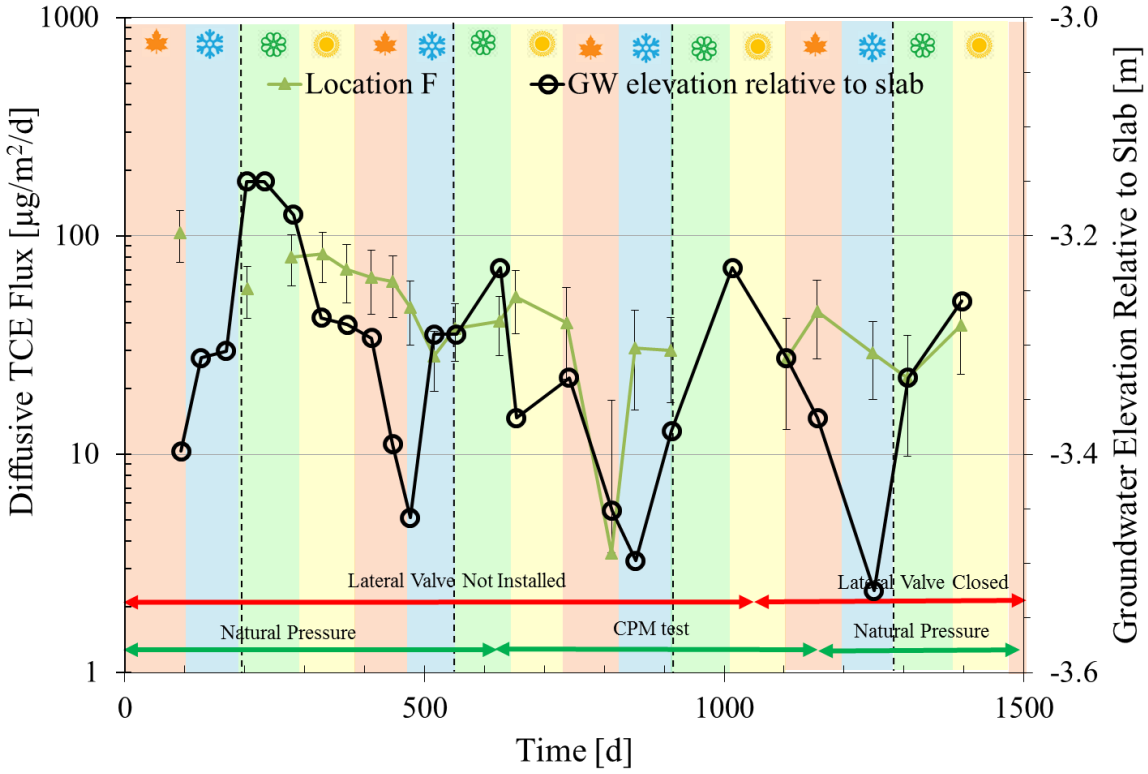

(j) TCE emissions per unit area at location F

: Spring : Summer : Autumn : Winter

Figure 2.5. Calculated diffusive TCE flux F_1 values (emissions per unit area) using synoptic soil gas survey data. Error bars span the uncertainty in each F_1 value calculation associated with uncertainty in concentration measurements.

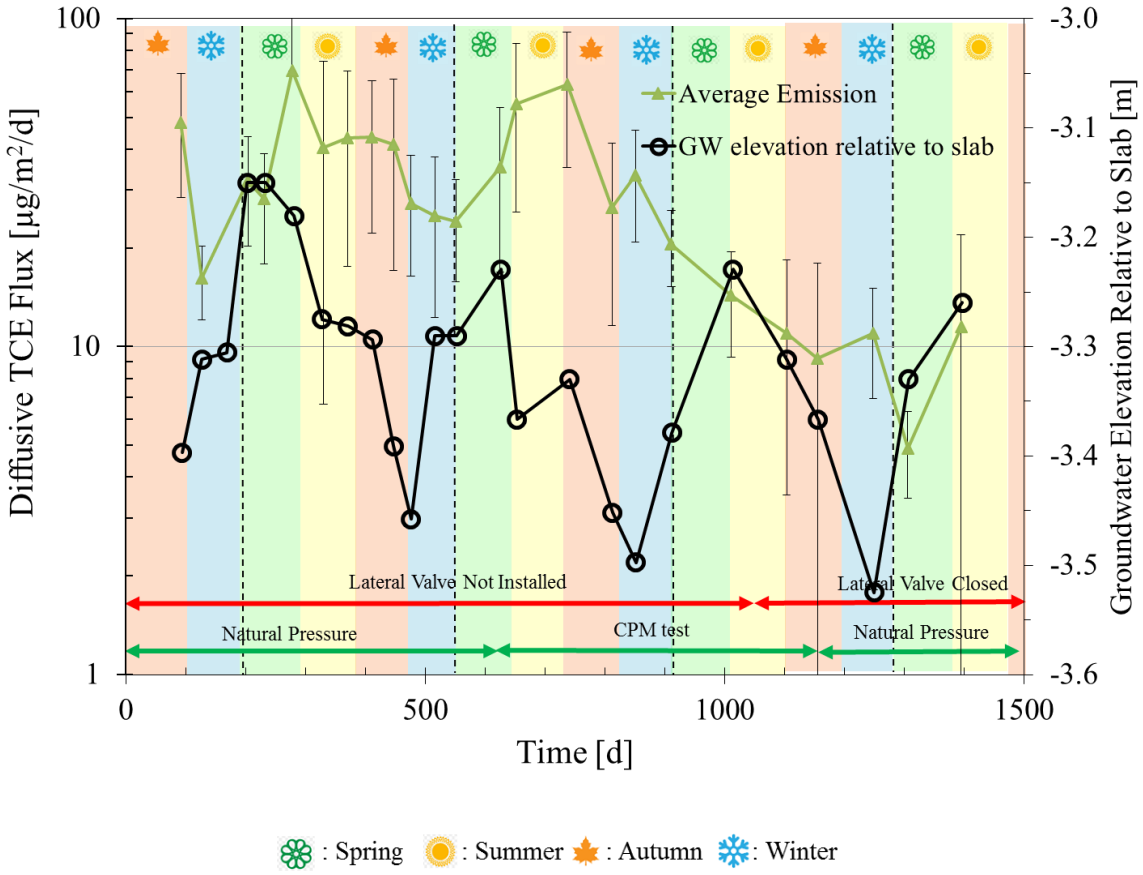

Figure 2.6. Averages of diffusive TCE flux F_1 values (emissions per unit area) for monitoring locations within the building footprint. Error bars span the standard deviation of each average value.

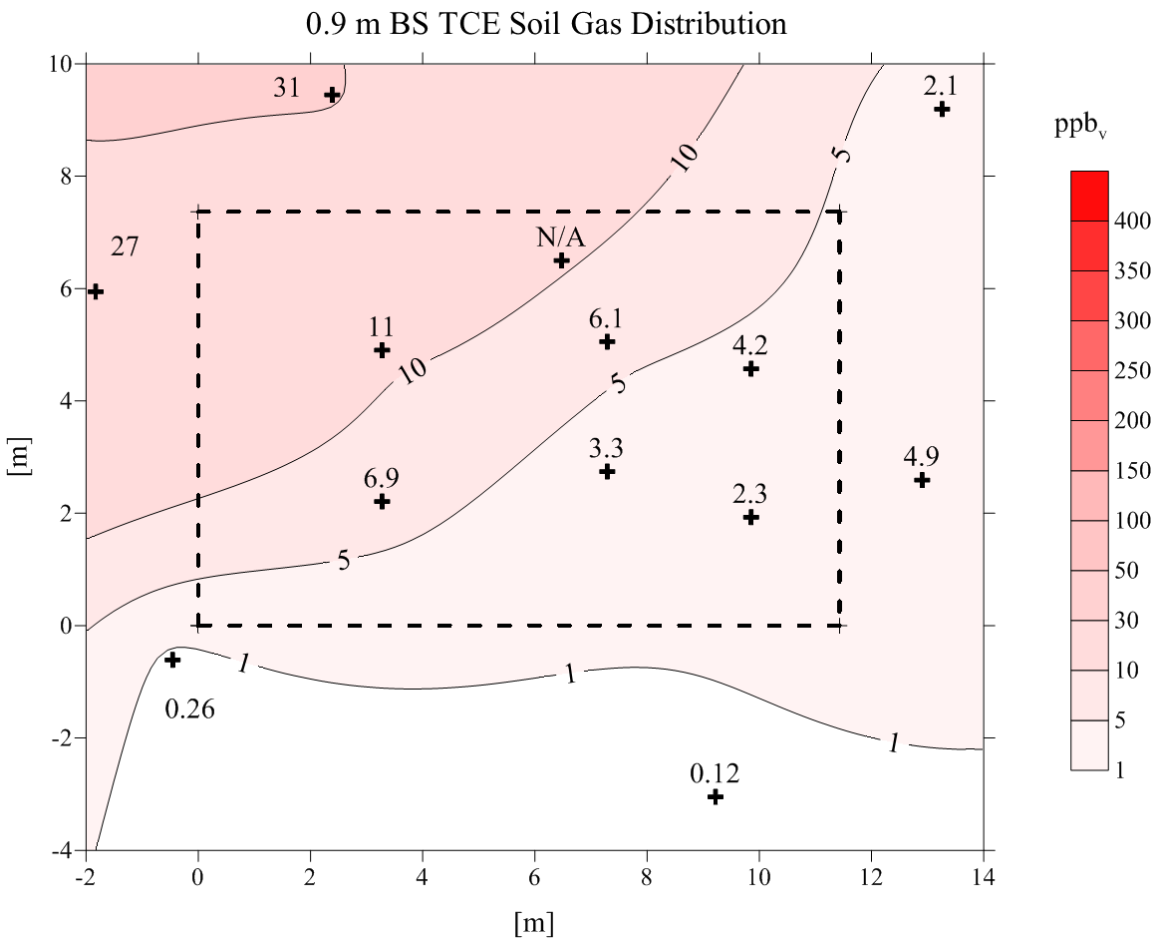
0.9 m BS TCE Soil Gas Distribution
31
2.1
27
N/A
11
6.1
4.2
6.9
3.3
4.9
2.3
0.26
0.12
10
5
1
[m]
[m]
ppb$_v$
400
350
300
250
200
150
100
50
30
10
5
1

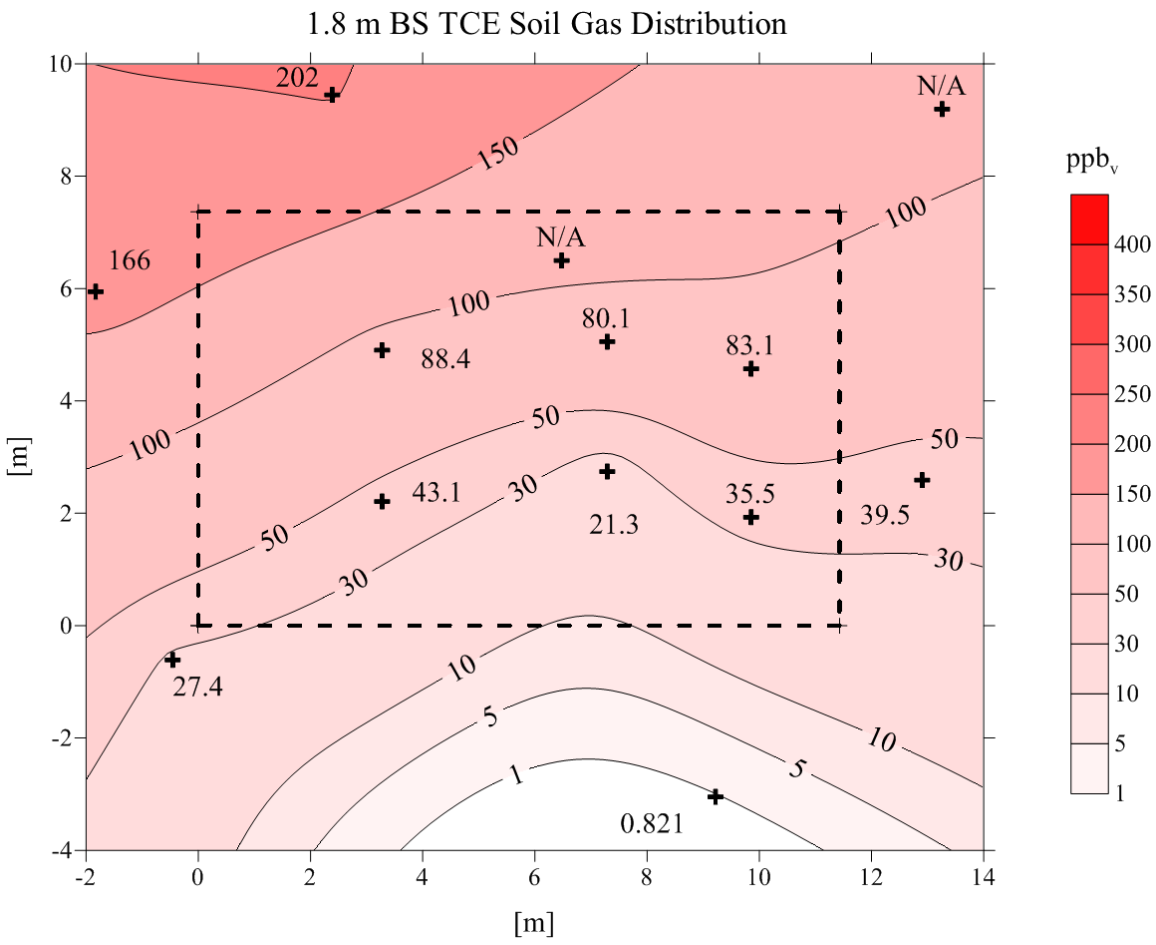
1.8 m BS TCE Soil Gas Distribution
202
N/A
166
N/A
80.1
88.4
83.1
43.1
21.3
35.5
39.5
27.4
0.821
150
100
100
100
50
50
50
30
30
30
10
10
5
5
1
[m]
[m]
ppbv
400
350
300
250
200
150
100
50
30
10
5
1

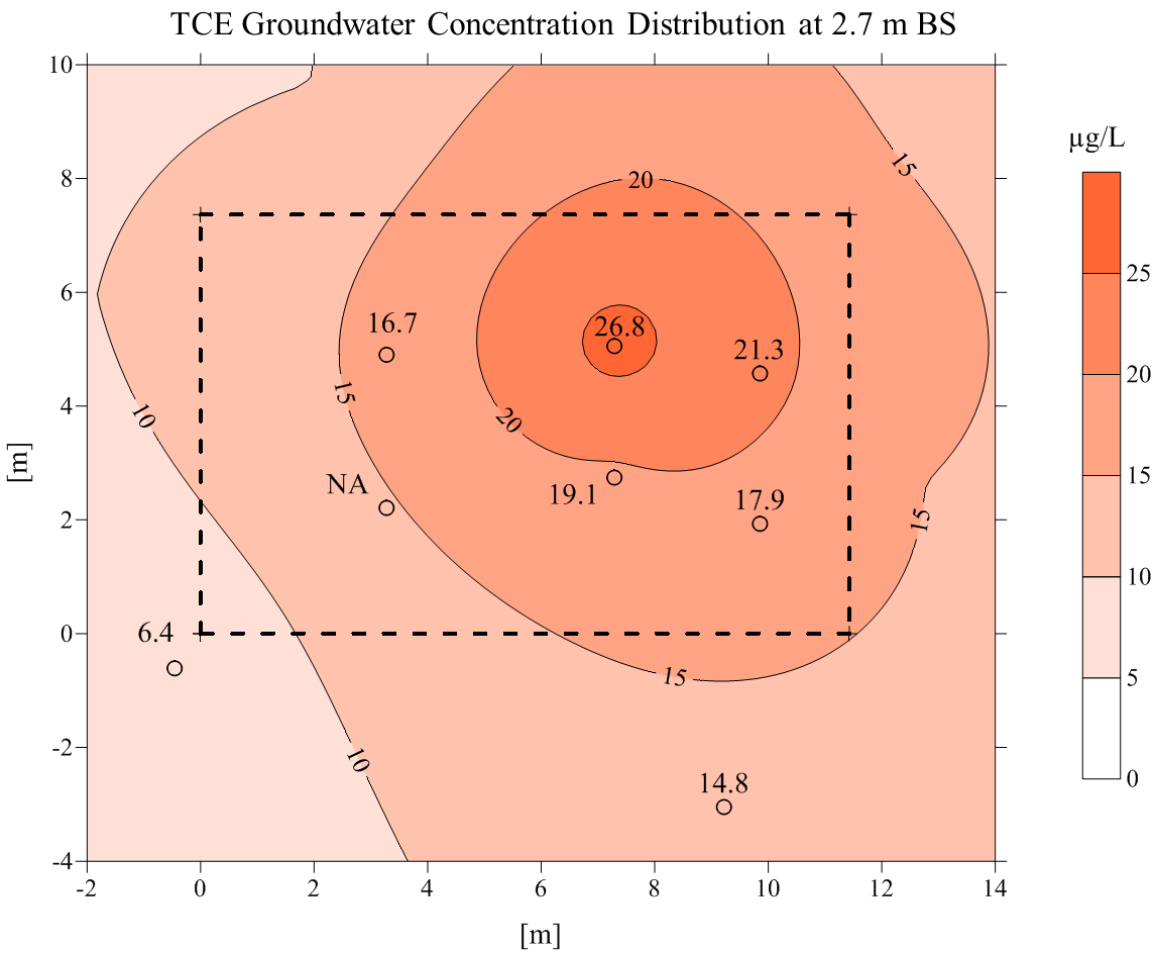
TCE Groundwater Concentration Distribution at 2.7 m BS
µg/L
25
20
15
10
5
0
[m]
[m]
10
8
6
4
2
0
-2
-4
-2
0
2
4
6
8
10
12
14
20
15
10
16.7
26.8
21.3
NA
19.1
17.9
6.4
14.8

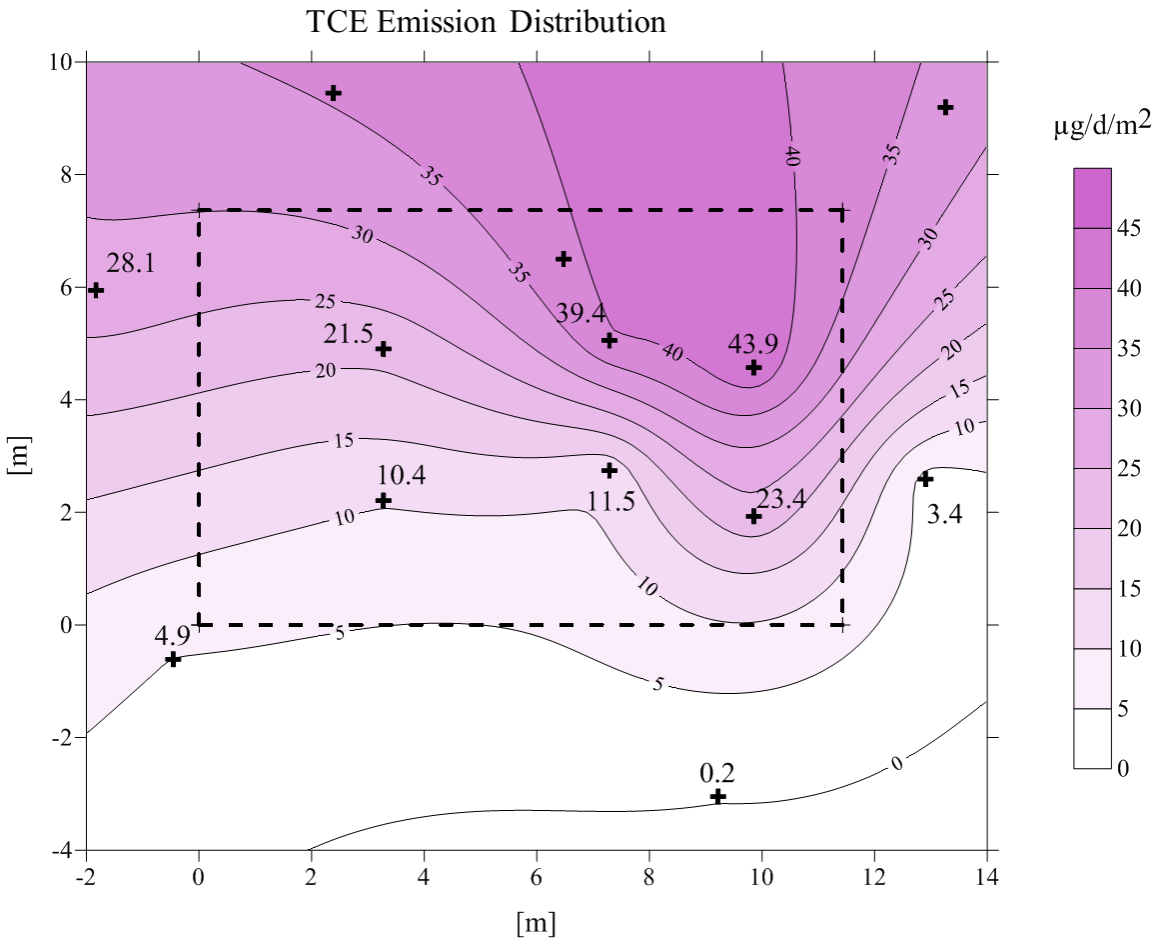

Figure 2.7. Representative 0.9 m BS, 1.8 m BS TCE soil gas concentrations, 2.7 m BS TCE groundwater concentrations and F_1 emission rates for the t = 514 d to t = 519 d sampling event.

Figure 2.8 presents TCE emissions calculated for CPM test conditions using method F_2 vs. time and groundwater table elevation. The data were collected during 1071 d < t < 1157 d when the lateral drain valve was closed and the real-time groundwater table elevation data were collected every 2 h. Short-term groundwater table elevation changes ranged from about 5 cm per day to 22 cm bi-weekly, with the longer term trends following the seasonal pattern observed in the synoptic measurements.

F_2 values varied ±50% about the mean emission rate of 6.0 µg/m^2-d. The standard deviation was ±1.3 µg/m^2-d and the maximum and minimum emission rates were 8.7 and 2.1 µg/m^2-d, respectively. The F_2 results agree well with the average F_1 values within the building footprint during the same period of time (e.g. 9.2 µg/m^2-d at t = 1155 d).

In summary, both F_1 and F_2 calculation methods produced emission rates that varied by at most approximately 50% about the average emissions for groundwater table elevations that changed by about 5 cm daily and 30 cm seasonally and for consistent operating conditions. This variability about the average is similar to the 36% uncertainty in each F_1 calculation. There was a noticeable decline in F_1 values for interior sampling points when the lateral land drain valve was closed, suggesting some influence of that feature. Results for the two calculation methods were similar during the time period when both methods overlapped; the F_2 results were comparable to spatially integrated F_1 results beneath the building footprint. Temporal changes in F_2 emissions were much smaller than the 2-3 orders of magnitude changes in indoor air concentrations under natural conditions at this site (Holton, et al., 2012). Thus, it is not likely that groundwater table elevation changes were major contributors to indoor air concentration variability at this site.

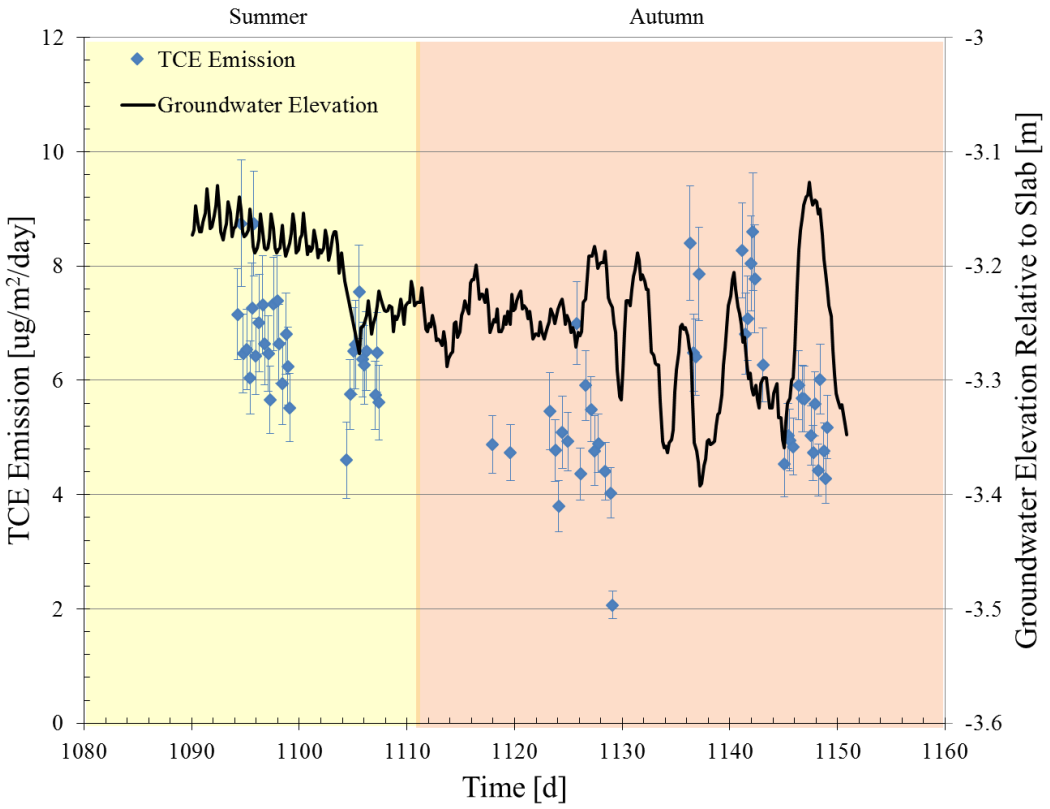

Figure 2.8. Real-time TCE emission rate per unit area (F_2) vs. groundwater table elevation during CPM test conditions when the lateral drain valve was closed. Error bars span the uncertainty in each F_2 value calculation.

2.3 STUDY OF VOC EMISSIONS WITH A FLUCTUATING WATER TABLE USING A TWO-DIMENSIONAL LABORATORY-SCALE PHYSICAL MODEL

Lab-scale, two-dimensional physical model experiments were performed to complement the field study results presented above. The experiments were designed to evaluate the significance of soil and chemical properties, and water table fluctuation rates on VOC emissions.

2.3.1 Experimental methods. *Physical model design*. The physical models used in this study were two 182-cm tall by 61-cm wide by 10-cm deep stainless steel frame

tanks with acrylic glass faces. The acrylic glass faces allow for visual observation and provide a readily configurable/reconfigurable face for sample port installation. Thirty-six (36) Swagelok® brass 1/8 in × 1/8 in NPT fittings were fitted with Thermolite® Shimadzu Plug septa and installed in the acrylic glass face of each tank. These fittings allowed for soil gas or groundwater sampling using a needle and syringe.

Five Decagon ECH$_2$O EC-5 soil moisture sensors (Decagon Devices, WA) were installed in the back window of each tank for real-time, volumetric soil moisture content measurement using an EM50 Digital/Analog data logger (Decagon Devices, WA) on 15-30 min intervals. The headspace for both sealed tanks was outfitted for sweep gas flushing and monitoring. A breathing grade air sweep gas flow of 120-150 mL/min was controlled and monitored real-time using a solenoid valve, an SRI gas sampling valve, mass flow controller, vacuum pump, and SRI GC with DELCD.

Two soils were used. One utilized Quikrete® Play Sand sieved to 50+ mesh size, whereas the other utilized a commercial 10-20 mesh washed silica sand. The hydraulic conductivity (K_w) and soil organic fraction (f_{oc}) for the play sand were 0.083 cm/s and 0.0019 g-OC/g-soil, respectively. For the silica sand, K_w and f_{oc} were 0.186 cm/s and 0.0009 g-OC/g-soil, respectively. When saturated, the play sand tank appeared to have a greater capillary fringe height (20 - 30 cm) than the silica sand tank (<5 cm).

Water levels in each tank were controlled by constant head overflow devices on the effluent, the elevations of which were controlled using STP-MTR-23079 stepper motors and STP-DRV-6575 stepper drives (Automation Direct, GA) equipped with pre-programmed D0-05DD PLCs (Koyo, China).

All experiments used three chlorinated hydrocarbons (CHCs) dissolved in water: TCE, 1,2-dichloroethane (1,2-DCA), and tetrachloroethene (PCE). In one set of experiments, they were introduced to the tanks via a constant lateral flow of water as shown in Figure 2.7a. This tank configuration was used when constant and vertically uniform water concentrations were desired. In another set of experiments, the water level in the tank was controlled by recharge/discharge from the bottom of the tank as shown in Figure 2.7b and new dissolved mass was not added to the system with time. This allowed a vertical concentration profile to develop over time similar to what might occur in a dissolved groundwater plume as it migrates down-gradient from a source.

CHC concentrations in the feed water were maintained using a syringe injection pump to constantly feed a high concentration dissolved solution into a mixing chamber with a constant flow of reverse osmosis (RO) water. Flow rates for both tanks were maintained at approximately 7.7 L/day.

The properties of chemicals used in these experiments are summarized below in Table 2.2.

Table 2.2

Chemical properties for TCE, PCE, and 1,2-DCA

	Unit	TCE	PCE	1,2- DCA
Dimensionless Henry's Law Constant (25 ℃)	-	0.42	0.75	0.04
Organic carbon water partition coefficient K_{ow}	cm^3-H_2O/g-OC	166	155	17.4
Diffusion Coefficient in Water (25 ℃)	cm^2/s	9.1×10^{-6}	8.2×10^{-6}	9.9×10^{-6}
Diffusion Coefficient in Air (25 ℃)	cm^2/s	7.9×10^{-2}	7.2×10^{-2}	1.0×10^{-1}
Solubility (25 ℃)	mg/L-H_2O	1.1×10^3	2.0×10^2	8.5×10^3

*: values from USEPA (2000)

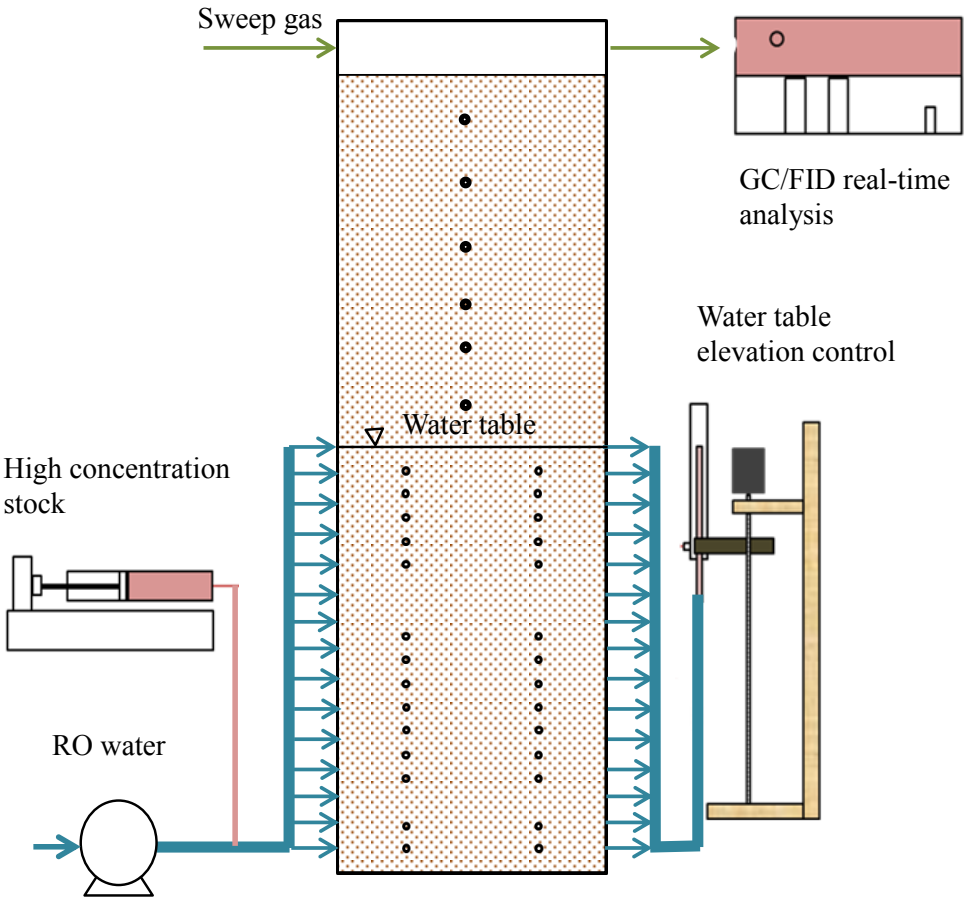
Sweep gas
GC/FID real-time analysis
Water table elevation control
Water table
High concentration stock
RO water

(a)

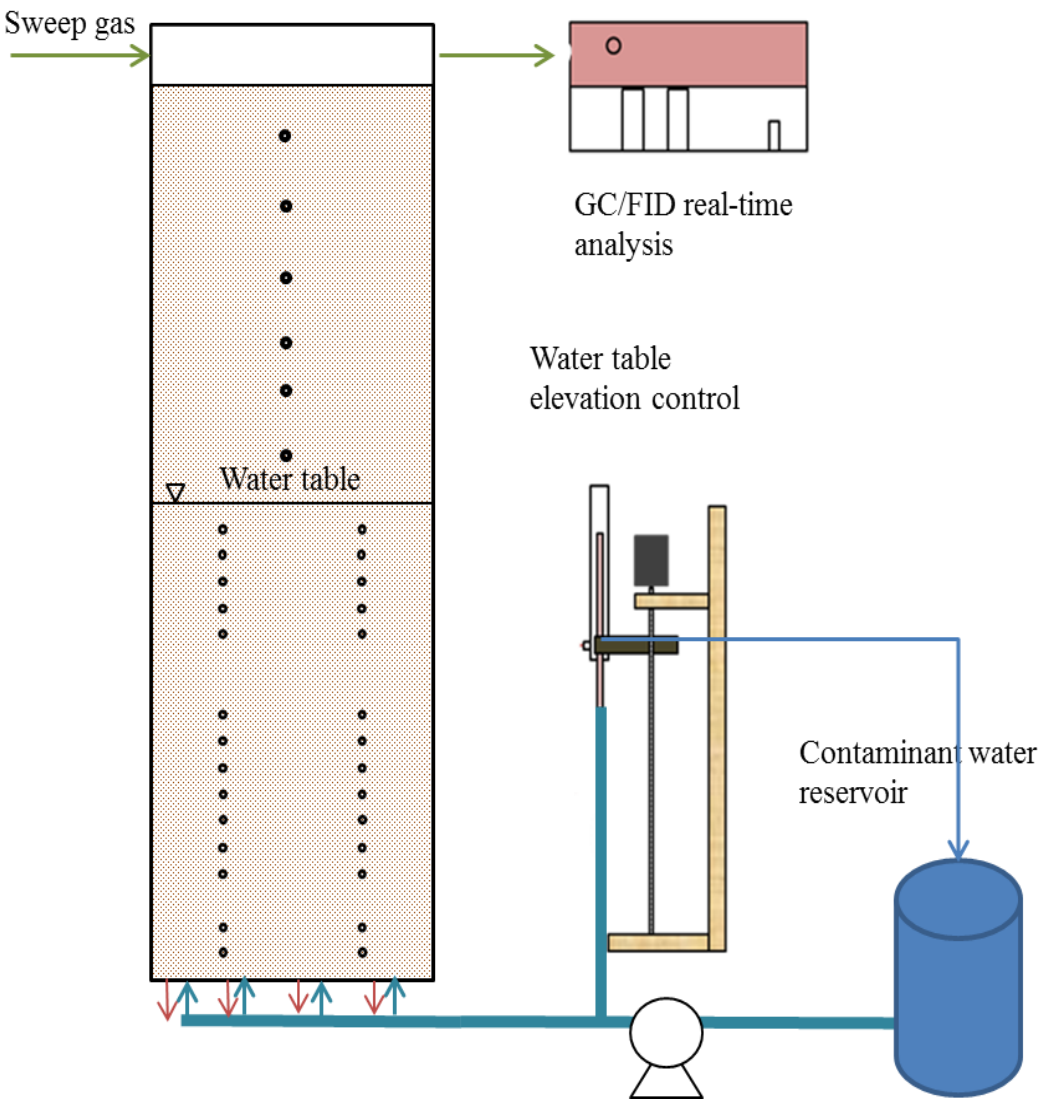
Sweep gas
GC/FID real-time
analysis
Water table
elevation control
Water table
Contaminant water
reservoir

(b)

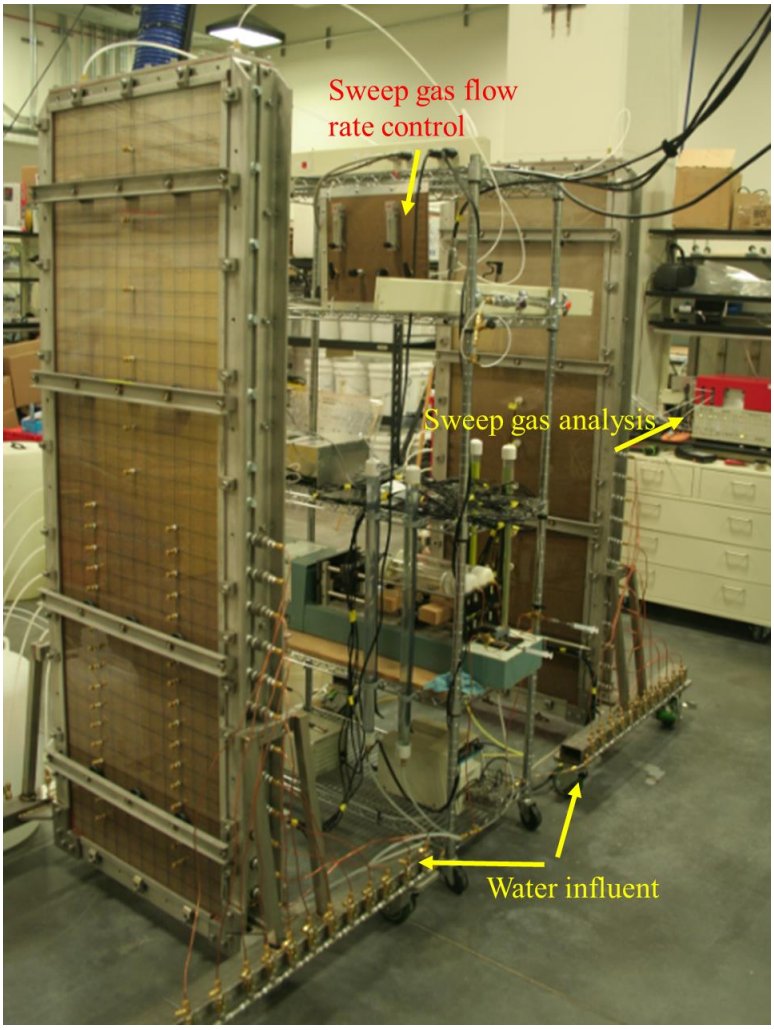

Figure 2.9. Schematic of physical models for a) horizontal flow experiments and b) fixed water volume experiments; and (c) photo of the physical model.

Tank operations. Initial scoping experiments were conducted with horizontal groundwater flow (Figure 2.7a) at an average linear velocity of about 60 cm/day while the water table was raised or lowered by 0.3 m across 3 days. CHC emission responses to water table fluctuation cycles were also tested with 0.3 m rises and drops across 6 and 12 days.

Following testing under uniform concentration conditions, experiments were performed using the test configuration shown in Figure 2.7b. Using this configuration, the water table was raised and lowered 0.3 m on 12-day cycles.

A summary of measurements and operational parameters for the experiments are given in Table 2.2.

Data collection and analysis. Soil gas and dissolved CHC concentrations were measured using analytical procedures similar to those described in the field experiment section. In this case, however, due to the small volumes that were extracted during water sampling, water samples required dilution from 1 mL to 30 mL using reverse osmosis treated water before head-space analysis using GC/DELCD.

CHC emission rates E_i [M/T] from groundwater were quantified by using the measured sweep-gas flow rate Q_{sweep} [m^3/d] and CHC concentration $C_{sweep,\,i}$ [g/ m^3], with $E = Q_{sweep} \times C_{sweep,i}$, where the subscript i denotes different chemicals. Sweep gas concentrations were continuously measured by an SRI GC equipped with a flame ionization detector (FID). Sweep gas samples were collected alternately from the tanks using a three-way solenoid valve (ASCO, NJ) controlled by SRI Peaksimple software. Sweep gas samples collected for analysis using the GC/FID were pulled onto a multi-bed sorbent tube trap (0.64 x 15.2 cm) packed with Tenax-GR and Carboxen-569 by a vacuum pump (Rena 301 series, model B E-302 vacuum/pressure pump), and a vacuum-configured 0-100 mL/min mass flow controller (Alicat Scientific, Tucson, AZ) at 40 mL/min. Sample collection time was controlled using SRI's PeakSimple software. Once a sample was collected, the sorbent tube was heated to 230°C and helium carried the sample onto a 60 m MXT-5 capillary column held at 40°C. After a 2.5-min delay, to

allow ample time for the trap heater to reach 240°C and for the sample to desorb from the trap, the GC column was heated from 40°C to 220°C at 12°C/min and the sample swept into the FID.

Table 2.3

Experimental conditions and measurements

Test	Operation Condition							Measurements			
	GW fluctuation range [m]	GW Flow	Initial water table elevation [m]	Final water table elevation [m]	GW velocity [m/d]	Water table change rate [cm/d]	Feed water concentrations [mg/L]	Sweep gas CHC concentration	Temperature and relative humidity in/out of sweep gas	GW contaminant profile	Real-time soil moisture content
Water table drop	0.3	horizontal	0.9	0.6	0.3	9.2	2.6 for 1,2-DCA, 2.1 for TCE and 1.2 for PCE.	Yes	No	Yes	Yes
Water table rise	0.3	horizontal	0.6	0.9	0.3	10		Yes	No	Yes	Yes
Water table fluctuation	0.3	horizontal	0.9	0.9	0.3	10	1.7 for 1,2-DCA, 1.6 for TCE and 0.9 for PCE.	Yes	No	Yes	Yes
Water table fluctuation	0.3	horizontal	0.9	0.9	0.3	5	1.8 for 1,2-DCA, 1.7 for TCE and 1.0 for PCE.	Yes	Yes	Yes	Yes
Water table fluctuation	0.3	no net flow into the tank	0.9	0.9	0	5	Initial concentrations were 1.1 for 1,2-DCA, 0.9 for TCE and 0.5 for PCE	Yes	Yes	Yes	Yes

2.3.2 Results and discussion. *Single-stage water table drop and rise tests.* The experiments were allowed to achieve steady-state depth versus normalized soil gas concentration profiles prior to initiating water table fluctuations. In preparing the normalized concentration profiles shown in Figure 2.8, measured soil gas concentrations at the sampling locations were divided by the equivalent equilibrium vapor phase concentrations corresponding to dissolved water concentrations at the water table (=dissolved concentrations x chemical-specific Henry's Law Constant).

All normalized concentrations decrease from about one to three orders-of-magnitude across the first two sampling points above the water table. This is similar to what McCarthy and Johnson (1993) observed in their experiments; their TCE concentrations decreased over three orders-of-magnitudes across an approximately 25 cm thick capillary fringe.

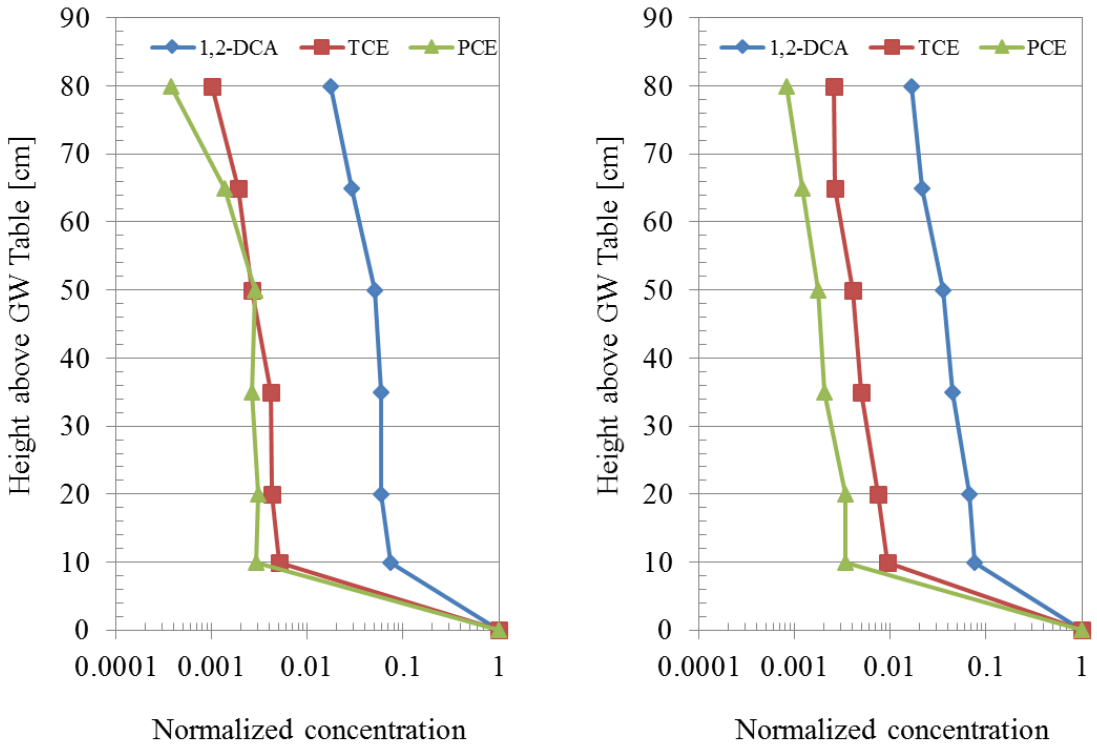

(a) Silica sand tank (b) Play sand tank

Figure 2.10. Normalized steady-state soil gas profiles for the (a) silica sand tank and (b) play sand tank. Normalized concentrations were obtained by dividing soil gas concentrations at sampling locations by the equivalent gas phase concentrations at the water table.

Figure 2.11 a-b and 2.12 a-b present CHC emission rates and water table elevations vs. time during single-stage drops and rises in the water table, respectively. In these figures, the emission rates were normalized to the averaged steady-state emission rate before the water table elevation change. A tank leak was discovered at t=110 h in the silica sand tank during the rising water table test, and as a result data after t=100 h were discarded. Overall, CHC emission rates in both tanks increased during falling water table tests and decreased during the rising water table tests. This observation agrees with

previous studies (e.g., Werner and Hohener, 2001). CHC emission rates did not return to their original level after the water table re-stabilized. With diffusion-dominated transport, steady-state emissions should be greater when the water table is 90 cm above the tank bottom vs. 60 cm above the tank bottom, because the distance to the soil surface is less. However, the opposite was observed during water table rise and drop tests. One possible explanation is that the emissions had not yet reached steady conditions when the experiment was terminated, and that appears plausible given the data trends in the single-stage water table drop tests (Figure 2.11). The explanation for the water table rise tests is that the result was an artifact of the way the experiments were conducted. The volumetric horizontal water flow for each tank was maintained at a constant rate, so that the linear horizontal flow rate of water was 33% slower when the elevation was 90 cm above the tank bottom vs. 60 cm. This might lead to more depletion at the emission interface as the water moves across the tank, thereby leading to a lower interface concentration and lower emissions for higher water table conditions.

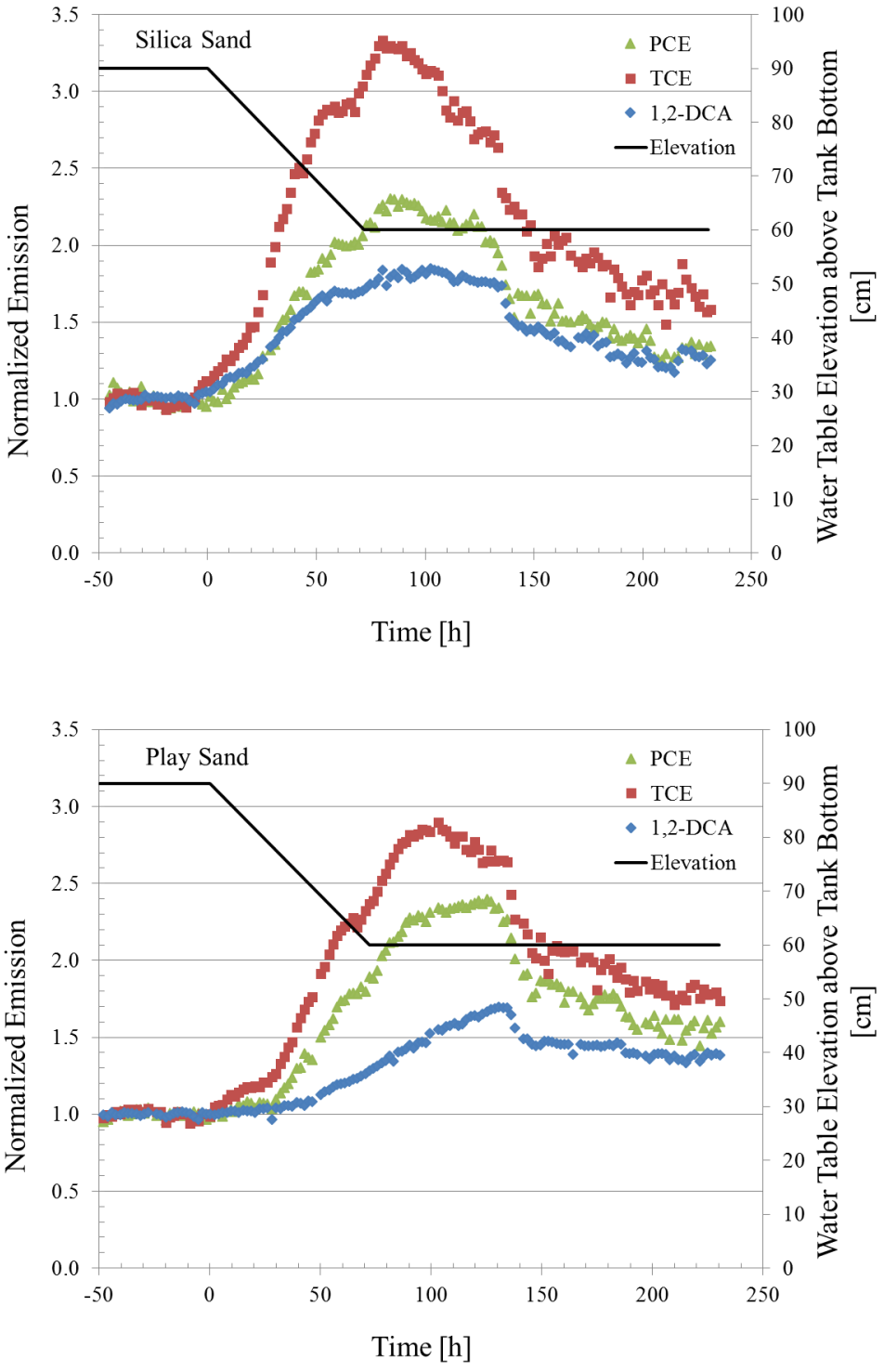

Figure 2.11. Normalized emissions and water table elevation vs. time in the (a) silica sand and (b) play sand tanks during the single-stage water table elevation drop test. Emissions are normalized to an averaged emission rate at steady-state before elevation changes.

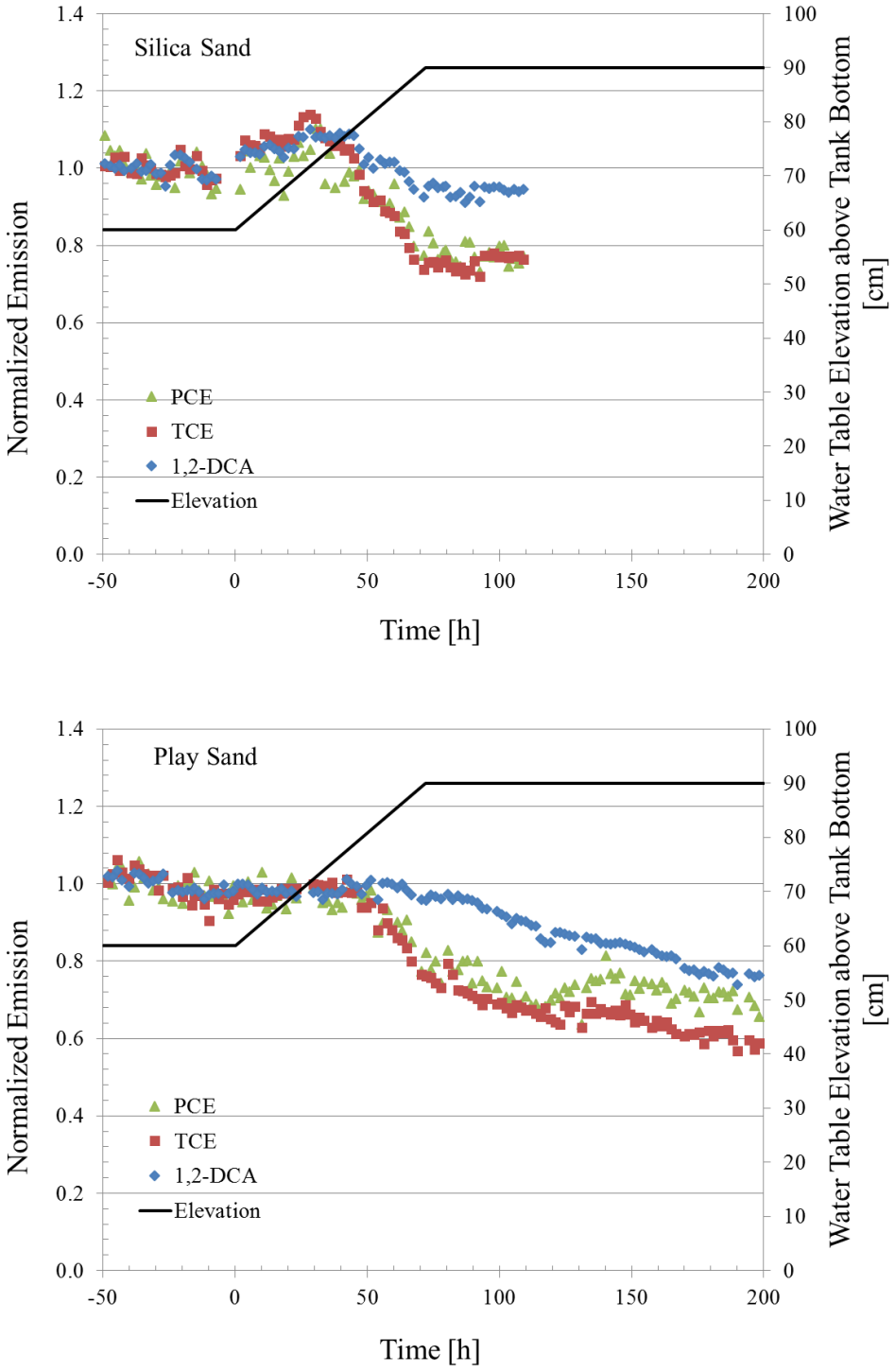

Figure 2.12. Normalized emissions and water table elevation vs. time in the a) silica sand and b) play sand tanks during the single-stage water table elevation rise test. Emissions are normalized to an averaged emission rate at steady-state before elevation changes.

The CHC emissions response to the single-stage water table drop was more rapid in the more permeable silica sand tank; the CHC emissions increases peaked in ≤100 h while they generally peaked at ≥100 h in the less permeable play sand tank. In addition, slight differences were observed in the emissions increases between tanks; peak TCE emissions were 3.3X greater than steady state conditions in the silica sand tank, whereas they were only 2.9X greater in the play sand tank. Since both tanks were tested simultaneously under the same operational conditions, these variations are likely a result of the different soil properties, and are probably linked to the rate of water drainage from the soil.

Alternating rising/falling groundwater elevation changes at different rates of change. Figures 2.13 and 2.14 present normalized CHC emission rates and water table elevations vs. time for water table elevation increases/decreases of 5 cm/day and 10 cm/day, respectively. In these experiments, water was continuously introduced by horizontal flow to maintain homogeneous dissolved CHC profiles across the water-saturated zone, and the change in water table elevation was about 30 cm. Four rise/fall cycles were implemented during the 5 cm/d experiment and three were implemented during the 10 cm/d experiment. Data gaps from 195 h to 225 h during the 5 cm/d experiment and from 195 h to 225 h and 403 h to 430 h during the 10 cm/day experiment were due to analytical instrument issues.

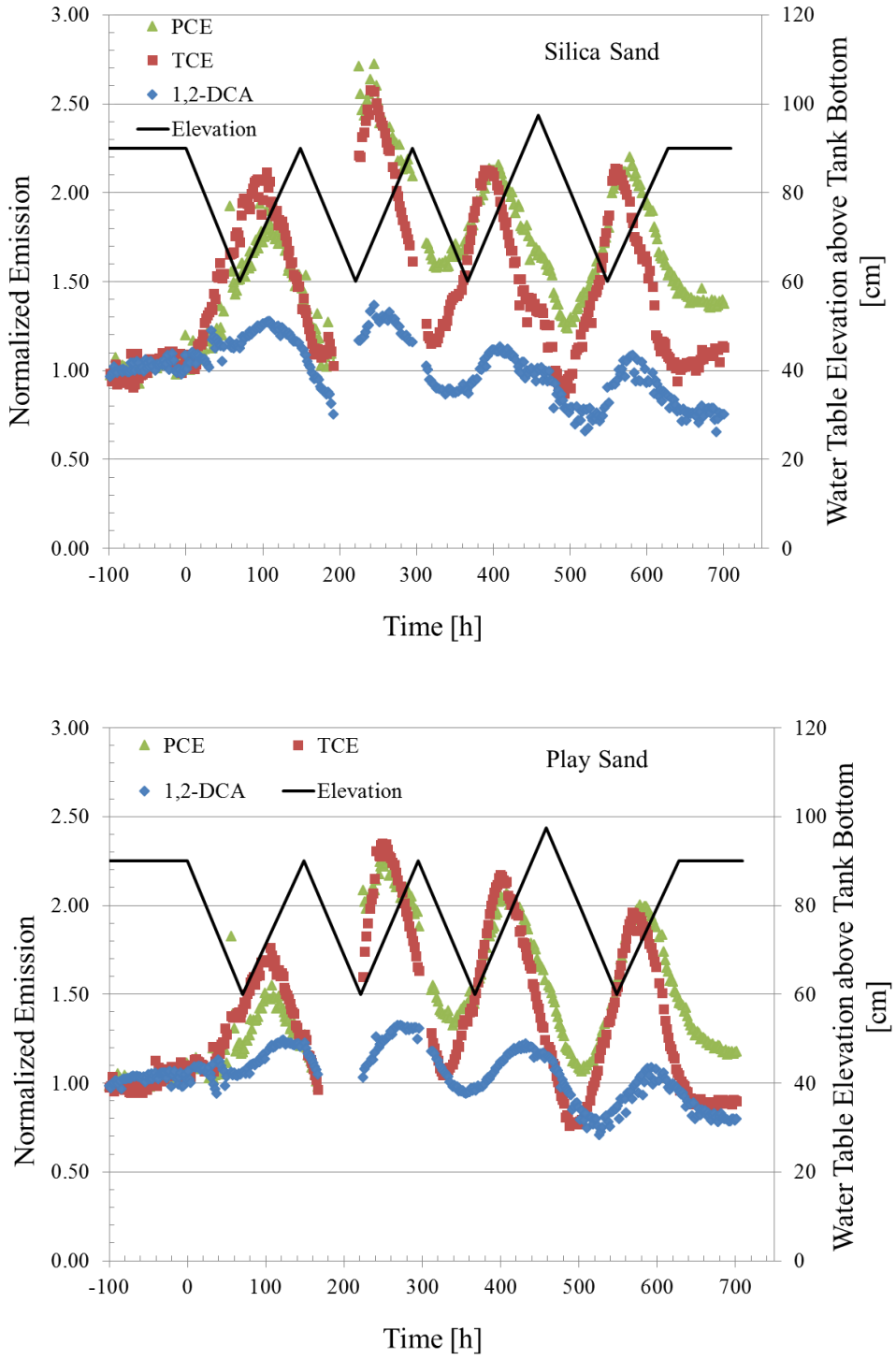

Figure 2.13. Normalized CHC emission rates and water table elevation vs. time during tests with 5 cm/d elevation change rate for a) silica sand and b) play sand tanks. Emissions are normalized to an averaged emission rate at steady-state before elevation changes.

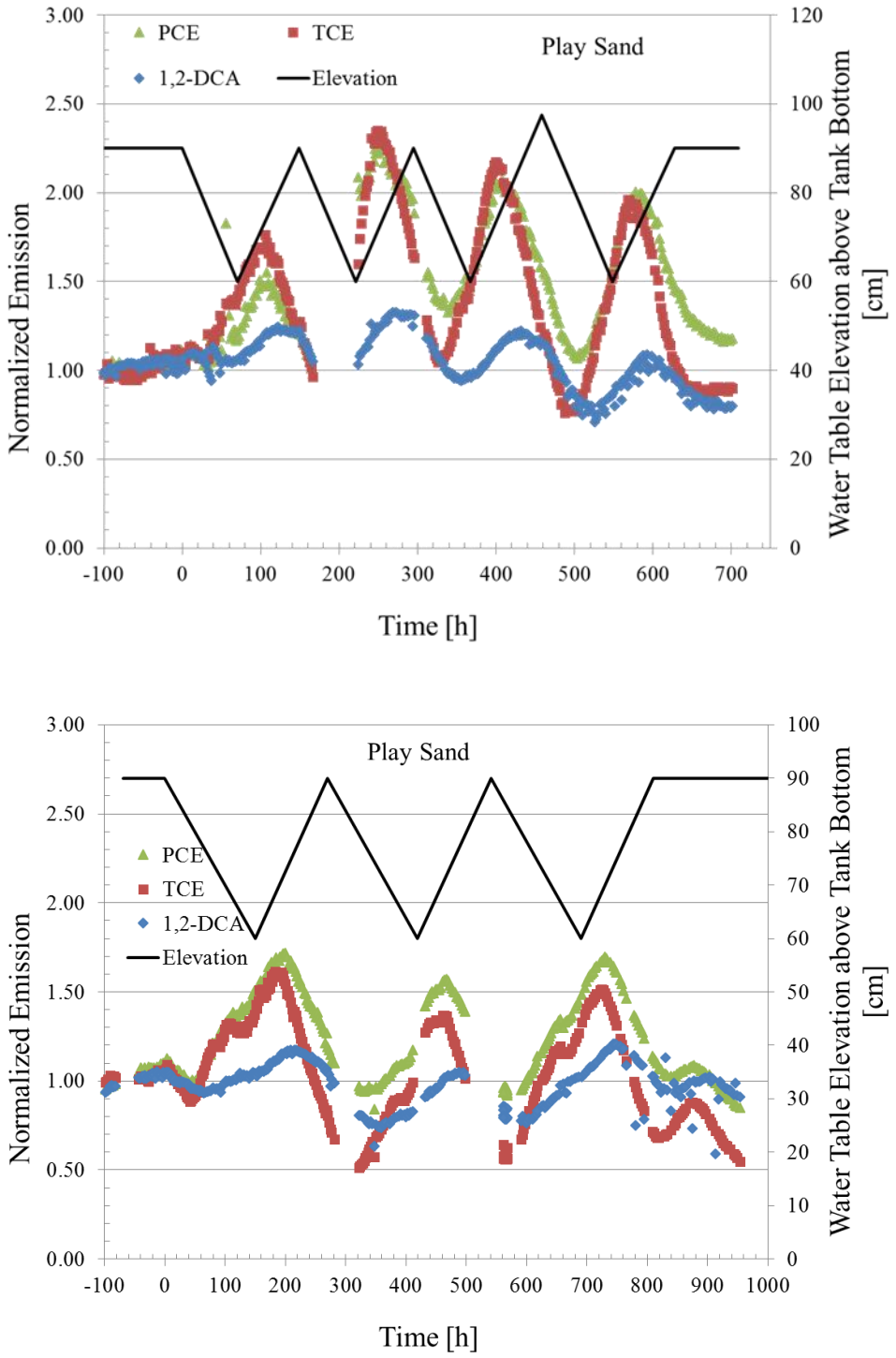

Figure 2.14. Normalized CHC emission rates and water table elevation vs. time during tests with 10 cm/d elevation change rate for a) silica sand and b) play sand tanks. Emissions are normalized to an averaged emission rate at steady-state before elevation changes.

The following observations were made from a review of Figures 2.13 and 2.14:

- All compounds respond to water table drops with an increase in emission rate, and that response begins shortly after the water table begins to fall. The TCE and PCE emissions responses to water table elevation changes were similar; the peak normalized TCE emission rates were within 10 % of the PCE peaks. The maximum increases in 1,2- DCA emissions were generally about 2X to 3X smaller than the other two CHCs. This appears to be influenced by differences in Henry's Law constants as TCE and PCE have similar H_i values and the H_i value for 1,2-DCA is 10X less than the other two (Table 2.1). In addition, the molecular diffusion coefficients are similar for all chemicals, with less than factor 2 difference across a wide range of chemicals.
- The magnitude of CHC emission increases during four 10 cm/day repeating water table fluctuations were less than in the single-stage 10 cm/day drop test (Figure 2.11). This is likely because the period of water table fluctuations was shorter than the time for emissions to peak following water table declines.
- CHC emissions increases were greater in the silica sand tank than in the play sand tank during the 5 cm/d oscillating water table level tests, but were similar for the 10/cm/d tests. For the 5 cm/d water table fluctuation cycles, the peak normalized CHC emissions in the silica sand tank were about 50% greater than those in the play sand tank. This may be a result of the differences in hydraulic conductivity between the silica sand (0.186

cm/s) and play sand (0.083 cm/s). Moisture profiles and water movement in the silica tank can respond more quickly to water head changes than in play sand tank.

- Emission responses changed when the rate of rise and fall changed from 5 to 10 cm/d. Peak normalized TCE emission rates increased from 1.50 ± 0.12 to 2.06 ± 0.26 in the play sand tank, while they were similar in the silica sand tank for both 5 and 10 cm/day.

In practice, uniform water concentration profiles with depth are unlikely to be observed aquifers. It is more probable that dissolved contaminant concentrations will decrease in approaching the water table because of depletion due to volatilization and infiltration of clean water onto dissolved groundwater plumes. For that reason, a second set of experiments was conducted in which the mass of chemical was allowed to deplete with time from the tank due to volatilization.

Groundwater fluctuation experiments with CHC mass depletion. In the second type of experiments, water table fluctuations of similar magnitude and frequency as above were implemented, but they were created by adding and removing water from the tank bottom, so the CHC mass was depleting with time by volatilization and there was no horizontal flow. Relatively uniform initial CHC distributions were created using lateral water flow and then that horizontal flow was stopped before the start of the vertical water table fluctuations.

A time progression of TCE concentration vs. depth profiles is presented in Figure 2.15. To show concentrations in both gas and water samples on the same plot, TCE concentrations are presented as “equivalent gas phase concentrations”, where dissolved

concentrations are converted to gas phase concentrations through multiplication by the Henry's Law constant.

At t= 0 h a strong concentration gradient exists near the water table. TCE concentrations decreased 60% and 37% within 5 cm of the water table in the silica sand and play sand tanks, respectively. This gradient was formed initially due to chemical volatilization during static water table conditions preceding the water table fluctuations.

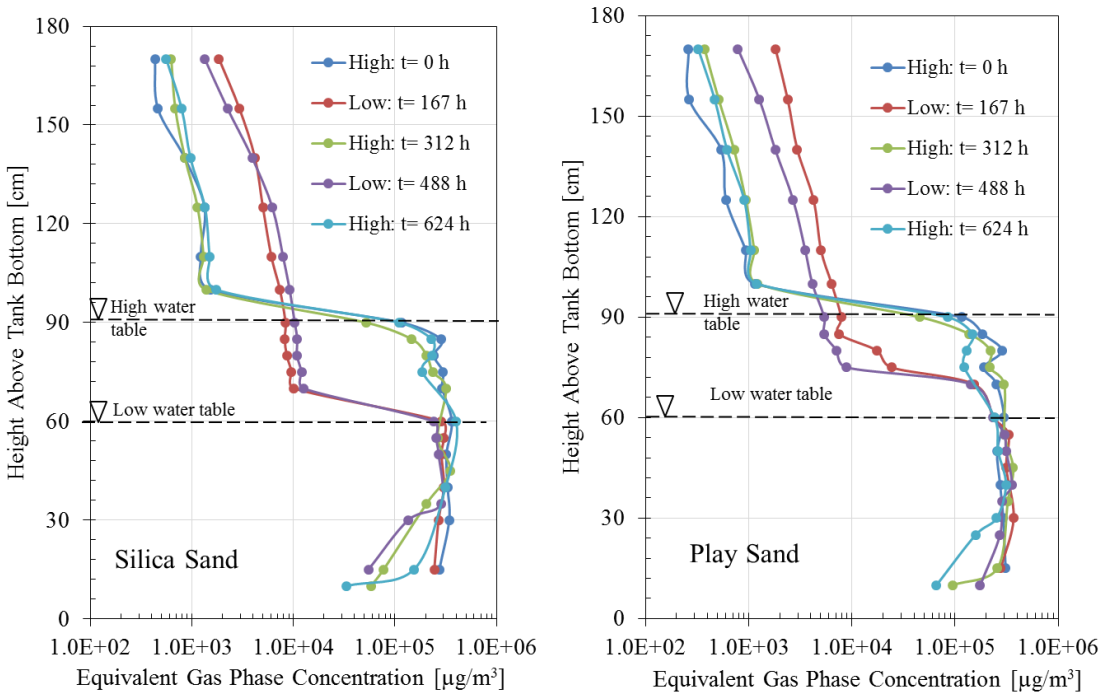

Figure 2. 15. Equivalent TCE gas phase concentration profiles during water level fluctuation tests for the silica sand (left) and play sand (right) tanks. Note that "high" and "low" in the legend refer to the highest and lowest water table elevations, respectively.

Real-time measured emissions were normalized to average steady-state emissions from each tank prior to water level fluctuations. Figure 2.16 presents results during two water table elevation fluctuation cycles. For both tanks, the rate of water level change

was 5 cm/d and maximum elevation changes were ± 0.3 m. Similar to the observations during uniform water concentration tests, CHC emissions changed when water table levels changed; however, in these tests the magnitude of the emissions increase decreased from the first cycle to the second. That indicates that the effect of groundwater table fluctuations will decrease with distance down-gradient in a dissolved plume. Again, as in all other tests, the effects of water table changes on TCE and PCE emissions is greater than for 1,2-DCA.

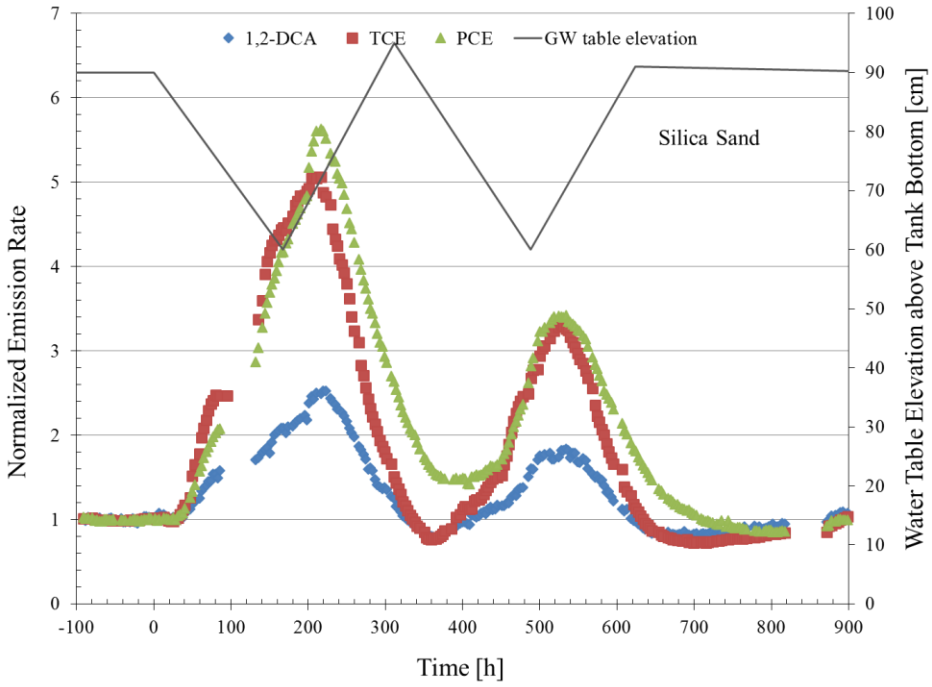

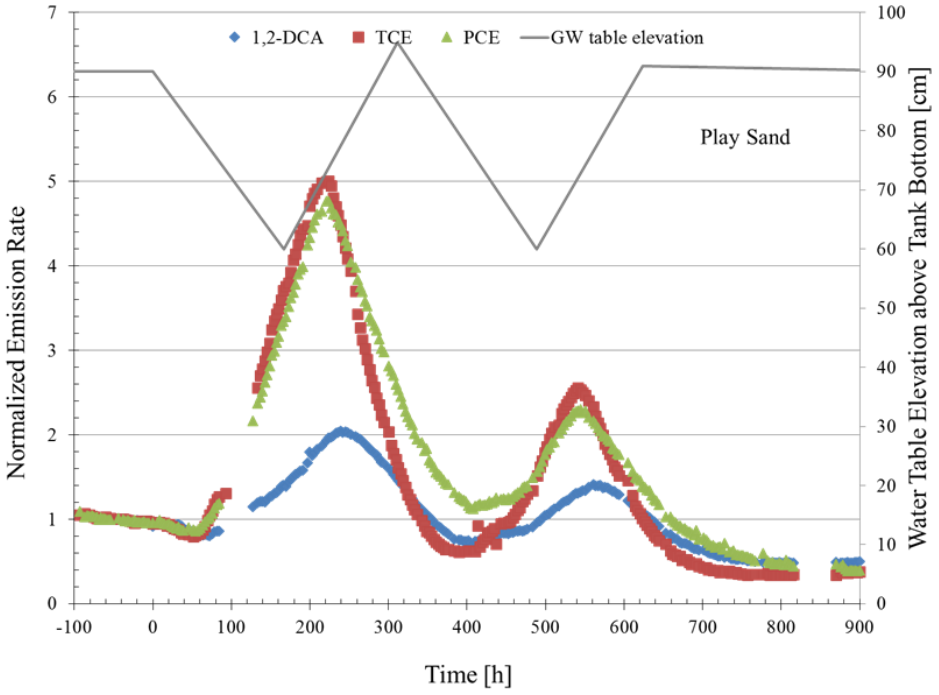

Figure 2.16. Normalized emission rates and water table elevations vs. time with depleting dissolved mass for the a) silica sand and b) play sand tanks. Emissions were normalized to averaged emissions from each tank prior to water level fluctuations.

In summary, the following are key observations from the laboratory studies:

- Emissions changed with changing water table elevation, with transient increases in emissions following water table declines and transient decreases in emissions following water table increases. The maximum temporary increases were <4X in the lab experiments. For reference, these are smaller than indoor air concentration changes with time reported Holton et al. (2013) but are similar to the roughly 3X seasonal variation reported by Folks et al. (2009).
- Chemical and soil properties appear to play a role in emission rate responses. For 1,2-DCA, with a Henry's law constant <1/10th of PCE and

TCE values, the maximum emissions increases were about a factor of 2X to 3X less than the other two chemicals.

- Greater emissions increases were observed for the more permeable and lower capillary rise silica sand during the water table level oscillation tests.
- Water table fluctuation frequency did affect the magnitude of emission increases for the play sand tank; the magnitude increased as the water level changed faster from 5 cm/d to 10 cm/d. The rate of change in water level did not appear to impact the peak emissions from the silica sand.
- The CHC depletion test showed the development of a decreasing concentration gradient with time near the water table and corresponding reduced emission increases over time. This suggests the responses of CHC emissions to water table fluctuations may be different in different regions of a dissolved groundwater plume.

2.4 SIMULATING VAPOR EMISSIONS FROM GROUNDWATER TO THE SOIL SURFACE WITH FLUCTUATING WATER TABLES

The field site and laboratory experiments encompass a small set of possible conditions, and it is difficult to state with confidence that the conclusions above will be true for all soil types, chemicals, and water table elevation vs. time patterns. Given the projected length of time required to evaluate a wider range of conditions, numeral modeling was utilized to expand the conditions explored. Simulations were conducted to

understand the effect of soil and chemical properties and water table fluctuation patterns (magnitude and frequency) on emission rate changes.

2.4.1 Modeling Approach. *Conceptual model and numerical modeling tool.* For simplicity, the conceptual model used for this modeling investigation was the one-dimensional soil column shown in Figure 2.17. Water table fluctuations were created by changing the lower water pressure boundary condition in the modeling domain. Contaminant transport included volatilization from the water phase, migration through the soil matrix, and emission to clean air at the modeling domain upper boundary.

HYDRUS-1D version 4.16 (Simunek, 2013) was used to perform simulations; it is public domain software and includes the one-dimensional finite element model HYDRUS for simulation of water, heat, and solute movement in variably water-saturated media. Only water and solute flow were considered in this study; the system was isothermal without hysteresis in saturation-capillary pressure profiles.

A constant pressure head was assigned at the upper boundary and a time-varying pressure head was assigned at the lower boundary. For solute transport, a 0.5 cm stagnant upper boundary layer thickness was selected, as it was recommended in HYDRUS-1 D (Simunek, 2013) when both water and gas phases are present at the soil surface. The vapor emission from the soil to the atmosphere is calculated based on the difference in gas concentrations above (atmosphere) and below (soil gas) this layer. The atmosphere concentration at the upper boundary of this stagnant layer was held at zero. A constant concentration was held at the lower model boundary for source below water table condition as shown in Figure 2.17.

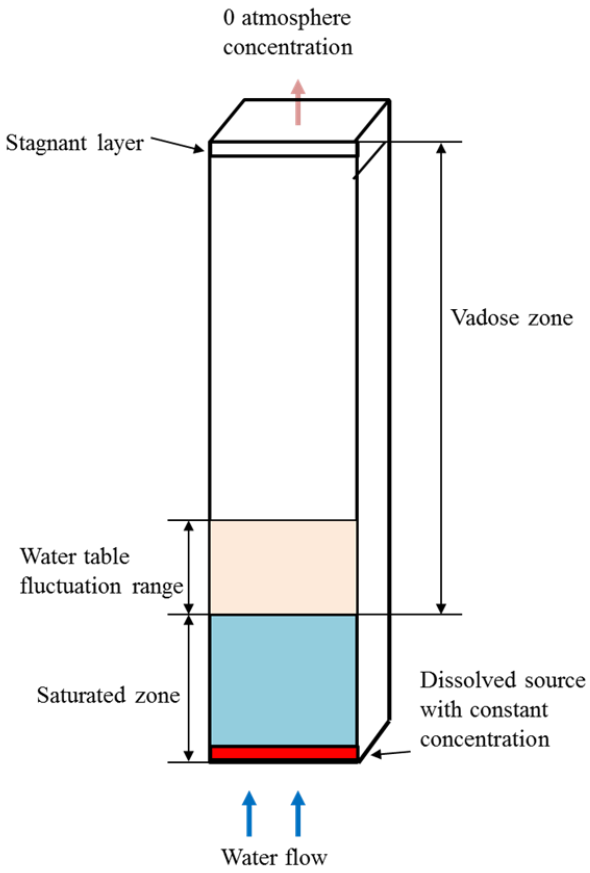

Figure 2.17. Conceptual models for simulation boundary condition.

Model validation. The groundwater table fluctuation lab experiment with water recharging/depleting from the lower boundary of the tank was similar to the mathematical modeling conditions. Thus, the experimental conditions for the play sand tank were input to the simulation and then the model output results were compared with experimental results. Table 2.3 summarizes model inputs for this simulation. Sorption was neglected in because the measured soil organic fraction (f_{oc}) for the play sand was very small (<0.1%).

Table 2.4

Model validation simulation inputs

Experimental Conditions and Soil Properties		
Total soil profile depth	cm	180
Initial water table elevation	cm	90
Residual soil water content	cm^3-H_2O)/cm^3-soil	0.079
Saturated soil water content	cm^3-H_2O)/cm^3-soil	0.35
Parameter *a* in the van Genuchten soil water retention function	cm^{-1}	0.2
Parameter *n* in the van Genuchten soil water retention function	-	2
Saturated hydraulic conductivity	cm/h	298.8
Tortuosity parameter in the conductivity function	-	0.5
Bulk density	g-soil/cm^3-soil	1.5
Longitudinal dispersivity	cm	0.1
Algorithm parameters		
Time weighting scheme		Crank-Nicholson implicit scheme
Space weighting scheme		Galerkin formulation
Minimum time step	s	0.864
Maximum time step	hour	50
Maximum number of iterations	-	10
Water content tolerance	-	0.001
Pressure head tolerance	cm	1

The van Genuchten capillary pressure-water saturation profile parameters used were obtained by fitting simulated to measured saturation profiles as shown in Figure 2.18. As mentioned in laboratory section, a concentration gradient was created by volatilization during the static water table condition preceding the water table fluctuations. A similar initial chemical profile was created in the simulation for a scenario where the water table elevation was maintained at 90 cm above the bottom boundary and groundwater contaminant concentrations were initially uniform in the saturated zone. Once this contaminant profile was generated in the model, it was used as the initial concentration input for the water table fluctuation simulations. This initial contaminant concentration profile for TCE is presented in Figure 2.19.

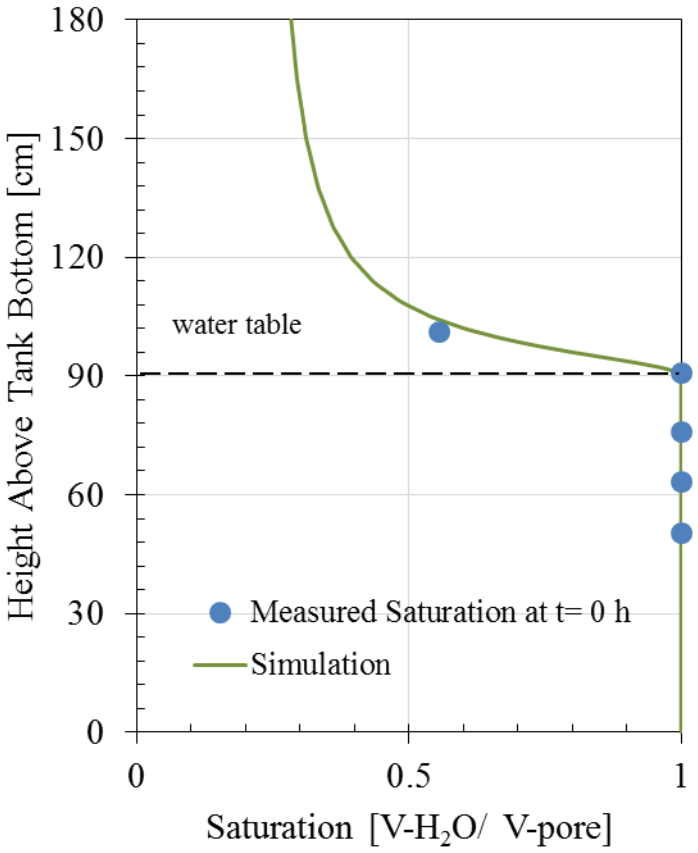

Figure 2.18. Measured and simulated water saturation in play sand tank after fitting van-Genuchten parameters.

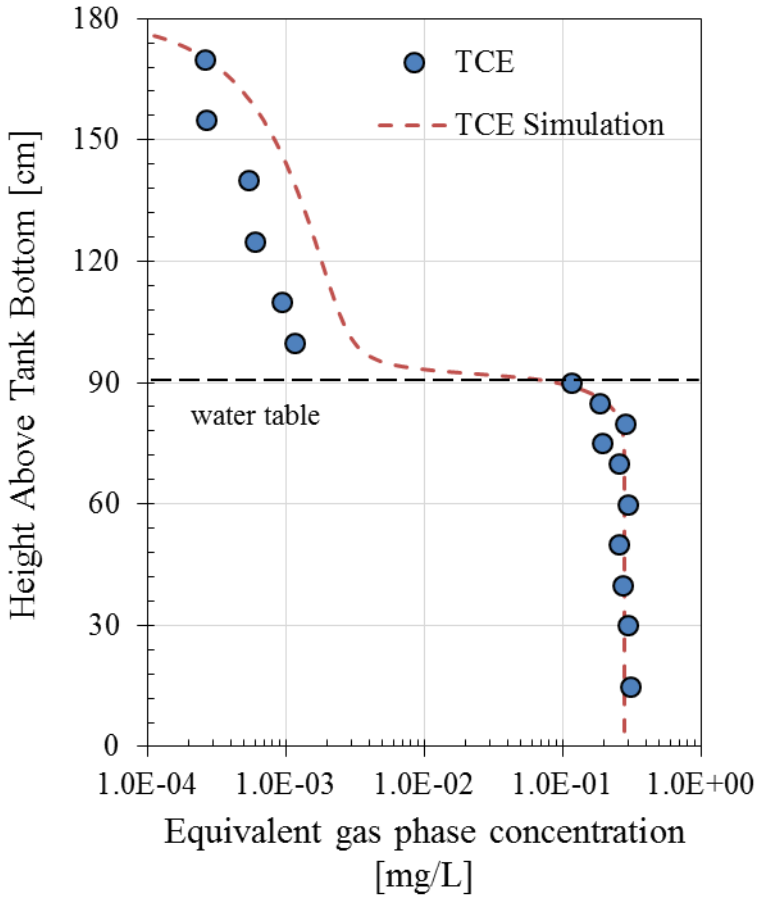

Figure 2.19. Measured and simulated initial chemical profiles.

2.4.2. Transport basis and parameter selection. It is helpful to identify parameters that can a) affect long-term VOC emission levels and b) control temporal VOC emission responses to water table fluctuations. The following analysis begins with a mass balance between groundwater and the soil surface:

$$\frac{\partial m}{\partial t} = A \times \left(\overrightarrow{F_{bot}} - \overrightarrow{F_{top}}\right) \quad (5)$$

where m is the total mass in the control volume [M]; A is cross-section area of the control volume [L^2]; and F_{bot} and F_{top} are mass fluxes at the bottom and top control volume boundaries, respectively [$M/L^2/T$].

Here the bottom water head fluctuates sinusoidally: $Head(bot) = L[sin(2\pi t/P - \pi/2)+1] + z_{initial}$, where L is the head change magnitude [L], P is the fluctuation period [T], and $z_{initial}$ is the initial water table elevation [L]. When the VOC transport reaches dynamic steady state, the total mass in the control volume is the same at the beginning and end of each water head change cycle. The integration of Equation (5) from t_0 to $t_0 + P$ yields:

$$\int_{t}^{t_0+P}\left(\frac{dm}{dt}\right)dt = \int_{t_0}^{t_0+P}\left(\overrightarrow{F_{bot}} - \overrightarrow{F_{top}}\right)dt = 0 \quad (6)$$

Thus:

$$\int_{t_0}^{t_0+P}\overrightarrow{F_{top}}dt = \int_{t_0}^{t_0+P}\overrightarrow{F_{bot}}dt \quad (7)$$

The left side of Equation (7) represents VOC emissions at the soil surface over the period P. This equation can help us to understand the long-term VOC emission changes relative to static water table condition. The long-term averaged emissions ($F_{average}$ [$M/L^2/T$]) can be written:

$$F_{average} = \frac{1}{p}\int_{t_0}^{t_0+P}\overrightarrow{F_{bot}}dt \quad (8)$$

In this case, $\overrightarrow{F_{bot}}$ involvs two transport mechanisms: advective dissolved flux from the lower boundary and chemical diffusive transport. Inserting Darcy's law and Fick's Law into equation (8) yields:

$$F_{average} = -C_{bot}\frac{K_s}{P}\int_{t_0}^{t_0+P}\frac{\partial H(z,t)}{\partial z}\Big|_{bot}dt + \frac{1}{P}\int_{t_0}^{t_0+P}\left(D_w^{eff}\frac{\partial C_w(z)}{\partial z} + D_g^{eff}\frac{\partial C_g(z)}{\partial z}\right)\Big|_{bot}dt \quad (9)$$

where C_{bot} is the lower boundary VOC concentration [M/L^3]; K_s is the saturated hydraulic conductivity [L/T]; $\frac{\partial H(z,t)}{\partial z}$ is the water head gradient at bottom boundary [L/L]; D_w^{eff} and D_g^{eff} are the effective diffusion coefficients in water and air [L^2/T]; $\frac{\partial C_w(z)}{\partial z}$ and $\frac{\partial C_g(z)}{\partial z}$ are water and soil gas concentration gradients at bottom boundary.

The first term in the right hand site of Equation (9) is the advective dissolved VOC flux associated with water movement caused by water head changes at the lower boundary. This term includes information about the water head change pattern and soil hydraulic conductivity. More mass is transferred in and out across the system as the boundary head fluctuation increases in magnitude (*L*) and frequency (1/*P*), in high-hydraulic conductivity soil (*Ks*).

The second term on the right-hand side is the diffusive flux. It depends on the effective diffusion coefficients (D_w^{eff} and D_g^{eff}), and concentration gradient with depth.

The transient VOC emission $\overrightarrow{F_{top}}$ is also of interest here, and can be obtained by rearranging Equation (5):

$$\overrightarrow{F_{top}} = \overrightarrow{F_{bot}} - \frac{\partial m}{A\partial t} \quad (10)$$

Assuming advection dominates the lower boundary flux term, and local equilibrium partitioning occurs in the control volume, Equation (10) can be written:

$$\overrightarrow{F_{top}} = -C_{bot} \times K_s \frac{\partial H(z,t)}{\partial z}\Big|_{bot} - \frac{\partial\left(\int_0^{D_{vadose}+z_{initial}}\left[\left(\theta_g(z,t)+\frac{\theta_W(z,t)}{H}+\frac{k_s\rho}{H}\right)C_g(z,t)\right]dz\right)}{A\partial t} \quad (11)$$

where $\theta_g(z,t)$ and $\theta_w(z,t)$ are gas- and water-filled porosities at depth *z* and time *t* [L^3/L^3]; *H* is the Henry's Law constant [L^3_{water}/L^3_{air}]; and k_s is the effective sorption coefficient [L^3/M].

The first term in right hand side of Equation (11) delivers mass through the lower boundary while the second term stores and releases mass, and acts like a capacitor in an electric circuit. Small k_s, D_{vadose}, $z_{initial}$ and large *H* values decrease the storage capacity and dampening of the fluctuating input.

Hence, Soil properties, chemical properties, and water table fluctuation patterns may affect vapor emissions from groundwater to the soil surface, based on field and lab observations as well as analysis above. A sensitivity analysis was performed for these parameters with the dissolved concentration source strength being 1 mg/L.

Two source zone conditions were simulated, one was a dissolved source located 50 cm below the initial water table, and the other was a dissolved source located 200 cm below the initial water table elevation. Both might be representative of regions where non-aqueous phase liquid (NAPL) source zones are submerged at or near the initial CHC spills.

Simulations for each scenario were conducted using the concentration distributions from fixed/non-moving water table conditions as the starting point for time-varying head condition simulations. The emission for the fixed water table elevation at $z_{initial} + L/2$ (E_{static}) was calculated to normalize time-varying simulation emissions, since the bottom pressure head followed: $Head(bot) = L[sin(2\pi t/P - \pi/2)+1] + z_{initial}$. For

example, Figure 2.20 illustrates the TCE emissions normalized to E_{static} during the transition process from a static water table (65 cm above lower boundary) to 30 cm monthly oscillation with a 50 cm initial vadose zone thickness and 50 cm source depth below the initial water table level. Maximum and minimum emission rates were obtained after t = 250 d, when the system reached dynamic steady state.

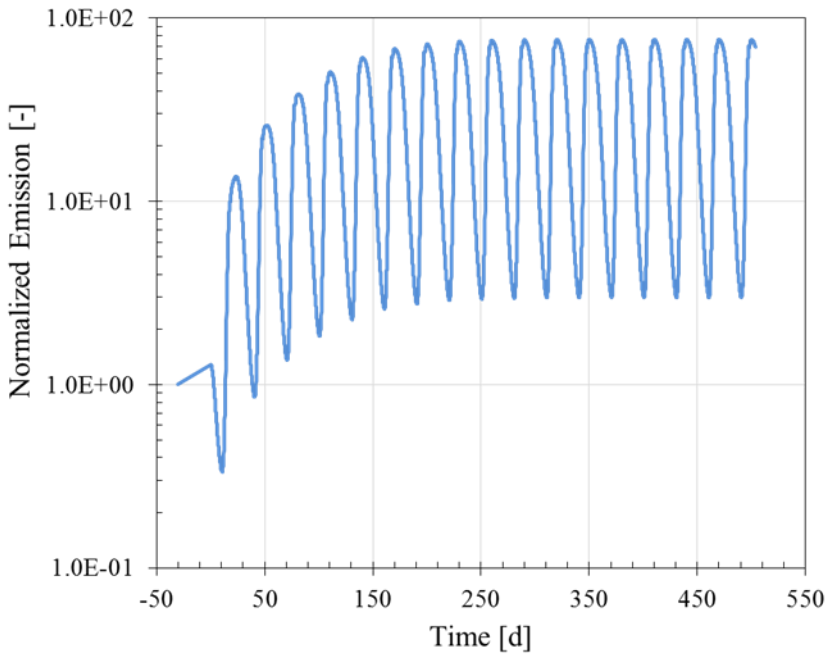

Figure 2.20. Normalized TCE emissions during the transition from static water table conditions to dynamic steady state for a source located 50 cm below the initial water table, 30 monthly water table oscillations, and 50 cm depth to the initial water table.

The reference scenario simulation involved a constant TCE concentration source, 150 cm vadose zone thickness above the initial water table elevation, and 30 cm monthly water table fluctuations. Changes in inputs about this reference scenario were then

evaluated with a focus on the following: (1) water table fluctuation pattern, (2) vadose zone thickness, (3) soil type, and (4) chemical properties.

Water table fluctuations were created by applying a sine-wave time-variable pressure head condition at the lower boundary ($Head(bot) = L[sin(2\pi t/P - \pi/2)+1] + z_{initial}$). Annual, monthly and daily water table variations of 30 cm were simulated, as well as monthly fluctuations ranging from 1 cm to 100 cm.

Soil capillary properties usually reflect soil hydraulic conductivity, and higher hydraulic conductivity soils commonly have smaller capillary fringe heights. Simulations were conducted using three types of soil: coarse sand, sand, and loam, with capillary fringe heights ranging from less than 5 cm to more than 200 cm, and their K_s values varied over 100X. Soil properties for sand and loam were obtained from values built-in HYDRUS 1-D. Soil properties for coarse sand were selected to match the silica sand tank steady-state saturation profiles. The soil saturation vs. elevation curves for these soil types are presented in Figure 2.21.

TCE was selected as a reference chemical for these studies, recognizing that diffusion coefficients in air and water for other CHCs are within about a factor of 2X and that Henry's Law constants might vary from TCE by as much as two orders of magnitude. Thus, simulations were run by varying its D_{air} and D_{water} values from 0.5X to 2X TCE values, and H from 0.1X to 10X the TCE value. The effective sorption coefficient (k_s) was also varied from 0 to 10 L/kg.

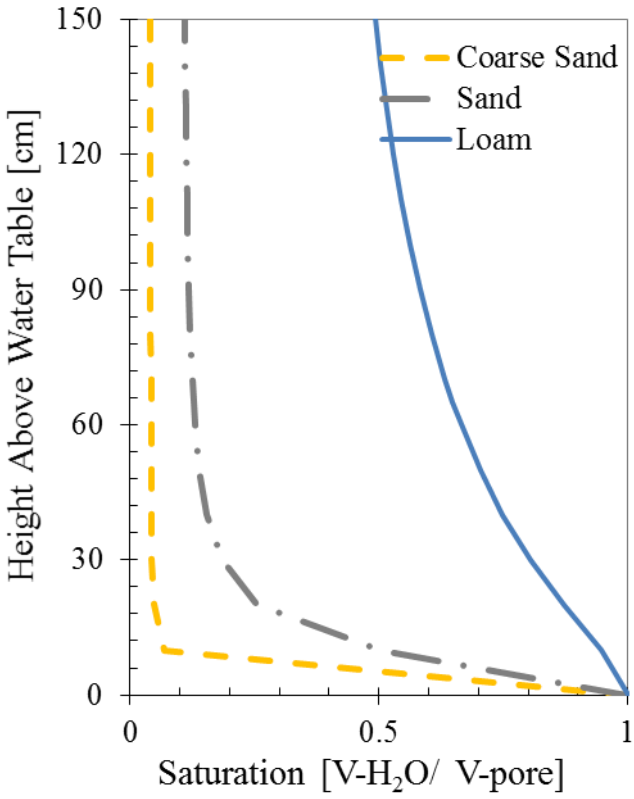

Figure 2.21. Soil saturation versus height above water table using coarse sand, sand and loam van Genuchten parameter values.

2.4.2 Results and discussion. *Validation simulation.* Figure 2.22 presents the comparison of measured vs. simulated TCE emission rates for the silica sand experiment discussed above. The results are qualitatively similar, with the emission peaks appearing at similar times in the simulation results and lab experiment data (approximately 210 h and 530 h after the beginning of the first water table fluctuation cycle). The maximum values for the first TCE emission peaks are about 2X greater than the second ones in both simulations and experiments. The normalized TCE emission values, however, were about 2X greater in the simulation results than in the measured lab results during water table fluctuations. This could be a result of the following uncertainties in model inputs:

- The fitted van Genuchten parameters may not perfectly reflect the soil saturation profiles and the fitting only occurred under static conditions. While the apparent match between measured and simulated profiles at steady state is good, the vertical resolution in soil moisture measurements is coarse and there is a significant change in moisture content immediately above the water table between the two moisture sensor locations.
- The simulation results are sensitive to the following input parameters: the saturated soil porosity, residual water content, the van Genuchten parameters defining the water flow and retention properties, and the Henry's Law Constant.
- Zero atmospheric TCE concentrations were set as an upper boundary condition in the simulation, whereas the TCE concentrations in the headspace of the experimental tank varied from less than 50 ppb_v (267 $\mu g/m^3$) to more than 250 ppb_v (1350 $\mu g/m^3$). However, this is unlikely to impact the experimental conditions because those levels are very small (nearly zero) relative to the source equivalent gas-phase TCE in the water (3×10^5 $\mu g/m^3$).
- Advective flow in the soil gas phase is not coupled in HYDRUS-1D, but does happen in the lab study. The movement of water table fills/depletes water in the soil pores, and consequently results in air movement out of and into the soil; the direction of air flow will be upward during water table rises and downward for water table drops. When the water table is moving downward, the direction of advective air flow is opposite to the diffusive flux, and this could reduce the magnitude of the emission peak. However, this is unlikely

an explanation as the model results are consistently greater than the measured results, independent of water table rise or fall conditions.

Overall, HYDRUS-1D results qualitatively mimic the emission changes observed on the laboratory, with modeled emission increases being about a factor of 2X greater than the observations. This provided confidence in continuing to explore how emissions changes with time might be impacted by soil properties, chemical properties, and water table elevation patterns with time.

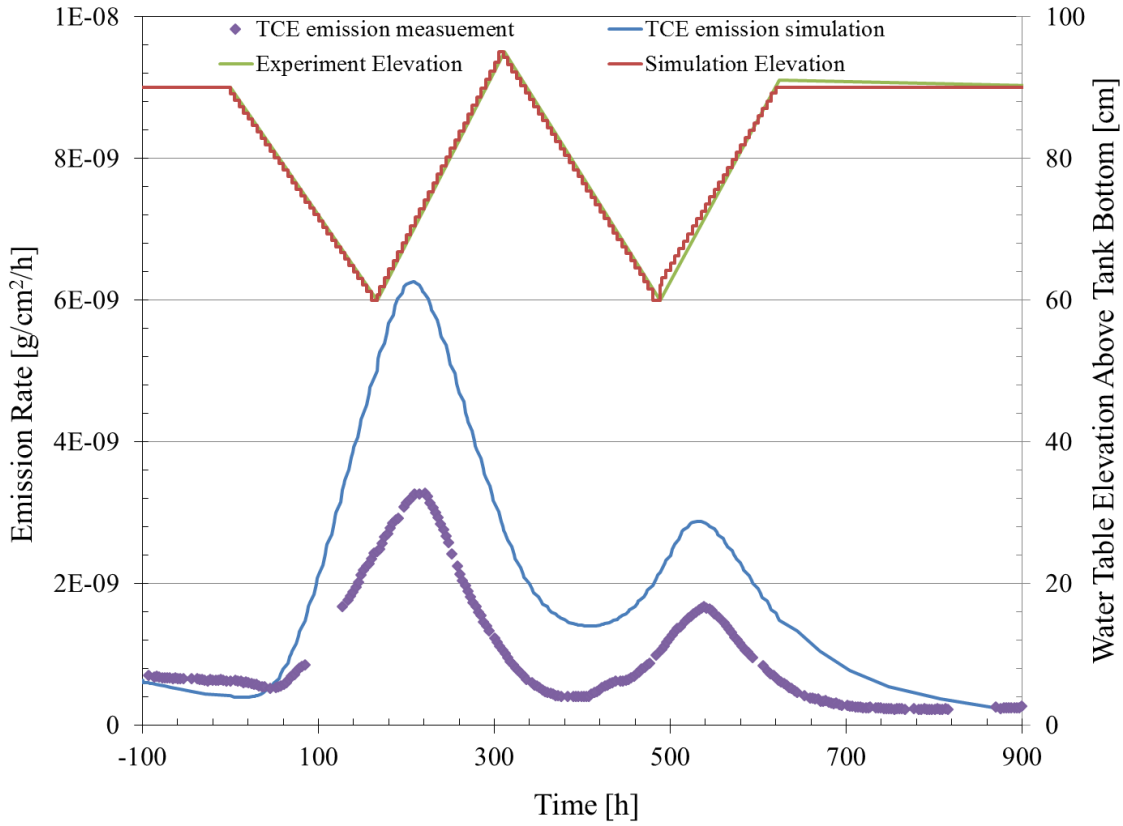

Figure 2.22. Simulated vs. measured emission rate and water table elevation for the silica sand experiment presented in Figure 2.4.

Sensitivity analysis for a range of water table fluctuation scenarios. Model inputs for HYDRUS 1-D simulations are summarized in Table 2.5. Simulation results for all scenarios, static water table ($z_{initial} + L/2$) condition emissions (E_{static}), maximum, minimum, and average emissions during fluctuation after the system reached dynamic steady state (E_{max}, E_{min}, and E_{mean}) as well as the ratios between them, are presented in Table 2.6.

Table 2.5

Summary of simulation inputs for sensitivity analyses.

HYDRUS 1-D algorithm inputs						
Time information	Initial time step [h]	0.0024	Iteration criteria	Maximum number of iteration	10	
	Minimum time step [s]	0.01		Water content tolerance	0.001	
	maximum time step [h]	200		Pressure head tolerance [cm]	1	
Time Weighing Scheme	Crank-Nicholson implicit scheme					
Space Weighting Scheme	Galerkin formulation					
Soil properties:	**Soil type: sand**		**Soil type: loam**		**Soil type: coarse sand**	
	Inputs	**Simulation ID**	**Inputs**	**Simulation ID**	**Inputs**	**Simulation ID**
Residual soil water content [cm^3-H_2O/cm^3-soil]	0.045	1-7, 10-24, 24-34	0.078	8, 25	0.016	9, 26
Saturated soil water content [cm^3-H_2O/cm^3-soil]	0.43		0.43		0.39	
Parameter *a* in the soil water retention function [1/cm]	0.145		0.036		0.6	
Parameter n in the soil water retention function [-]	2.68		1.56		3	
Saturated hydraulic conductivity [cm/h]	29.7		1.04		669.6	
Tortuosity parameter in the conductivity function [-]	0.5		0.5		0.5	
Bulk density [g/cm^3]	1.5	These values were kept as the software defaults for all simulations				
Longitudinal dispersivity [cm]	0.1					

(continued on the next page)

Table 2.5 (cont.)

Summary of simulation inputs for sensitivity analyses.

Solute specific parameters:	**Inputs**	**Simulation ID**
Molecular diffusion coefficient in water, *Dwater* [cm^2/h]	0.01638	16, 33
	0.03276	1-15, 18-33
	0.06552	17, 34
Molecular diffusion coefficient in air, *Dair* [cm^2/h]	142.2	14, 31
	284.4	1-13, 16-30, 33-34
	568.8	15, 32
Adsorption isotherm coefficient, *ks* [cm^3/g]	0	1-9, 12-26, 29-34
	1	11, 28
	10	10, 27
Henry's Law constant, *H* [V-water/V-gas]	0.042	12, 29
	0.42	1-11, 14-28, 31-34
	4.2	13, 30

(continued on the next page)

Table 2.5 (cont.)

Summary of simulation inputs for sensitivity analyses.

Water table fluctuation patterns:	**Inputs**	**Simulation ID**		
Fluctuation magnitude [cm]	1	4, 21		
	30	1-3, 6-20, 23-34		
	100	5, 22		
Fluctuation frequency [1/day]	1	3, 20		
	1/30	1, 4-18, 21-34		
	1/360	2, 19		
Domain information:	**Inputs**	**Simulation ID**		
Depth of modeling domain [cm]	Source 50 cm below water table		Source 100 cm below water table	
	Inputs	Simulation ID	Inputs	Simulation ID
	100	6	250	23
	200	1-5, 8-17	350	18-22, 25-34
	550	7	700	24
Initial water table elevation above bottom of the domain [cm]	50	1--17		
	200	18-- 34		

Table 2.6

Model Results for Hydrus 1-D Simulations

	Simulation Number	Description	Source 50 cm below water table							
			E_{static} [g/cm^2-h] x 10^7	E_{max} [g/cm^2-h] x 10^7	E_{min} [g/cm^2-h] x 10^7	E_{mean} [g/cm^2-h] x 10^7	E_{max}/ E_{static}	E_{min}/ E_{static}	E_{mean}/ E_{static}	E_{max}/ E_{min}
	1	Reference (TCE, monthly 30 cm water table fluctuation, no adsorption)	1.55	5.04	0.634	2.50	3.25	0.41	1.61	7.95
Water table fluctuation pattern	2	Annual, 30 cm	1.55	2.54	1.24	1.83	1.64	0.80	1.18	2.04
	3	daily, 30cm	1.55	17.7	16.7	17.0	11.44	10.80	10.99	1.06
	4	Monthly, 1 cm	1.96	2.07	1.92	1.99	1.06	0.98	1.02	1.08
	5	Monthly, 100 cm	1.02	11.7	0.00692	3.33	11.45	0.01	3.26	1687
Vadose zone thickness	6	50 cm	1.55	118	4.61	53.2	76.47	2.98	34.43	25.67
	7	500 cm	1.54	2.73	2.20	2.45	1.77	1.42	1.59	1.24
Soil types	8	Loam	1.28	3.85	2.77	2.52	3.02	2.17	1.97	1.39
	9	Coarse sand	1.43	5.18	0.71	2.34	3.63	0.50	1.64	7.31
Chemical properties	10	k_s = 10 cm^3/g	1.55	2.25	2.22	2.23	1.45	1.43	1.44	1.01
	11	ks = 1 cm^3/g	1.55	3.33	1.53	2.33	2.15	0.99	1.50	2.17
	12	H= 0.042	1.50	3.10	1.59	2.33	2.07	1.06	1.56	1.95
	13	H= 4.2	1.58	5.71	0.52	2.51	3.62	0.33	1.59	10.93
	14	D_{air} = 142.2 cm^2/h	1.54	4.15	1.03	2.49	2.70	0.67	1.62	4.03
	15	D_{air} = 568.8 cm^2/h	1.56	5.94	0.53	2.55	3.81	0.34	1.64	11.14
	16	D_{water}= 0.016 cm^2/h	0.78	3.71	0.204	1.54	4.75	0.26	1.97	18.19
	17	D_{water} = 0.066cm^2/h	3.07	7.61	1.54	4.20	2.48	0.50	1.37	4.94

Table 2.6 (cont.)

Model Results for Hydrus 1-D Simulations

	Simulation Number	Description	Source 200 cm below water table							
			E_{static} [g/cm^2-h] x 10^8	E_{max} [g/cm^2-h] x 10^8	E_{min} [g/cm^2-h] x 10^8	E_{mean} [g/cm^2-h] x 10^8	E_{max}/E_{static}	E_{min}/E_{static}	E_{mean}/E_{static}	E_{max}/E_{min}
	18	Reference (TCE, monthly 30 cm water table fluctuation, no adsorption)	4.87	1.26	0.214	0.66	2.59	0.44	1.36	5.89
Water table fluctuation pattern	19	Annual, 30 cm	4.87	0.744	0.338	0.521	1.53	0.69	1.07	2.20
	20	daily, 30cm	4.87	3.82	3.67	3.74	7.84	7.54	7.67	1.04
	21	Monthly, 1 cm	5.22	0.55	0.499	0.521	1.06	0.96	1.00	1.11
	22	Monthly, 100 cm	4.2	3.36	0.00832	1.10	8.01	0.02	2.61	404
Vadose zone thickness	23	50 cm	4.87	170	7.26	66.2	348.11	14.92	135.94	23.34
	24	500 cm	4.87	0.731	0.617	0.680	1.50	1.27	1.40	1.19
Soil types	25	Loam	4.56	3.01	2.21	2.57	6.60	4.84	5.64	1.36
	26	Coarse sand	4.32	1.67	0.045	0.608	3.86	0.10	1.41	34.43
Chemical properties	27	k_s = 10 cm^3/g	4.87	0.611	0.604	0.607	1.25	1.24	1.25	1.01
	28	k_s = 1 cm^3/g	4.87	0.921	0.431	0.649	1.89	0.88	1.33	2.14
	29	H= 0.042	4.81	0.843	0.467	0.654	1.75	0.97	1.36	1.80
	30	H= 4.2	4.90	1.45	0.148	0.688	2.96	0.30	1.40	9.79
	31	D_{air} = 142.2 cm^2/h	4.86	1.04	0.270	0.616	2.14	0.56	1.27	3.86
	32	D_{air} = 568.8 cm^2/h	4.88	1.47	0.185	0.645	3.01	0.38	1.32	7.94
	33	D_{water} = 0.016 cm^2/h	2.44	0.840	0.101	0.414	3.45	0.42	1.70	8.29
	34	D_{water} = 0.066cm^2/h	9.72	2.06	0.486	1.19	2.12	0.50	1.22	4.24

Water table fluctuation pattern. The emission response to daily, monthly and annual water table fluctuations was examined under the two source zone conditions discussed above (sources 50 and 200 cm below the initial water table). Figures 2.23 and 2.24 present the chemical emissions responses to water table oscillations of different frequencies and magnitudes. In these two figures, dynamic steady state chemical emission rates are normalized to emission rates under static water table conditions for each set of conditions (E_{static} in Table 2.6). The emissions plotted here are dynamic steady state emissions and the time plotted on the x-axis is relative to the repeating water table elevation pattern and not to the initial start of the model run.

The following observations come from those simulation results and Table 2.6:

- As discussed above (e.g. Equation 9), larger magnitude water fluctuations over shorter periods are expected to result in more advective mass flux into the water table fluctuation region and result in increased long-term VOC emissions. E_{mean}/E_{static} increased with decreasing water table oscillation period (P) from years to days, and with increasing water table fluctuation magnitude (L) from 1 cm to 100 cm. The most significant increases were found at daily oscillations, for which simulated E_{mean}/E_{static} were 10.99 and 7.67 for 50 cm and 200 cm source depths below the initial water table level, respectively.
- The temporal variability in emissions can also be evaluated using E_{max}/E_{min} values. These values increased with increasing water table fluctuation magnitude from 1 cm to 100 cm. Over two orders of magnitude variation was found under 100 cm monthly water table oscillations. This can be

expected from Equation (11). While E_{max}/E_{min} values were less predictable regarding oscillation frequency, the temporal changes were all less than 8X for 30 cm water table fluctuation simulations.

E_{mean}/E_{static} is >1 for all simulations. This suggests that models assuming static water table conditions will likely underestimate long-term average emissions and VI impacts, although that difference between the simulations with and without water table fluctuations is <50% for most cases modeled.

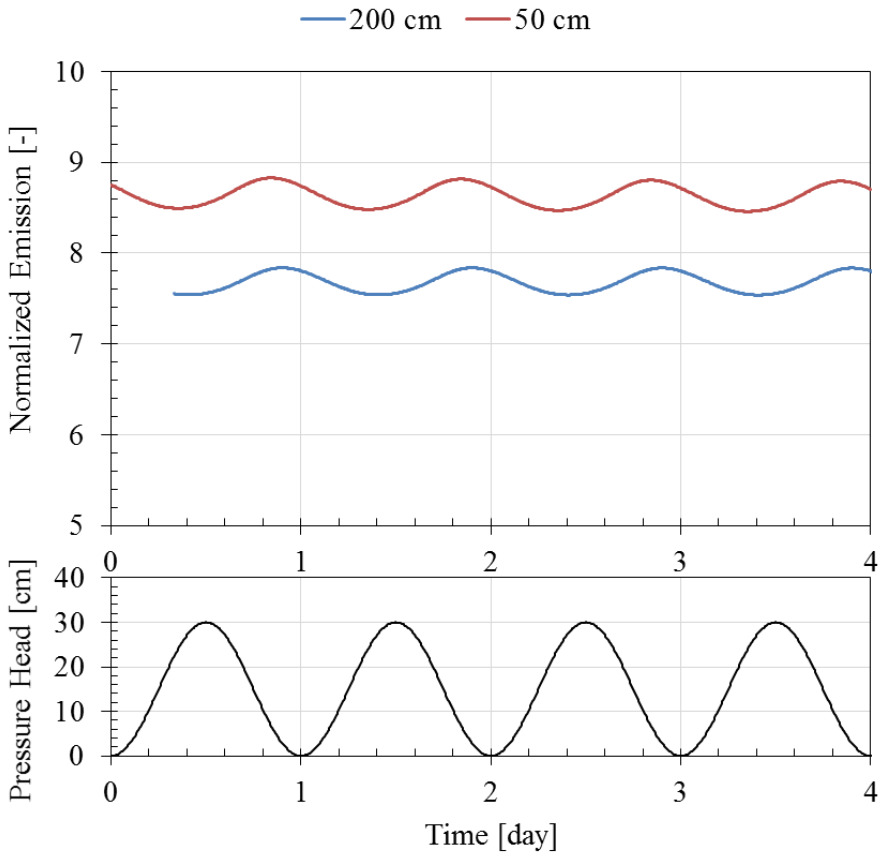

(a)

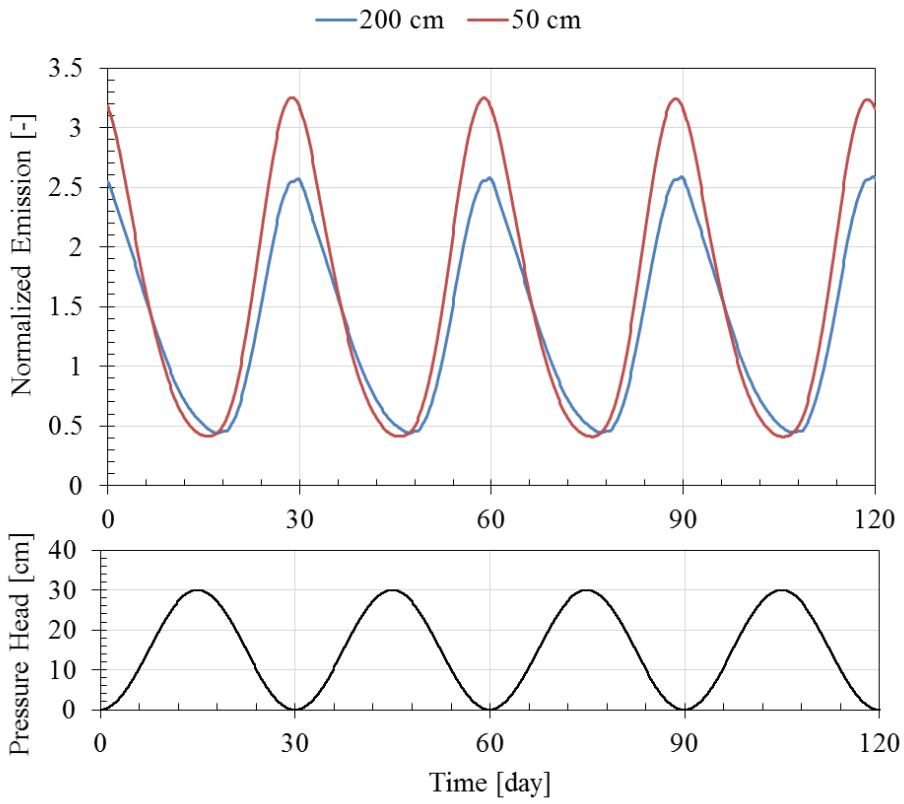
200 cm
50 cm
Normalized Emission [-]
3.5
3
2.5
2
1.5
1
0.5
0
0
30
60
90
120
Pressure Head [cm]
40
30
20
10
0
0
30
60
90
120
Time [day]

(b)

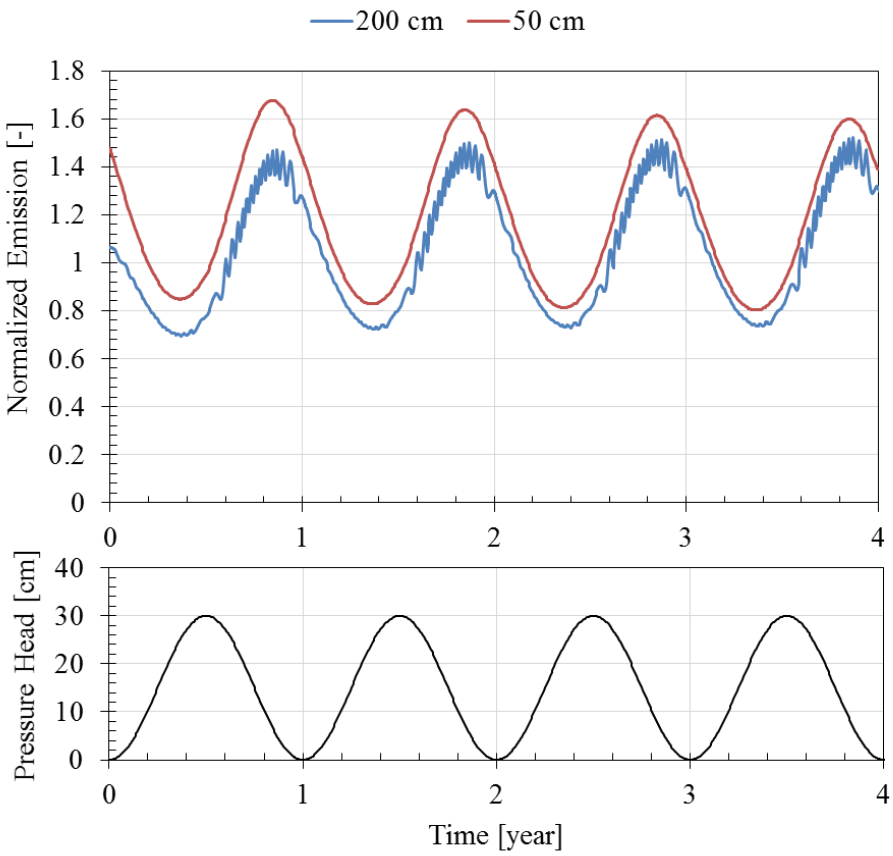

(c)

Figure 2.23. Dynamic steady state TCE emissions normalized to static water table condition emissions. Simulation results for 30 cm water table fluctuations and a contaminant source located 50 and 200 cm below the water table. Various water table fluctuation frequencies are shown (a) daily fluctuation, (b) monthly fluctuation and (c) annual fluctuation. Water pressure head is plotted relative to the initial water table elevation at the bottom boundary vs. time.

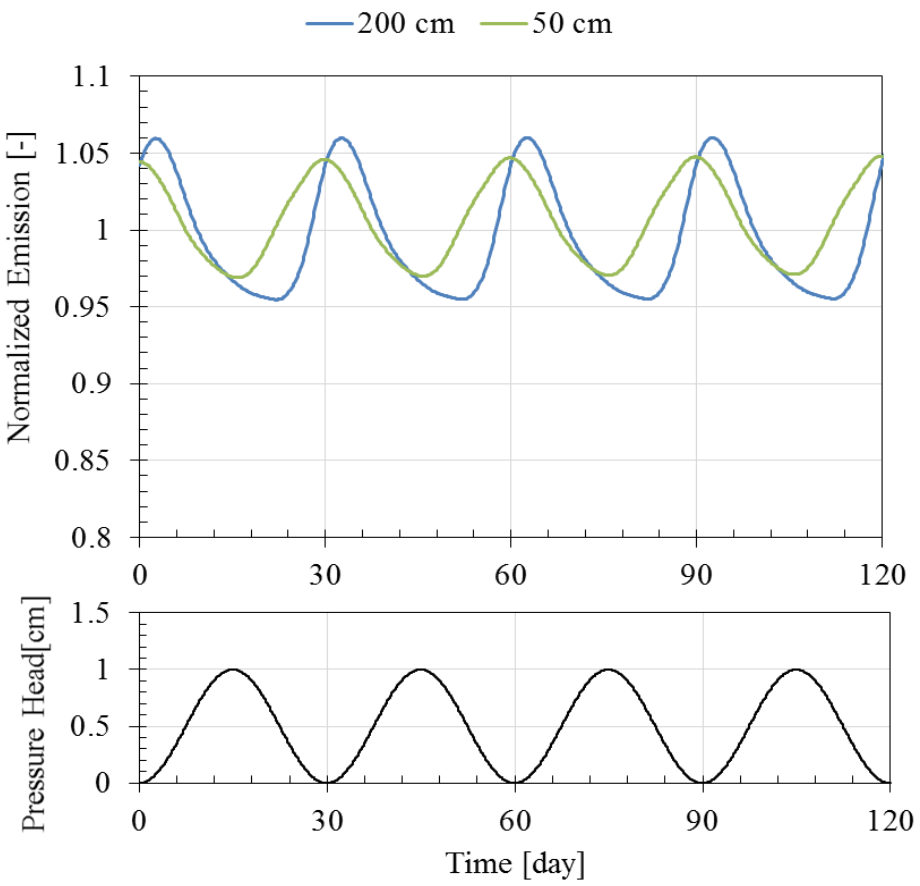
200 cm
50 cm
Normalized Emission [-]
1.1
1.05
1
0.95
0.9
0.85
0.8
0
30
60
90
120
Pressure Head[cm]
1.5
1
0.5
0
0
30
60
90
120
Time [day]

(a)

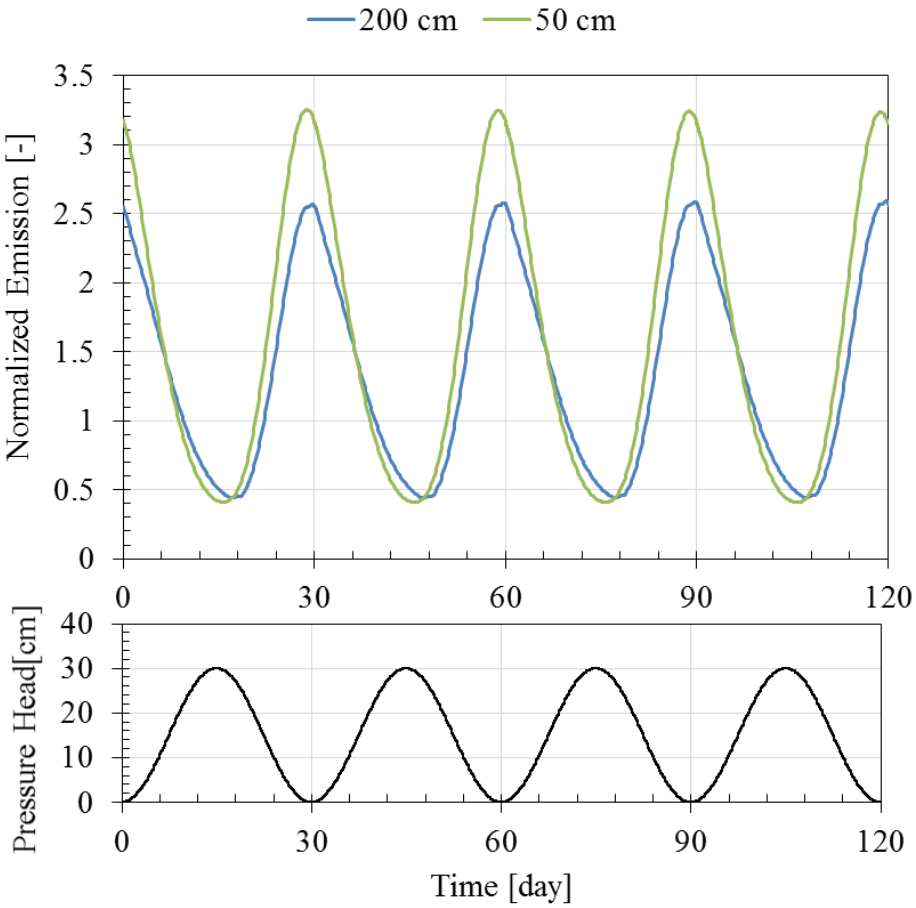
200 cm
50 cm
Normalized Emission [-]
3.5
3
2.5
2
1.5
1
0.5
0
0
30
60
90
120
Pressure Head[cm]
40
30
20
10
0
0
30
60
90
120
Time [day]

(b)

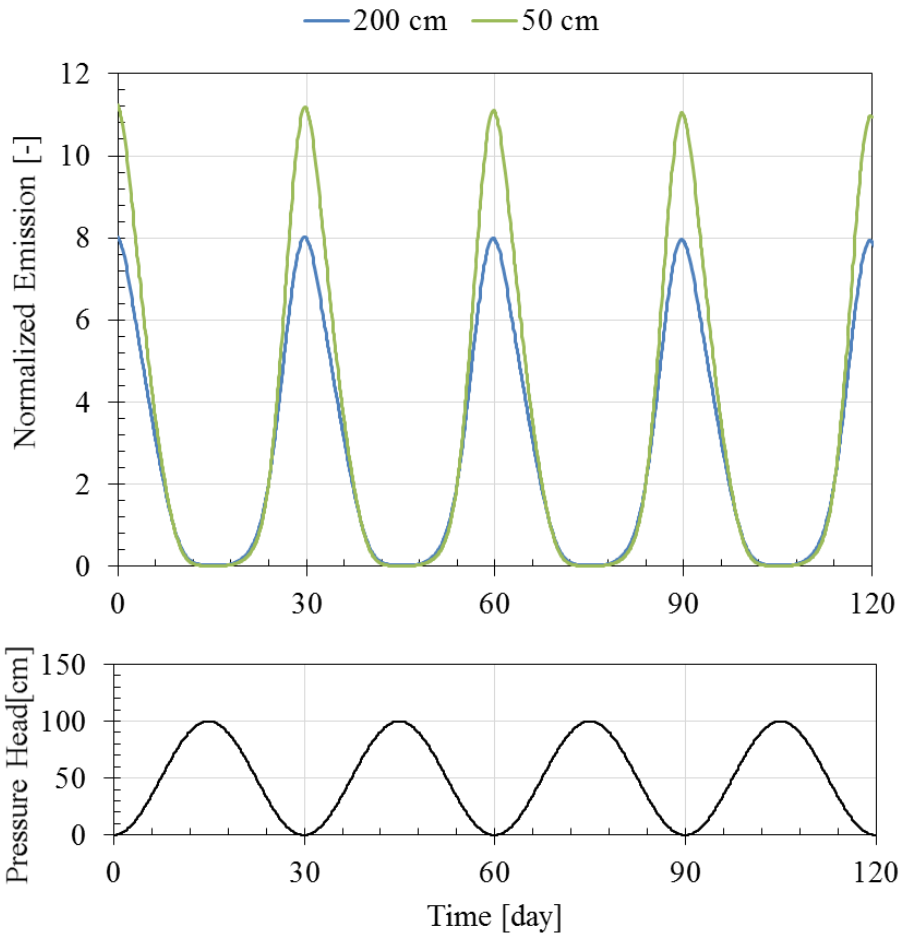

(c)

Figure 2.24. Dynamic steady state TCE emissions normalized to initial static water table condition emissions. Simulation results for monthly water table fluctuations of 1 cm, 30 and 100 cm magnitude, where the source zone is located at (a) 50 cm below water table and (b) 200 cm below water table. Water pressure head is plotted relative to the initial water table elevation at the bottom boundary vs. time.

Vadose zone thickness. Figure 2.25 presents TCE emissions for 50 cm, 150 cm and 500 cm vadose zone thicknesses. E_{max}/E_{min} values increased as the depth to groundwater decreased. From a 500 cm vadose zone thickness to a 50 cm thickness, E_{max}/E_{min} increases from 1.24 to 25.6 for a source zone 50 cm below the water table, and from 1.19 to 23.3 for a source zone 200 cm below water table. This can be explained by

the mass capacitance term in Equation (11), where decreased D_{vadose} reduced the value of this term, which decreases its dampening effect

The greatest E_{mean}/E_{static} values (34.4 and 135.9) were found for simulations with 50 cm vadose zone thickness. This reflects the contributions of two factors: smaller diffusion distances that decrease significantly during the water table fluctuation cycle and less mass storage between the emission point and ground surface. Overall, the most significant temporal changes and long-term emission increases were found for simulations with D_{vadose} = 50 cm, so attention should be paid when assessing shallow water table VI sites.

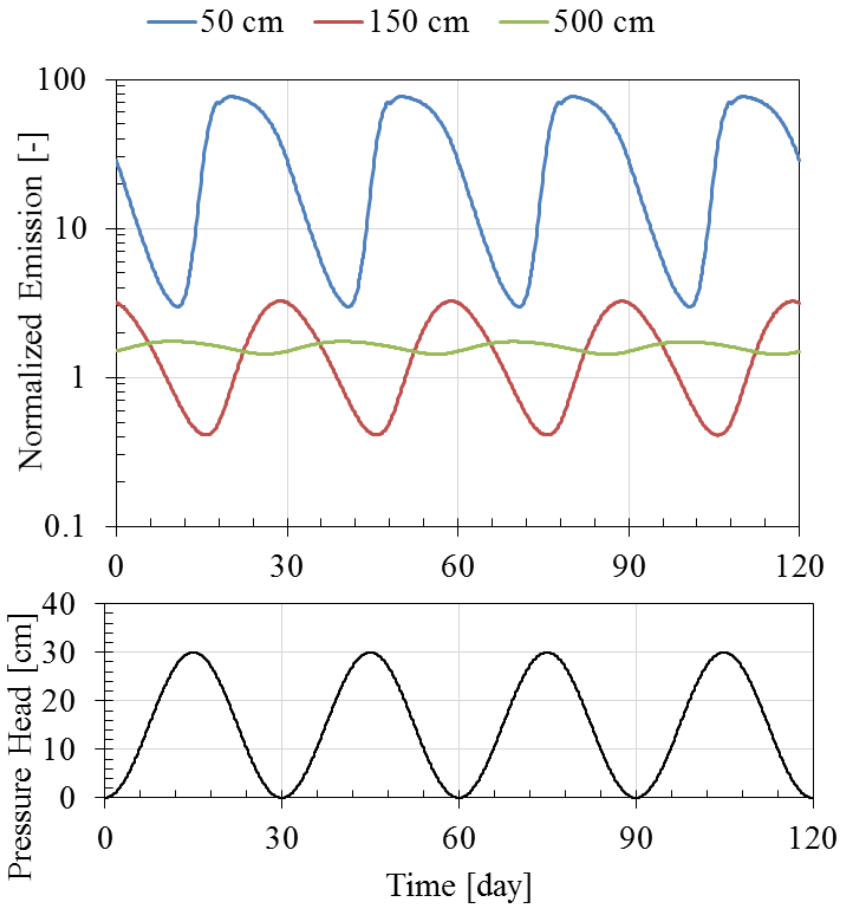

(a) Source 50 cm below water table

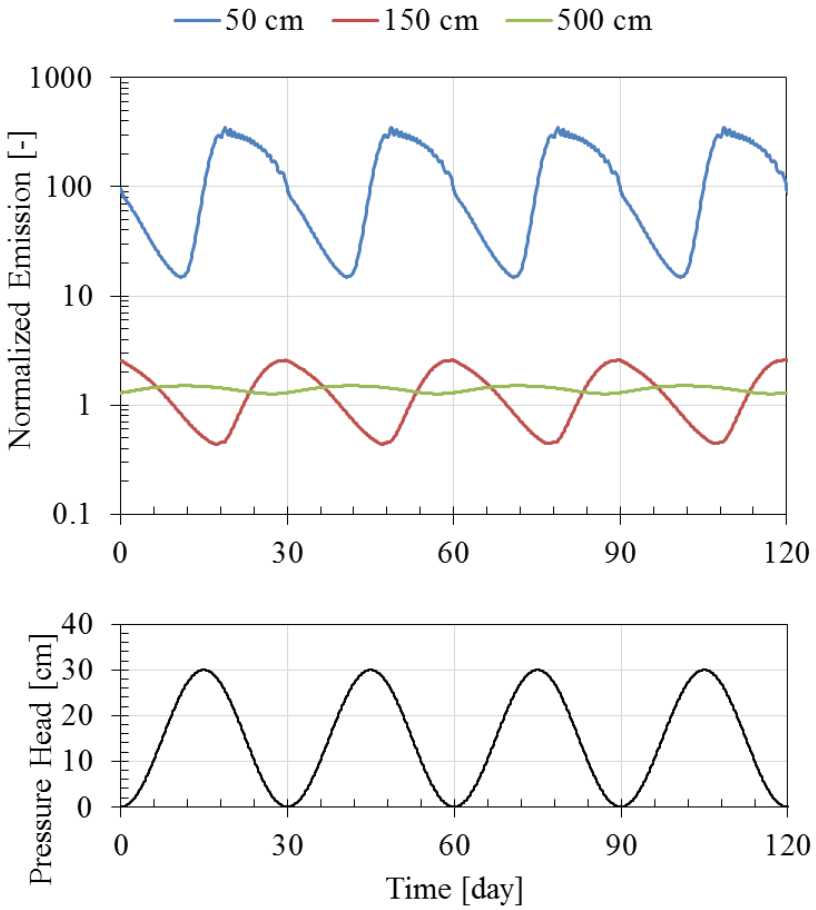

(b) Source 200 cm below water table

Figure 2.25. Dynamic steady state TCE emissions normalized to static water table condition emissions. Simulation results for scenarios with vadose zone thicknesses of 50, 150 and 500 cm where (a) the source zone is 50 cm and (b) 200 cm below water table. Water pressure head is plotted relative to the initial water table elevation at the bottom boundary vs. time.

Soil types. Simulations were run for three types of soil (coarse sand, sand, and loam) under monthly 30 cm water table oscillations. The estimated capillary rise for each is about 5 cm, 20 cm and over 200 cm, respectively. The normalized TCE emissions are shown in Figure 2.26. E_{max}/E_{min} values were greater for the coarse sand than loam - indicating more temporal variability. This is because the flow of water (up and down)

responds more quickly and completely to head changes in the higher permeability soil. As the permeability decreases, the actual water level rise and fall (not the head changes) are dampened (slower and of smaller magnitude). This can be seen in the out-of-phase emissions behavior for loam in Figure 2.26.

The E_{max}/E_{min} values that were close to unity for the finer-grained loam soil are consistent with observations from the field site which had fine-grained silts and clays. The E_{mean}/E_{static} values were greater for loam than the other two types of soil – indicating greater amplification of emissions relative to a static water table case.

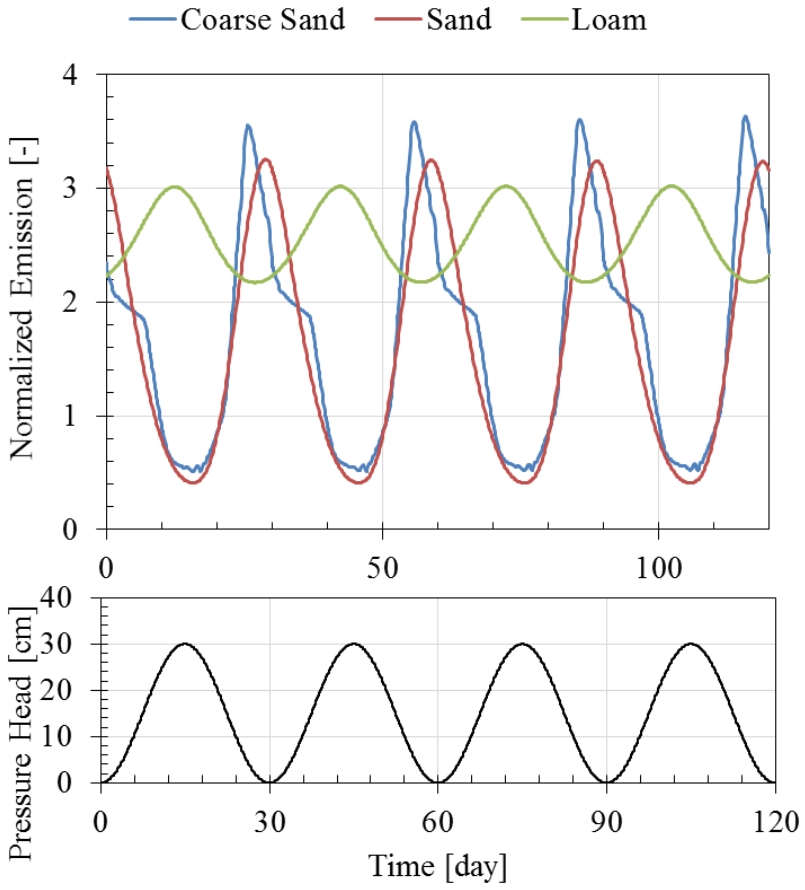

(a) Source 50 cm below water table

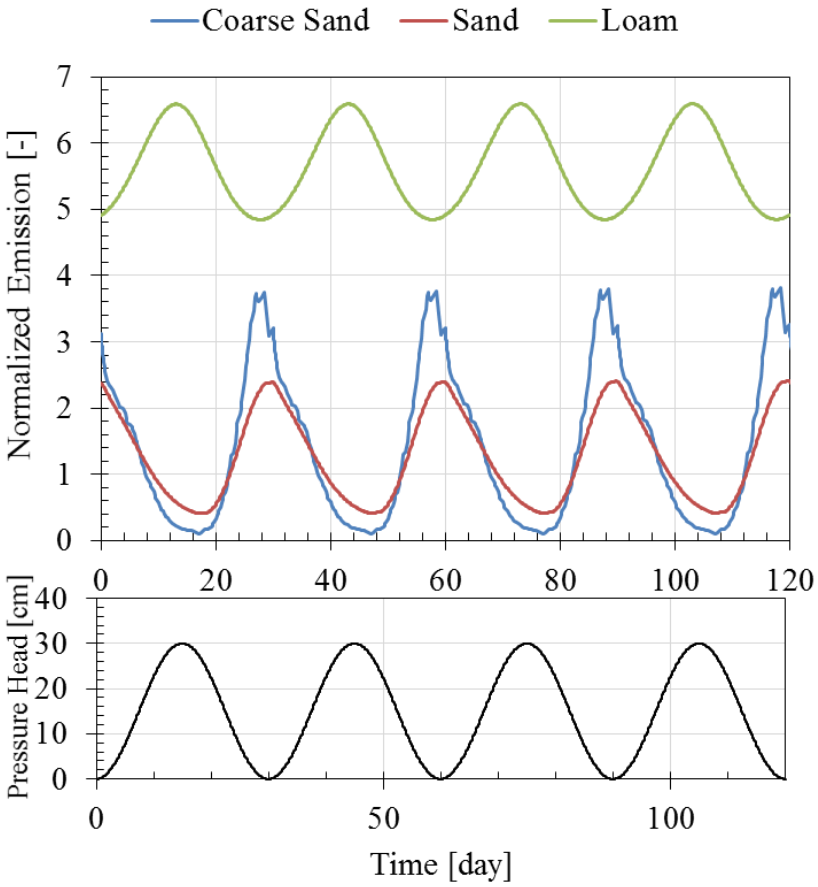

(b) Source 50 cm below water table

Figure 2.26. Dynamic steady state TCE emissions normalized to initial static water table condition emissions. Simulation results for scenarios with monthly water table fluctuations at coarse sand, sand and loam soils, and the source zone a) 50 cm below water table and (b) 200 cm below water table. Water pressure head is plotted relative to the initial water table elevation at the bottom boundary vs. time.

Chemical properties. The influences of effective absorption coefficient (k_s), Henry's law constant (H_i), and the diffusion coefficients in air and water (D_{air} and D_{water}) were tested by varying the reference chemical (TCE) properties by two orders of magnitude for H_i and 4X for diffusion coefficients. The normalized emissions are shown in Figures 2.27 to 2.30. Overall, changing the chemical properties had little effect on

long-term average emission levels, as E_{mean}/E_{static} values varied less than 100 % from static water level results. In general:

- Water table fluctuations caused greater emission rate changes for more volatile chemicals. When H_i increased about 100X, the E_{max}/E_{min} values increased about 5X for both source zone conditions. This is consistent with the laboratory observations, where TCE emissions increases were greater than those for 1,2-DCA in all tests by about 2X and the H_i values differed by about 10X.
- k_s values equal to 0, 1 and 10 cm^3-H_2O/g-soil were input for monthly 30 cm water table fluctuations in sand. Partitioning between soil organic matter and water/gas can be seen as a buffering effect that reduces variation. As seen, the amplitude of TCE emissions decreased when k_s changed from 0 to 10 cm^3-H_2O/g-soil.
- The simulation results for different k_s and H_i values agreed with Equation (11), the dampening of emissions at the water table decreased with increasing H_i and decreasing k_s because of less capacitance for mass storage in the vadose zone.
- As shown in Table 2.6 and Figures 2.28 and 2.29, increasing magnitude in emission fluctuations is likely to occur for lower D_{water} and higher D_{air}. Greater E_{max}/E_{min} values are found when D_{water} was set at 50% of TCE properties vs. set at 2X greater. High D_{air} values lead to greater temporal variations, approximately 10X variations were found when D_{air} value was

set at 568.8 cm^2/h, whereas only 4X differences are found for the simulations using a D_{air} value of 142.2 cm^2/h.

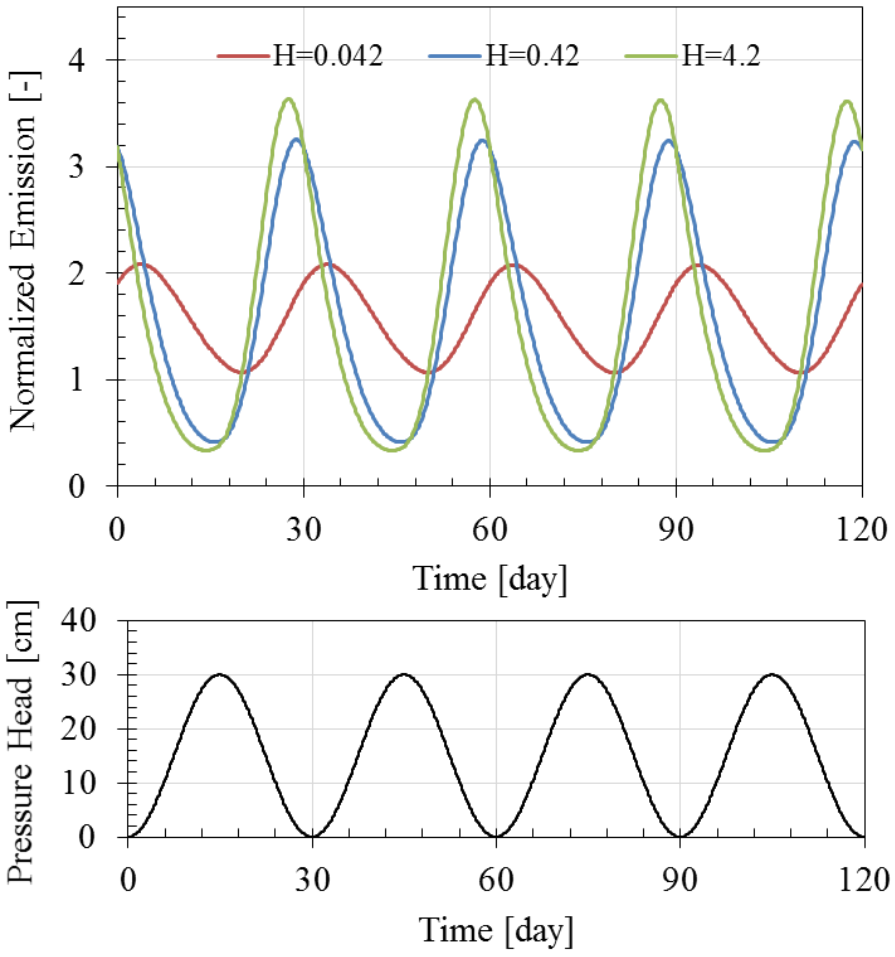

(a) Source 50 cm below water table

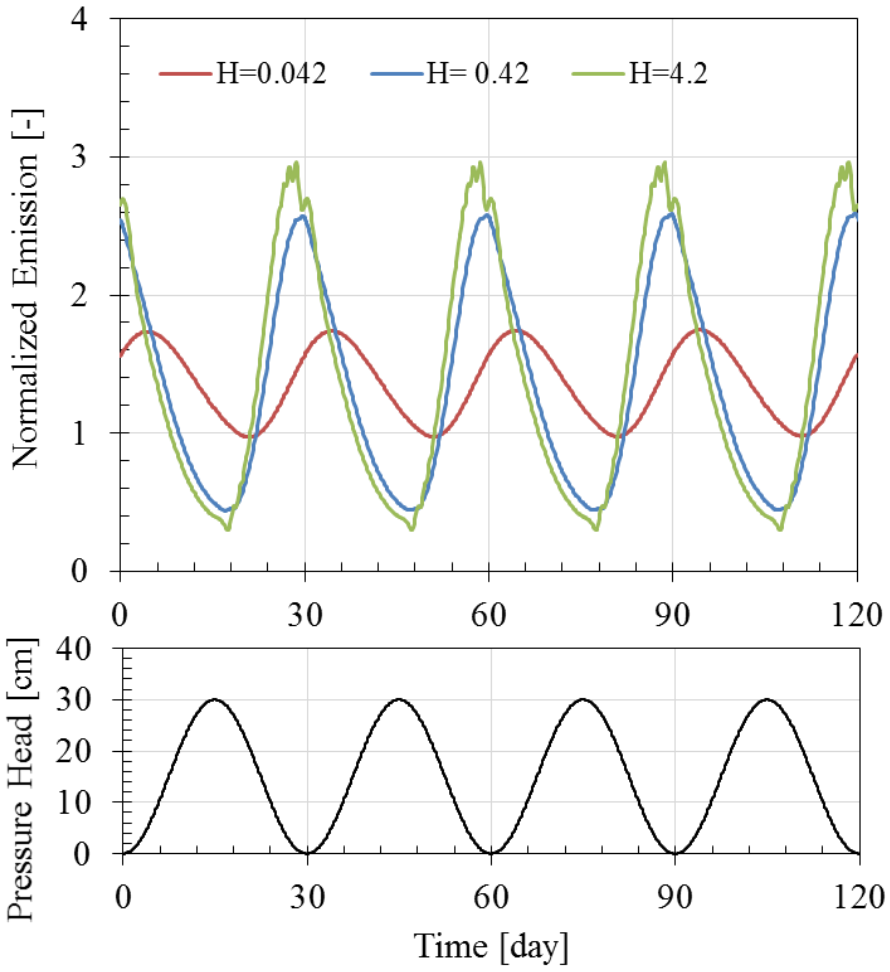

(b) Source 200 cm below water table

Figure 2.27. Dynamic steady state TCE emissions normalized to static water table condition emissions. Simulation results for scenarios with monthly water table fluctuations and Henry's Law constant values of 0.042, 0.42 and 4.2, and the source zone a) 50 cm below water table and (b) 200 cm below water table. Water pressure head is plotted relative to the initial water table elevation at the bottom boundary vs. time.

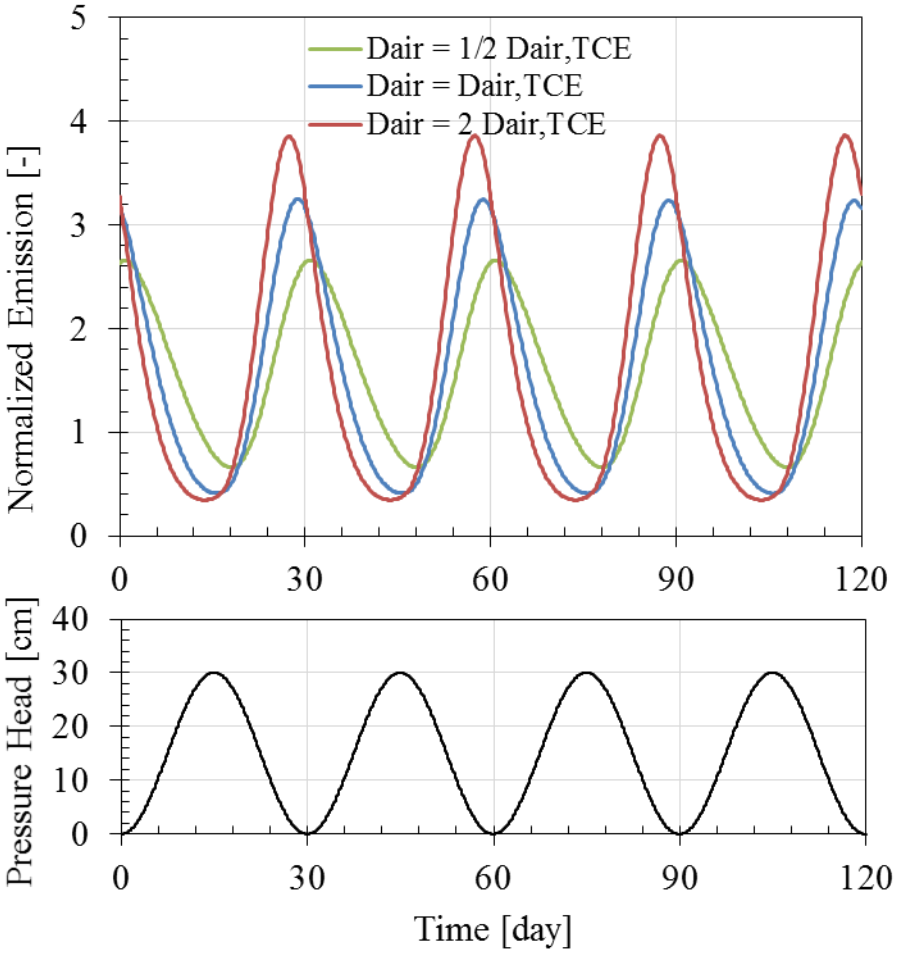

(a) Source 50 cm below water table

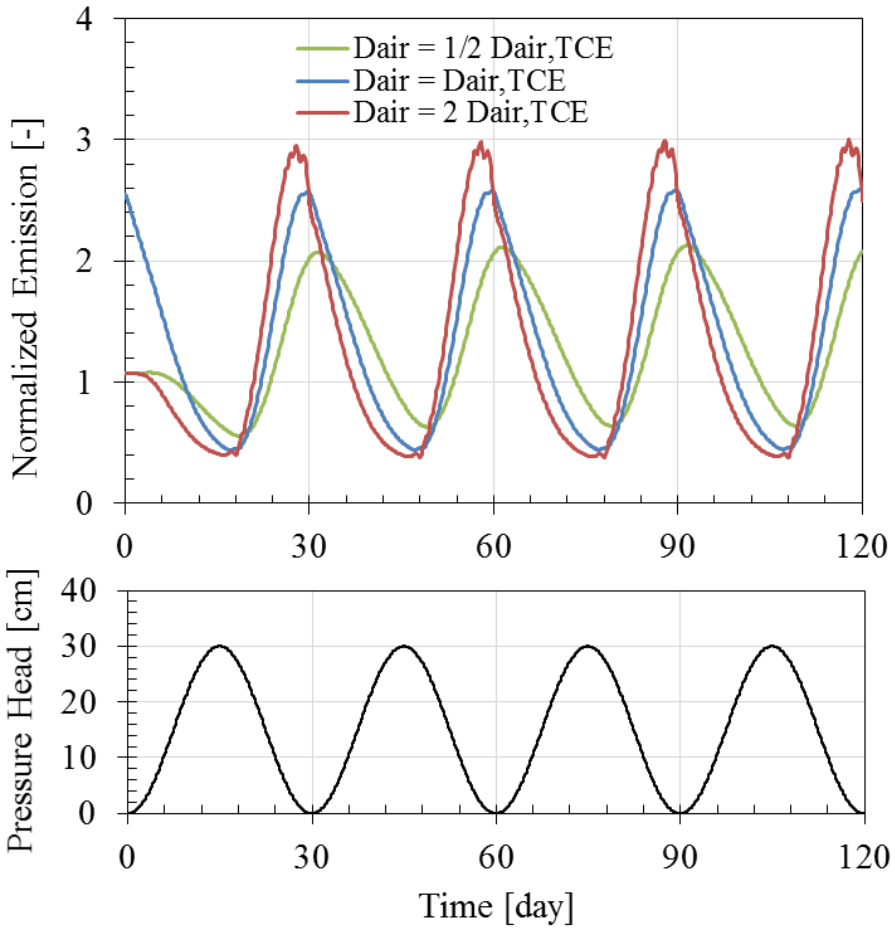

(b) Source 200 cm below water table

Figure 2.28. Dynamic steady state TCE emissions normalized to static water table condition emissions. Simulation results for scenarios with monthly water table fluctuations and chemical molecular diffusion coefficients in air of 0.142.2, 284.4 and 568.8 cm^2/h, and the source zone a) 50 cm below water table and (b) 200 cm below water table. Water pressure head is plotted relative to the initial water table elevation at the bottom boundary vs. time.

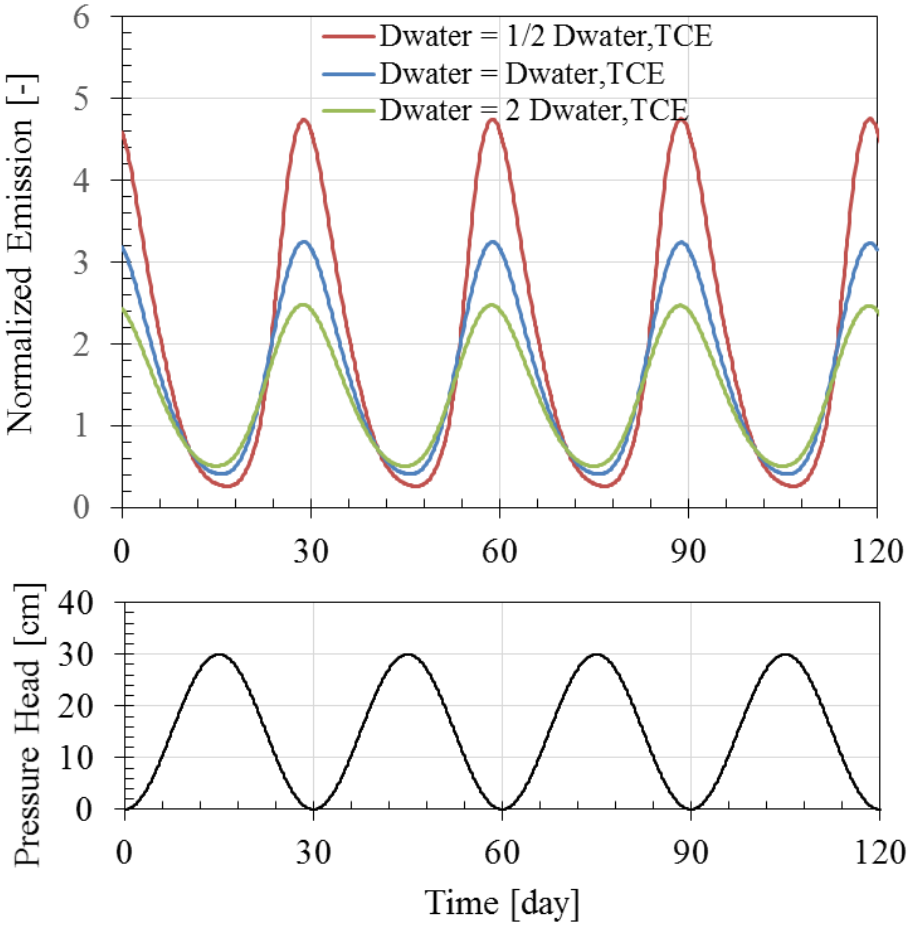

(a) Source 50 cm below water table

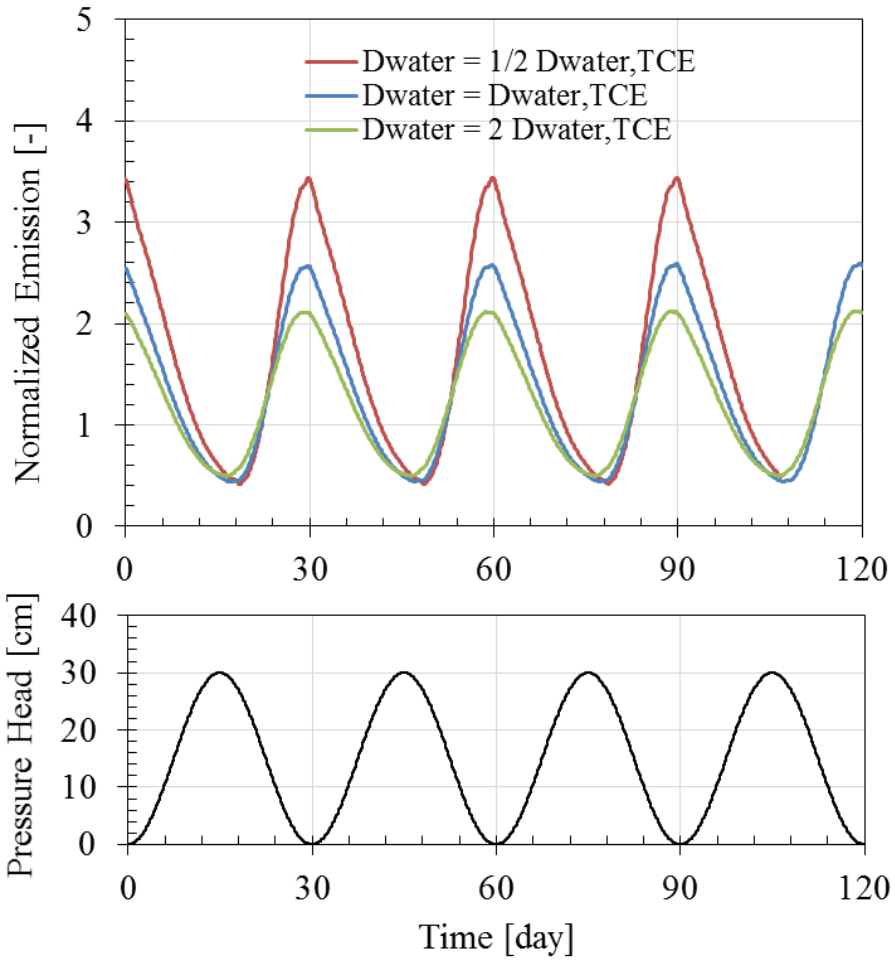

(b) Source 200 cm below water table

Figure 2. 29. Dynamic steady state TCE emissions normalized to static water table condition emissions. Simulation results for scenarios with monthly water table fluctuations and chemical molecular diffusion coefficients in water of 0.016, 0.033 and 0.066 cm^2/h, and the source zone a) 50 cm below water table and (b) 200 cm below water table. Water pressure head is plotted relative to the initial water table elevation at the bottom boundary vs. time.

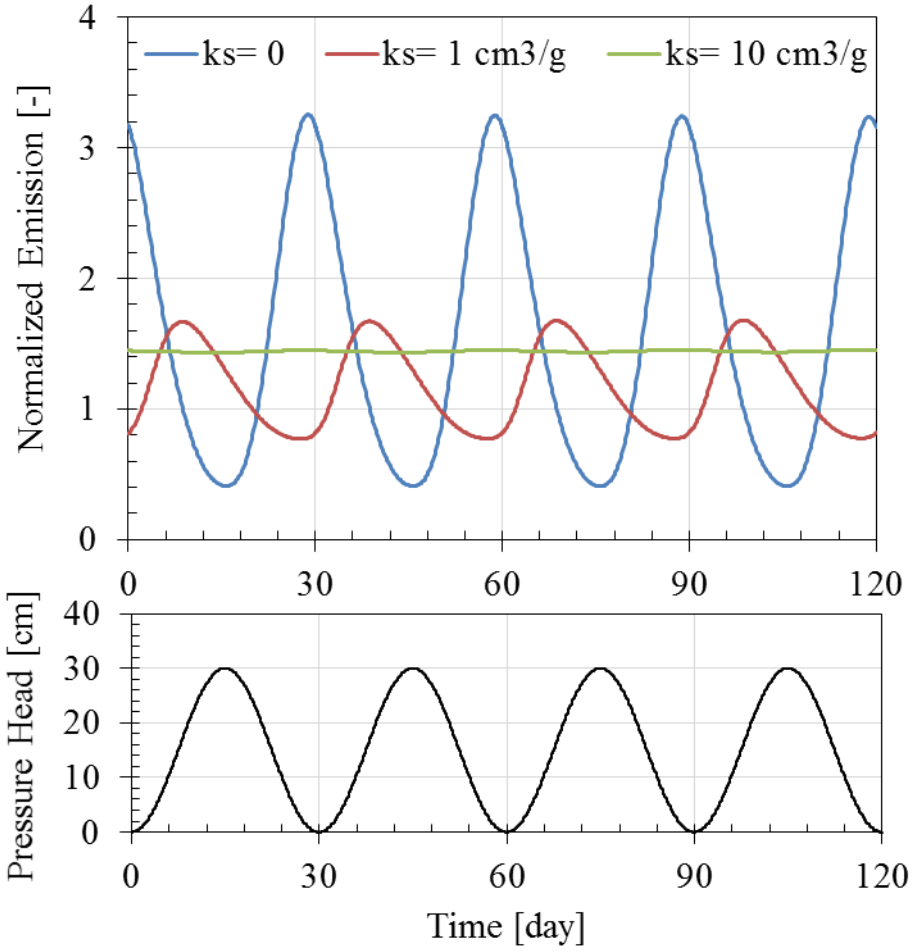

(a) Source 50 cm below water table

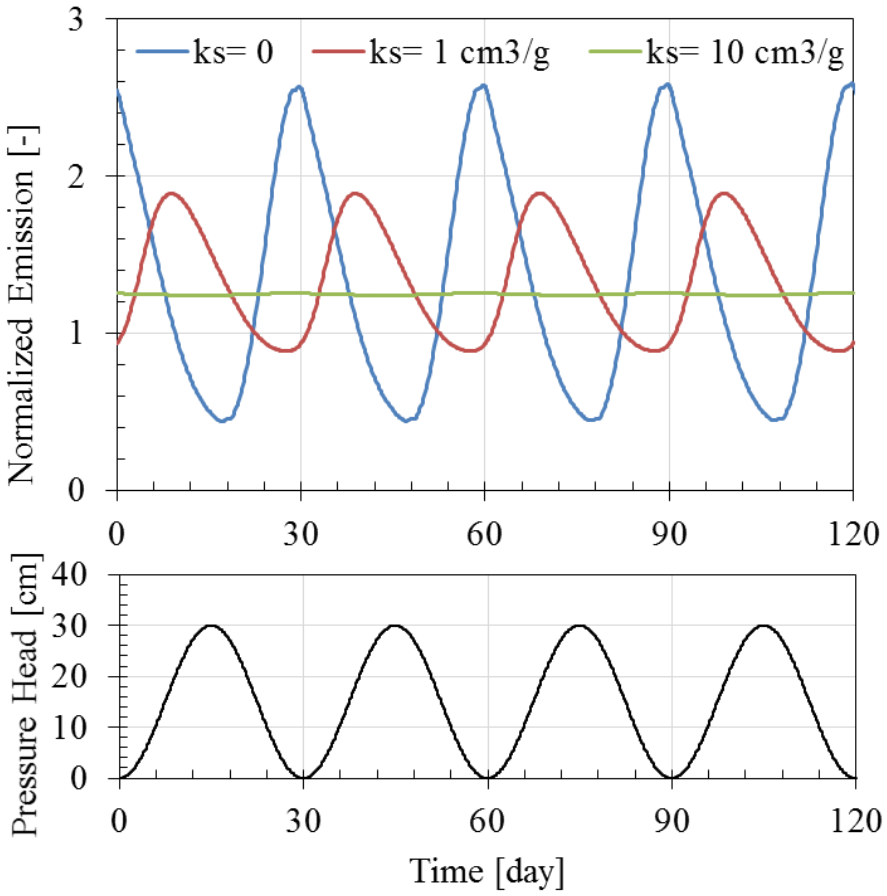

(b) Source 200 cm below water table

Figure 2.30. Dynamic steady state TCE emissions normalized to static water table condition emissions. Simulation results for scenarios with monthly water table fluctuations and effective sorption coefficients of 0, 1 and 10 L/kg, and the source zone at a) 50 cm below water table and (b) 200 cm below water table. Water pressure head is plotted relative to the initial water table elevation at the bottom boundary vs. time.

2.5 CONCLUSION

This chapter focused on improving our understanding of the connection between temporal changes in water table fluctuations and vapor intrusion (VI) impacts. This was accomplished through analysis of field site data, direct measurement in lab tests, and simulation studies. With respect to the two main issues raised at the beginning of this

chapter: a) identifying conditions for which temporal variations in emissions will and will not be significant, and b) identifying scenarios where fluctuating groundwater tables produce emissions that are significantly different from the base-case static water table scenario:

- Water table fluctuations will cause temporal changes in emission rates from dissolved plumes, but in many cases the short- and long-term average magnitude of these changes may be small relative to observed temporal variability in VI impacts (Folkes et al. 2009, USEPA 2012, Holton et al. 2013) caused by other factors like time-varying indoor-outdoor pressure differentials. For example, temporal variations in emissions calculated by two different methods for the field site were 50% or less about the long-term average, while indoor air concentrations varied by two to three orders-of-magnitude under natural conditions.
- For the scenarios examined in the simulation exercise, the long-term mean emission rate was greater, but usually within about 50% of the emissions for the static water table case. Exceptions occurred in cases with high frequency water table fluctuations (e.g., daily oscillations in simulations #3 and #20) and large water table elevation changes relative to the vadose zone thickness (e.g., simulations #6 and #23 with 30 cm fluctuations and 50 cm vadose zone; and simulations #5 and #22 with 100 cm fluctuations and 150 cm vadose zone).
- Short-term peak increases in emissions measured in laboratory experiments were less than about 4X the base case with a static water

table. The E_{max}/E_{min} ratio for most simulation results was less than this as well except in conditions with greater amplitude water table fluctuations (e.g., 100 cm oscillations in simulations #5 and #22), shallower vadose zones (e.g., simulations #9 and #26 with coarse sand). It should be noted that scenarios with higher E_{max}/E_{min} ratios did not always have high long-term increases in emissions. For example, for simulation scenario #5 with E_{max}/E_{min} = 1687, the long-term mean was only 3.26X greater than the emission rate with a static groundwater table.

While more simulations are needed to explore a fuller range of conditions, the field data, lab results, and model simulation output suggest that the scenarios most likely to result in significant temporal changes in emission rates (10X or greater) and rates that are greatly amplified relative to static water table conditions are those involving water table fluctuations that are large relative to the vadose zone thickness; either because the groundwater is shallow (<1 m below ground surface) and fluctuations are moderate (e.g., 50 cm at any reasonable frequency) or because the groundwater table is deeper and the magnitude of fluctuations is larger and significant relative to the average vadose zone thickness.

2.6 REFERENCES

Abreu, L., Johnson, P. C. (2005). Effect of vapor source-building separation and building construction on soil vapor intrusion as studied with a three-dimensional numerical model. *Environmental Science and Technology*, *39* (12), 4550-4561.

Bozkurt, O., Pennell, K. G., Suuberg, E. M. (2009). Simulation of the vapor intrusion process for nonhomogeneous soils using a three-dimensional numerical model. *Groundwater Monitoring and Remediation*, *29* (1), 92-104.

Escobar Melendez, E. A. (2012). Transport and Biodegradation of Petroleum Hydrocarbon Vapors in the Subsurface. A Laboratory Soil Column Study (Doctoral dissertation). Arizona State University.

Folkes, D., Wertz, W., Kurtz, J., Kuehster, T. (2009). Observed spatial and temporal distributions of CVOCs at Colorado and New York vapor intrusion sites. *Ground Water Monitoring and Remediation*, *29*, 70-80.

Hubbard, L. M., Mellander, H., Swedjemark, G. A. (1996). Studies on temporal variations of radon in Swedish single-family houses. *Environment International*, 22, 715-722.

Holton, C.; Luo, H., Dahlen, P., Gorder, K. A., Dettenmaier, E. M.; Johnson, P. C. (2013). Temporal variability of indoor air concentrations under natural conditions in a house overlying a dilute chlorinated solvent groundwater plume. *Environmental Science and Technology, 47*, 13347-13354.

Johnson, P. C., Bruce, C., Johnson, R. L., Kemblowski, M. W. (1998). In situ measurement of effective vapor-phase porous medium diffusion coefficient. *Environmental Science and Technology*, 32, 3405-3409.

Leduc, C., Bromley, J., Schroeter, P. (1997). Water table fluctuation and recharge in semi-arid climate: some results of the HAPEX-Sahel hydrodynamic survey (Niger). *Journal of Hydrology*, 188, 123-138.

Li, H., Jiao, J. J. (2005). One-dimensional airflow in unsaturated zone induced by periodic water table fluctuation. *Water resources research, 41*(4).

Luo, H. (2009). Field and modeling studies of soil gas migration into buildings at petroleum hydrocarbon impacted sites (Dissertation). Arizona State University, Tempe, AZ.

Interstate Technology & Regulatory Council. (2007). *Vapor intrusion pathway: A practical guideline*. Washington, DC: Interstate Technology & Regulatory Council.

McCarthy, K. A.; Johnson, R. L. (1993). Transport of volatile organic compound across the capillary fringe. *Water Resources Research, 29* (6), 1675-1683.

New Jersey Department of Environmental Protection. (2013). *Vapor intrusion technical guidance.* Trenton, NJ: New Jersey Department of Environmental Protection.

Parker, J. C. (2003). Modeling volatile chemical transport, biodecay, and emission to indoor air. *Groundwater Monitoring & Remediation*, 23(1), 107-120.

Picone, S., Valstar, J., van Gaans, P., Grotenhuis, T., Rijnaarts, H. (2012). Sensitivity analysis on parameters and processes affecting vapor intrusion risk. *Environmental Toxicology and Chemistry, 31* (5), 1042-1052.

Shen, R., Pennell, K. G., Suuberg, E. M. (2012). A numerical investigation of vapor intrusion – the dynamic response of contaminant vapors to rainfall events. *Science of the Total Environment*. *437*, 110-120.

Šimůnek, J.; Šejna, M.; Saito, H.; Sakai, M.; van Genuchten, M. Th. The HYDRUS-1D software package for simulating the one-dimensional movement of water, heat, and multiple solutes in variably-saturated media. California, Riverside: University of California Riverside.

Turk, L. J. (1975). Diurnal fluctuations of water tables induced by atmospheric pressure changes. *Journal of Hydrology*. 26(1), 1-16.

U.S. Environmental Protection Agency. (2000). Johnson and Ettinger (1991) Model for Subsurface Vapor Intrusion into Buildings (3-Phase System Models and Soil Gas Models). Washington, DC: U.S. Environmental Protection Agency.

U.S. Environmental Protection Agency. (2002). *OSWER draft guidance for evaluation the vapor intrusion to indoor air pathway from groundwater and soils (Subsurface vapor intrusion guidance).*Washington, DC: U.S. Environmental Protection Agency.

U.S. Environmental Protection Agency. (2012). *Conceptual model scenarios for the vapor intrusion pathway*. Washington, DC: U.S. Environmental Protection Agency.U.S. Environmental Protection Agency. (2015). *OSWER TECHNICAL GUIDE FOR ASSESSING AND MITIGATING THE VAPOR INTRUSION PATHWAY FROM SUBSURFACE VAPOR SOURCES TO INDOOR AIR*. Washington, DC: U.S. Environmental Protection Agency.

U.S. Environmental Protection Agency. (2012). *Fluctuation of indoor radon and VOC concentrations due to seasonal variations*. Washington, DC: U.S. Environmental Protection Agency.

Wener, D.; Hohener, P. (2002). The influence of water table fluctuations on the volatilization of contamination from groundwater. *IAHS PUBLICATION*, 213-218.

Yao, Y., Pennell, K. G., Suuberg, E. M. (2010). The influence of transient processes on vapor intrusion processes. In Air and Waste Management Association Vapor Intrusion Conference. Chicago, IL (pp. 29-30).

CHAPTER 3

IDENTIFICATION OF ALTERNATIVE VAPOR INTRUSION PATHWAYS USING CONTROLLED PRESSURE TESTING, SOIL GAS MONITORING, AND SCREENING MODEL CALCULATIONS

Text adapted from, "Identification of Alternative Vapor Intrusion Pathways Using Controlled Pressure Testing, Soil Gas Monitoring, and Screening Model Calculations" with associated supporting information (Guo et al., 2015).

3.0 ABSTRACT

Vapor intrusion (VI) pathway assessment and data interpretation have been guided by an historical conceptual model in which vapors originating from contaminated soil and/or groundwater diffuse upward through soil and are swept into a building by soil gas flow induced by building under-pressurization. Recent studies reveal that alternative VI pathways involving neighborhood sewers, land drains, and other major underground piping can also be significant VI contributors, even to buildings beyond the delineated footprint of soil and groundwater contamination. This work illustrates how controlled pressure method testing (CPM), soil gas sampling, and screening level emissions calculations can be used to identify significant alternative VI pathways that might go undetected by conventional sampling under natural conditions at some sites. The combined utility of these tools is shown through data collected at a long-term study house where a significant alternative VI pathway was discovered and altered so that it could be manipulated to be on or off. Data collected during periods of natural and CPM conditions show that the alternative pathway was significant but its presence was not

identifiable under natural conditions; it was identified under CPM conditions when measured emission rates were two orders of magnitude greater than screening model estimates and sub-foundation vertical soil gas profiles changed and were no longer consistent with the conventional VI conceptual model.

3.1 INTRODUCTION

Guidance for assessing the vapor intrusion (VI) to indoor air pathway varies (USEPA, 2002; ITRC, 2007; NJDEP, 2013), but most emphasize multiple-lines-of-evidence (MLE) approaches involving combinations of point-in-time indoor air, sub-slab soil gas, deeper soil gas, groundwater, and soil sampling, along with screening-level or more complex transport modeling. The VI pathway assessment strategy and data interpretation are guided by a conceptual site model (CSM). A generic conventional VI pathway CSM for a site over contaminated groundwater is shown in Figure 3.1a: vapors diffuse upward through soil and away from impacted groundwater and are swept into the building through foundation cracks and perforations by advective flow induced by building under-pressurization. This route to indoor air is referred to as the "soil VI" pathway in this paper, and is the route focused on in most modeling and data interpretation paradigms (Johnson and Ettinger, 1991; USEPA, 2002; Abreu and Johnson, 2005; Bozkurt et al., 2009; USEPA, 2012).

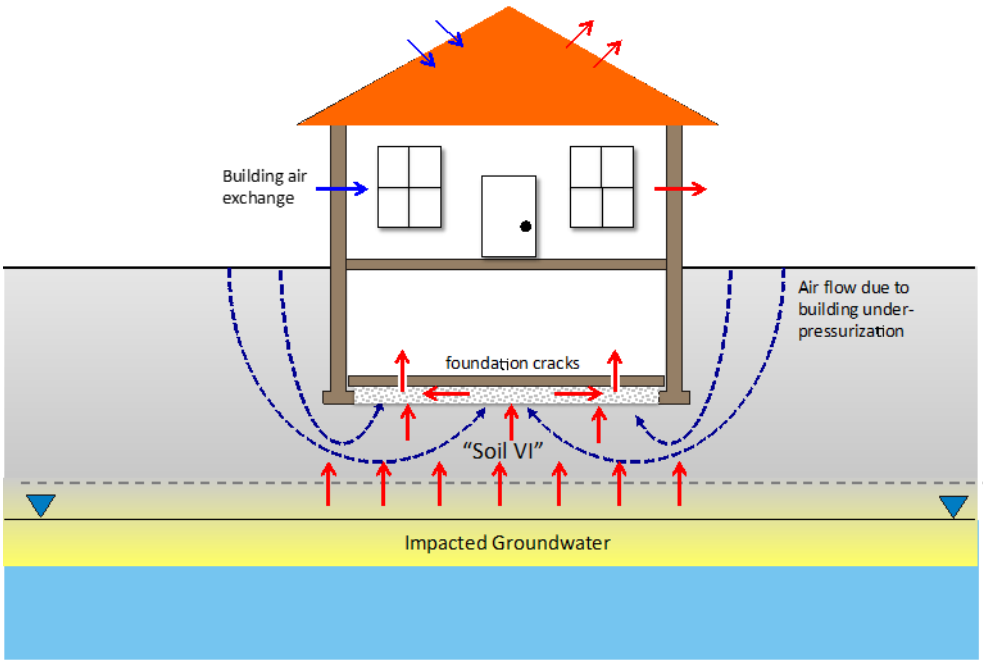

(a) Conventional vapor intrusion pathway conceptualization showing only the "*soil VI*" pathway.

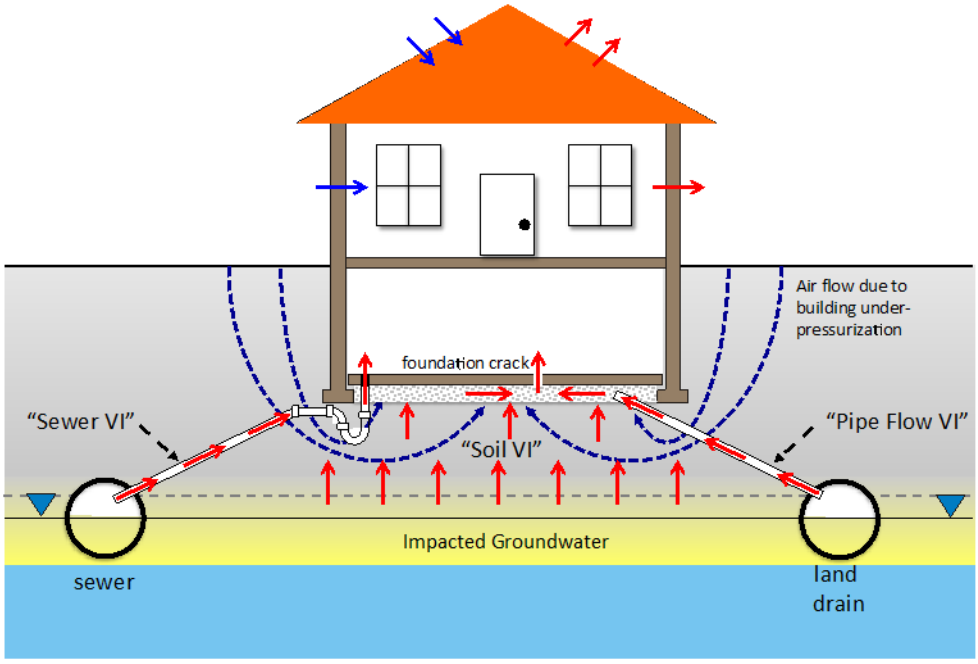

(b) Vapor intrusion pathway conceptualization showing the "*pipe flow VI*" and "*sewer VI*" alternative VI pathways.

Figure 3.1. Conceptualization of vapor intrusion pathways.

In addition to contaminated soils and aquifers, subsurface pipe networks (e.g., sewer mains and land drains) may also contain contaminants of concern either from chemical discharge to those systems or from inflow of contaminated groundwater or vapors originating from subsurface contamination. These neighborhood sewers, land drains, and other major underground piping can distribute chemical-containing water and vapor beyond delineated footprints of regional dissolved groundwater plumes. Vapors in them can be drawn into indoor air through two routes as shown in Figure 3.1b: a) flow through piping or conduits to the sub-foundation region and subsequent migration to indoor air via foundation cracks and permeations, and b) through direct connection of plumbing fixtures to indoor air. These alternative VI pathways are referred to as the "pipe flow VI pathway" and "sewer VI pathway" here. The significance of alternative VI pathways has recently begun to be reported; for example, Riis et al (2010) confirmed that VI impacts to homes outside a chlorinated hydrocarbon-impacted groundwater plume were due to vapors emanating from contaminated groundwater flowing into the sewer system. Similarly, Pennell et al. (2013) concluded that tetrachloroethylene (PCE) in indoor air at their study site was the result of sewer VI.

Identifying VI pathways and understanding their significance is critical when VI mitigation system selection and design are needed. Sub-slab depressurization (SSD), which is the presumptive remedy for VI impacts (USEPA, 2008), is known to be effective where soil VI is the dominant pathway, but it might not be protective for homes where pipe flow and sewer VI pathways are significant. While this has not yet been demonstrated in a well-controlled study, passive sub-slab ventilation was ineffective for

the buildings reported by Riis et al. (2010), and we are aware of another site where SSD has been ineffective at mitigating VI impacts in a building screened for indoor sources.

Most buildings have plumbing connections and subsurface infrastructure and therefore the potential for alternative VI pathways; however, the presence of these VI pathways and their significance are not easily discerned via simple observation, building drawings, or traditional site characterization. For example, alternative VI pathways were discovered by Riis et al. (2010) and Pennell et al. (2013) because they had more temporally and spatially extensive data sets than is typical. Riis et al. (2010) suspected alternative sewer VI pathways because VI-impacts were detected in homes outside of a plume footprint. They determined through indoor air, sub-slab and sewer sampling that sewers were serving as alternate VI pathways. Pennell et al. (2013) reached a similar conclusion at a home where indoor air contaminant concentrations were higher on an upper level than the lowest level.

Below we present our experiences at a well-studied and documented house (Holton et al., 2013; Holton et al., 2015) where a significant alternative pipe-flow VI pathway went undetected during multi-year high-frequency sampling under natural conditions, and was only discovered through the combined use of indoor air and soil gas sampling during manipulation of the building pressure and screening-level modeling. After detection, the alternative pathway was modified to allow on/off control of it during testing. This provided a unique opportunity to collect VI pathway assessment data under natural and controlled under-pressurization conditions, with and without the connection of the alternative VI pathway.

3.2 SITE DESCRIPTION

The study site is described in Holton et al. (2013, 2015). It includes a two-story, split-level house built into a slope with a 2.5 m elevation drop from the back to front yard. There is a living space and attached garage on the lower level. Multi-level soil gas and groundwater sampling points were installed inside through the foundation and outside of the building, with the soil gas points installed to the following depths relative to the slab elevation: sub-slab (SS), 0.9 m below slab (BS) and 1.8 m BS. The building footprint and sampling locations are shown in Figure 3.2. The house was equipped with attic blower fans to control building under-pressurization as described in Holton et al. (2015).

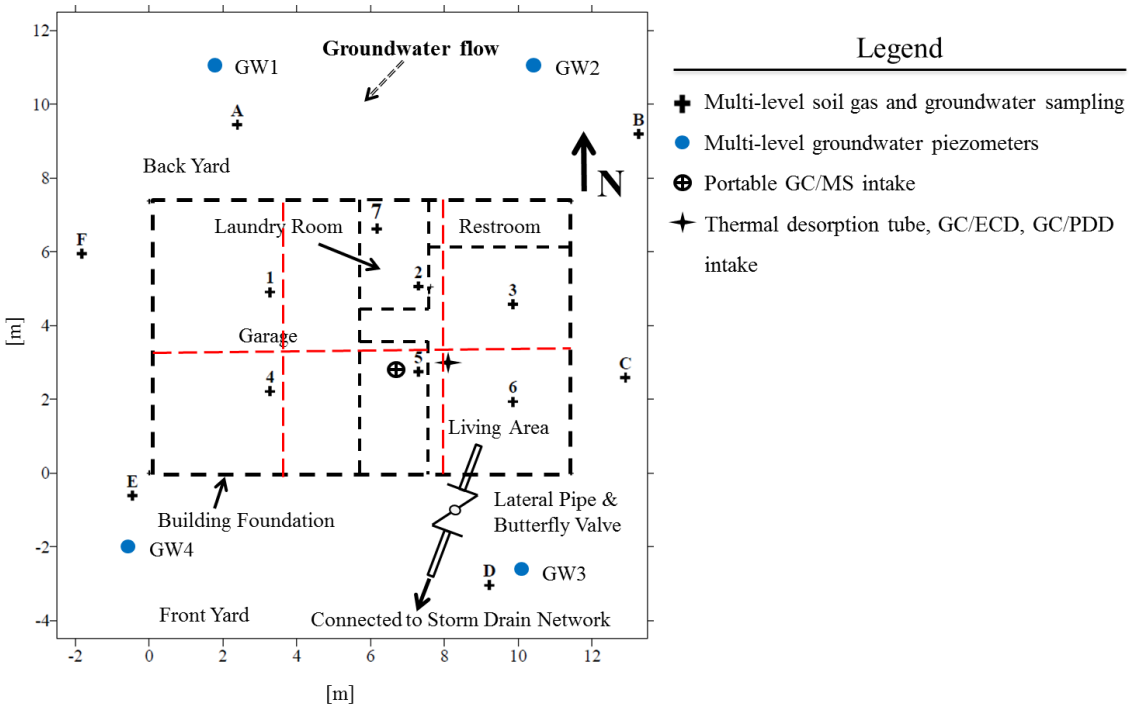

Figure 3.2. Schematic of building footprint, sample locations and lateral land drain pipe with valve installed for this study. Red dashed lines delineate sub areas used for high-resolution screening-level emission estimates.

The study house overlies a dilute dissolved chlorinated solvent groundwater plume containing 1,1-dichlorethylene (1,1-DCE), 1,1,1-trichloroethane (1,1,1-TCA), and trichloroethylene (TCE). Groundwater is at about 2.5 m BS. TCE concentrations in water samples collected below the building foundation ranged from approximately 10 - 50 µg/L over the four years of this study with an average concentration of 24 ± 9 µg/L and no clear long-term temporal trend; the groundwater concentration history is provided in Appendix IV Figure IV.1.

The sub-foundation gravel zone is connected to a neighborhood land drain system running across the southern property boundary through a lateral pipe having one end

open in the sub-foundation gravel near locations 5 and 6. Unknown at the beginning of this study, its presence was suspected from the data presented below. A series of diagnostic tests, (land drain and lateral pipe vapor sampling, land drain manhole water and vapor sampling, SF_6 and Helium tracer release study, videography) confirmed the active lateral pipe connection between the sub-foundation region and the neighborhood land drain system. The lateral pipe was modified at t=1071 d with the installation of a manual butterfly valve to control the connection between the sub-foundation area and the land drain system. Tracer gases (SF_6 and Helium) were released up- and down-stream of the valve with it open and closed to verify its ability to seal the connection between the sub-foundation area and the land drain system. Figure 3.2 presents a schematic of the lateral pipe and valve positions; photos of the lateral pipe and valve can be found in Appendix IV Figure IV.2.

3.3 DIAGNOSTIC TOOLS OVERVIEW

The diagnostic toolset employed at the study site and discussed below includes controlled pressure method (CPM) testing, soil gas sampling, and screening level calculations using typical site characterization data. CPM use was proposed by McHugh et al. (2012) for VI pathway assessment and indoor source identification, and Holton et al. (2015) recently validated its use for quickly and confidently identifying maximum VI impacts without false negative results at their study home overlying a dilute chlorinated solvent plume. CPM test results can be reported as an indoor air concentration and as a mass emission rate into a building. While the former is of interest for human health risk assessment, the latter is of interest here. It can be compared with a screening-level mass

emission calculation as one line of evidence to discern if significant alternative VI pathways are present as outlined below. For example, if the CPM test emission rate greatly exceeds the emission rate predicted with a screening level calculation, then that suggests an inconsistency between actual site conditions and the soil VI conceptual site model, and this could be an indicator of a significant alternative VI pathway. CPM testing will also influence soil gas profiles and the responses could be indicative of significant alternative VI pathways. Specifics of these two data analyses approaches are outlined below.

3.3.1 Comparison of screening-level mass emission rate estimate with emission rate measured during CPM testing. Screening-level mass emission estimates can be calculated from vertical soil gas profiles or source zone vapor concentrations using a one-dimensional diffusion-dominated screening model. For example, when vertical soil gas profiles $C_{g,i}(z)$ [mg/m^3] are available for n sub-areas of the building foundation, a soil VI pathway emission estimate $E_{estimate,i}$ [mg/d] can be calculated for each sub-area i using the soil gas data and measured or estimated overall effective diffusion coefficients D_i^{eff} [m^2/d] obtained from multi-depth sampling locations representative of each sub-area. The total emission then can be obtained by the summation of all sub-area emission rates:

$$E_{estimate} = \sum_{i=1}^{i=n} \left(\frac{D_i^{eff}}{L_i} \right) \Delta C_{g,i} \Delta A_{F,i} \qquad (1)$$

where $\Delta A_{F,i}$ [m^2] is the area of sub-area i, $\Sigma \Delta A_{F,i} = A_F$ is the total building foundation area, and within sub-area i $\Delta C_{g,i}$ is the soil gas concentration difference over the vertical

distance L_i, , and D_i^{eff} [m^2/d] is the overall in situ effective diffusion coefficient for the vertical interval L_i. The effective diffusion coefficient can be measured using the Johnson et al. (1998) tracer method or estimated using the empirical Millington-Quirk expressions as described in Johnson and Ettinger[4]. When the interval L_i has multiple estimated or measured values $D_{i,j}^{eff}$ over m sub-layers of thickness $\Delta L_{i,j}$, where $\Sigma\Delta L_{i,j} = L_i$, and j denotes the sub-layer, then:

$$\left(\frac{D_i^{eff}}{L_i}\right) = \frac{1}{\sum_{j=1}^{j=m} \frac{\Delta L_{i,j}}{D_{i,j}^{eff}}} \qquad (2)$$

When only vapor source concentrations are available, the USEPA spreadsheet implementation of the Johnson and Ettinger model[15] can be used to generate a screening-level emission estimate. In that case $E_{J\&E\text{-}estimate}$ is calculated from the user-specified building exchange rate E_B [1/d] and building volume V_B [m^3], and the indoor air concentration estimate $C_{J\&E\text{-}indoor}$ [mg/m^3] output in the spreadsheet:

$$E_{J\&E\text{-}estimate} = E_B \times V_B \times C_{J\&E\text{-}indoor} \qquad (3)$$

While the building volume V_B and building exchange rate E_B are inputs to the Johnson and Ettinger model and the concentration output C is dependent on them, the emission rate $E_{J\&E\text{-}estimate}$ is not sensitive to their choice for reasonable values. Once $E_{estimate}$ or $E_{J\&E\text{-}estimate}$ is obtained, it is compared with the measured emission rate $E_{measured}$ from CPM testing (2015). When $E_{measured}$ is more than an order or magnitude greater than $E_{estimate}$ (or $E_{J\&E\text{-}estimate}$), then this might indicate a significant alternative pathway, or other discrepancies between actual site conditions and a simplistic VI site conceptual model.

The discrepancies could also include mischaracterization of soil properties and soil gas concentrations, or the presence of constituent production mechanisms (e.g., daughter product production from parent decay) not accounted for in the screening-level modeling.

3.3.2 Response of soil gas profiles during CPM testing. Soil gas profile response to CPM testing could be different in the presence and absence of alternative VI pathways, as is illustrated below for the study site. For example, for a site with only the soil VI pathway present, shallow soil gas concentrations might increase or decrease during CPM testing, but they should always remain lower than vapor source concentrations (these are referred to as "conforming" soil gas profiles here). With the pipe flow VI pathway present and connected to a relatively high concentration vapor source, it is conceivable that shallow sub-slab soil gas concentrations could become greater than intermediate depth soil gas concentrations. Thus, observation of "non-conforming" soil gas profiles (those that do not match the conventional conceptual model) could indicate significant pipe flow VI at a site. The absence of non-conforming soil gas profiles, however, does not necessarily prove the absence of a significant alternative VI pathway. For example, it is unlikely that non-conforming soil gas profiles would be observed for sewer VI pathways as their contaminant vapor sources are directly connected to indoor air.

Below we illustrate use of the diagnostic tools and analyses discussed above for a home where a significant pipe flow VI pathway was discovered and then modified to be manipulated on and off.

3.4 EXPERIMENTAL METHODS

Data presented below were obtained over four years involving natural and controlled building under-pressurization conditions, and both with the lateral pipe valve open and closed. The time sequence of experimental conditions is summarized in Table 3.1.

Table 3.1

Building operation conditions and indoor air sampling methods.

Period	120 d to 740 d[a]	780 d to 1045 d[b]	1071 d to 1157 d	1157 d +
Building pressure condition	Natural	Controlled under-pressurization	Controlled under-pressurization	Natural
Lateral pipe valve	Open (NI)	Open (NI)	Closed	Closed
Mean of the 24-h averaged pressure differentials (outdoor - indoor)	0.02 ± 0.9 Pa	11 ± 4 Pa	12 ± 1 Pa	0.7 ± 2 Pa
Indoor air sample location: analysis method	Lower level: TD-GC/MS	Lower level: TD-GC/MS Attic: TD-GC/MS Attic: GC/ECD	Lower level: TD-GC/MS Attic: TD-GC/MS Attic: GC/ECD	Lower level: TD-GC/MS

[a]Note: Between 740 d to 780 day, blower system was installed and tested.
[b]Note: Blower speed changed from "High" to "Low" at 1046 d, and switched back to "High" at 1071 d.
NI – butterfly valve not installed on the land drain lateral during this phase of the study.

Indoor air concentrations of chlorinated chemicals and the SF_6 tracer, indoor - outdoor and sub-slab soil gas - indoor pressure differentials, and external environmental

conditions were monitored continuously at frequencies of minutes to hours as described in Holton et al. (2013, 2015).

TCE concentrations in soil gas beneath and around the building foundation were measured 25 times over four years. Soil gas samples were collected in Tedlar bags using a vacuum box. TCE concentrations were quantified on-site using an SRI 8610C gas chromatograph equipped with a dry electrolytic conductivity detector (DELCD). Both direct injection and sorbent-concentration methods were used. The method detection limit (MDL) is 4.9 ppb_v (26 $\mu g/m^3$) for the former and 0.019 ppb_v (0.1 $\mu g/m^3$) for the latter.

Effective diffusion coefficients were measured at the sampling points during five of the soil gas sampling events using the method presented by Johnson et al. (1998) with helium as the tracer.

3.5 DATA REDUCTION

Measured TCE emission rates to indoor air ($E_{measured}$) were determined for CPM test conditions using the Holton et al. (2015) approach: $E_{measured} = C_i \times (C^o_{tracer}/C_{tracer}) \times Q_{tracer}$, with known indoor SF_6 tracer release rate (Q_{tracer}) and concentration (C^o_{tracer}) and measured indoor air tracer and TCE concentrations (C_{tracer} and C_i). Building air exchange flow rates (Q_B) can also be calculated from SF_6 tracer release rate (Q_{tracer}) and tracer concentration data (C_{tracer}) $Q_B = (C^o_{tracer}/C_{tracer}) \times Q_{tracer}$.

For comparison, screening-level TCE emission estimates ($E_{estimate}$ and $E_{J\&E\text{-}estimate}$) were generated using equations (1) – (3) and two different data reduction approaches. In both cases a single "high resolution" estimate was generated using all data collected beneath the foundation footprint and multiple "low resolution" estimates were generated

using the data from each individual 1.8 m BS sampling location exterior to the foundation. This was done to assess if reliance on low resolution exterior sampling yields emission estimates similar to high resolution through-the-foundation sampling, as the former is more likely to be implemented in practice than the latter.

More specifically, $E_{estimate}$, values were generated using TCE soil gas data sets and equations (1) and (2). For the high-resolution estimates, soil gas concentrations from locations 1 to 6 were assigned to 6 foundation footprint sub-regions with 14.1 m^2 areas as shown in Figure 2. The sub-slab and 1.8 m BS concentrations were used to calculate $\Delta C_{g,i}$. Equation (2) was used to calculate $(D_{i,j}^{eff}/L_i)$ by conceptualizing a three-layer soil system beneath the house, with layers of uniform effective diffusion coefficients from 0-30 cm, 30-90 cm and 90-180 cm BS. Effective diffusion coefficients for each sub-region $(D_{i,j}^{eff})$ were obtained by averaging results from the five field surveys for each depth interval. Using equation (1), low resolution estimates were generated using each individual 1.8 m BS TCE exterior sampling point concentration from the 25 soil gas surveys collected across the 4 year study. Each low resolution estimate utilized the same average effective diffusion coefficient $(D_{i,j}^{eff})$ calculated for the five $D_{i,j}^{eff}$ measurements at that 1.8 m BS sampling location.

EJ&E-estimate values were generated using equation (3) and the USEPA spreadsheet implementation (USEPA, 2000) of the Johnson and Ettinger model (1991). As above, high resolution calculations made use of the sub-foundation data and low resolution calculations employed the 1.8 m BS exterior data values. For high resolution estimates, the 1.8 m BS TCE concentrations averaged within the building footprint from each soil gas data set were used as the vapor source concentration input. A three-layer

soil system was also modeled as above with soil properties selected to obtain layer-specific effective diffusion coefficients that are the same as those used above for high resolution Eestimate calculations. Low resolution EJ&E-estimate values were computed in a similar fashion, except with use of individual exterior sampling location data consistent with the low resolution Eestimate calculations above. With respect to soil permeability, each layer was assigned a generic value from the USEPA spreadsheet (USEPA, 2000) based on qualitative soil descriptions; these included sand for the sub-slab layer and sandy clay for the next two layers. All model inputs are summarized in Table 3.2.

Table 3.2

Johnson and Ettinger Model USEPA Spreadsheet Inputs

Depth below grade to bottom of enclosed floor [	30
Soil gas sampling depth below grade [cm]	210
Average soil temperature, C	25
Thickness of soil stratum A [cm]	60
Thickness of soil stratum B [cm]	60
Thickness of soil stratum C [cm]	90
Enclosed floor thickness [cm]	10
Building under-pressurization [Pa]	5
Enclosed space floor length [cm]	1140
Enclosed space floor width [cm]	740
Enclosed space floor height [cm]	210
Floor-wall crack with [cm]	0.1
Air exchange rate [1/h]	0.5
Stratum A soil type permeability (sand) [cm^2]	1.02×10^{-7}
Stratum B soil type permeability (sandy clay) [c	1.79×10^{-9}
Stratum C soil type permeability (sandy clay) [c	1.79×10^{-9}
High Resolution Approach Effective Diffusion Coefficient [cm^2/s]	
Stratum A	1.42×10^{-2}
Stratum B	4.52×10^{-3}
Stratum C	3.80×10^{-3}
Low Resolution Approach Effective Diffusion Coefficients [cm^2/s] are provided in Supplemental Information Table S1	

3.6 RESULTS AND DISCUSSION

The raw data used for calculation of measured and estimated emission rates are presented in Appendix IV Table IV.1 and IV.2 and Figures IV.3 and IV.4. These include measured TCE effective diffusion coefficients $D_{i,j}^{eff}$ (Table IV.1), soil gas TCE concentrations (Table IV.2), indoor air exchange flow rates Q_B (Figure IV.3) and indoor air TCE concentrations (Figure IV.4). Figure IV.2 also presents daily (24-h) average pressure differentials. In brief, $D_{i,j}^{eff}$ values range from 0.001 to 0.02 cm^2/s for tests conducted at 0.9 m BS and 1.8 m BS and for sub-slab depth locations outside the

foundation footprint. Beneath the foundation at the sub-slab depth the $D_{i,j}^{eff}$ values are consistently the largest of all locations, ranging from 0.01 to 0.03 cm^2/s. The ($D_{i,j}^{eff}/L_i$) values calculated using equation (2) are also presented in Table S1. With respect to pressure differential and Q_B values, it was noted that under natural and controlled pressure conditions, both were not significantly influenced by the state (open/closed) of the land drain lateral control valve.

3.6.1 Calculation and Comparison of Measured and Estimated TCE

Emission Rates. Figure 3.3 presents the TCE emission rates measured during CPM testing, first with the land drain lateral connection open to the sub-foundation region (780 – 1045 d) and then later with it closed (1071 – 1157 d). Summary statistics are presented in Table 3.3 for both conditions. The results for 780 – 1045 d were presented previously in Holton et al. (2015), while the latter are being published here for the first time. Under both experimental conditions, the emissions were relatively consistent with time, having minimal variations from day-to-day and across long time periods.

Table 3.3

Summary statistics for measured and estimated TCE emissions rates.

	Measured TCE Emission Rates [g/d]		TCE Emission Rate Estimates [g/d]			
Pressure condition	Controlled Pressure Method Test*	Controlled Pressure Method Test*	High Resolution Data Reduction Approach**		Low Resolution Data Reduction Approach***	
Land Drain Lateral Valve Condition	Open [780 – 1040 d]	Closed [1071 – 1157 d]	$E_{estimate}$	$E_{J\&E\text{-}estimate}$	$E_{estimate}$	$E_{J\&E\text{-}estimate}$
Mean	0.18	1.3×10^{-3}	8.0×10^{-4}	2.7×10^{-4}	7.9×10^{-4}	3.3×10^{-4}
Maximum	0.29	6.3×10^{-3}	1.9×10^{-3}	6.2×10^{-4}	4.6×10^{-3}	1.7×10^{-3}
Minimum	0.09	1.2×10^{-4}	1.3×10^{-4}	4.6×10^{-5}	1.3×10^{-6}	5.4×10^{-7}
90^{th} Percentile	0.26	4.5×10^{-3}	1.3×10^{-3}	4.2×10^{-4}	2.5×10^{-3}	9.5×10^{-4}
10^{th} Percentile	0.12	2.8×10^{-4}	3.2×10^{-4}	1.0×10^{-4}	5.6×10^{-6}	2.4×10^{-6}

* - summary statistics of all daily 24-h average emission rate values determined during the measurement period,

** - summary statistics of high resolution estimates; one high resolution estimate calculated for each of 20 soil gas snapshot sampling events

*** - summary statistics of low resolution estimates; four low resolution estimates calculated for each soil gas snapshot sampling events (one for each of four exterior sampling locations)

TCE emission rate estimates are also presented in Table 3.3 for comparison. There are four columns capturing the different combinations possible with the two calculation approaches (equations 1 and 3) and the high- and low-resolution data analysis approaches discussed above. The ranges of the emission rate estimates are also presented in Figure 3.3 with the measured values.

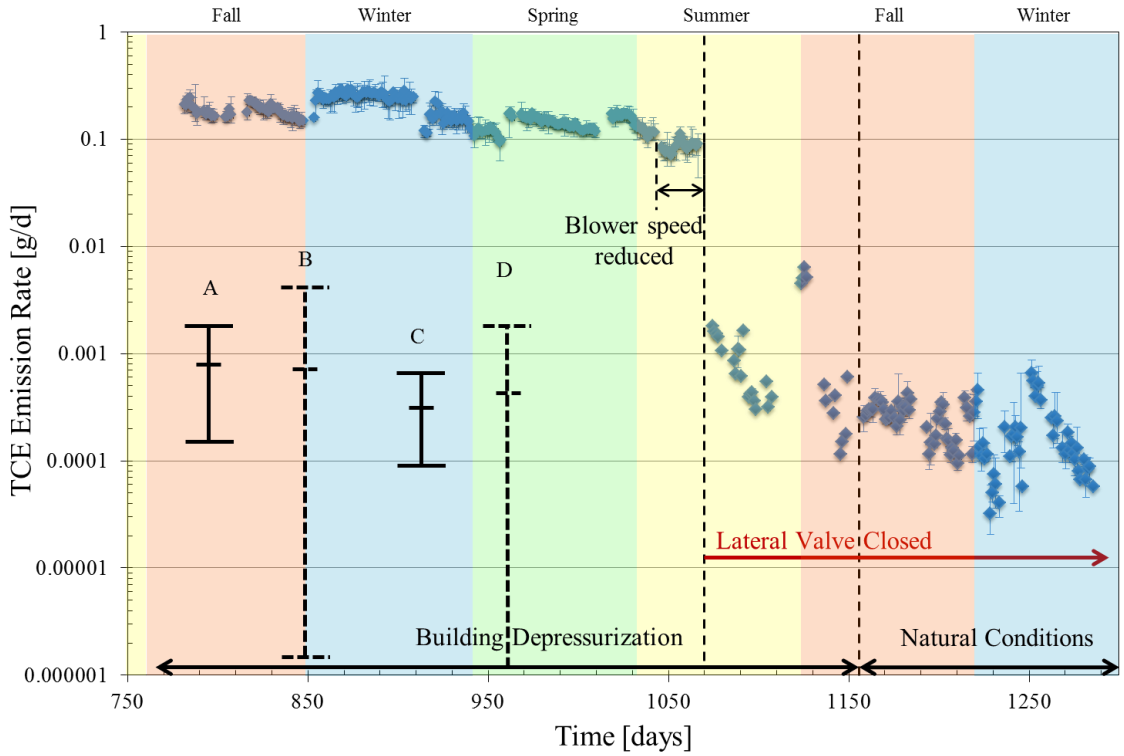

Figure 3.3. Measured 24-h average TCE emission rates for the four building conditions tested with ranges of screening level model estimates, including: A) $E_{estimate}$ using the high-resolution approach, B) $E_{estimate}$ using the low-resolution approach, C) $E_{J\&E\text{-}estimate}$ using the high-resolution approach, and D) $E_{J\&E\text{-}estimate}$ using the low-resolution approach. Horizontal bars on the estimated emission rate ranges indicate the maximum, mean and minimum modeling results (ordered from top to bottom).

The following observations come from a review of Table 3 and Figure 3:

- The contribution of the alternative vapor intrusion pathway (land drain lateral valve open) is clearly evident as the mean measured emission rate with the land drain lateral valve open (0.18 g/d) is about two orders of magnitude greater than the mean emission rate measured with the land drain valve closed (0.0013 g/d).
- The emission rate measured with the land drain valve open is about two orders of magnitude or more greater than any of the emission rate estimates. This supports the hypothesis that an inconsistency between estimated and measured emission rates can be a line of evidence for identifying alternative VI pathways, especially when the emission rate measured during CPM testing is much greater than estimated values.
- All mean emission rate estimates are within about 2X to 4X of the mean emission rate measured with the land drain valve closed; this provides confidence in the use of simple screening equations to estimate the maximum impact from the soil VI pathway.
- The high-resolution method emission rate estimates span less than an order of magnitude and 14 of the 21 values (67%) are within about 50% of their mean value, independent of the screening calculation approach used. This suggests that only a few sampling events would be required to generate a reliable emission estimate and it provides some confidence in the use of the high resolution approach, even though its practicability is questionable.
- The less data intensive and arguably more practicable low resolution method leads to emission rate estimates spanning about three orders of magnitude at this

site, independent of the screening calculation approach used. This variation reflects both spatial and temporal variability in the soil gas concentration data. While they span a wide range, all estimates are significantly less than the emission rate measured with the land drain lateral valve open, so comparison of any with the measured CPM test emission rates would lead to suspicion of the presence of an alternative VI pathway. These results suggest, however, that practitioners should be cautious about relying on a single exterior sampling location and a single sampling event when estimating soil VI pathway emission rates.

- While not shown in Table 3, the mean of the estimates for each of the four exterior location data sets is generally within about 50% of the mean measured emission rate during CPM testing after lateral valve was closed, independent of the screening calculation approach used. This suggests that reliable emission rate estimates might be obtained at other sites with a small number of exterior sampling locations and a few sampling events.

3.6.2 Soil gas distribution response to CPM testing. Figures 3.4 and 3.5 present representative soil gas distributions across the four years of this study. These contour plots were prepared using the soil gas concentrations and locations, and Surfer 12 (Golden Software, Inc.) with its Kriging gridding algorithm. Each plot presents TCE concentration distributions at sub-slab (SS), 0.9 m BS and 1.8 m BS depths. For location C, the ground surface is below the sub-slab elevation, so a 0 ppb_v TCE concentration was assigned to this point when creating contours. The building footprint is shown as a

dashed outline on the sub-slab depth plot with the back of the house being the north side of the plot.

Holton et al. (2013) characterized the indoor air concentration vs. time behavior at this house under natural conditions and with an open land drain lateral valve as having "VI-active" and "VI-inactive" periods. The VI-active behavior was prevalent in fall, winter and early spring, while the VI-inactive behavior was prevalent in late spring and summer. Causes for VI-active and –inactive periods were not identified in that work, although increasing VI activity appeared to be related to increasing indoor-outdoor temperature difference more than any other factor. Figures 4 and 5 present representative TCE soil gas distributions from VI-active and VI-inactive periods, respectively. There are similarities between them at the 0.9 m BS and 1.8 m BS depths, with TCE concentrations generally decreasing when moving from the north to the south (back to front of the house). This reflects the influence of the sloping ground surface, which decreases in elevation by about 2 m from back to front of the house, so sampling points at equivalent elevations are closer to ground surface in the front of the house.

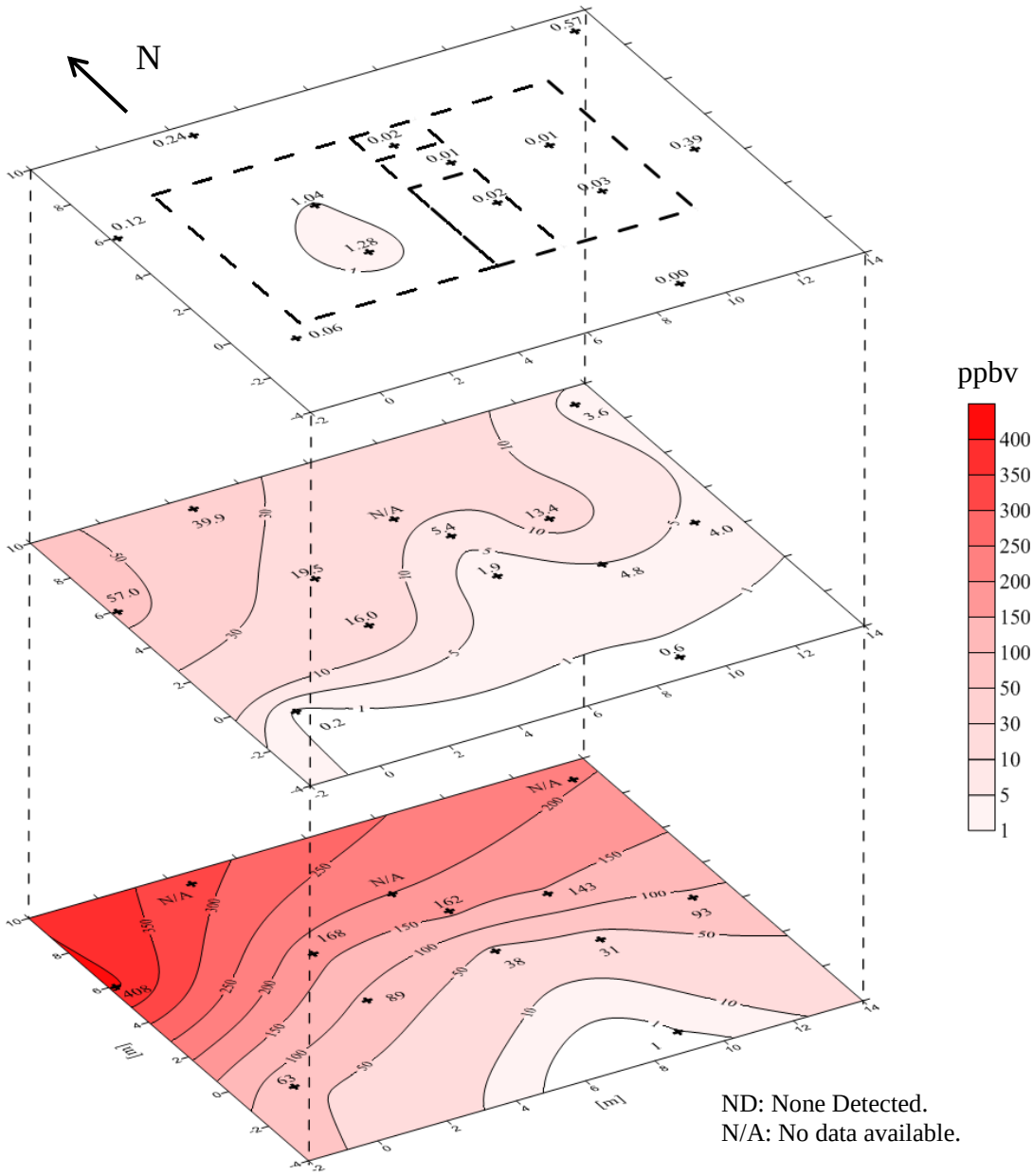

Figure 3.4. Representative TCE soil gas concentrations collected from t=368 d to 370 d during a VI-active period under natural conditions with the land drain lateral valve open. SS, 0.9 m BS and 1.8 m BS contours are shown from top to bottom. The bold dashed line in the SS surface delineates the building perimeter.

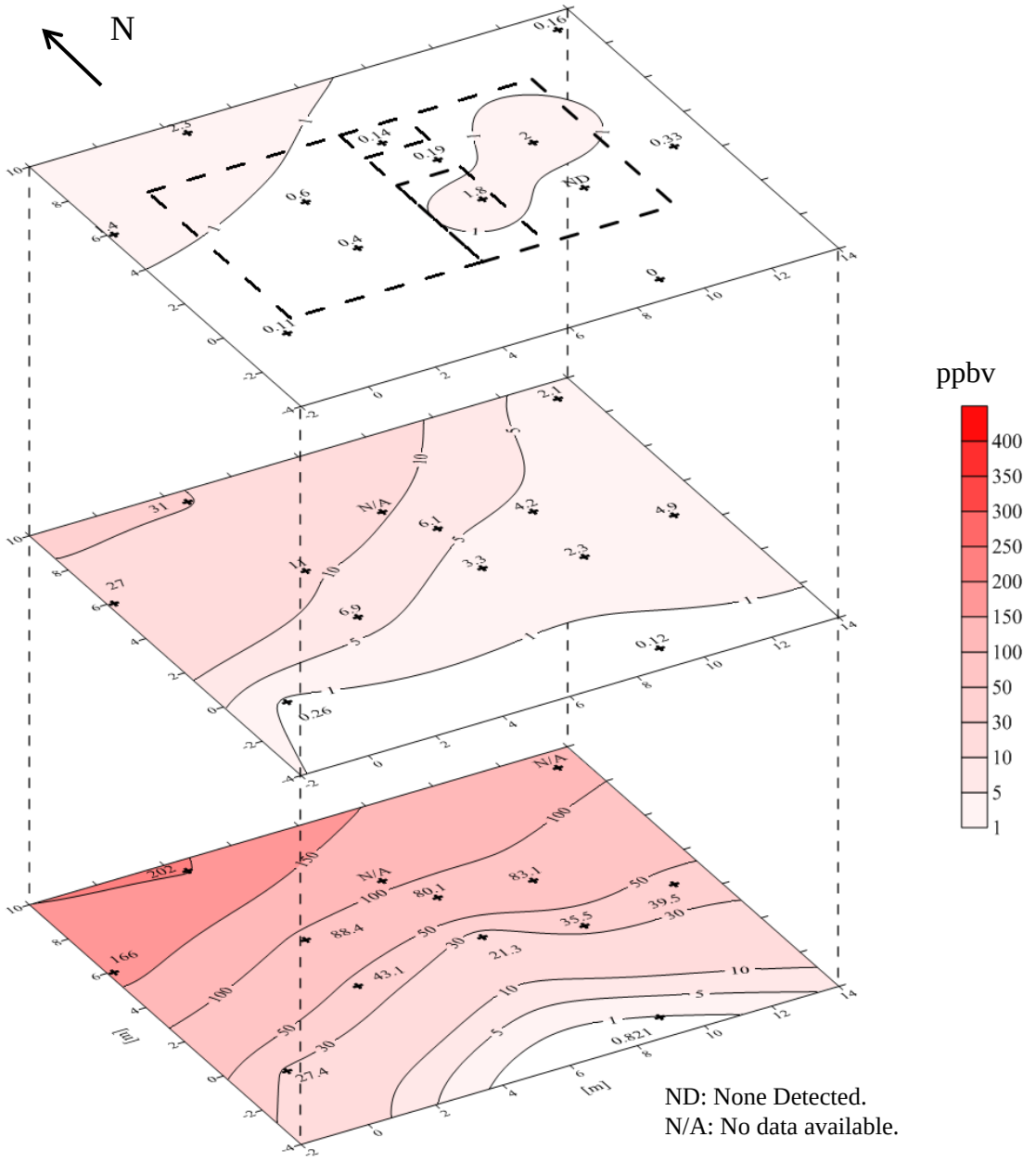

Figure 3.5. Representative TCE soil gas concentrations collected from t=514 d to 516 d during a VI-inactive period under natural conditions with open land drain lateral valve. SS, 0.9 m BS and 1.8 m BS contours are shown from top to bottom. The bold dashed line in the SS surface delineates the building perimeter.

The soil gas profiles under natural conditions do not provide any indication that a significant alternative VI pathway is present at this site. The distributions in Figures 3.4 and 3.5 are both consistent with the conventional diffusion-driven soil gas VI pathway conceptualization prevalent in the vapor intrusion literature (Johnson and Ettinger, 1991; Atteia and Hohener, 2010). Soil gas concentrations decrease from the source to the building and ground surface as expected. For example, the concentration attenuation from 1.8 m BS to the sub-slab depth ranges from 10^{-2} to 10^{-3} and this is comparable to the modeling results for "*soil VI*" only conceptual models (Abreu and Johnson, 2005; Bozkurt et al., 2009; USEPA, 2012).

Four soil gas sampling events separated by one to three months occurred during the long-term CPM test. Representative results are presented in Figure 3.6. TCE concentration distributions at 0.9 m BS and 1.8 m BS depths remain similar to those in Figures 4 and 5 under natural conditions, with concentration differences at each location and depth being within 3X of values in Figures 3.4 and 3.5. A significant change, however, can be seen in the sub-slab depth TCE concentrations beneath the house living area (right-hand portion of the footprint). The increases are 100X or greater in comparison to concentrations measured under natural conditions.

Under CPM conditions, the vertical distribution of soil gas concentrations is no longer consistent with the conventional diffusion-driven soil gas VI pathway conceptualization. Concentrations decrease from 1.8 m BS to 0.9 m BS but then increase to the sub-slab depth. Sub-slab depth concentrations at some locations are now greater than 1.8 m BS near-source concentrations. For example, at one central sampling location the sub-slab TCE concentration was 91.1 ppb_v while it was 6.6 ppb_v and 43.3 ppb_v for the

0.9 m BS and 1.8 m BS samples. Thus, the data support the hypothesis that soil gas profiles under CPM test conditions can at some sites provide an indication of a significant alternative VI pathway.

Once the "pipe VI" pathway was closed, CPM testing did not significantly alter the soil gas distribution at this site from that observed under natural conditions. Figure 3.7 presents a representative TCE soil gas distribution for CPM test conditions with the lateral drain valve closed (no alternative VI pathway). In comparison to Figure 3.6, the previously elevated TCE concentrations at the sub-slab depth beneath the house living area decreased after the valve was closed and the deep soil gas (0.9 m and 1.8 m BS) concentrations remained relatively unchanged. The soil gas profile resembles that anticipated for a soil VI-dominated setting. It is also very similar to that shown in Figure 3.8, which presents data measured under natural conditions and with the land drain valve closed.

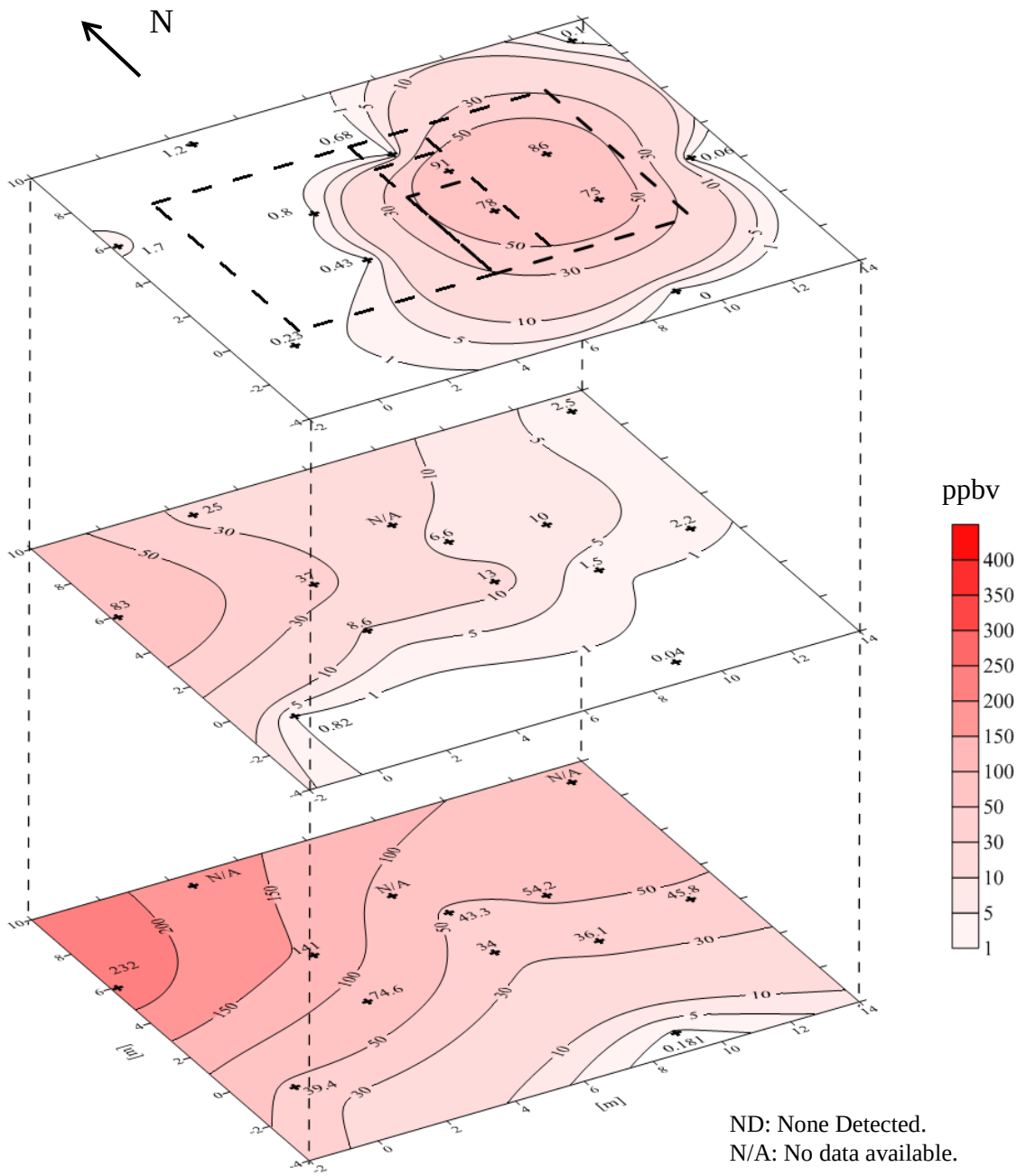

Figure 3.6. Representative TCE soil gas concentrations collected from t=910 d to 911 d during CPM conditions with open land drain lateral valve. SS, 0.9 m BS and 1.8 m BS contours are shown from top to bottom. The bold dashed line in the SS surface delineates the building perimeter.

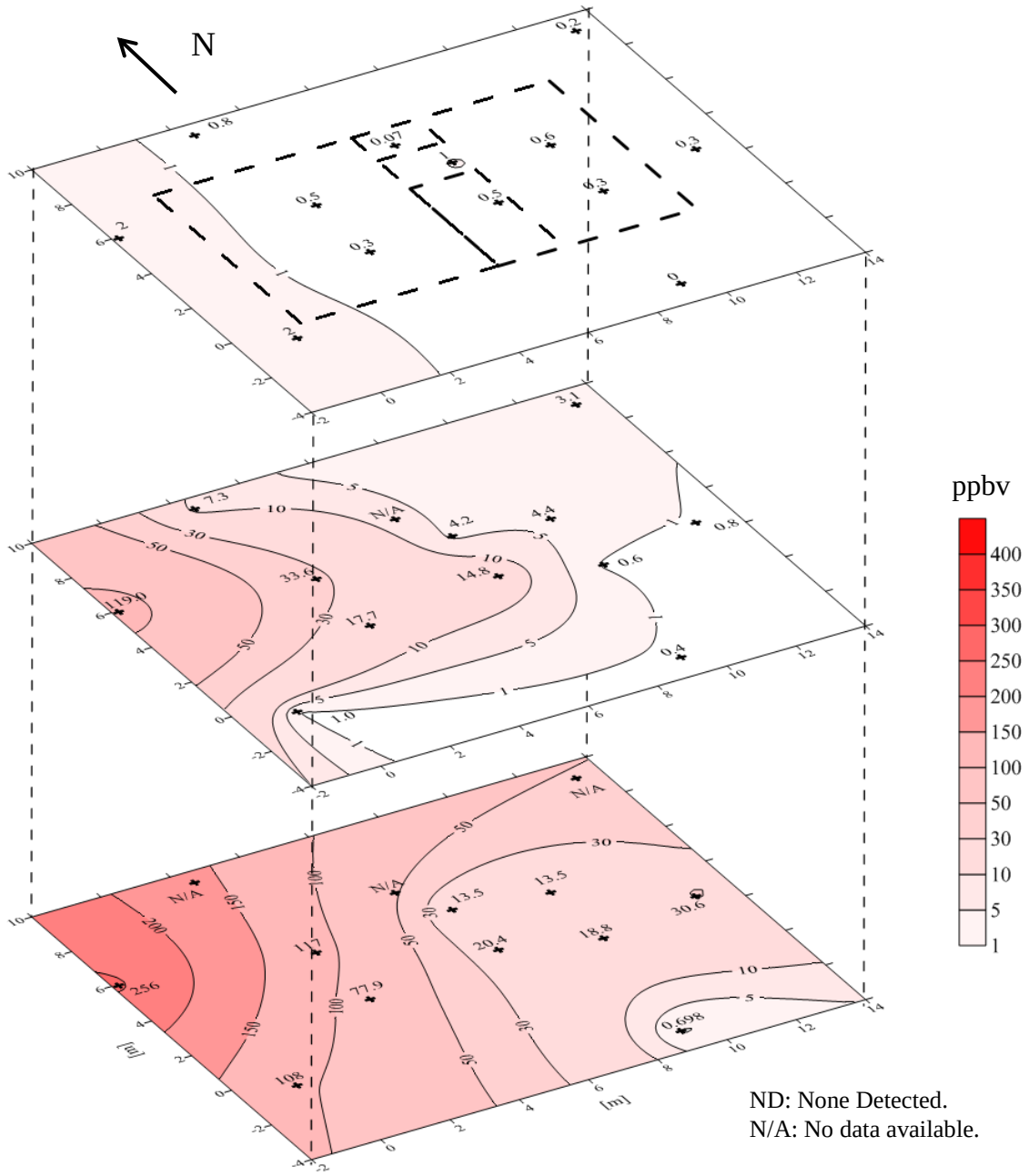

Figure 3.7. Representative TCE soil gas concentrations collected from t=1012 d to 1013 d during CPM conditions with closed land drain lateral valve. SS, 0.9 m BS and 1.8 m BS contours are shown from top to bottom. The bold dashed line in the SS surface delineates the building perimeter

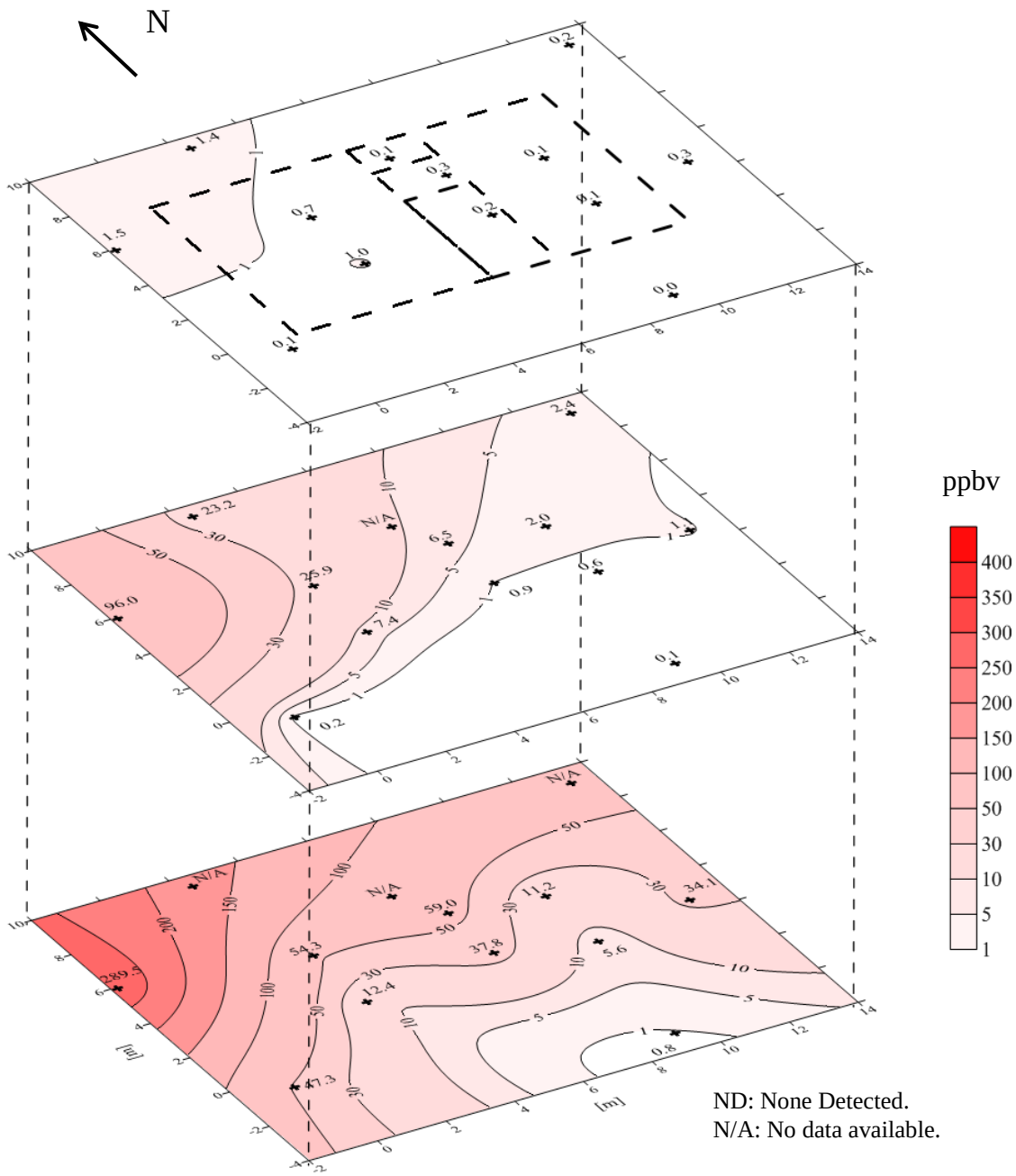

Figure 3.8. Representative TCE soil gas concentrations collected from t=1394 d to 1395 d during natural conditions with closed land drain lateral valve. SS, 0.9 m BS and 1.8 m BS contours are shown from top to bottom. The bold dashed line in the SS surface delineates the building perimeter.

3.6.3 Reflection on key lessons-learned and future research. The experiences and results from this study illustrate that the presence of a significant alternative VI pathway is not easily detected by visual observation or routine VI pathway assessment measurements under natural conditions. In particular, the soil gas profiles under natural conditions conformed to typical soil VI-dominated conceptual models at this site, with and without the presence of the significant alternative VI pathway. The presence of the significant pipe flow VI pathway was only revealed by data collected during CPM testing; more specifically the observations that measured emission rates greatly exceeded emission rate screening estimates and soil gas profiles that changed and no longer conformed to traditional soil VI conceptual models of the vapor intrusion pathway.

In summary, this work in addition to the work of Riis et al. (2010) and Pennell et al. (2013) suggest that the following conditions might be indicative of the presence of significant pipe flow and sewer VI pathways: a) VI impacts under natural or CPM testing conditions in buildings outside the delineated boundaries of the vapor source(s) indicate one or more alternative VI pathways, b) CPM test emission rates that greatly exceed screening-level estimates in combination with conforming soil gas profiles might indicate a significant sewer VI pathway, and c) CPM test emission rates that greatly exceed screening-level estimates in combination with non-conforming soil gas profiles might indicate a significant pipe flow VI pathway.

There are a number of reasons why there should be interest in being able to quickly identify significant alternative VI pathways. One is that conventional pathway characterization paradigms, data analyses, and decisions have been built on a soil VI-only conceptualization of the VI pathway, and these might lead to erroneous decisions when

significant alternative VI pathways are present. The second is that VI mitigation system design and monitoring is also based on the soil VI-only conceptualization and it is not known if presumptive remedies are effective when significant alternative VI pathways are present. This should be examined in future research studies.

The proposed method was tested at a chlorinated hydrocarbon impacted site with a known "*pipe flow VI*" pathway, and its effectiveness was well demonstrated. However, when assessing petroleum hydrocarbon-impacted sites or other site conceptual models, such as sites with a "*sewer VI*" pathway present, its effectiveness is unknown. Further research is necessary to evaluate this method under different scenarios.

3.7 REFERENCES

Abreu, L., Johnson, P. C. (2005). Effect of vapor source-building separation and building construction on soil vapor intrusion as studied with a three-dimensional numerical model. *Environmental Science and Technology, 39* (12), 4550-4561.

Atteia, O.; Hohener, P. (2010). Semianalytical model predicting transfer of volatile pollutants from groundwater to the soil surface. *Environmental Science and Technology,* 44, 6228-6232.

Bozkurt, O., Pennell, K. G., Suuberg, E. M. (2009). Simulation of the vapor intrusion process for nonhomogeneous soils using a three-dimensional numerical model. *Groundwater Monitoring and Remediation, 29* (1), 92-104.

Holton, C.; Luo, H.; Dahlen, P.; Gorder, K. A.; Dettenmaier, E. M.; Johnson, P. C. (2013). Temporal variability of indoor air concentrations under natural conditions in a house overlying a dilute chlorinated solvent groundwater plume. *Environmental Science and Technology, 47*, 13347-13354.

Holton, C.; Guo, Y.; Luo, H.; Dahlen, P.; Gorder, K. A.; Dettenmaier, E. M.; Johnson, P. C. (2015). Long-Term Evaluation of the Controlled Pressure Method for Assessment of the Vapor Intrusion Pathway. *Environmental Science and Technology, 49*, 2091-2098.

Interstate Technology & Regulatory Council. (2007). *Vapor intrusion pathway: A practical guideline*. Washington, DC: Interstate Technology & Regulatory Council.

Johnson, P. C., Ettinger, R. A. (1991). Heuristic model for predicting the intrusion rate of contaminant vapors into buildings. *Environmental Science and Technology, 25* (8), 1445-1452.

Johnson, P. C., Bruce, C., Johnson, R. L., Kemblowski, M. W. (1998). In situ measurement of effective vapor-phase porous medium diffusion coefficient. *Environmental Science & Technology*, 32, 3405-3409.

McHugh, T. E., Beckley, L., Bailey, D., Gorder, K., Dettenmaier, E., Rivera-Duarte, I., Brock, S., MacGregor, I. C. (2012). Evaluation of vapor intrusion using controlled building pressure. *Environmental Science & Technology*, *46*, 4792-4799.

New Jersey Department of Environmental Protection. (2013). *Vapor intrusion technical guidance.* Trenton, NJ: New Jersey Department of Environmental Protection.

Pennell, K. G.; Scammell, M. K.; McClean, M. D.; Ames, J.; Weldon, B.; Friguglietti, L.; Suuberg, E. M.; Shen, R.; Indeglia, P. A.; Heiger-Bernays, W. J. (2013). Sewer gas: An indoor air source of PCE to consider during vapor intrusion investigations. *Groundwater Monitoring and Remediation, 33* (3), 119-126.

Riis, C. E.; Christensen, A. G.; Hansen, M. H.; Husum, H.; Terkelsen, M. (2010). Vapor Intrusion through Sewer Systems: Migration Pathways of Chlorinated Solvents from Groundwater to Indoor Air. Presentation at the 7th Battelle International Conference on Remediation of Chlorinated and Recalcitrant Compounds, Monterey.

U.S. Environmental Protection Agency. (2000). *Johnson and Ettinger (1991) Model for Subsurface Vapor Intrusion into Buildings (3-Phase System Models and Soil Gas Models).* Washington, DC: U.S. Environmental Protection Agency. http:// www.epa.gov/oswer/riskassessment/airmodel/ johnson_ettinger.htm.

U.S. Environmental Protection Agency. (2002). *OSWER draft guidance for evaluation the vapor intrusion to indoor air pathway from groundwater and soils (Subsurface vapor intrusion guidance).*Washington, DC: U.S. Environmental Protection Agency.

U.S. Environmental Protection Agency. (2008). *Engineering Issue: Indoor Air Vapor Intrusion Mitigation Approaches*. Washington, DC: U.S. Environmental Protection Agency.

U.S. Environmental Protection Agency. (2012). *Conceptual model scenarios for the vapor intrusion pathway*. Washington, DC: U.S. Environmental Protection Agency.

CHAPTER 4

EFFECTIVENESS OF A SUB-SLAB DEPRESSURIZATION SYSTEM AT AN ALTERNATIVE VAPOR INTRUSION PATHWAY SITE

4.0 ABSTRACT

Subsurface conduits, such as land drain and sewer pipes, can serve as significant alternative vapor intrusion (VI) pathways at some soil- and groundwater-impacted sites. The effectiveness of current VI mitigation approaches at these sites with significant alternative VI pathways is unknown. This study conducted long-term monitoring of conventional VI mitigation system performance at a site with an alternative VI pathway that could be manipulated to be on or off. There, a house overlying a chlorinated solvent groundwater plume was equipped with a sub-slab depressurization (SSD) system. A lateral pipe connecting the sub-foundation region to a neighborhood land drain network provided an alternative pathway for chlorinated hydrocarbon (CHC) vapors to migrate to indoor air. The response of CHCs and radon indoor air concentrations and subsurface soil gas, differential vacuums between the sub-slab region and indoor air were monitored with SSD operation and control of the alternative VI pathway. There were differences and similarities in SSD system performance with the alternative VI pathway disconnected and connected. For example, the vacuum between the sub-slab region and indoor air was about 20-45% less near the land drain lateral connection point and sub-slab soil gas TCE concentrations were significantly increased with it connected and they persisted for days to months after the SSD system was switched off. Indoor air concentrations, however,

were similarly low (<0.04 ppb_v) under both conditions. Whether or not SSD mitigation will provide enough protection at all sites with alternative pathways requires more study.

4.1 INTRODUCTION

Vapor intrusion (VI), a process in which volatile contaminants migrate from subsurface sources into overlying buildings, can pose health risks to occupants. Sources can include impacted soils and groundwater and sewers and other underground drainage systems. At sites where concentrations are known, or are thought to have the potential to exceed target thresholds, and where subsurface contaminant sources cannot be quickly remediated, mitigation is necessary to protect building occupants (ITRC, 2007; USEPA, 2015).

VI mitigation usually involves sub-slab depressurization (SSD) systems that extract sub-slab soil gas and vent it to the atmosphere as shown in Figure 4.1. The functional design goal for SSD systems is to maintain the sub-slab region at a lower pressure than the building interior, thereby ensuring that any cross-foundation gas flow occurs toward the subsurface. Operational performance monitoring focuses on this metric. SSD systems were first developed for protecting against radon intrusion into homes (USEPA, 1993) and they have become the presumptive remedy for buildings with unacceptable VI impacts associated with volatile organic chemicals (VOCs) and other anthropogenic chemicals (USEPA, 2008; USEPA, 2012; USEPA, 2015). SSD systems, when designed and operated properly, have been shown to be effective at sites where impacts are due to the "*soil VI pathway*"; at these locations contaminant vapors diffuse through soil to the near-foundation region and then enter the building through foundation

cracks and perforations by a combination of advective and diffusive transport (Johnson and Ettinger, 1991, Rydock and Skaret, 2002; Babyak and Welt, 2006; Jiranek, 2012).

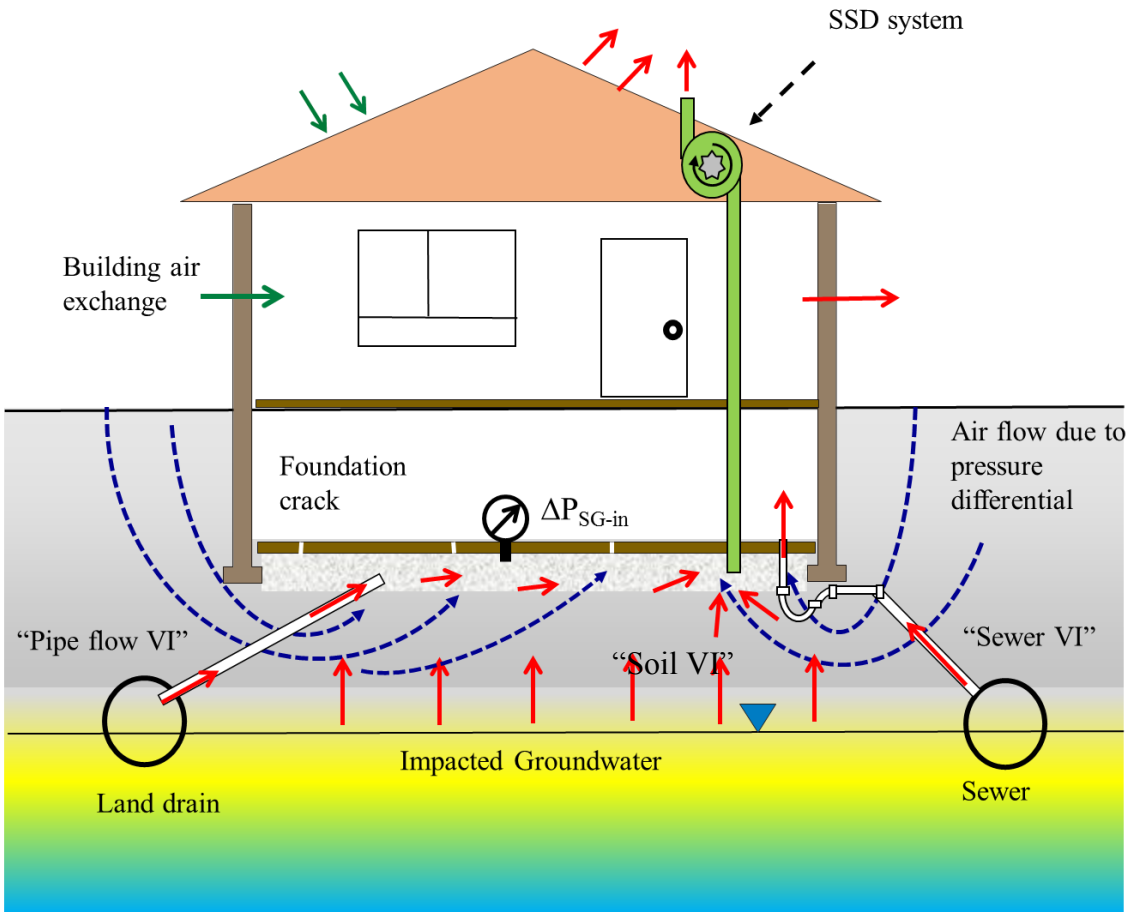

Figure 4.1. Conceptual drawing of conventional and alternative vapor intrusion pathways and a sub-slab depressurization (SSD) system.

In addition to the soil VI pathway discussed above, subsurface conduits, such as sewer lines and land drains have been identified as significant "*alternative VI pathways*" at some sites (Riis et al., 2010; Pennell et al., 2013; Guo et al., 2015). These alternative VI pathways can provide connections between vapor sources and the sub-foundation region ("*pipe flow VI pathway*") or the building interior ("*sewer VI pathway*") as shown

in Figure 4.1. It is not difficult to conceptualize that SSD systems might not provide sufficient protection for buildings having significant sewer VI pathways, because controlling the pressure differential between sub-slab soil gas and indoor air should not affect vapor transport in well-sealed sewer lines, and lowered sub-slab pressures could induce more flow along land drain and other pipe flow VI pathways toward the sub-foundation region. Although it has not been demonstrated in a well-controlled study, anecdotal experience suggests that this might be true. For example, Riis et al. (2010) reported that passive sub-slab ventilation was ineffective for their buildings affected by sewer VI pathways.

Assessing the effectiveness of SSD systems for sites having a significant pipe flow VI pathway is the focus of this study. As demonstrated in Guo et al. (2015) at a field study site, the pipe flow VI pathway is unlikely to be discovered through routine VI pathway assessment and it is possible that SSD systems will be installed and operated at sites having pipe flow VI pathways without knowing they are present. At such sites, it is unknown if SSD systems designed and monitored according to typical guidance will sufficiently mitigate VI impacts. The presence of the pipe flow VI pathway could influence performance in a number of ways; for example, if significant SSD system flow is drawn through the pipe flow VI conduit, then the SSD system radius of influence could be smaller than expected. SSD system operation is also expected to amplify flow along the pipe flow VI conduit relative to natural conditions and this can lead to increased contaminant concentrations in the subsurface region. The combination of increased concentrations and reduced pressure distribution extent could lead to scenarios where episodic VI impacts could occur.

This is the first study focused on the effectiveness of a conventional SSD system at a site with a known and controllable pipe flow VI pathway. The response of chlorinated hydrocarbon (CHC) and radon concentrations in indoor air and soil gas to the operation of a SSD system was monitored at the Guo et al. (2015) house having a lateral pipe connecting its sub-foundation soil and a neighborhood land drain system, with the latter containing trichloroethylene (TCE) vapors.

4.2 EXPERIMENTAL DESIGN AND METHODS

4.2.1 Site description. The study building is a two-story split-level house located in a residential neighborhood. This house has an 85 m^2 footprint and was built into a sloped lot with a 2.5 m ground surface elevation drop from the back to front yard. Multi-level soil gas and groundwater sampling points were installed inside through the foundation and outside of the building. Soil gas points were installed to the following depths: sub-slab (SS), 0.9 m below slab (BS) and 1.8 m BS, as shown in Figure 4.2.

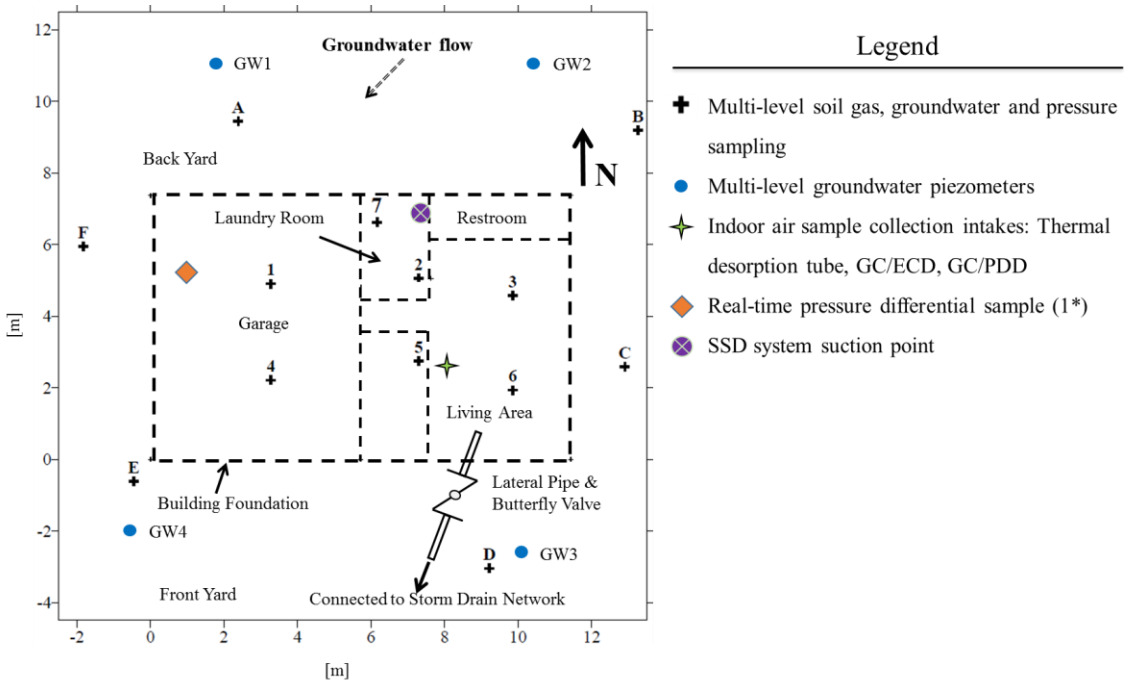

Figure 4.2. Schematic of study house footprint and sampling locations.

The house overlies a dilute dissolved chlorinated solvent groundwater plume containing 1,1-dichlorethylene (1,1-DCE), 1,1,1-trichloroethane (1,1,1-TCA), and trichloroethylene (TCE). Groundwater is encountered at about 3 m BS, which fluctuates by about 0.3 m seasonally. TCE concentrations in water samples collected 5 times over this 7-month study below the building foundation ranged spatially and temporally from approximately 10 - 80 µg/L with an average concentration of 28 ± 16 µg/L.

The sub-foundation gravel zone is connected to a neighborhood land drain system running across the southern property boundary via a lateral pipe having one end open in the sub-foundation gravel near locations 5 and 6 in Figure 4.2. This land drain system was confirmed as a pipe flow VI pathway by Guo et al. (2015) as discussed in the previous chapter. The connection between the sub-foundation area and the land drain system can be controlled by a manual butterfly valve that was installed along the lateral

pipe in the Guo et al (2015) study. Photos of the valve installation and lateral pipe can be found in Appendix I.

A SSD system was installed at the house on December 20, 2006 before the house was purchased for this study. The suction point (a hole cored through the foundation and sealed to a PVC pipe riser) is located at the northeast corner of the laundry room near sampling locations 2 and 7 shown in Figure 4.2. A KT-150 turbine fan (Radon PDS, CO) installed in the attic draws air through a 4-inch PVC pipe connected to the suction point.

4.2.2 Experimental conditions. Data presented below were obtained over 7 months and involved combinations of SSD system operation (on/off) and lateral pipe valve manipulation (open/closed). The history of experimental conditions is summarized in Table 4.1. It should be noted that this data set uses a different reference time than previous chapters; here time t = 0 is 8:00 AM on 1/11/2015.

Table 4.1

History of SSD system operation and land drain lateral valve manipulation.

Period	0 to 33 d	33 to 71 d	71 to 172 d	172 d +
SSD system	Off	On	On	Off
Lateral pipe valve	Closed	Closed	Open	Open

Permanent multi-level soil gas monitoring probes were installed inside and outside of the house. Their locations and other key house features are shown in Figure 4.2. Bentonite seals were placed above and below each sampling interval in the multi-level sampling probes to ensure isolation of intervals from each other and the atmosphere.

Sampling probes installed through the foundation were sealed at the foundation with a cement plug topped with silicone caulk. The integrity of the seals and probe connections was verified by sampling through a helium-filled shroud covering the sampling probe and connectors, and confirming no helium in the sample. Indoor air samples were collected at approximately 1 m above the floor in the lower level of the house at the location shown in Figure 4.2.

4.2.3 Experimental Methods. 24-h time-averaged indoor air samples were collected in the lower level of the house at the location shown in Figure 4.2. Two customized SRI Instruments (SRI Instruments, Torrance, CA) 20-stream gas sampling valves were utilized to configure a 38 sample collection sequence. For each sample, 72 L of indoor air were pulled through a multi-bed sorbent tube at a consistent flowrate of 50 mL/min controlled by a vacuum-configured 0-100 mL/min mass flow controller (Alicat Scientific, Tucson, AZ). Multi-bed sorbent tubes (0.64 cm x by 15.2 cm-long) were packed with Tenax-GR and Carboxen-569 and fitted with Markes DiffLok™ caps (Markes International, UK) for tube/sample preservation. Once all 38 samples were collected, they were sent back to the analytical lab.

Sorbent tubes were analyzed using a Markes Ultra auto-sampler and Markes Unity thermal desorber (Markes International, UK) connected to an HP7890A gas chromatograph equipped with a Restek 60-m Rxi-5 capillary column and an HP5975C mass spectrometer. Samples were analyzed using selective ion (SIM) mode with a method detection limit (MDL) for TCE of 0.00007 ppb_v (0.0004 $\mu g/m^3$).

Soil gas VOC samples were collected and analyzed using two methods: a) high frequency real-time collection and b) synoptic multi-depth survey. High-frequency real-

time gas sampling focused on the transient CHC concentration responses at sub-slab depths at locations 1 through 6 and 0.9 m BS depth at location 5. Those samples were collected and analyzed approximately every 6 h by a sorbent-concentration method using a 10-stream auto-sampling valve connected to an SRI 8610C GC equipped with an electron capture detector (ECD) (SRI Instruments, Torrence, CA). The MDL for TCE for this method was 0.009 ppb_v (0.048 $\mu g/m^3$). CHC concentrations in the SSD system vent pipe were also quantified using this real-time sampling technique.

Five synoptic multi-depth soil gas surveys were performed at 1-2 month intervals to provide insight to subsurface soil gas distribution changes with time. For each survey, samples were collected at sub-slab, 0.9 m below-slab (BS), and 1.8 m BS depths at the locations shown in Figure 4.2. Samples were collected in 1-liter Tedlar bags (SKC 232-01) using a custom-built vacuum chamber sampler. Analyses were conducted within 3 hours of sample collection using the SRI 8610C GC equipped with a dry electrolytic conductivity detector (DELCD). Direct injection and sorbent trap pre-concentration were used as needed based on the soil gas concentration. The detection limit was 4.9 ppb_v (26 $\mu g/m^3$) for direct injection and 0.019 ppb_v (0.1 $\mu g/m^3$) for the pre-concentration method.

Radon concentrations in both indoor air and soil gas were quantified using a Durridge RAD7 (Durridge Company, Inc., Billerica, MA). The RAD7 is calibrated annually by the manufacturer and the manufacturer-stated accuracy is ±5% or better with a 0.5 pCi/L lower confidence level. Real-time indoor air samples were collected throughout the test; the RAD7 was configured to sample continuously and report concentrations representative of 2 h intervals. Synoptic multi-depth soil gas radon concentrations were obtained by averaging five 5-minute sampling cycle results.

Differential pressures between soil gas and indoor air and between outdoor air and indoor air were monitored using electronic differential pressure transducers (Model P300-0.4"-D, Pace Scientific Inc., Mooresville, NC). Data were logged every 2 minutes using a data acquisition module (Model OMB-DAQ-56, Omega Engineering Inc., Stamford, CT). The pressure transducers were re-zeroed daily using an automated valve system.

Before the SSD was turned on (t< 33 d), there was only one sampling port available for the sub-slab depth at each multi-level sampler location, and differential pressure and real-time soil gas concentrations could not be monitored at the same time without interference. Therefore, additional sampling ports dedicated to differential pressure monitoring were installed at locations 2, 3, 4, 5 and 6; these were installed within 15 cm of the original sampling points. A new pressure differential monitoring location was also installed at the northwest corner of the garage foundation; it is labeled "1*" in Figure 4.2.

4.3 RESULTS AND DISCUSSION

4.3.1 SSD system operation. Between 33 < t < 172 d, the SSD system was on constantly. The flowrate was determined to be 2.1 m^3/min by three independent measurement approaches: a helium tracer dilution test method, an in-line thermal flow meter, and a Pitot tube method. Values from the three methods agreed within 10%. Detailed calculations and results can be found in Appendix V.

Figures 4.3 through 4.7 present hourly-averaged differential vacuums between sub-slab and indoor air measured at locations 1*, 2, 3, 5 and 6. Statistical characteristics of these measurements are summarized in Table 4.2. The sub-slab region was

consistently depressurized during the period of SSD system operation as indicated by the positive vacuums and small relative standard deviations (<10%). The greatest vacuum was observed at location 2, which is closest to the SSD system suction point, and the least vacuum was observed at location 6, which is located farthest from the SSD system suction point.

The impact of opening the land drain lateral valve is evident in the time trend of differential vacuum at locations 5 and 6; these are located closest to the land drain lateral pipe opening beneath the foundation. The mean hourly-average sub-slab to indoor air vacuum decreased about 20% at location 5 and about 45% at location 6 when the lateral pipe valve was opened. Little or no response to land drain lateral valve operation was observed at the other monitoring locations.

According to USEPA (2008), approximately 4-10 Pa vacuum between indoor air and sub-slab soil gas over the building footprint is considered sufficient for protective SSD system operation. During this study, the time-average vacuum measured at all locations satisfied this criterion, except at location 6 where it was 3.9 ± 0.4 Pa and at some time it was only 2.2 Pa when the land drain lateral valve was open.

Table 4.2

Characteristics of sub-slab soil gas – indoor air vacuum during the test.

Condition	Pressure differential to indoor air [Pa]				
	Lateral valve closed (33 < t <71 d)				
Location	1-SS	2-SS	3-SS	5-SS	6-SS
Average	45.7	106.7	57.3	15.3	7.1
Minimum	37.7	103.9	55.6	13.6	6.3
Maximum	50.9	111.0	60.1	16.1	7.7
Standard Deviation	1.2	1.0	0.7	0.4	0.3
	Lateral valve open (71 < t < 172 d)				
	1-SS	2-SS	3-SS	5-SS	6-SS
Average	45.9	103.4	54.1	12.1	3.9
Minimum	37.5	94.2	48.9	8.3	2.2
Maximum	49.0	107.1	56.0	13.1	4.7
Standard Deviation	1.0	1.6	7.3	0.5	0.4

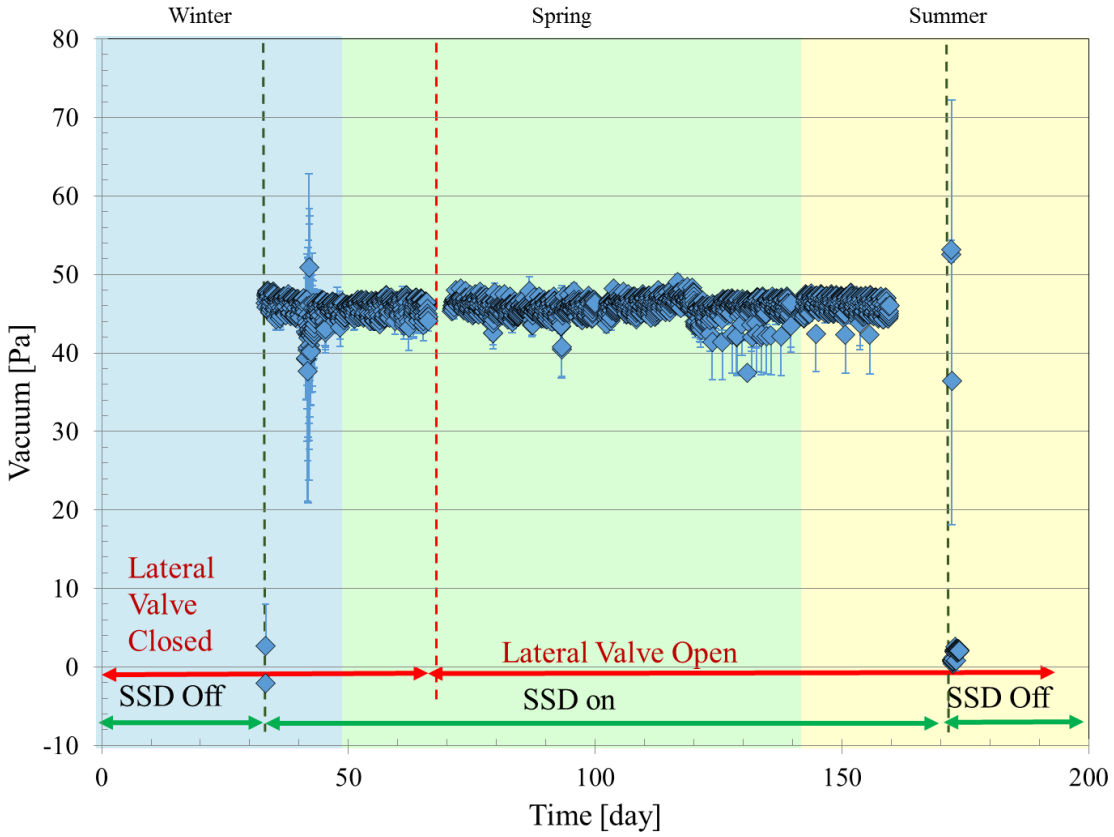

Figure 4.3. Hourly average vacuum between sub-slab soil gas and indoor air at location 1*, with error bars spanning the 90th and 10th percentile of the hourly data sets. Positive values indicate lower sub-slab pressure than indoor air.

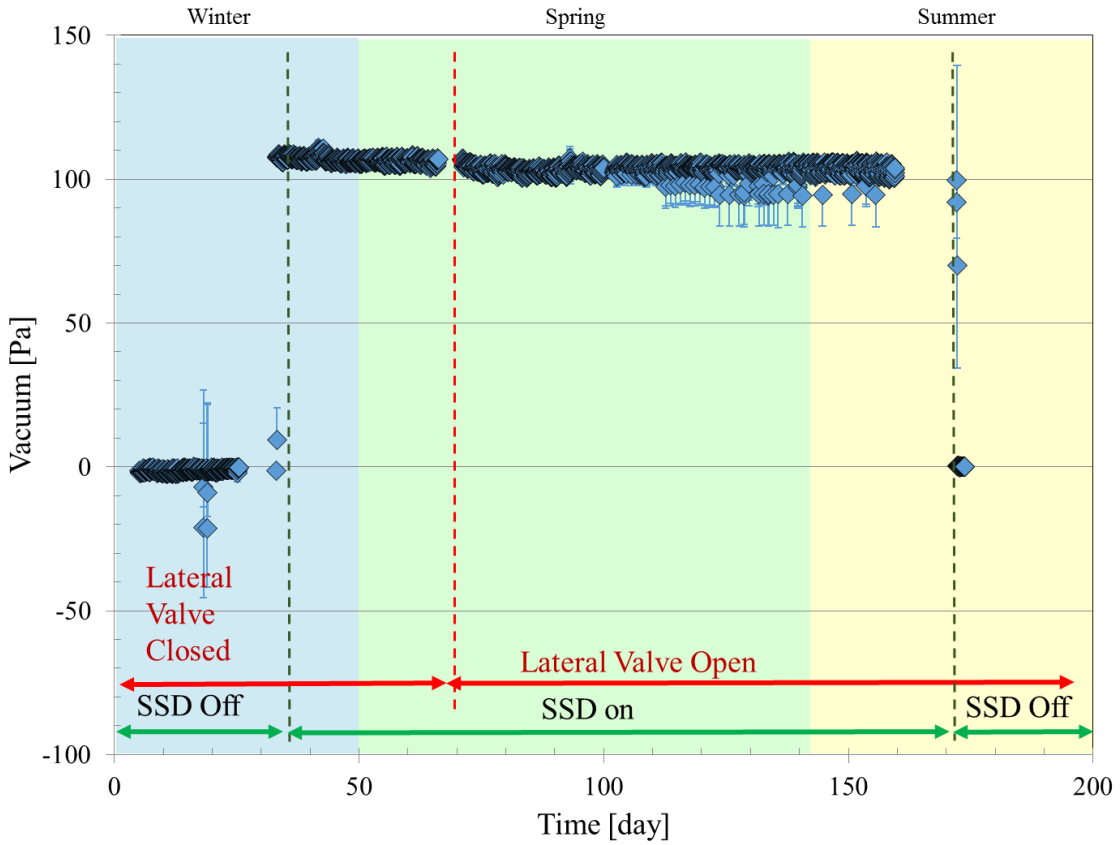

Figure 4.4. Hourly average vacuum between sub-slab soil gas and indoor air at location 2 with error bars spanning the 90th and 10th percentile of the hourly data sets. Positive values indicate lower sub-slab pressure than indoor air.

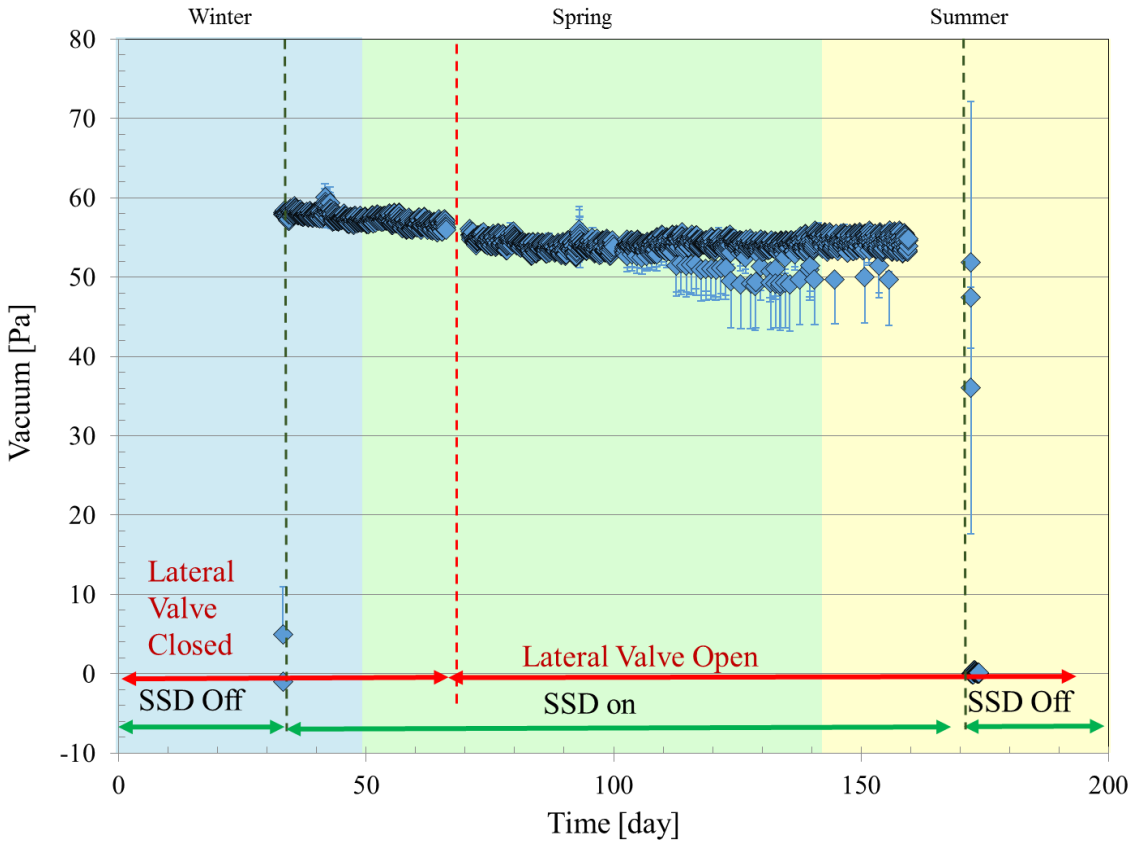

Figure 4.5. Hourly average vacuum between sub-slab soil gas and indoor air at location 3, with error bars spanning the 90th and 10th percentile of the hourly data sets. Positive values indicate lower sub-slab pressure than indoor air.

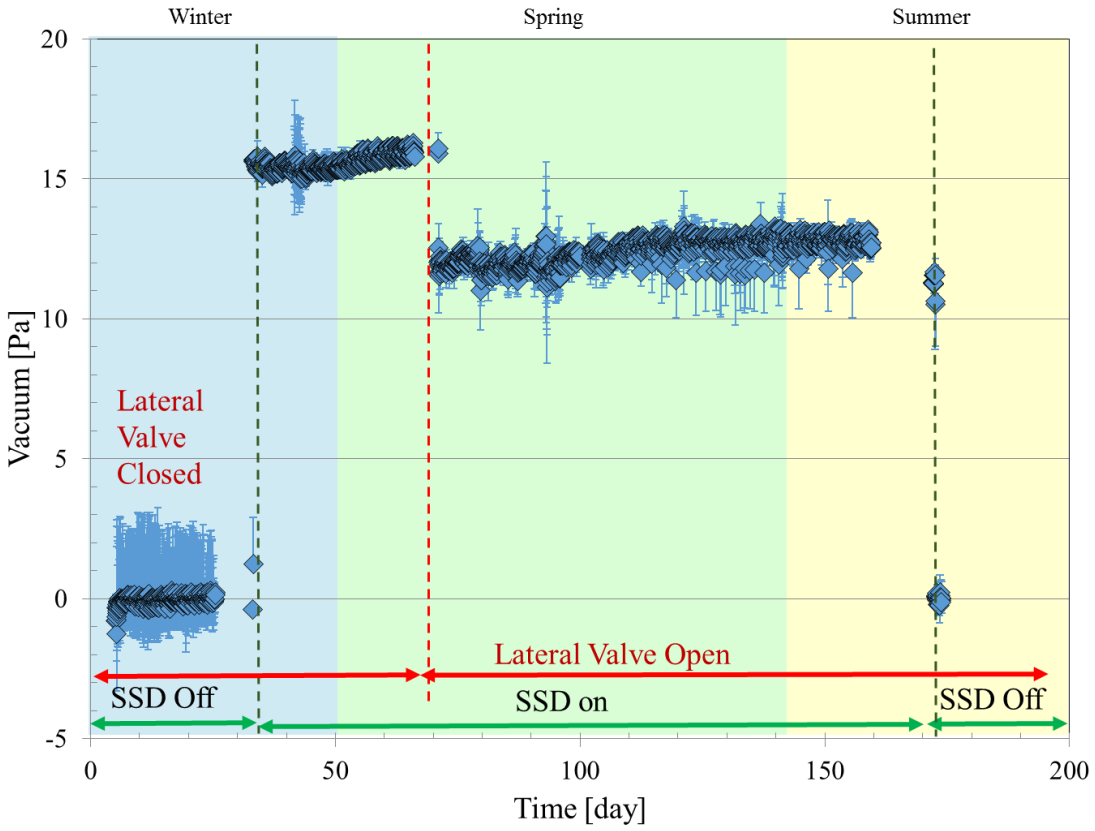

Figure 4.6. Hourly average vacuum between sub-slab soil gas and indoor air at location 5, with error bars spanning the 90th and 10th percentile of the hourly data sets. Positive values indicate lower sub-slab pressure than indoor air.

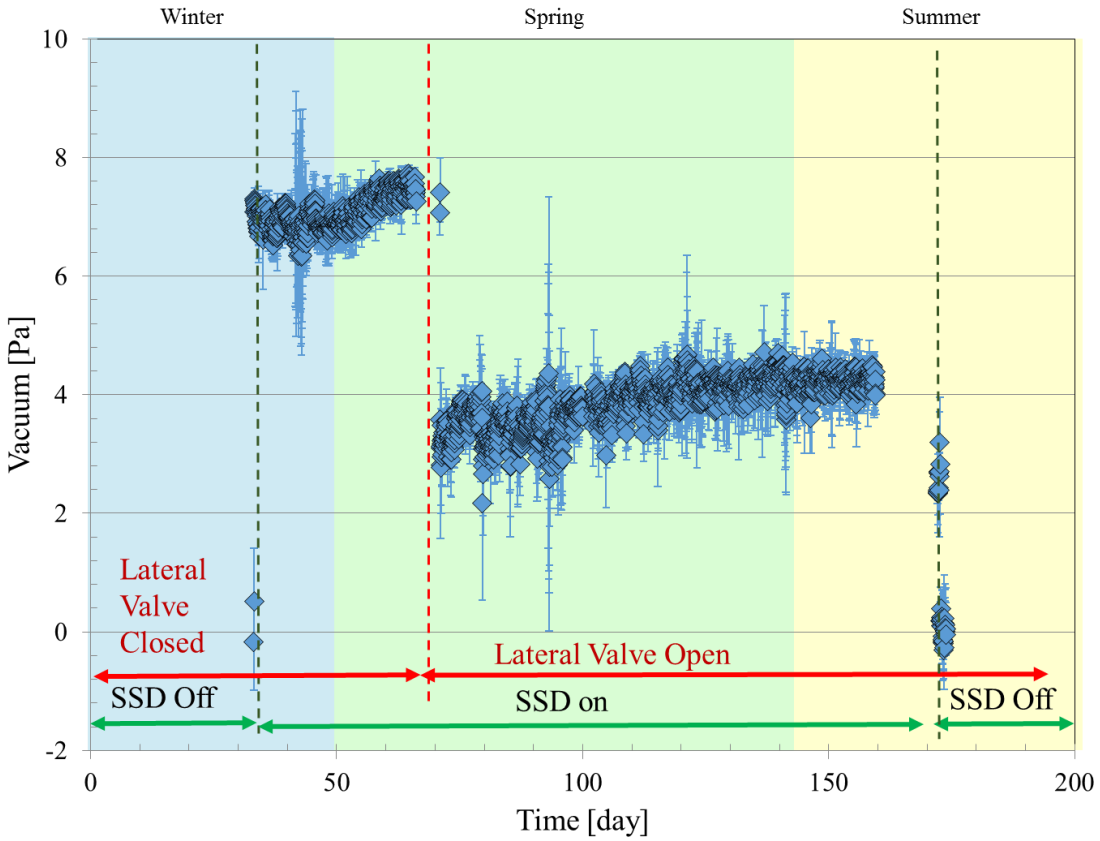

Figure 4.7. Hourly average vacuum between sub-slab soil gas and indoor air at location 6, with error bars spanning the 90th and 10th percentile of the hourly data sets. Positive values indicate lower sub-slab pressure than indoor air.

Figure 4.8 presents TCE concentrations for samples collected from the SSD system vent pipe. The impact of manipulating the land drain lateral valve is apparent as TCE concentrations (C_{vent}) increase quickly from below the MDL to 5.2 ± 1.5 ppb_v when the valve is opened. The air flow rate through the lateral pipe ($Q_{lateral}$) can be estimated using the measured TCE concentration in the lateral pipe and SSD vent pipe ($C_{lateral}$) and SSD pipe flow rate (Q_{vent}): $Q_{lateral}/Q_{vent} = C_{vent}/C_{lateral}$. TCE vapor concentrations ($C_{lateral}$) in the land drain system near the lateral valve were quantified four times from t= 0 d to t= 171 d, with an average concentration of 105 ppb_v. Using the calculation outlined above, it

was estimated that about 5% of the total SSD system extraction flow was contributed by the lateral pipe.

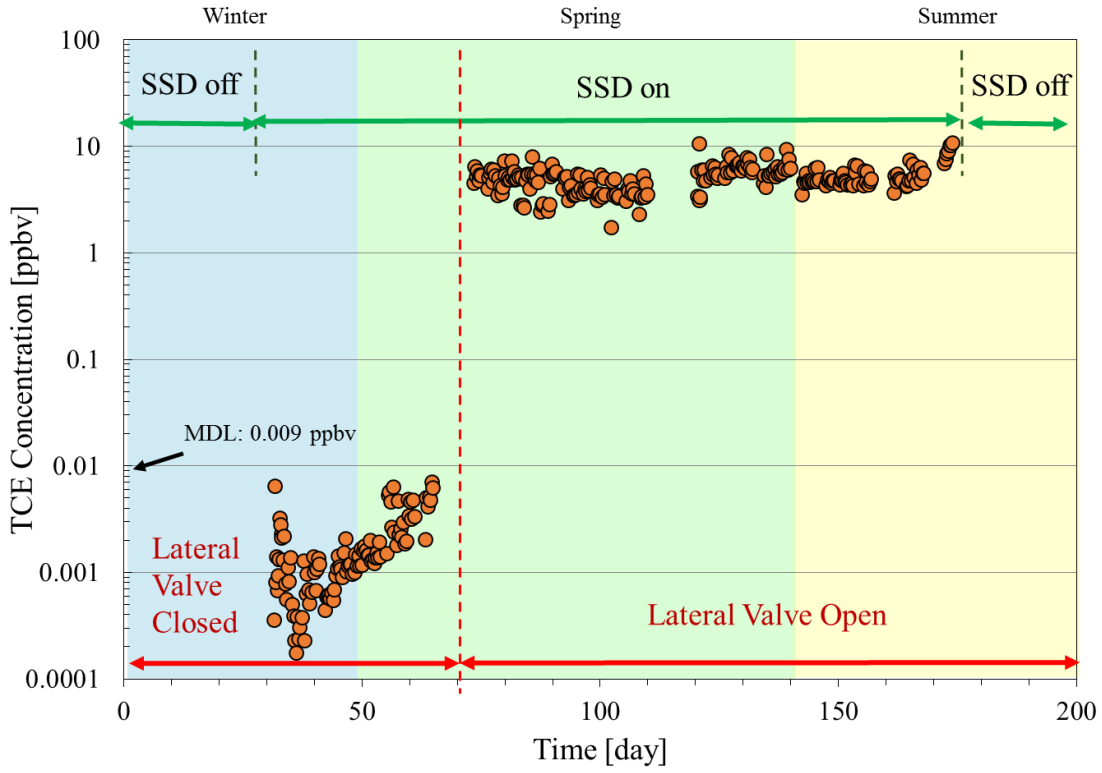

Figure 4.8. TCE concentrations in the SSD vent pipe.

Radon concentrations in the SSD system vent pipe during SSD system operation are shown in Figure 4.9. Once the lateral valve was opened, radon concentrations in SSD vent pipe increased, but less significantly than the TCE concentrations; the increase was about a factor of 3X (from 3.0 ± 0.3 pCi/L to 10.6 ± 1.6 pCi/L). This is because the <20 pCi/L radon vapor concentrations in the lateral pipe were less than the <100 to about 1500 pCi/L soil gas radon concentrations, which was opposite the case for TCE concentrations.

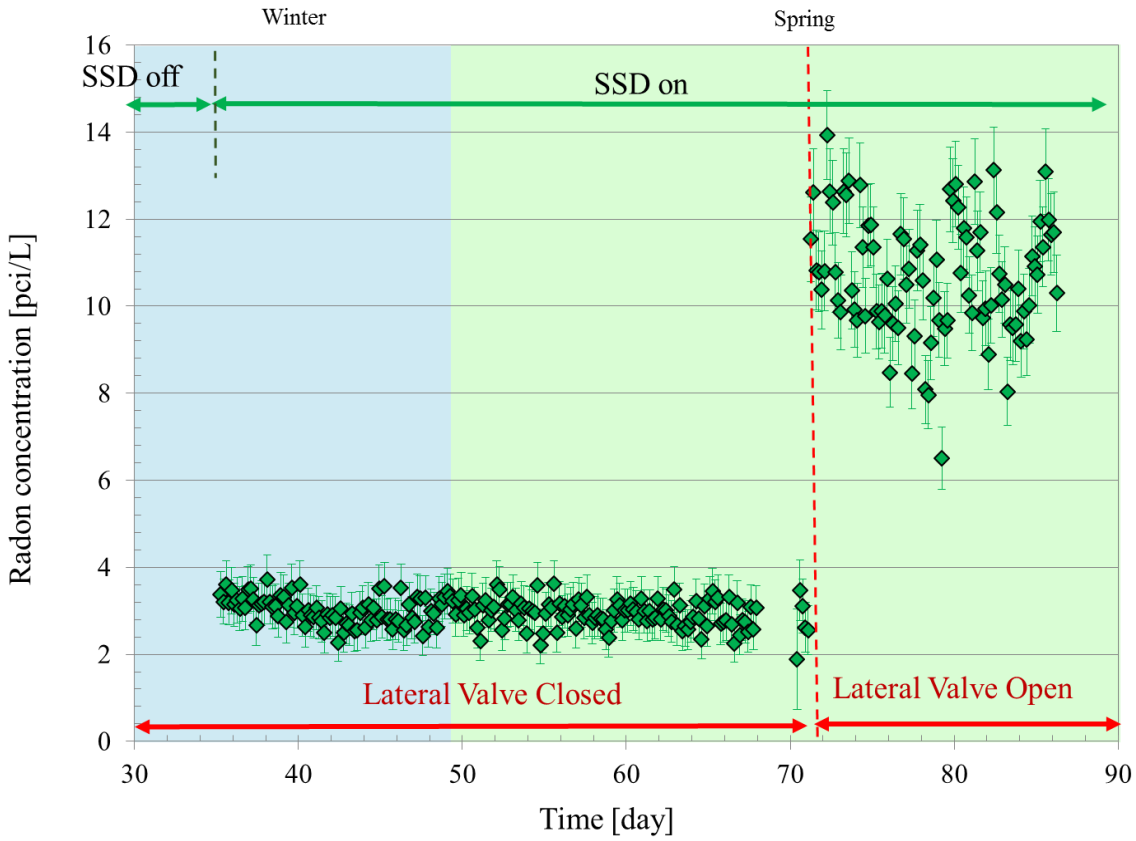

Figure 4. 9. Radon concentrations in the SSD vent pipe.

4.3.2 Indoor air TCE and Radon concentrations. Figure 4.10 presents the indoor air TCE concentrations from the two different sampling and analysis methods. For the real-time GC/ECD samples, analytical results <0.009 ppb_v are plotted as 0.009 ppb_v, so that it is clear that samples were collected at those times. From 44 d < t < 71 d, 24-h average sorbent tube samples were not collected due to a failure of the auto-sampling equipment.

Figure 4.11 presents the indoor air radon concentrations after the lateral pipe valve was opened. Prior to t= 90 d, the radon sampler was used to collect air samples from the SSD system vent pipe and indoor air alternatively, and it was discovered that

significant carry-over from vent pipe to indoor air samples occurred, thus the indoor air radon data from that period were discarded.

With respect to effectiveness of the SSD system, the 24-h average indoor air TCE concentration collected by sorbent tubes during SSD system operation was 0.0023 ± 0.0015 ppb_v with the land drain lateral valve closed and 0.0027 ± 0.0042 ppb_v with it open. The indoor air radon concentration was 0.22 ± 0.09 pCi/L with the land drain lateral open. These can be compared with concentrations reported by Holton et al. (2015) for multi-year periods under natural conditions and prior to installation of the land drain lateral valve: 0.065 ± 0.19 ppb_v long-term TCE average and 0.15 ppb_v 90^{th} percentile and 0.45 ± 0.2 pCi/L long-term radon average and 0.68 pCi/L 90^{th} percentile. Based on comparison of the long-term averages, the operation of the SSD system reduced indoor air concentrations by 96.9 % for TCE and 51.7 % for radon with the pipe flow VI pathway active (land drain lateral valve open).

The percentage reductions of indoor air concentrations by SSD operation can vary depending on pre-mitigation concentrations (USEPA, 2008; Engler, 2006). Higher-percentage reductions are often associated with higher pre-mitigation concentrations. With initial 1,1-DCE indoor air concentrations that ranged up to 131 $\mu g/m^3$ (33 ppb_v), Folkes and Kurz (2002) reported that SSD systems achieved over 99.9 % reduction at the Redfield site over 3 years of monitoring in 189 houses with SSD systems. Lutes et al (2015) reported a 61% average reduction for tetrachloroethylene (PCE) in indoor air at a duplex with averaged pre-mitigation concentrations less than 8 $\mu g/m^3$ (1.2 ppb_v). It is important to keep in mind, however, that the key performance metric is the indoor air concentration and not a percentage reduction.

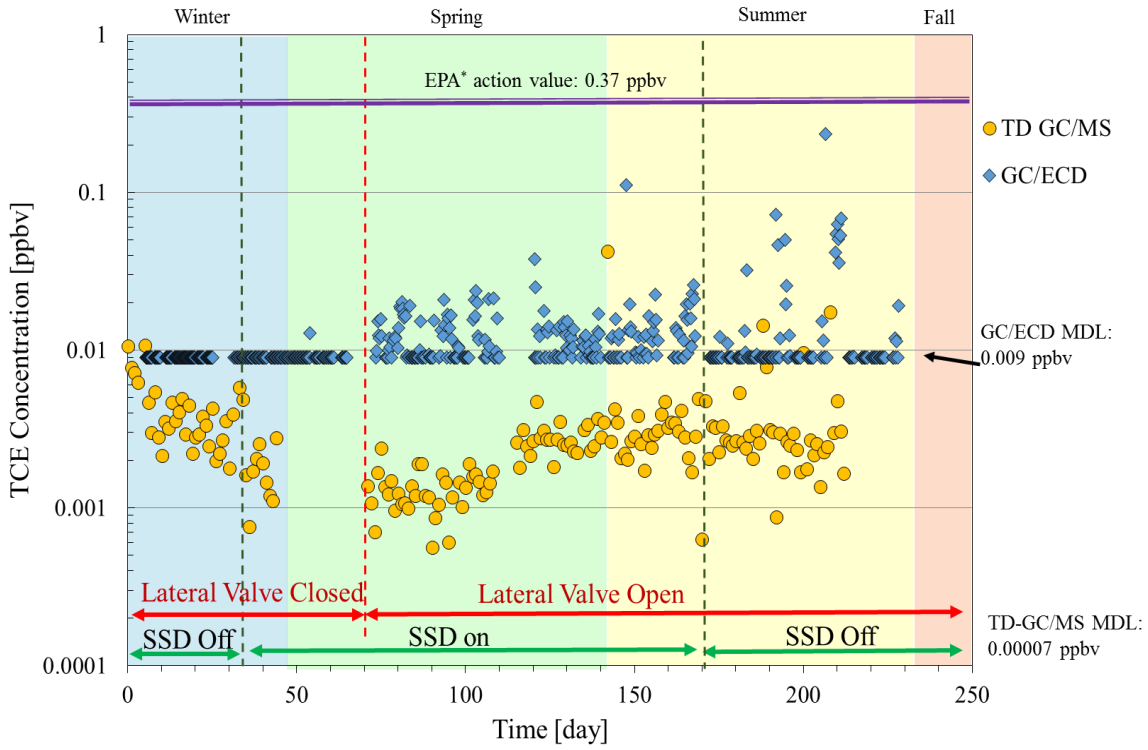

Figure 4.10. Indoor air TCE concentrations from real-time GC/ECD and 24-h averaged sorbent tubes GC/MS methods.

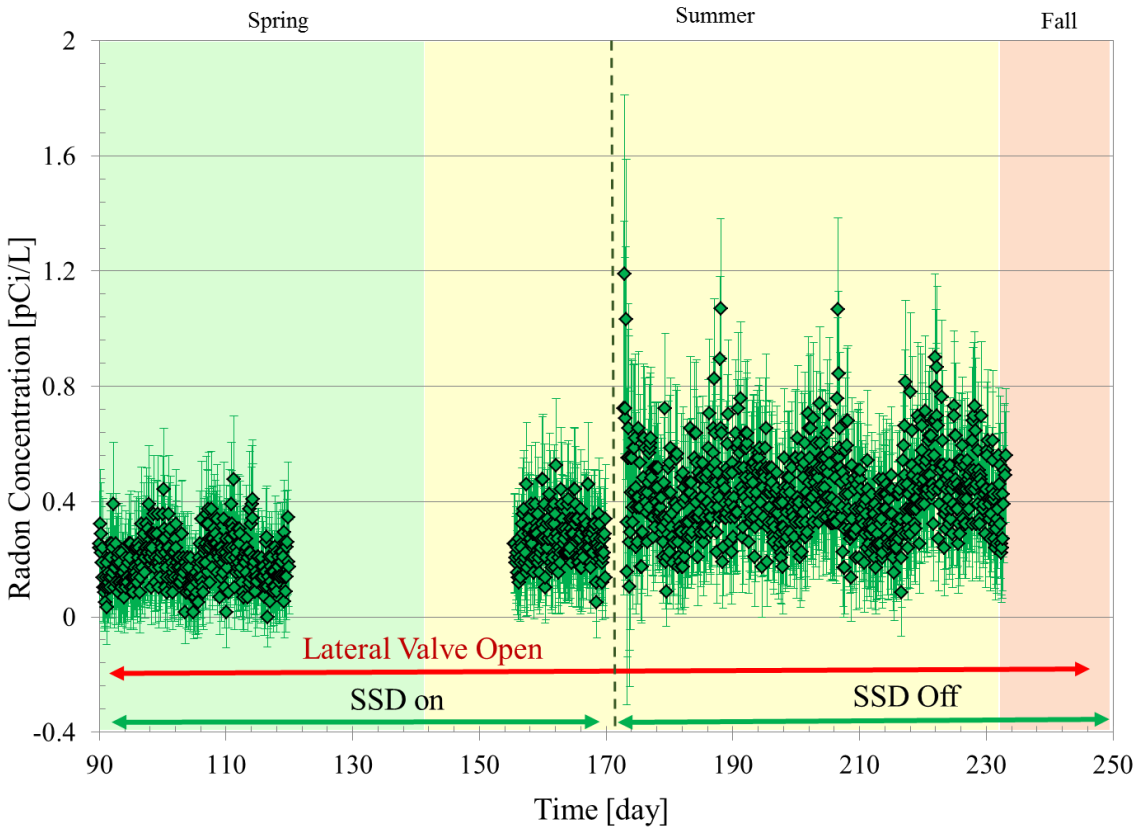

Figure 4.11. Indoor air radon concentrations with error bars indicating the uncertainty calculated by the detector.

4.3.3. Subsurface TCE and radon responses to SSD. This section presents synoptic soil gas TCE/radon profiles as well as real-time sub-slab soil gas TCE monitoring results under different experimental conditions.

Synoptic TCE and radon soil gas profiles. Figures 4.12 to 4.15 present representative TCE and radon soil gas concentration distributions for four scenarios in the time sequence of operating conditions. These contour plots were generated using the soil gas concentrations and locations and Surfer 12 (Golden Software, Inc.) with its Kriging gridding algorithm. Each plot presents TCE concentration distributions at sub-slab (SS),

0.9 m BS and 1.8 m BS depths. For location C, the ground surface is below the sub-slab elevation, so 0 ppb_v TCE and 0 pCi/L radon concentrations were assigned to the sub-slab depth when creating contours. The building footprint is shown as a dashed outline on the sub-slab depth plot with the back of the house being the north side of the plot. The averaged TCE and radon soil gas concentrations within building footprint at each depth were calculated for each synoptic data set and were summarized in Table 4.3.

Table 4.3

Summary of average TCE and radon soil gas concentrations at each depth for synoptic data sets within the building footprint.

	Averaged TCE soil gas concentration [ppbv]		
Operation conditions	Sub-slab	0.9 m BS	1.8 m BS
SSD off, no land drain VI	0.06	3.2	25.2
SSD on, no land drain VI	0.02	17.2	79.1
SSD on, land drain VI	7.4	17.7	38.2
SSD off, land drain VI	0.4	16.1	38.3
	Averaged radon soil gas concentration [pCi/L]		
SSD off, no land drain VI	364.6	1538.3	1779.1
SSD on, no land drain VI	26.0	808.4	1415.0
SSD on, land drain VI	48.2	1020.3	1604.0
SSD off, land drain VI	350.9	1850.3	2031.4

Distributions shown in Figure 4.12 were generated using on-site survey results collected under natural pressure conditions when the lateral valve was closed. These are comparable to the TCE soil gas profiles collected earlier at this site and shown in Figure 3.8 and in Guo et al. (2015). In general TCE concentrations decrease from the north to the south (back to front of the house) at the 0.9 m BS and 1.8 m BS depths, and TCE soil

gas concentrations decreased in moving from the deepest depths to the building and ground surface.

Operation of the SSD system with the lateral valve closed generally caused decreases in TCE and radon concentrations in the sub-slab soil gas zone, the averaged TCE and radon concentration decreased about 3X and over 100X respectively. This was likely caused by increased lateral flow immediately below the foundation, with clean atmospheric air being pulled from ground surface. There were also increases in TCE concentrations at some deeper depths; for example, From Figure 4.12 to 4.13, it can be seen that TCE soil vapor concentrations increased at some 0.9 m BS depth locations; the spatially-averaged concentration beneath the building footprint increased by about 5X from 3.2 ppb_v to 17.2 ppb_v. This increase could be the result of increased source strength as the spatially averaged TCE concentration at 1.8 m BS was 25.2 ppb_v before SSD operation and it increased about 3X to 79.1 ppb_v during SSD operation.

Opening of the lateral valve resulted in additional changes in the soil gas distribution as shown in Figure 4.14. TCE concentrations in the sub-slab region increased significantly, similar to observations from the controlled pressure method (CPM) test discussed in Chapter 3. The SSD system created a depressurized pressure field beneath the house but with greater vacuums than during the CPM test. Therefore, an increase in the sub-slab depth TCE concentrations was expected when the SSD system was on and the lateral valve was open; for example, the TCE sub-slab soil gas concentration at location 2 was 100X greater than it was under any other conditions. The radon concentrations increased by about 2X beneath the garage portion of the foundation and

increases also occurred at the 0.9 m BS depth, both of which might reflect a reduction in the vacuum field and air flow from the atmosphere to beneath the foundation.

The elevated soil gas concentrations at the sub-slab depth during SSD system operation and the land drain lateral valve open raised questions about the potential for transient CHC impacts to indoor air during SSD system shut-downs (e.g., blower failure, power failure, or intentional shut-down) or during times when significant indoor-outdoor under-pressurization occurs naturally (e.g., during high wind events or significant indoor-outdoor temperature differences).

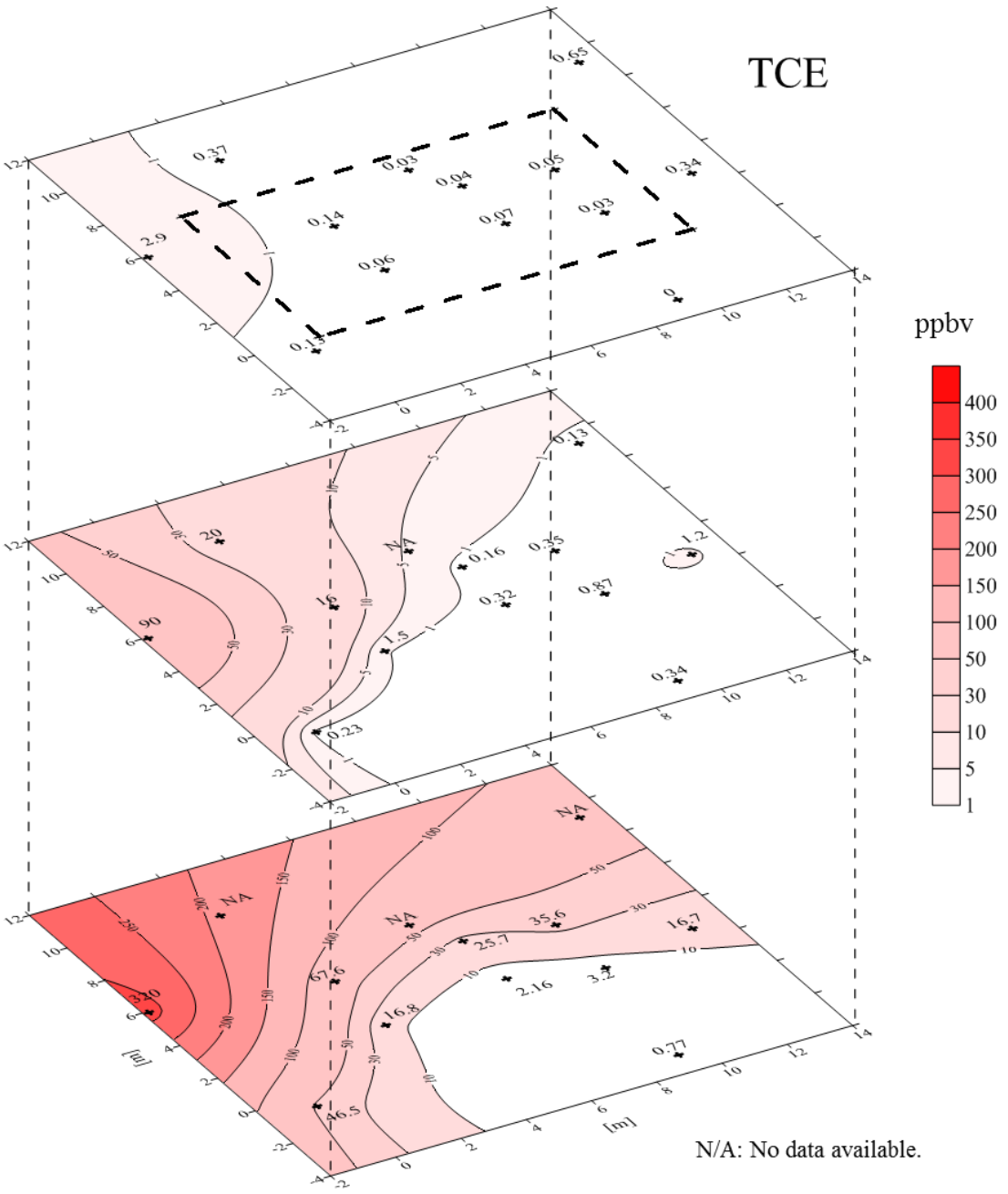
TCE
ppbv
400
350
300
250
200
150
100
50
30
10
5
1
[ft]
[m]
N/A: No data available.

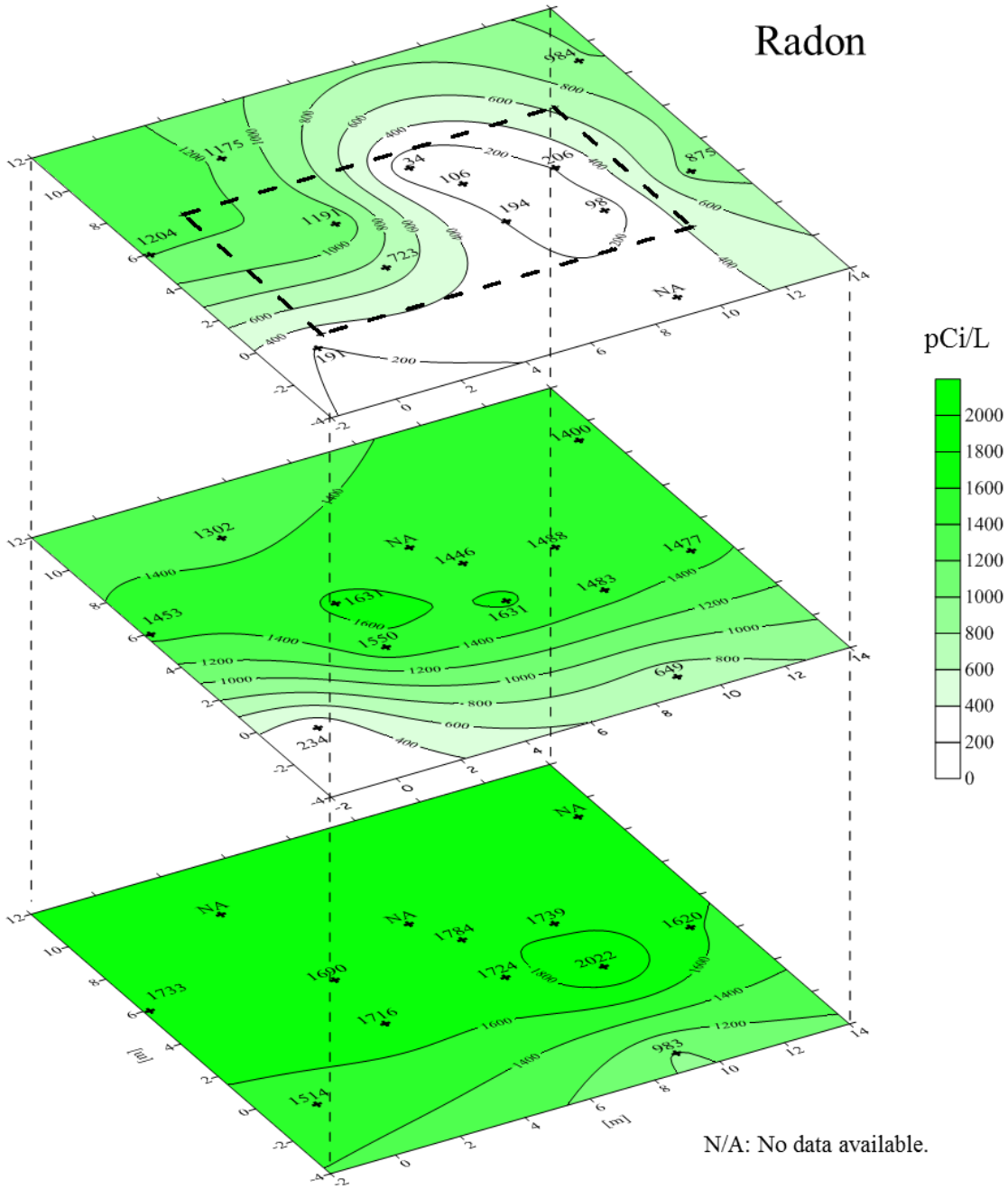

Figure 4.12. Representative TCE soil gas concentrations collected from t=28 d to 30 d before SSD system operation with closed land drain lateral valve. Sub-slab, 0.9 m BS and 1.8 m BS contours are shown from top to bottom. The bold dashed line in the sub-slab surface delineates the building perimeter.

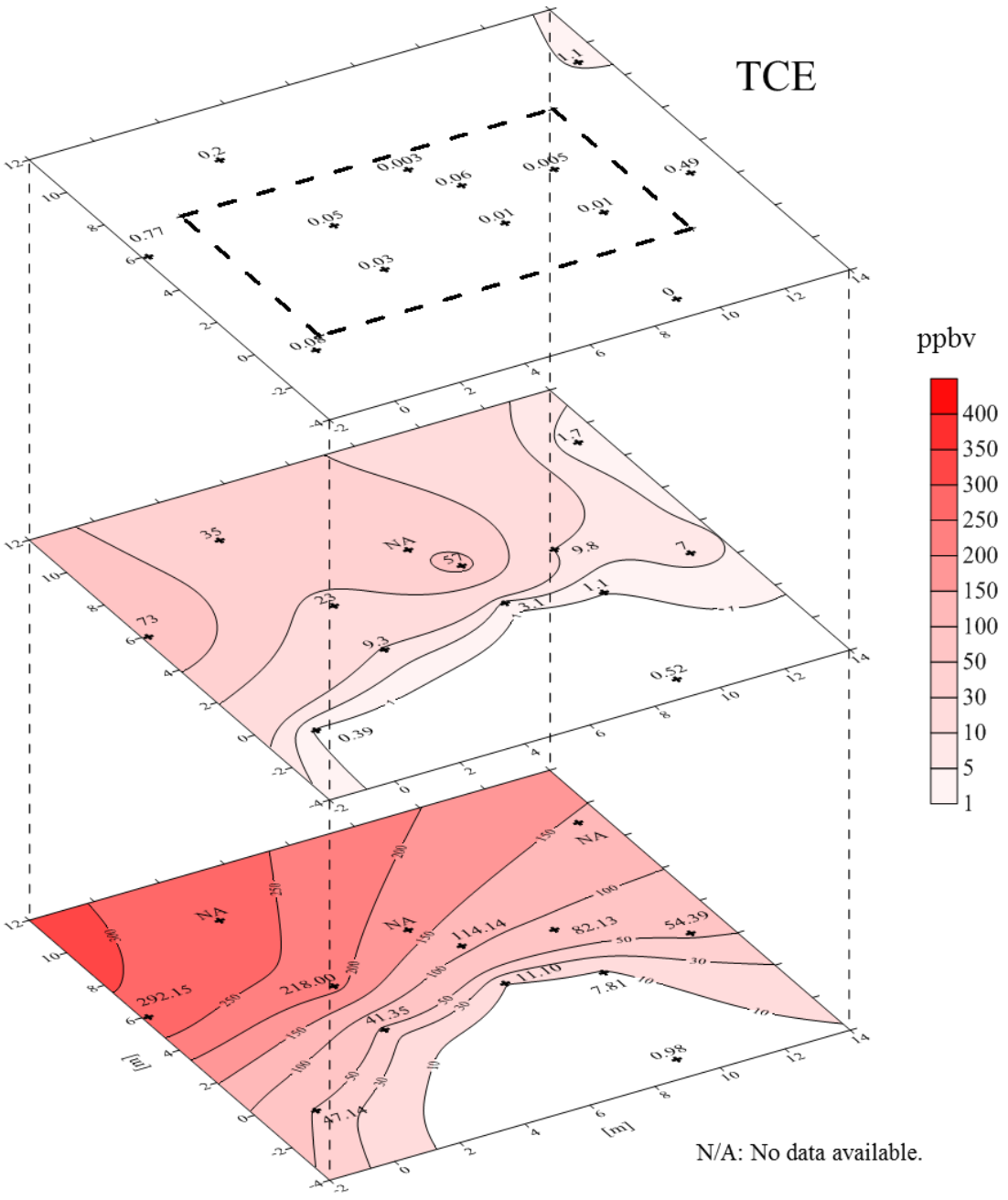
TCE
ppbv
400
350
300
250
200
150
100
50
30
10
5
1
[m]
[m]
N/A: No data available.

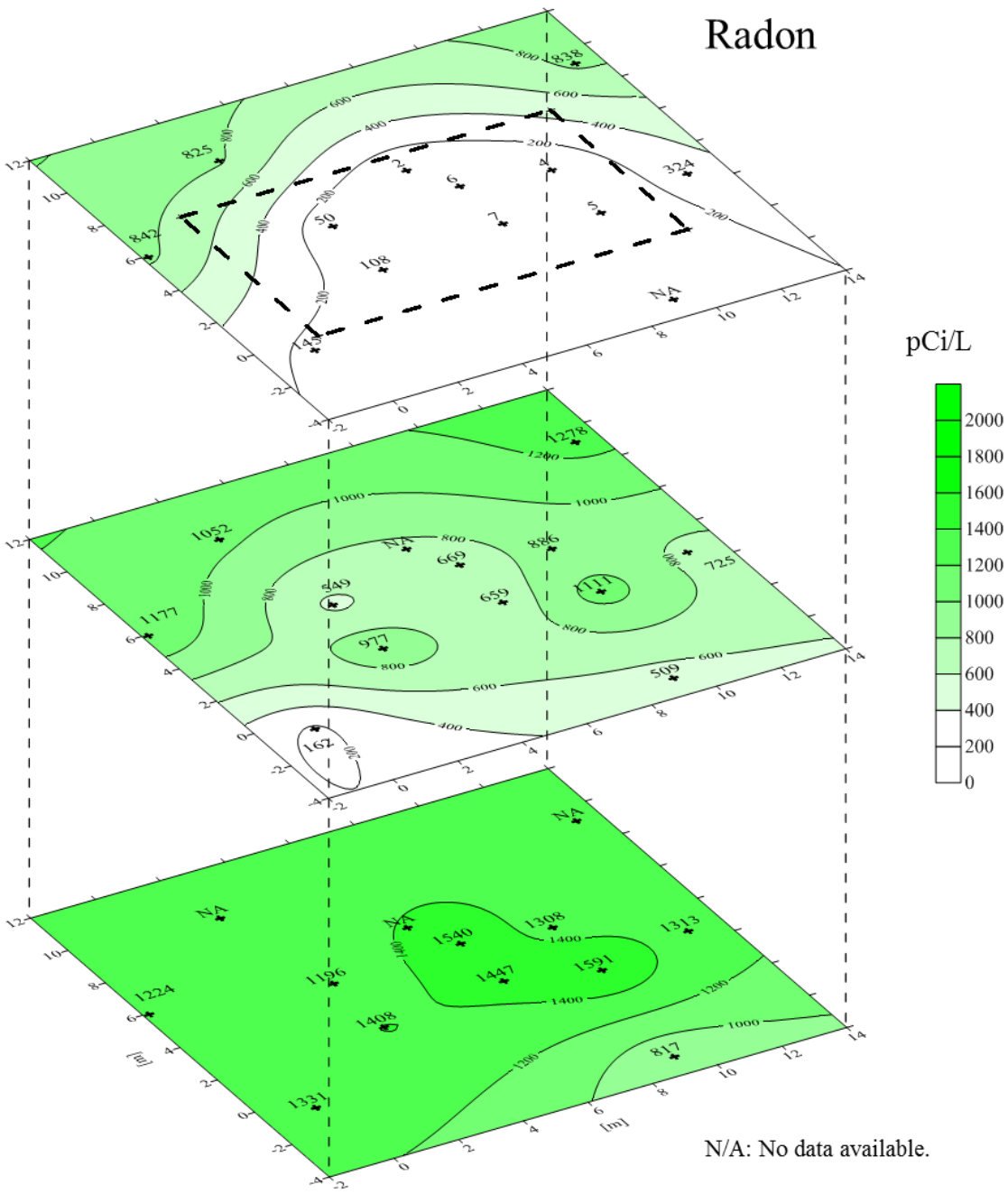

Figure 4.13. Representative TCE soil gas concentrations collected from t=66 d to 68 d during SSD system operating with closed land drain lateral valve. Sub-slab, 0.9 m BS and 1.8 m BS contours are shown from top to bottom. The bold dashed line in the sub-slab surface delineates the building perimeter.

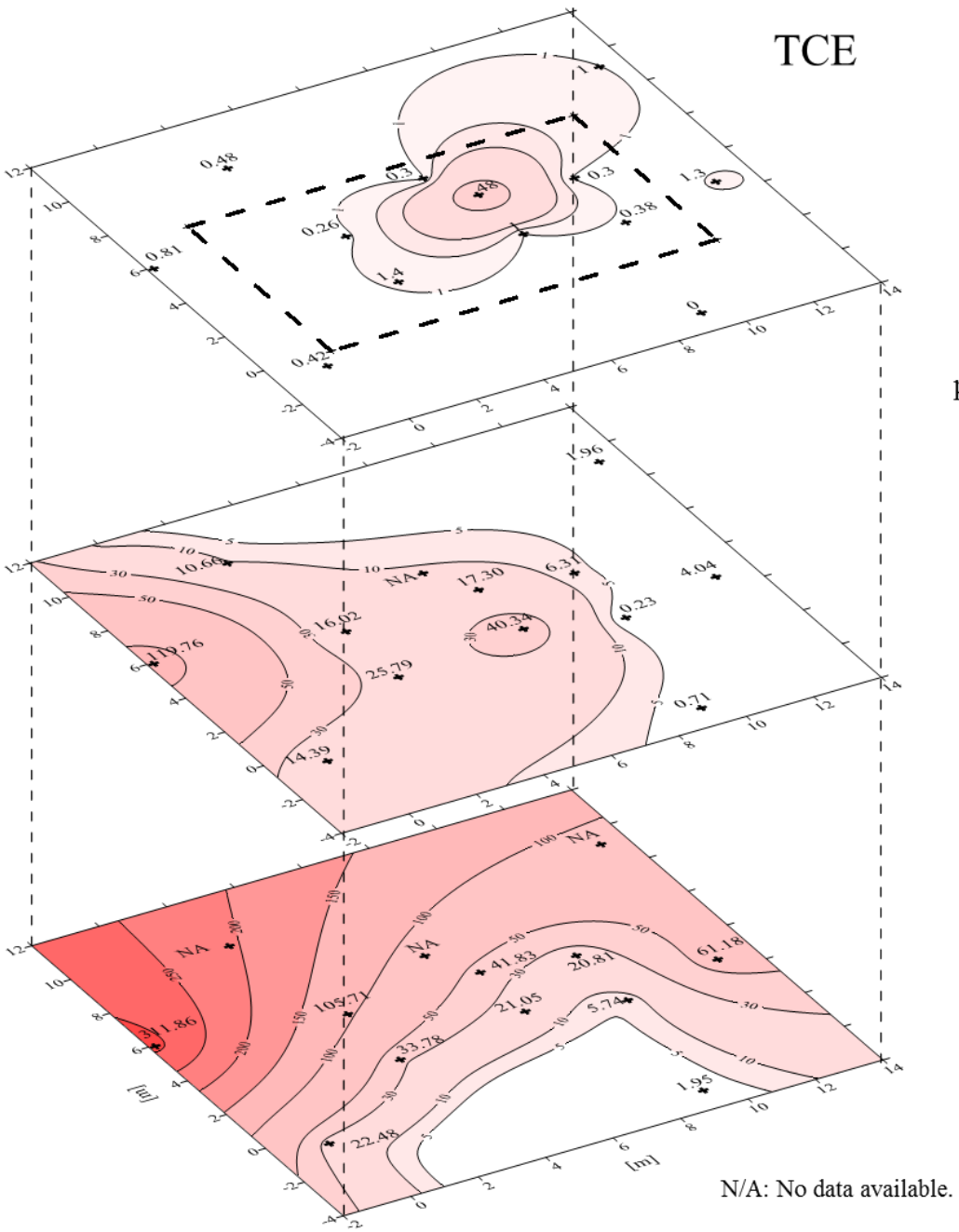
TCE
ppbv
400
350
300
250
200
150
100
50
30
10
5
1
[m]
[m]
N/A: No data available.

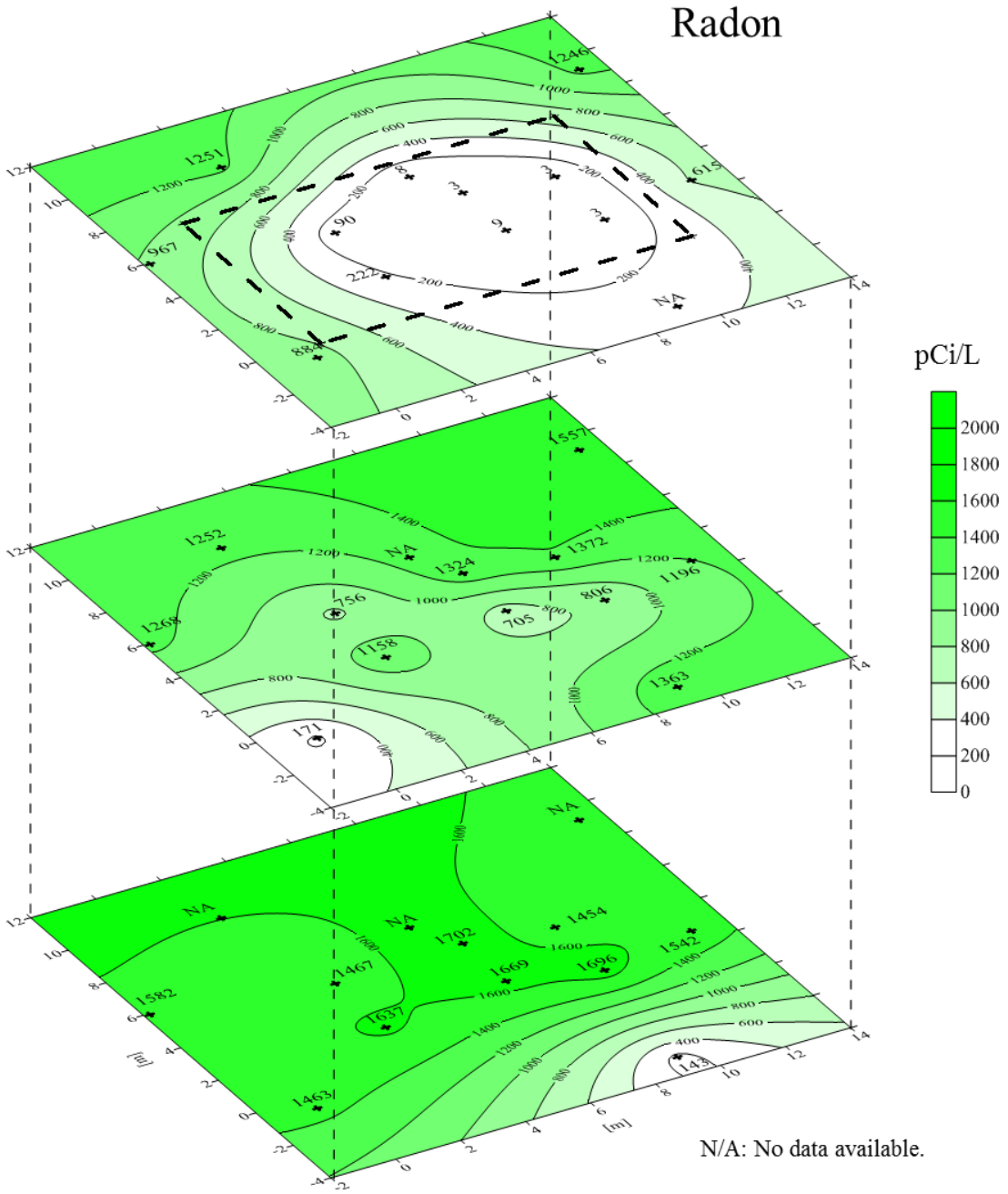

Figure 4.14. Representative TCE soil gas concentrations collected from t=167 d to 169 d during SSD system operating with open land drain lateral valve. Sub-slab, 0.9 m BS and 1.8 m BS contours are shown from top to bottom. The bold dashed line in the sub-slab surface delineates the building perimeter.

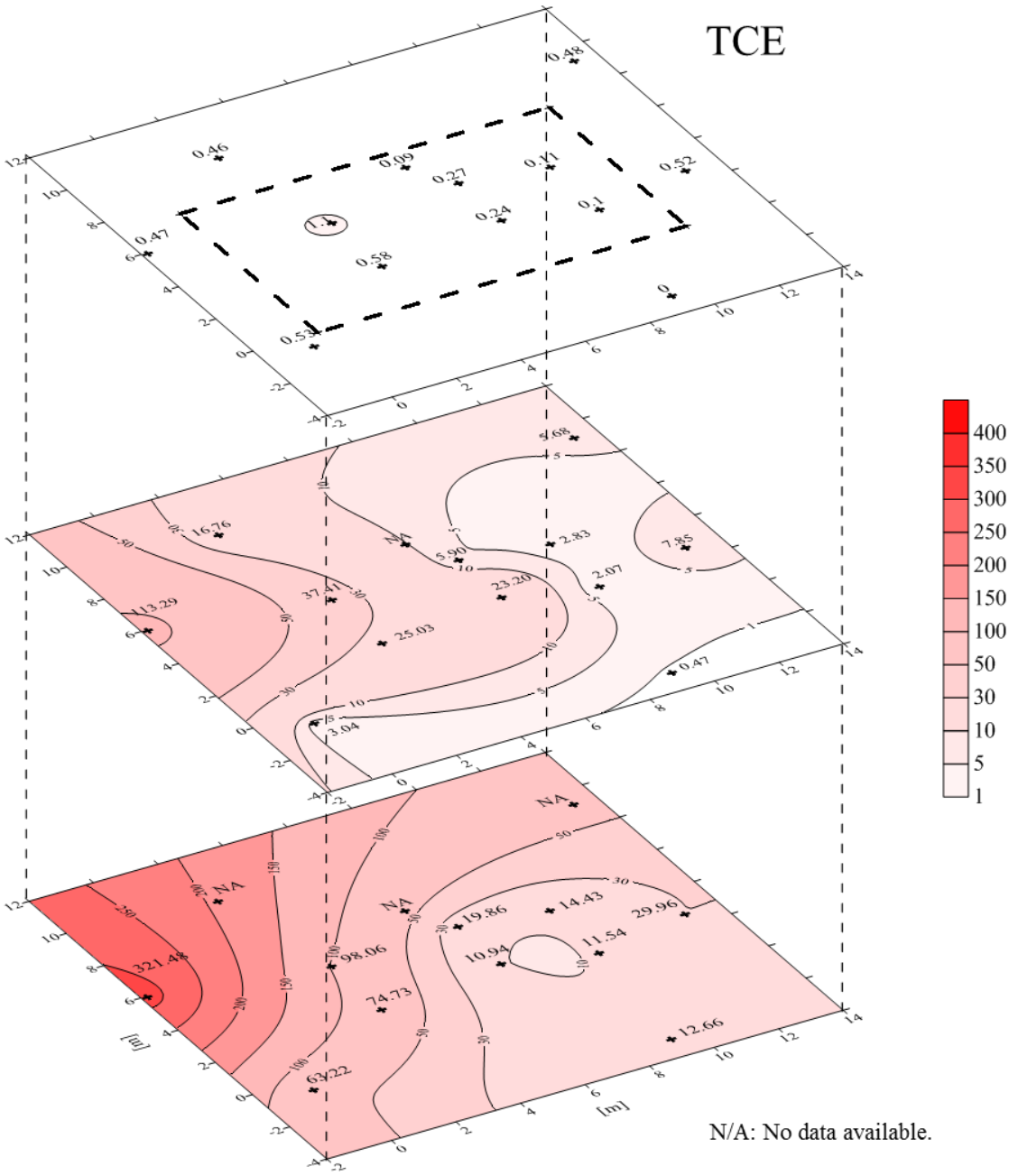
TCE
[ul]
[m]
400
350
300
250
200
150
100
50
30
10
5
1
N/A: No data available.

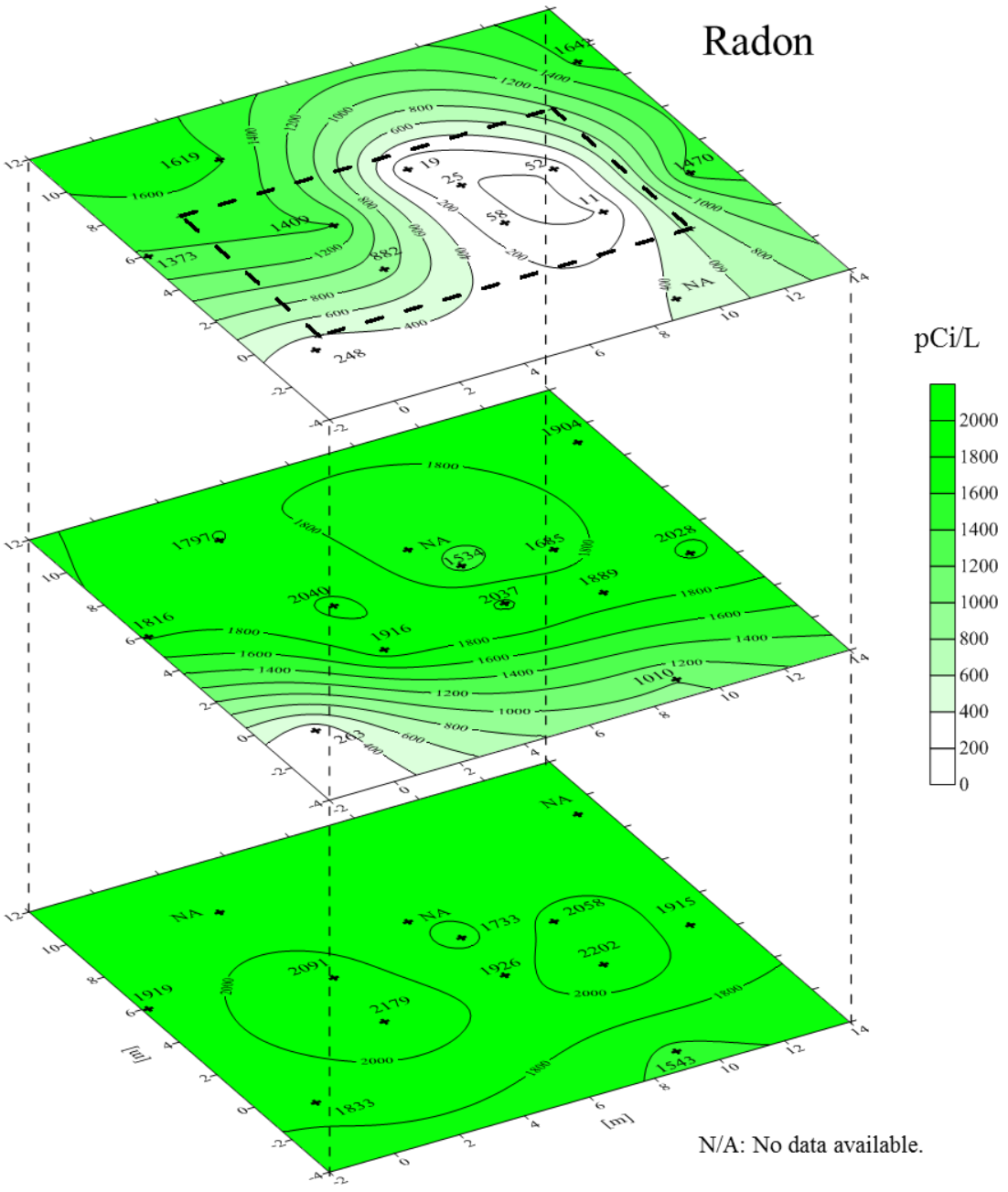

Figure 4.15. Representative TCE soil gas concentrations collected from t=231 d to 233 d after SSD system turned off with open land drain lateral valve. Sub-slab, 0.9 m BS and 1.8 m BS contours are shown from top to bottom. The bold dashed line in the sub-slab surface delineates the building perimeter.

Real-time soil gas TCE concentrations. Figure 4.16 to 4.21 present real-time soil gas TCE concentration at locations 1 through 6 at the sub-slab depth as well as 0.9 m BS at location 5. In this case, the TCE soil gas concentrations are less than the MDL, but the trends provide insight to TCE fate and transport beneath slab.

SSD systems are designed to collect chemical vapors in the sub-slab region and discharge them to the atmosphere. The vacuum induced by the SSD exhaust blower is expected to increase lateral sub-slab air flow from the atmosphere, which then causes a dilution or reduction in concentrations relative to natural conditions. Monitoring conducted during SSD operation shows that the SSD system behaved as expected when the lateral valve was closed. TCE soil gas concentration reductions were found at all sub-slab sampling ports once the SSD system was turned on.

In a pipe flow VI scenario, however, SSD operation can preferentially amplify chemical transport along the pipe flow VI pathway relative to natural conditions. During SSD operation there is a constant pressure difference in the sub-slab zone, rather than the time-varying and alternating pressure differential that occurs under natural conditions. That constant differential causes constant pipe flow, so the balance of diffusive-driven soil VI transport and advective pipe flow VI transport shifts to favor the pipe flow transport. This can be seen in the TCE soil gas concentration profiles presented above and transient responses shown below. Once the lateral valve was opened, TCE concentrations in sub-slab soil gas quickly increased in all monitoring locations. The greatest TCE concentration increases (over five orders of magnitude) were found at locations 2 and 5, which are located in between the SSD suction point and the lateral pipe

opening beneath the foundation. About one to two orders of magnitude increases can be seen at other locations.

After turning off the SSD system, sub-slab TCE vapor concentrations at location 2 declined from about 30 ppb_v to <1 ppb_v in 4 days. In contrast, it took more than 50 days for 0.9 m BS TCE concentrations at location 5 to decline by about 50%. The persistence of increased concentrations relative to natural conditions raises concerns about possible VI impacts anytime the SSD is turned off or it fails to create a sufficient vacuum. In this case, the TCE indoor air concentrations remained low after the SSD was turned off as seen in Figure 4.10. That, however, is not unexpected as the SSD system was turned off in the middle of summer, which is when the indoor air pressure is typically greater than the sub-slab pressure at this study house, which drives flow of indoor air to the subsurface. For example, Figure 4.23 presents two years of daily-average pressure differentials from sub-slab region to indoor air at location 5 (Holton 2015). As can be seen, the pressure differential generally favors downward flow in the summer and upward flow into the house in the winter. The shut-down test would need to be conducted in the winter to see if indoor air impacts could be caused by temporary SSD system shut-down.

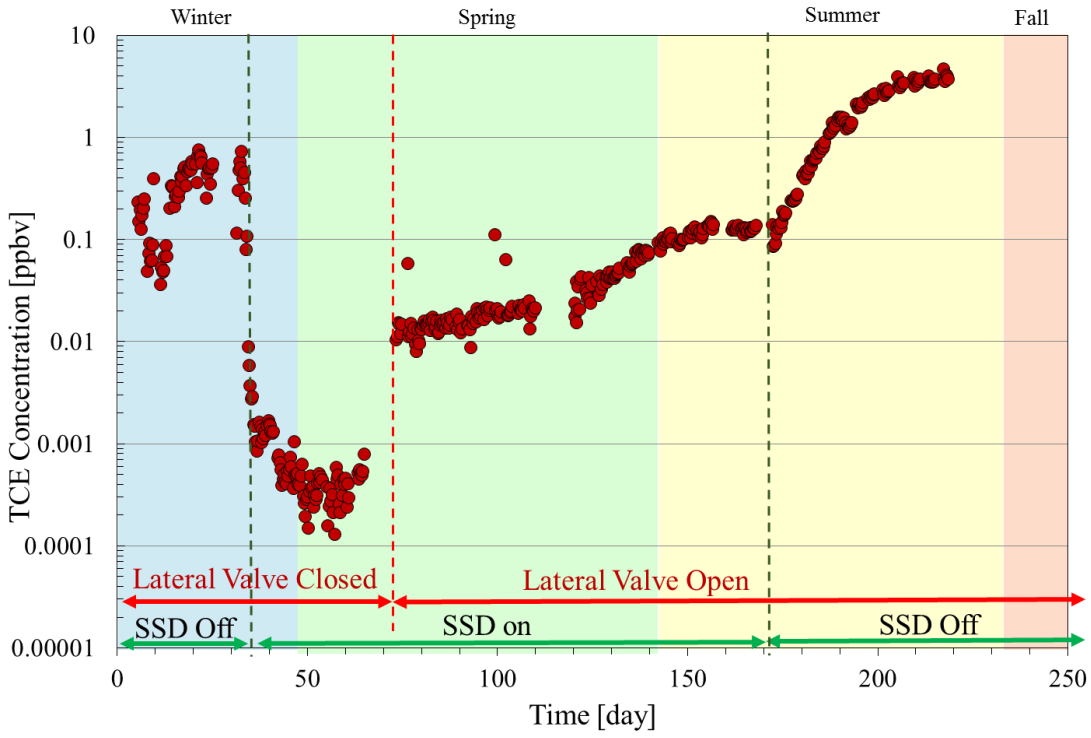

Figure 4.16. Real-time TCE sub-slab soil gas concentrations at location 1.

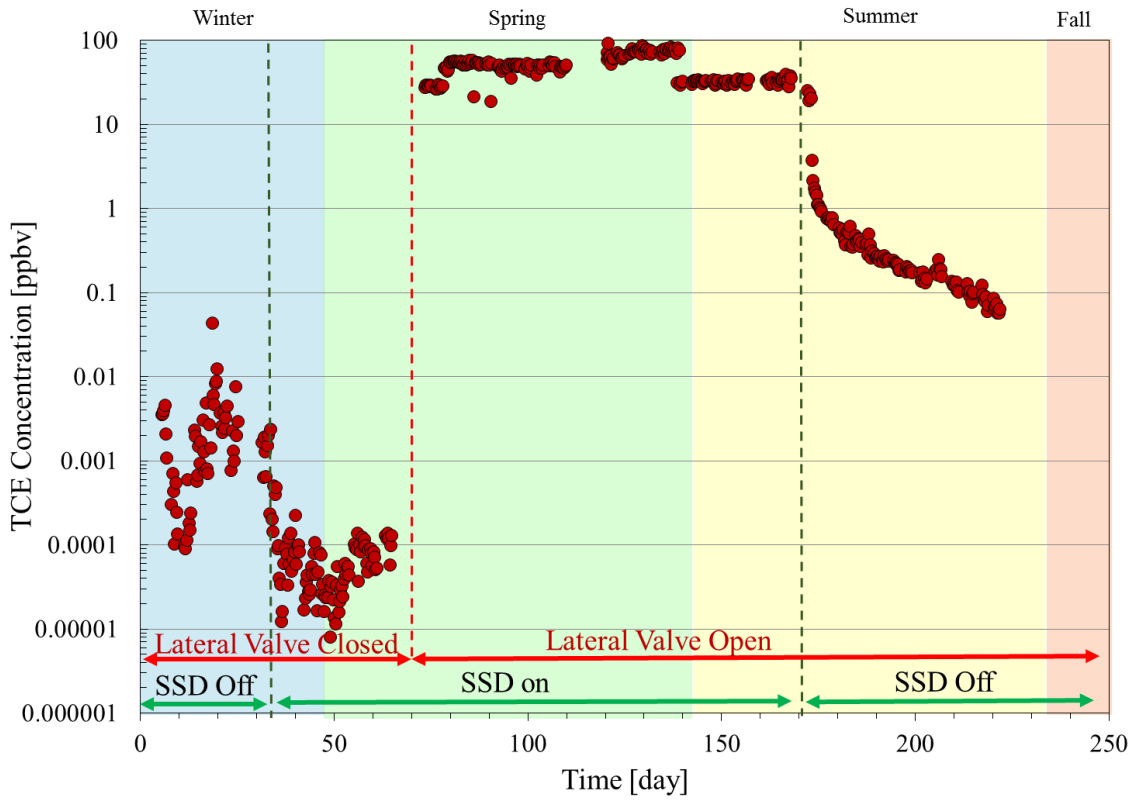

Figure 4.17. Real-time TCE sub-slab soil gas concentrations at location 2.

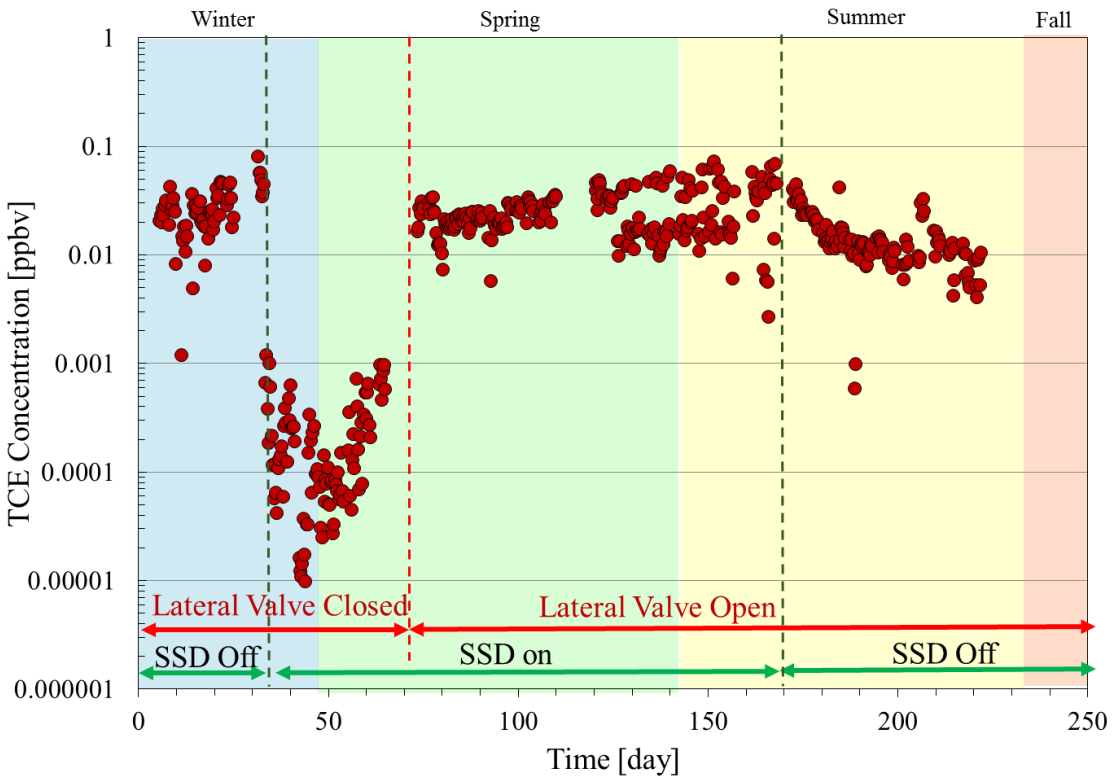

Figure 4.18. Real-time TCE sub-slab soil gas concentrations at location 3.

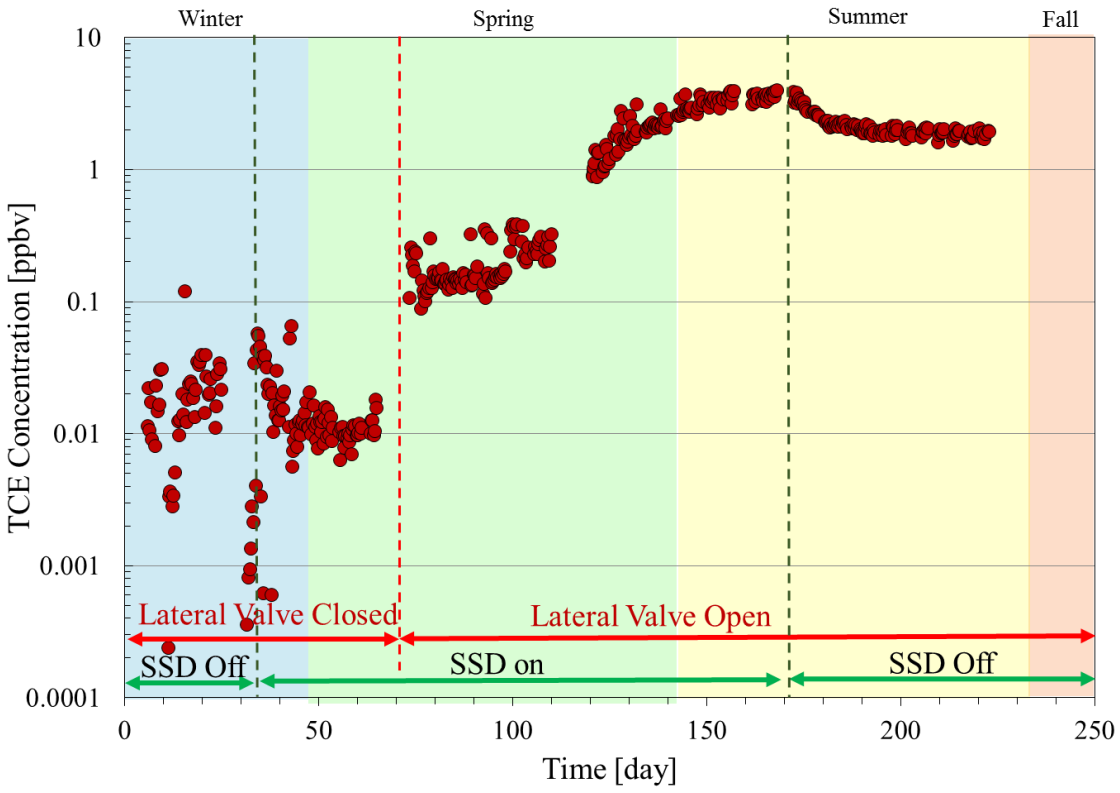

Figure 4.19. Real-time TCE sub-slab soil gas concentrations at location 4.

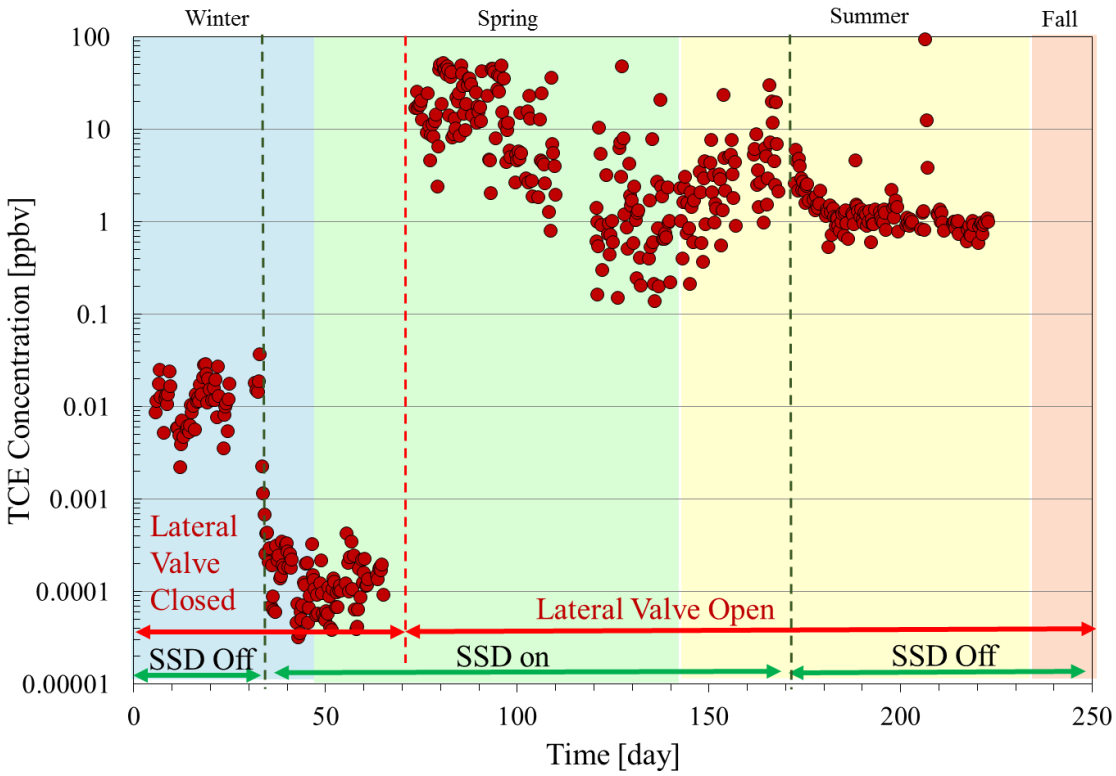

Figure 4.20. Real-time TCE sub-slab soil gas concentrations at location 5.

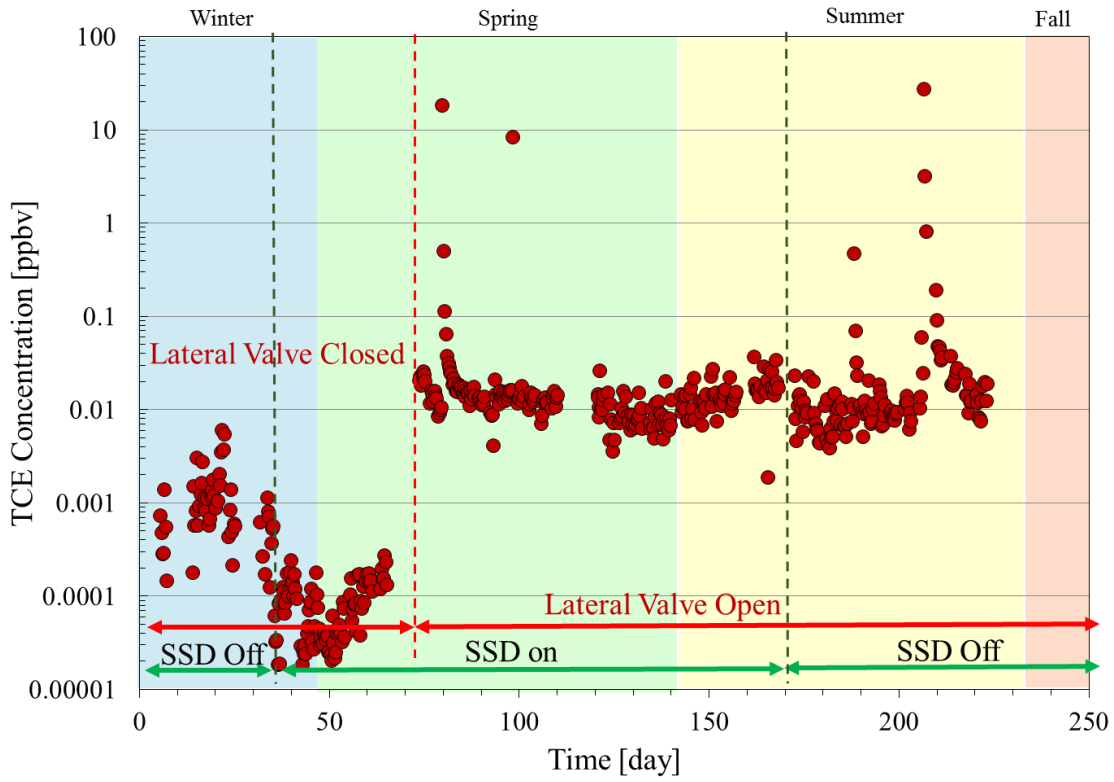

Figure 4.21. Real-time TCE sub-slab soil gas concentrations at location 6.

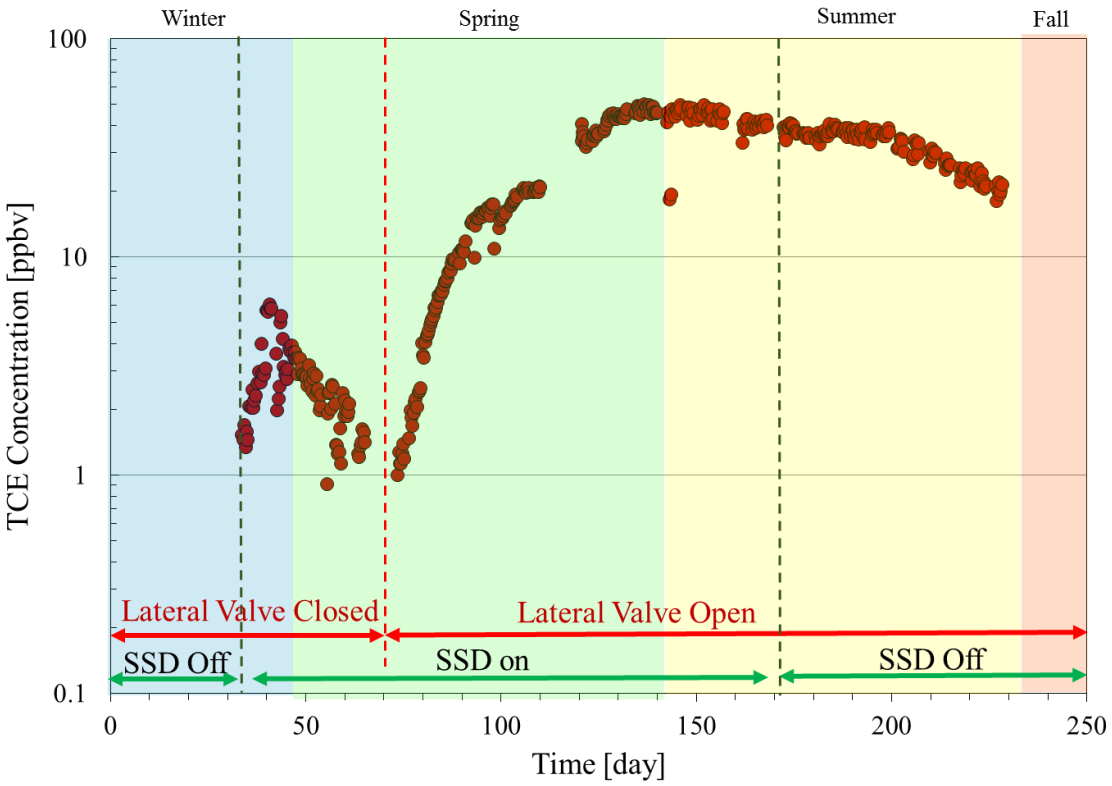

Figure 4.22. Real-time TCE 0.9 m BS soil gas concentrations at location 5.

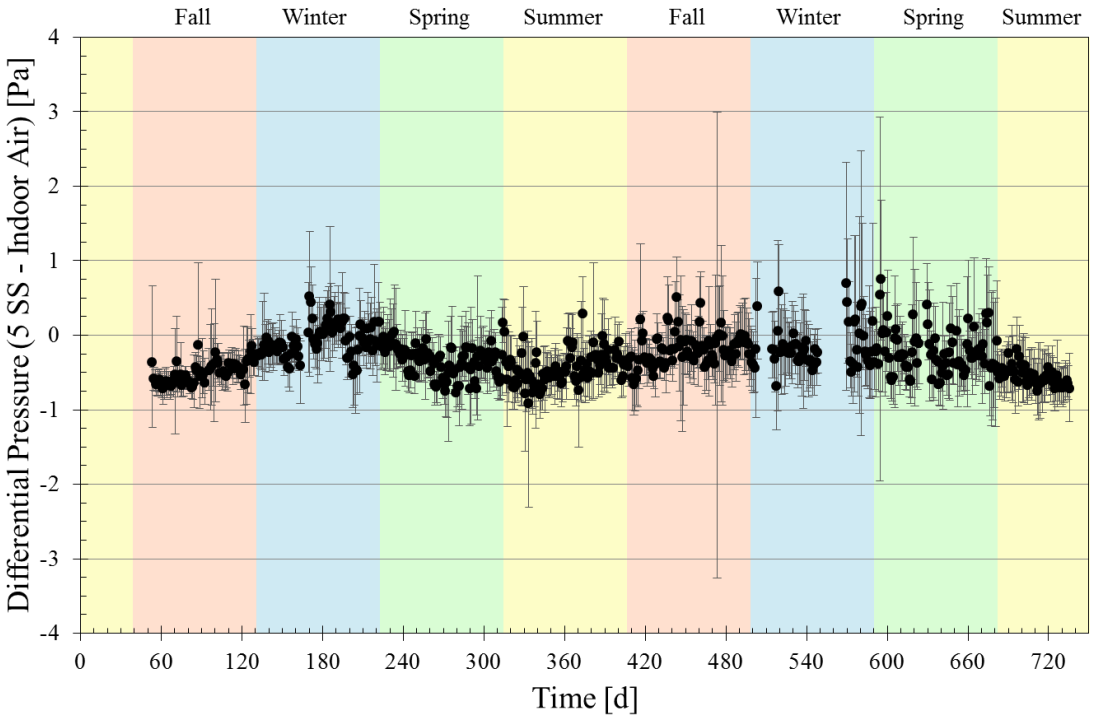

Figure 4.23. Daily-average differential pressure values between sub-slab soil gas and indoor air at location 5 with error bars spanning the 90th and 10th percentile of the daily data sets. (Holton, 2015)

4.4 CONCLUSIONS

This study is the first to report monitoring of CHC and radon concentrations in indoor air and soil gas during extended SSD system operation. The SSD system significantly reduced indoor air concentrations relative to long-term time averages under natural conditions with and without the alternative VI pathway. The 24-h average indoor air TCE concentration during SSD system operation was 0.0023 ± 0.0015 ppb_v with the land drain lateral valve closed and 0.0027 ± 0.0042 ppb_v with it open.

The presence of a pipe flow VI pathway reduced the sub-slab vacuum distribution during SSD operation. For example, at location 6, the vacuum between indoor air and sub-foundation decreased about 45% once the lateral valve changed from closed to open; and

it approached the lower design limit suggested by USEPA (4-10 Pa vacuum over the entire building footprint, 2008). Relative to typical design metrics, this SSD appears to be over-designed from an extraction flow perspective as it created excessive vacuums at some locations (e.g. over 100 Pa vacuum at location 2). Given that there is growing emphasis on reducing energy use for SSD systems, it is easy to conceptualize the installation of systems with much lower flow rates and that marginally meet the target design metrics for pressure differentials. More study is needed to determine if those systems will be equally protective with and without the presence of significant alternative pathways. It might be valuable to explore a range of scenarios through mathematical modeling might and identify cases that should be tested with field studies.

Soil gas TCE concentrations increased at sub-slab and intermediate depths during SSD operation when the pipe flow VI pathway as active. The concentrations dissipated slowly over many days when the SSD system was turned off (e.g. sub-slab TCE vapor concentrations at location 2 declined from about 30 ppb_v to <1 ppb_v in 4 days). Although the TCE indoor air concentrations were unchanged, the slow post-SSD operation dissipation of elevated sub-foundation soil gas concentrations might have posed a risk to indoor air if the experiment was conducted at a time when the building was naturally under-pressurized (e.g. during the winter). This scenario should be tested in the future and until that is better understood, caution is needed when considering turning off SSD systems temporarily at pipe flow VI sites.

4.5 REFERENCES

Engler, C. D. (2006). Design considerations of VI mitigation systems. Paper presented at the Vapor Intrusion-The next great environmental challenge. 2006 Air and Waste Management Conference, Philadelphia, PA. Pittsburgh, PA: Air & Waste Management Association.

Guo, Y., Holton, C. W., Luo, H., Dahlen, P., Gorder, K., Dettenmaier, E. M., & Johnson, P. C. (2015). Identification of Alternative Vapor Intrusion Pathways Using Controlled Pressure Testing, Soil Gas Monitoring, and Screening Model Calculations. *Environmental Science and Technology*. DOI: 10.1021/acs.est.5b03564.

Holton, C.; Luo, H.; Dahlen, P.; Gorder, K. A.; Dettenmaier, E. M.; Johnson, P. C. (2013). Temporal variability of indoor air concentrations under natural conditions in a house overlying a dilute chlorinated solvent groundwater plume. *Environmental Science and Technology*. 47, 13347-13354.

Holton, C.; Guo, Y.; Luo, H.; Dahlen, P.; Gorder, K. A.; Dettenmaier, E. M.; Johnson, P. C. (2015). Long-Term evaluation of the controlled pressure method for assessment of the vapor intrusion pathway. *Environmental Science and Technology*. 49, 2091-2098.

Interstate Technology & Regulatory Council. (2007). *Vapor intrusion pathway: A practical guideline*. Washington, DC: Interstate Technology & Regulatory Council.

Jiránek, M. (2014). Sub-slab depressurization systems used in the Czech Republic and verification of their efficiency. *Radiation protection dosimetry*. 162(1-2), 63-67.

Lutes, C. C., Truesdale, R. S., Cosky, B. W., Zimmerman, J. H., & Schumacher, B. A. (2015). Comparing Vapor Intrusion Mitigation System Performance for VOCs and Radon. *Remediation Journal*. 25(4), 7-26.

Pennell, K. G.; Scammell, M. K.; McClean, M. D.; Ames, J.; Weldon, B.; Friguglietti, L.; Suuberg, E. M.; Shen, R.; Indeglia, P. A.; Heiger-Bernays, W. J. (2013) Sewer gas: An indoor air source of PCE to consider during vapor intrusion investigations. *Ground Water Monit. Rem. 33* (3), 119-126.

Riis, C. E.; Christensen, A. G.; Hansen, M. H.; Husum, H.; Terkelsen, M. (2010) Vapor Intrusion through Sewer Systems: Migration Pathways of Chlorinated Solvents from Groundwater to Indoor Air. Presentation at the 7th Battelle International Conference on Remediation of Chlorinated and Recalcitrant Compounds, Monterey.

Rydock, J. P., & Skåret, E. (2002). A case study of sub-slab depressurization for a building located over VOC-contaminated ground. *Building and environment*. 37(12), 1343-1347.

U.S. Environmental Protection Agency. (1993). Radon reduction techniques for existing detached houses -Technical guidance (third edition) for active soil depressurization systems. Washington, DC: U.S. Government Printing Office.

U.S. Environmental Protection Agency. (2008). Engineering issue: Indoor air vapor mitigation approaches. Washington, DC: U.S. Environmental Protection Agency.

U.S. Environmental Protection Agency. (2015). *OSWER TECHNICAL GUIDE FOR ASSESSING AND MITIGATING THE VAPOR INTRUSION PATHWAY FROM SUBSURFACE VAPOR SOURCES TO INDOOR AIR*. Washington, DC: U.S. Environmental Protection Agency.

CHAPTER 5

CONCLUSIONS AND RECOMMENDATIONS FOR FUTURE WORK

5.1 CONCLUSIONS

The research presented in this dissertation focused on improving our understanding of the significance of groundwater fluctuations and alternative VI pathways on vapor intrusion (VI) impacts and how they should be addressed during VI pathway assessment and mitigation. Long-term field monitoring studies, lab-scale physical model experiments, and modeling analyses were conducted.

Key conclusions from this study related to groundwater table fluctuations include:

- Groundwater table elevation changes with time can result in increased volatile organic chemical (VOC) emissions from groundwater to indoor air relative to emissions from static water table conditions. This was shown clearly in lab experiments and mathematical modeling. These results, however, suggest that long-term average emission increases are likely to be less than 2x for most site conditions encountered, and that was consistent with results at the field study house. The implication here is that emissions from groundwater and near-building upward VOC fluxes are not expected to vary significantly with time and that it is defensible to assume static water table conditions when performing screening-level estimates of VI impacts. The results also suggest that the exception to this conclusion occurs under conditions with shallow water tables (<1 m below a building) and higher-frequency elevation changes (daily-monthly).

Under those conditions, emissions could be up to about 10X greater than expected for static water table conditions. Further examination of a broader range of scenarios is needed to increase confidence in this conclusion.

- As discussed above and in the literature (Wener and Hohener, 2002; Picone et al., 2012), VOC emissions increase and decrease during water table drops and rises, respectively. However, none of the published results or results from this work suggest emission changes of the magnitude observed in long-term indoor air monitoring (one to three orders-of-magnitude) (e.g., Folks, et al. 2009; Holton, et al. 2013). This suggests that water table fluctuations are not likely the major cause for indoor air temporal variability. The most likely causes are the dynamic pressure changes surrounding the building envelope as they control the rate of flow into and out of the building across the building foundation.
- The only significant VOC emission variations >100X were found under the scenarios with 100 cm water table oscillations and shallow depths to groundwater.

Key conclusions related to alternative VI pathway assessment and mitigation include:

- The contribution of the alternative vapor intrusion pathway (land drain lateral valve open) was clearly evident at the field study site as the mean emission rate with the land drain lateral valve open (0.18 g/d) was about

two orders-of-magnitude greater than the mean emission rate with the land drain valve closed (0.0013 g/d). It was also about two orders-of-magnitude or more greater than any of the emission rate estimates generated from subsurface concentration and effective diffusion coefficient data.

- The presence of this significant pipe flow alternative VI pathway was not discovered during two-years of intensive indoor air, soil gas, groundwater, and building pressure differentials monitoring under natural conditions. It was only found and confirmed by analysis of CPM test data.
- Inconsistency between estimated and measured emission rates can be a line of evidence for identifying alternative VI pathways.
- Soil gas distributions can be used to identify pipe flow alternative VI pathway presence. In this case, the inconsistency between measured soil gas concentration distribution and what is expected for diffusion-driven soil gas VI pathway scenarios was a key indicator of the pipe flow VI pathway. Sub-slab depth concentrations at some locations were greater than 1.8 m BS near-source concentrations.

With respect to the effectiveness of SSD system operation at the field study site:

- The presence of the pipe flow VI pathway at this site reduced the vacuum effectiveness of the SSD system. At location 6, the vacuum between indoor air and sub-slab air decreased by about 45% when the pipe flow pathway was opened. It declined to the lower limit of suggested operational conditions (4-10 Pa; USEPA, 2008).

- Although this SSD provided enough protection throughout the test (< 0.1 ppb_v indoor air TCE concentrations under all conditions), it is not clear that this will be universally true for all sites and SSD systems (e.g large-footprint buildings with multiple VI pathways).
- TCE concentrations increased significantly at both sub-slab and 0.9 m below slab depth depths beneath the building during SSD operation when the pipe flow VI pathway was open. These concentrations dissipated slowly over many days when the SSD system was turned off. While this was not observed at the study house, it seems that this could result in indoor air impacts under other scenarios not studied; for example, cases with consistent soil gas flow into a building under natural conditions.

5.2 RECOMMENDATIONS FOR FUTURE WORK

The conclusions above have added to our understanding of the significance of groundwater fluctuations and alternative VI pathways on vapor intrusion (VI) impacts and how they should be addressed during VI pathway assessment and mitigation; however, further research is needed as discussed below:

- Groundwater fluctuation
    - Other than this work, there have been few attempts to understand the effect of groundwater table fluctuation on VI impacts. This work suggests little impact, except at shallow sites with frequent groundwater table elevation changes. Thus, it would be useful verify or refute that by conducting a study at a site with these

conditions – for example, at a building overlying impacted groundwater in a tidally-influenced area.

  - The modeling tool used for these studies does not include advective gas flow transport, and as such, the simulation results may not fully predict the response of high-frequency and high magnitude water table oscillations. Thus, more comprehensive modeling analyses are recommended to more fully understand VOC emission responses to fast water table movement.

- Identifying alternative VI pathways
  - The conclusion here is obtained from a specific site and with the pipe flow VI pathway. Thus, the utility and value of CPM tests and soil gas monitoring at other sites and other alternative VI pathways should be tested.
  - Given the practical limitations of test site availability, numerical modeling could be used to explore other field test conditions.
  - The proposed site assessment methodology incorporates CPM testing. However, there are only a few data sets demonstrating the effectiveness of CPM testing and no standard CPM test protocols can be found. As such, the development of standard procedures for conducting and interpreting CPM test and its results would provide a baseline standard for use of the technology.
- SSD mitigation on alternative VI pathways

- The SSD at the study site was over-designed relative to minimum SSD design guidelines. Thus, it might be useful to test its effectiveness under other operating conditions that might occur and that are consistent with today's design guidelines.
- Concerns regarding possible VI impacts associated with interruptions of SSD system operation and the slow dissipation of sub-slab TCE concentrations were raised. Since there are no data to support or refute these concerns, modeling of various SSD operational scenarios with failures and with varying alternative VI pathways would provide insight into these areas of concern.
  This study encompasses experiences at a field site with pipe flow VI and an SSD mitigation system. The effectiveness of other VI mitigation systems (e.g. passive venting, sub-slab pressurization) and/or the effect of different types of alternative pathways (e.g. sewer VI) is unknown. Both field and modeling studies are recommended to better understand other types of mitigation systems and other types of alternative VI pathways.

BIBLIOGRAPHY

Abreu, L. (2009). A transient three dimensional numerical model to simulate vapor intrusion into buildings. (Dissertation), Arizona State University, Tempe, AZ, 2005.

Abreu, L., Johnson, P. C. (2005). Effect of vapor source-building separation and building construction on soil vapor intrusion as studied with a three-dimensional numerical model. *Environmental Science and Technology*, *39* (12), 4550-4561.

Abreu, L.; Johnson, P. C. (2006). Simulating the Effect of Aerobic Biodegradation on Soil Vapor Intrusion into Buildings: Influence of Degradation Rate. Source Concentration, and Depth. *Environmental Science and Technology, 40,* 2304-2315.

American Petroleum Institute. (2005). *A practical strategy for assessing the subsurface vapor-to-indoor air migration pathway at petroleum hydrocarbon sites*. Washington, DC: American Petroleum Institute.

Atteia, O.; Hohener, P. (2010). Semianalytical model predicting transfer of volatile pollutants from groundwater to the soil surface. *Environmental Science and Technology,* 44, 6228-6232.

Bozkurt, O., Pennell, K. G., Suuberg, E. M. (2009). Simulation of the vapor intrusion process for nonhomogeneous soils using a three-dimensional numerical model. *Groundwater Monitoring and Remediation*, *29* (1), 92-104.

California Department of Toxic Substances Control. (2011). *Guidance for the evaluation and mitigation of subsurface vapor intrusion to indoor air (Vapor intrusion guidance).*

Department of Defense. (2009). *Vapor intrusion handbook*. Washington, DC: Department of Defense.

Engler, C. D. (2006). Design considerations of VI mitigation systems. Paper presented at the Vapor Intrusion-The next great environmental challenge. 2006 Air and Waste Management Conference, Philadelphia, PA. Pittsburgh, PA: Air & Waste Management Association.

Escobar Melendez, E. A. (2012). Transport and Biodegradation of Petroleum Hydrocarbon Vapors in the Subsurface. A Laboratory Soil Column Study (Doctoral dissertation). Arizona State University.

Folkes, D., Wertz, W., Kurtz, J., Kuehster, T. (2009). Observed spatial and temporal distributions of CVOCs at Colorado and New York vapor intrusion sites. *Ground Water Monitoring and Remediation*, *29*, 70-80.

Garbesi, K., Sextro, R. G. (1989). Modeling and field evidence of pressure-driven entry of soil gas into a house through permeable below grade walls. *Environmental Science and Technology, 23* (12), 1481-1487.

Guo, Y., Holton, C. W., Luo, H., Dahlen, P., Gorder, K., Dettenmaier, E. M., & Johnson, P. C. (2015). Identification of Alternative Vapor Intrusion Pathways Using Controlled Pressure Testing, Soil Gas Monitoring, and Screening Model Calculations. *Environmental Science and Technology.* DOI: 10.1021/acs.est.5b03564.

Gribovszki, Z.; Szilagyi, J.; Kalicz, P. (2010). Diurnal fluctuation in shallow groundwater levels and streamflow rates and their interpretation – A review. *Journal of Hydrology, 385*, 371-383.

Hawkins, J. (2008). Vapor Intrusion in Texas- Evaluating the Indoor Air Pathway. Presentation at Society of Texas Environmental Professionals (STEP). Texas.

Hintenlane, D.E.; Al-Ahmady, K.K. (1992). Pressure Differentials for Radon Entry Coupled to Periodic Atmospheric Pressure Variations. *Indoor Air, 2* (12), 208-215.

Holton, C.; Luo, H.; Dahlen, P.; Gorder, K. A.; Dettenmaier, E. M.; Johnson, P. C. (2013). Temporal variability of indoor air concentrations under natural conditions in a house overlying a dilute chlorinated solvent groundwater plume. *Environmental Science and Technology, 47*, 13347-13354.

Holton, C.; Guo, Y.; Luo, H.; Dahlen, P.; Gorder, K. A.; Dettenmaier, E. M.; Johnson, P. C. (2015). Long-Term Evaluation of the Controlled Pressure Method for Assessment of the Vapor Intrusion Pathway. *Environmental Science and Technology, 49,* 2091-2098.

Howard, P.H. (1991). *Handbook of Environmental Degradation Rates*. Lewis Publishers, Chelsea, MI.

Hubbard, L. M., Mellander, H., Swedejemark, G. A. (1995). Studies on temporal variations of radon in Swedish single-family houses. *Environment International, 22*, S715-S722.

Interstate Technology & Regulatory Council. (2007). *Vapor intrusion pathway: A practical guideline*. Washington, DC: Interstate Technology & Regulatory Council.

Jiránek, M. (2014). Sub-slab depressurization systems used in the Czech Republic and verification of their efficiency. *Radiation protection dosimetry*. 162(1-2), 63-67.

Johnson, J. E. (2013). Assessing Exposure to Chlorinated Solvents from the Subsurface to Indoor Air Pathway. Ph.D. Dissertation, University of North Carolina, Chapel Hill, NC.

Johnson, P. C., Ettinger, R. A. (1991). Heuristic model for predicting the intrusion rate of contaminant vapors into buildings. *Environmental Science and Technology, 25* (8), 1445-1452.

Johnson, P. C., Bruce, C., Johnson, R. L., Kemblowski, M. W. (1998). In situ measurement of effective vapor-phase porous medium diffusion coefficient. *Environmental Science & Technology*, 32, 3405-3409.

Leduc, C.; Bromley, J.; Schroeter, P. (1997). Water table fluctuation and recharge in semi-arid climate: some results of HAPEX-Sahel hydrodynamic survey (Niger). *Journal of Hydrology, 188-189*, 123-138.

Li, H., Jiao, J. J. (2005). One-dimensional airflow in unsaturated zone induced by periodic water table fluctuation. *Water resources research, 41*(4).

Little, J. C., Daisey, J. M., Nazaroff, W. W. (1992). Transport of subsurface contaminants into buildings: An exposure pathway for volatile organics. *Environmental Science and Technology*, *26* (11), 2058-2066.

Loureiro, C. O. (1987). Simulation of Steady-state transport of radon from soil into houses with basement under constant negative pressure (Dissertation). Lawrence Berkeley Laboratory, Berkeley, CA.

Loureiro, C. O., Abriola, L. M., Martin, J. E., Sextro, R. G. (1990). Three-dimensional simulation of radon transport into houses with basements under constant negative pressure. *Environmental Science and Technology*, *24*, 1338-1348.

Luo, H. (2009). Field and modeling studies of soil gas migration into buildings at petroleum hydrocarbon impacted sites (Dissertation). Arizona State University, Tempe, AZ.

Luo, H., Dahlen, P., Johnson, P. C., Peargin, T., Creamer, T. (2009). Spatial variability of soil-gas concentrations near and beneath a building overlying shallow petroleum hydrocarbon-impacted soils. *Ground Water Monitoring and Remediation*, *29*, 81-91.

Lutes, C. C., Truesdale, R. S., Cosky, B. W., Zimmerman, J. H., & Schumacher, B. A. (2015). Comparing Vapor Intrusion Mitigation System Performance for VOCs and Radon. *Remediation Journal*. 25(4), 7-26.

Massachusetts Department of Environmental Protection. (2011). *Interim final vapor Intrusion guidance*. Boston, MA: Massachusetts Department of Environmental Protection.

McCarthy, K. A.; Johnson, R. L. (1993). Transport of volatile organic compound across the capillary fringe. *Water Resources Research, 29* (6), 1675-1683.

McHugh, T. E., Nickels, T. N., Brock, S. (2007). Evaluation of spatial and temporal variability in VOC concentrations at vapor intrusion investigation sites. Proceedings of Air and Waste Management Association's *Vapor intrusion: Learning from the challenges*, Providence, RI, 129-142.

McHugh, T. E., Beckley, L., Bailey, D., Gorder, K., Dettenmaier, E., Rivera-Duarte, I., Brock, S., MacGregor, I. C. (2012). Evaluation of vapor intrusion using controlled building pressure. *Environmental Science & Technology*, *46*, 4792-4799.

Moseley, C. L., Meyer, M. R. (1993). Petroleum contamination of an elementary school: A case history involving indoor air, soil-gas, and groundwater monitoring. *Environmental Science and Technology*, *26*, 185-192.

Nazaroff, W. W., Fuestel, H., Nero, A. V. Revzan, K. L., Grimsruf, D. T. (1985). Radon transport into a detached one-story house with a basement. *Environmental Science and Technology*, *19* (1), 31-46.

Nazaroff, W. W., Doyle, S. M. (1985). Radon entry into house having a crawl space. *Health Physics*, *48* (3), 265-281.

Nazaroff, W. W., Lewis, S. R., Doyle, S. M., Moed, B. A., Nero, A. V. (1987). Experiments on pollutant transport from soil into residential basements by pressure-driven airflow. *Environmental Science and Technology*, *21* (5), 459-466.

Nazaroff, W. W. (1992). Radon transport from soil to air. *Reviews of Geophysics*, *30* (2), 137-160.

New Jersey Department of Environmental Protection. (2013). *Vapor intrusion technical guidance.* Trenton, NJ: New Jersey Department of Environmental Protection.

New York State Department of Health. (2006). *Guidance for Evaluating Soil Vapor Intrusion in the State of New York*. Troy, NY: New York State Department of Health.

Parker, J. C. (2003). Modeling volatile chemical transport, biodecay, and emission to indoor air. *Groundwater Monitoring & Remediation*, 23(1), 107-120.

Patterson, B. M. and Davis, G. B. (2009). Qualification of Vapor Intrusion Pathways into a Slab-on-Ground Building under Varying Environmental Conditions. *Environmental Science and Technology, 43*, 650-656.

Pennell, K. G.; Scammell, M. K.; McClean, M. D.; Ames, J.; Weldon, B.; Friguglietti, L.; Suuberg, E. M.; Shen, R.; Indeglia, P. A.; Heiger-Bernays, W. J. (2013). Sewer gas: An indoor air source of PCE to consider during vapor intrusion investigations. *Groundwater Monitoring and Remediation, 33* (3), 119-126.

Picone, S., Valstar, J., van Gaans, P., Grotenhuis, T., Rijnaarts, H. (2012). Sensitivity analysis on parameters and processes affecting vapor intrusion risk. *Environmental Toxicology and Chemistry, 31* (5), 1042-1052.

Riley, W. J., Robinson, A. L., Gadgil, A. J., Nazaroff, W. W. (1999). Effects of variable wind speed and direction on radon transport from soil into buildings: Model development and exploratory results. *Atmospheric Environment, 33*, 2157-2168.

Riis, C. E.; Christensen, A. G.; Hansen, M. H.; Husum, H.; Terkelsen, M. (2010). Vapor Intrusion through Sewer Systems: Migration Pathways of Chlorinated Solvents from Groundwater to Indoor Air. Presentation at the 7th Battelle International Conference on Remediation of Chlorinated and Recalcitrant Compounds, Monterey.

Robinson, A. L. (1993). Radon Entry into Buildings: Effects of Atmospheric Pressure Fluctuations and Building Structural Factors (Dissertation). University of California, Berkeley.

Robinson, A. L., Sextro, R. G., Fisk, W. (1997). Soil-gas entry into an experimental basement driven by atmospheric pressure fluctuations – measurements spectral analysis, and model comparison. *Atmospheric Environment, 31* (10), 1477-1485.

Rydock, J. P., & Skåret, E. (2002). A case study of sub-slab depressurization for a building located over VOC-contaminated ground. *Building and environment*. 37(12), 1343-1347.

Shen, R., Pennell, K. G., Suuberg, E. M. (2012). A numerical investigation of vapor intrusion – the dynamic response of contaminant vapors to rainfall events. *Science of the Total Environment*. *437*, 110-120.

Šimůnek, J.; Šejna, M.; Saito, H.; Sakai, M.; van Genuchten, M. Th. The HYDRUS-1D software package for simulating the one-dimensional movement of water, heat, and multiple solutes in variably-saturated media. California, Riverside: University of California Riverside.

Turk, L. J. (1975). Diurnal fluctuations of water tables induced by atmospheric pressure changes. *Journal of Hydrology*. 26(1), 1-16.

U.S. Environmental Protection Agency. (1993). Radon reduction techniques for existing detached houses -Technical guidance (third edition) for active soil depressurization systems. Washington, DC: U.S. Government Printing Office.

U.S. Environmental Protection Agency. (2000). Johnson and Ettinger (1991) Model for Subsurface Vapor Intrusion into Buildings (3-Phase System Models and Soil Gas Models). Washington, DC: U.S. Environmental Protection Agency.

U.S. Environmental Protection Agency. (2002). *OSWER draft guidance for evaluation the vapor intrusion to indoor air pathway from groundwater and soils (Subsurface vapor intrusion guidance).*Washington, DC: U.S. Environmental Protection Agency.

U.S. Environmental Protection Agency. (2008). *Engineering Issue: Indoor Air Vapor Intrusion Mitigation Approaches*. Washington, DC: U.S. Environmental Protection Agency.

U.S. Environmental Protection Agency. (2010). *Review of the draft 2002 subsurface vapor intrusion guidance*. Washington, DC: U.S. Environmental Protection Agency.

U.S. Environmental Protection Agency. (2011). Toxicological review of trichloroethylene: In support of summary information on the integrated risk information system (IRIS). Washington, DC: U.S. Environmental Protection Agency.

U.S. Environmental Protection Agency. (2012). *Petroleum hydrocarbons and chlorinated hydrocarbons differ in their potential for vapor intrusion*. Washington, DC: U.S. Environmental Protection Agency.

U.S. Environmental Protection Agency. (2012). *Fluctuation of indoor radon and VOC concentrations due to seasonal variations*. Washington, DC: U.S. Environmental Protection Agency.

U.S. Environmental Protection Agency. (2012). *EPA's vapor intrusion database: Evaluation and characterization of attenuation factors for chlorinated volatile organic compounds and residential buildings*. Washington, DC: U.S. Environmental Protection Agency.

U.S. Environmental Protection Agency. (2012). *Conceptual model scenarios for the vapor intrusion pathway*. Washington, DC: U.S. Environmental Protection Agency.

U.S. Environmental Protection Agency. (2012). *Toxicological review of tetrachloroethylene (perchloroethylene): In support of summary information on the integrated risk information system (IRIS)*. Washington, DC: U.S. Environmental Protection Agency.

U.S. Environmental Protection Agency. (2013). *OSWER FINAL GUIDANCE FOR ASSESSING AND MITIGATING THE VAPOR INTRUSION PATHWAY FROM SUBSURFACE SOURCES TO INDOOR AIR (EXTERNAL REVIEW DRAFT)*. Washington, DC: U.S. Environmental Protection Agency.

U.S. Environmental Protection Agency. (2015). *OSWER TECHNICAL GUIDE FOR ASSESSING AND MITIGATING THE VAPOR INTRUSION PATHWAY FROM SUBSURFACE VAPOR SOURCES TO INDOOR AIR*. Washington, DC: U.S. Environmental Protection Agency.

U.S. Environmental Protection Agency. (2015). *Technical Guide for Addressing Petroleum Vapor Intrusion At Leaking Underground Storage Tank Sites*. Washington, DC: U.S. Environmental Protection Agency.

U.S. Environmental Protection Agency. (2014) *Vapor Intrusion Screening Level (VISL) Calculator, User's Guide*. Washington, DC: U.S. Environmental Protection Agency.

Wener, D.; Hohener, P. (2002). The influence of water table fluctuations on the volatilization of contamination from groundwater. *IAHS PUBLICATION*, 213-218.

Yao, Y., Pennell, K. G., Suuberg, E. M. The influence of transient processes on vapor intrusion processes. Paper for the AWMA Vapor Intrusion Conference, September 2010.

Yao, Y.; Shen, R.; Suuberg, E. M. (2012). Estimation of Contaminant Subslab Concentration in Vapor Intrusion Including Lateral Source-Building Separation. *Vadose Zone Journal*, doi:10.2136/vzj2012.0157.

APPENDIX A

SITE DESCRIPTION

The field works for this study were performed as part of continuous work as that was reported by Holton (2015) at the same study house. Thus, following descriptions of the site history and research house were adopted from the dissertation by Holton (2015) with updated data. Field monitor results from Chapter 2 and 3 used same time line as it was reported in Holton's dissertation, while Chapter 4, which involved the operation of sub-slab depressurization (SSD) system, placed a new timeline, where time (t) = 0 is 8:00 AM on 1/11/2015. The description of this SSD mitigation system was not included in Holton's report, and can be found in the later part of this section.

A.1 SITE HISTORY

Hill Air Force Base (Hill AFB) has been a site for repair and maintenance of aircrafts since the early 1940s (Hill AFB, 2008). In part from maintenance activities, including chemical storage and waste treatment, contamination of soil and groundwater occurred over time. In 1987, Hill AFB was placed on the National Priorities List (NPL) under the Comprehensive Environmental Response, Compensation, and Liability Act (CERCLA) for environmental cleanup (Hill AFB, 2008; Hill AFB, 2012). Currently, the contaminated sites are divided into 13 operable units (OUs), with several extending beyond Hill AFB's boundaries.

In 1993, the presence of chlorinated solvents was discovered in shallow groundwater below Layton, UT (Hill AFB, 2008; Hill AFB, 2012). The contaminated area is designated as OU8 and includes approximately 301 acres of land within Hill AFB's boundaries and 434 acres outside the boundaries (Hill AFB, 2012). The chlorinated solvent-impacted groundwater plume is primarily beneath Layton with a small amount below the city of Clearfield. A hydraulic containment system was installed

along the boundary of Hill AFB to inhibit additional spread of the contaminated groundwater. The area of OU8, the extent of the contaminated groundwater plume, and other pertinent features are shown in Figure A.1. The map, created by Hill AFB's Environmental Management Division (Hill AFB, 2012), shows an approximation of plume concentration for 1,1-dichloroethane (1,1-DCA) and trichloroethylene (TCE) based on the maximum concentration of groundwater samples measured in off-base monitoring wells from 2005 to 2007. Due to the extent of contamination, both on- and off-base, completion of cleanup is estimated to be in the 2040s (Hill AFB, 2012).

The risks associated with the groundwater contamination have been primarily associated with potential impacts to indoor air from vapor intrusion. As of 2012, Hill AFB has conducted indoor air sampling at 645 homes. Of the houses samples, 55 required mitigation systems (Hill AFB, 2012). The drinking water for Layton and surrounding communities is provided by deep groundwater aquifers and mountain reservoirs and has not shown evidence of being affected by the contamination.

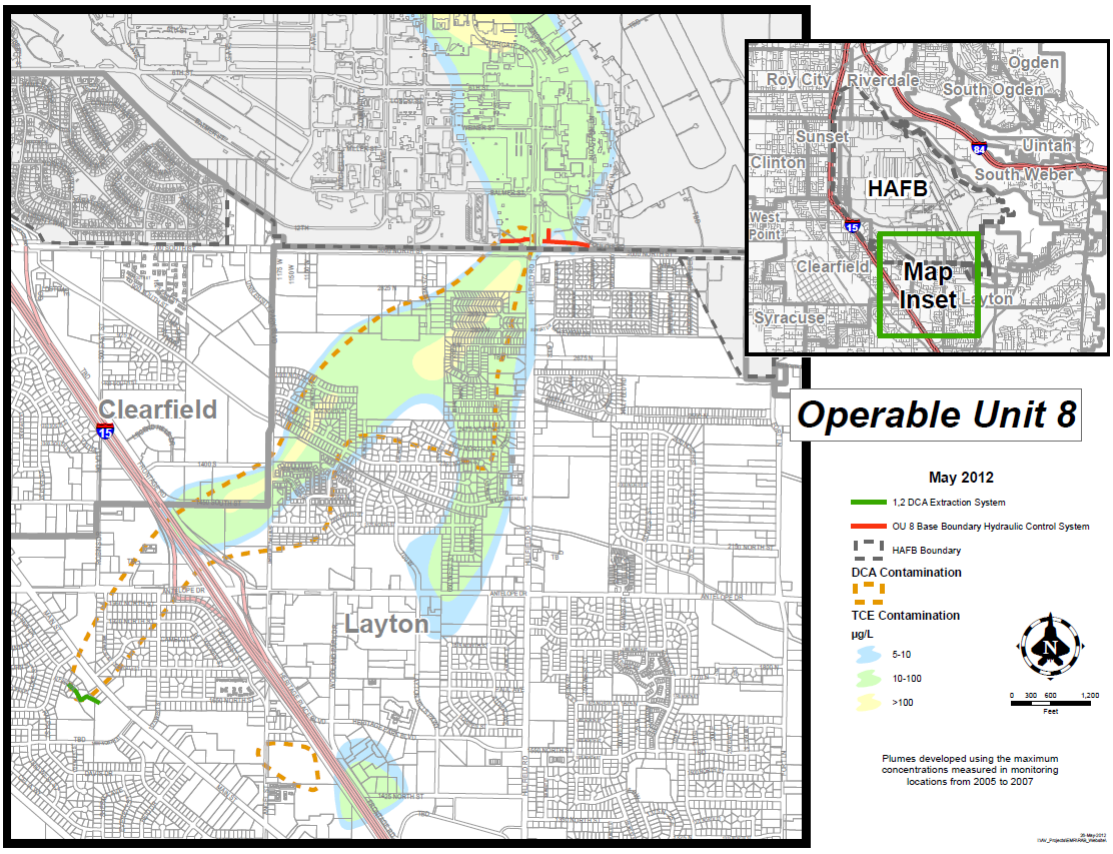

Figure A.1. Map Operable Unit 8 (OU8) showing the extent of groundwater contamination in Layton and Clearfield Utah (from Hill AFB, 2012).

A.2 DESCRIPTION OF RESEARCH HOUSE

The field work for this project was performed at a site above the chlorinated solvent-impacted groundwater in OU8. The study site is a split-level, two-story, three-bedroom house with a garage on the lower level in a residential community in Layton, UT, south of Hill AFB. The house has been affectionately nicknamed Sun Devil Manor (SDM). The house covers a footprint of approximately 85 m^2 (915 ft^2). Figure A.2 present a photo of the study house. The house sits on a south-facing slope with an elevation drop of approximately 2.5 m from the back to front of the property.

Figure A.2. Photo of the front of the study house.

Permanent multi-depth soil gas and groundwater monitoring points were installed through and exterior to the house foundation at locations shown in Figure A.3. Figure A.4 shows a photo of a multi-depth indoor soil gas and groundwater monitoring location. Each was sealed with bentonite above and below sampling intervals and perforations through the foundation were sealed with a cement plug topped with a silicone caulk seal to ensure no connection with the subsurface. Sampling network specifics are summarized in Table A.1.

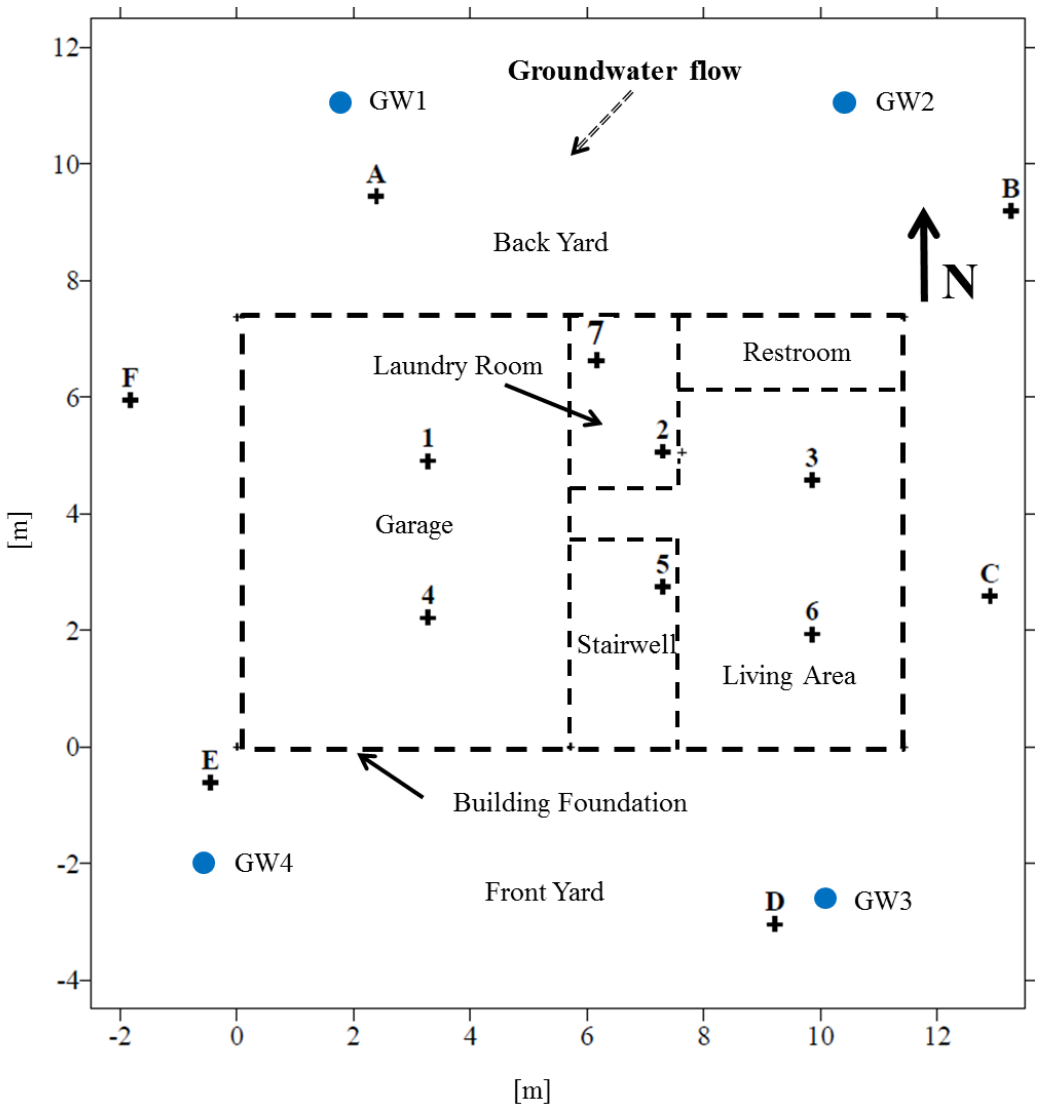

Figure A.3. Schematic of the lower level of the study house including interior and exterior subsurface monitoring locations.

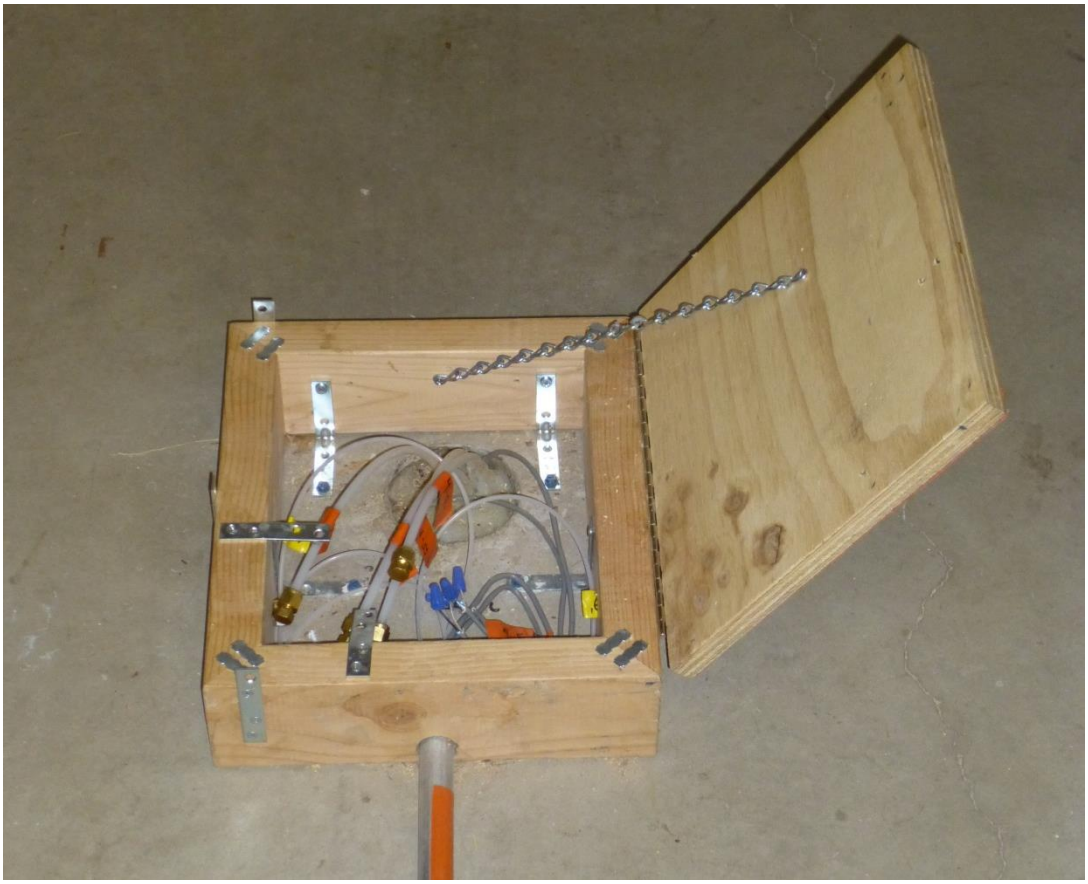

Figure A.4. Photo of a multi-depth soil gas and groundwater monitoring location at the house

Table A. 1

Sampling network specifics for groundwater and soil gas monitoring locations (see Figure 3 for locations).

Soil Gas Sampling					Groundwater Sampling			
Location	Depth [m Below Slab]				Location	Depth [m Below Ground Surface]		
A	SS	0.9	1.8	2.7	GW1	4.9	10.0	12.8
B	SS	0.9	1.8	2.7	GW2	4.9	10.0	12.8
C	SS	0.9	1.8	2.7	GW3	4.3	7.0	9.1
D	SS	0.9	1.8	2.7	GW4	4.0	6.4	9.1
E	SS	0.9	1.8	2.7	IGW1	2.7*		
F	SS	0.9	1.8	2.7	IGW2	2.7*		
1	SS	0.9	1.8	2.7*	IGW3	2.7*		
2	SS	0.9	1.8	2.7*	IGW4	2.7*		
3	SS	0.9	1.8	2.7*	IGW5	2.7*		
4	SS	0.9	1.8	2.7*	IGW6	2.7*		
5	SS	0.9	1.8	2.7*				
6	SS	0.9	1.8	2.7*				
7	SS	--	--	--				

*water-saturated conditions sometimes exist at soil gas sampling depths of 2.7 m below slab, and may be used as groundwater sampling points labelled as IGW1, IGW2, etc.

Building slab thickness ranges from approximately 12 to 16 cm and the gravel pack below the slab ranges from 20 to 30 cm. A photo of the foundation thickness, relative to the step from the garage to the inside of the house, is shown in Figure I.5.

The sub-foundation gravel zone drains to a local land drain system running across the southern border of the property through a lateral pipe. The lateral pipe was modified on t=1072 d with the addition of a butterfly valve to allow for control of the connection between the sub-foundation gravel zone and the land drain system. Tracer gases (SF_6 and helium) were released up- and down-stream of the butterfly valve with it open and closed to confirm its integrity and ability to close the connection between the sub-foundation

area and the land drain system. Figure A.6 presents a schematic and photos of the lateral pipe.

As mentioned, the house overlies a regional dilute groundwater plume containing 1,1-dichloroethene (1,1-DCE), 1,1,1-trichloroethane (1,1,1-TCA) and trichloroethylene (TCE). Regional groundwater flow is predominately to the southwest (consistent with Hill AFB's OU8 Fact Sheet). Depth to groundwater is estimated to be 2.5 m (8.3 ft) below the house slab (BS), based on absence of water in the 1.8 m (6 ft) sub-slab monitoring points and the presence of water in the 2.7 m (9 ft) sub-slab monitoring points. Figure A.7 shows the average groundwater concentrations for TCE from samples collected below the house slab from August 2010 to March 2014. Field monitor results generated during this period were used to support discussions in Chapter 2 and Chapter 3. On average, dissolved TCE concentrations in groundwater collected beneath the foundation ranged from about 10-50 µg/L with the mean TCE concentration of 24 ± 9 µg/L. Figure I.8 presents the groundwater monitor results during the field test that was discussed in Chapter 4 (January 2015 to September 2015). TCE concentrations in groundwater collected beneath the foundation ranged from about 10-80 µg/L with the mean TCE concentration of 28 ± 16 µg/L. These figures place different timelines, where time (t) = 0 is 8:00 AM on 8/151/2010 for Figure I.7 and time (t) = 0 is 8:00 AM on 1/11/2015 for Figure A.8.

Figure A.5. Photo of a slab core taken during the installation of internal subsurface monitoring locations. The photo is shown next to the step from the garage to inside of the house.

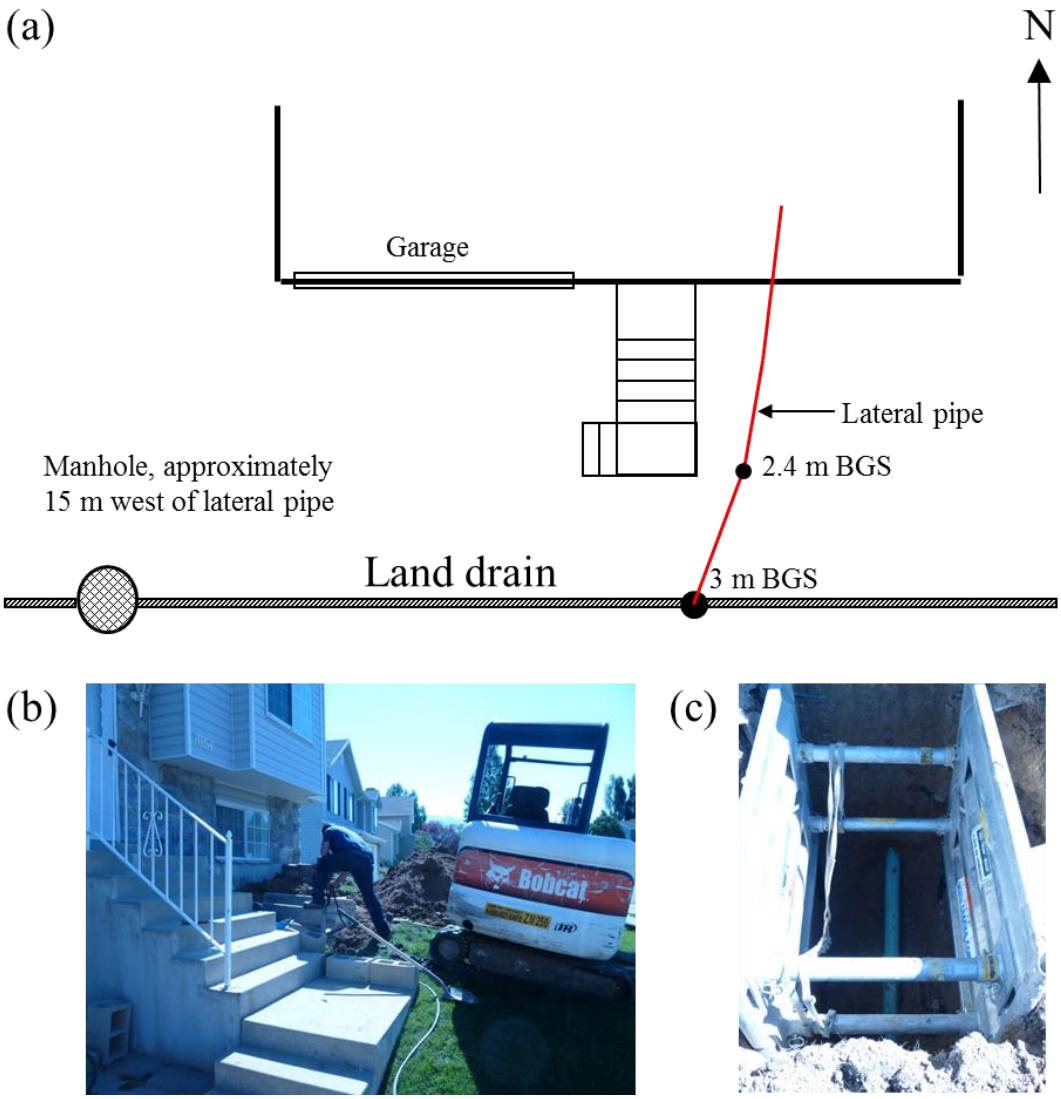

Figure A.6. (a) Schematic showing the location of the lateral pipe and land drain system relative to the front of the study house; photos (b) of the excavation process to uncover the lateral pipe and (c) the uncovered lateral pipe.

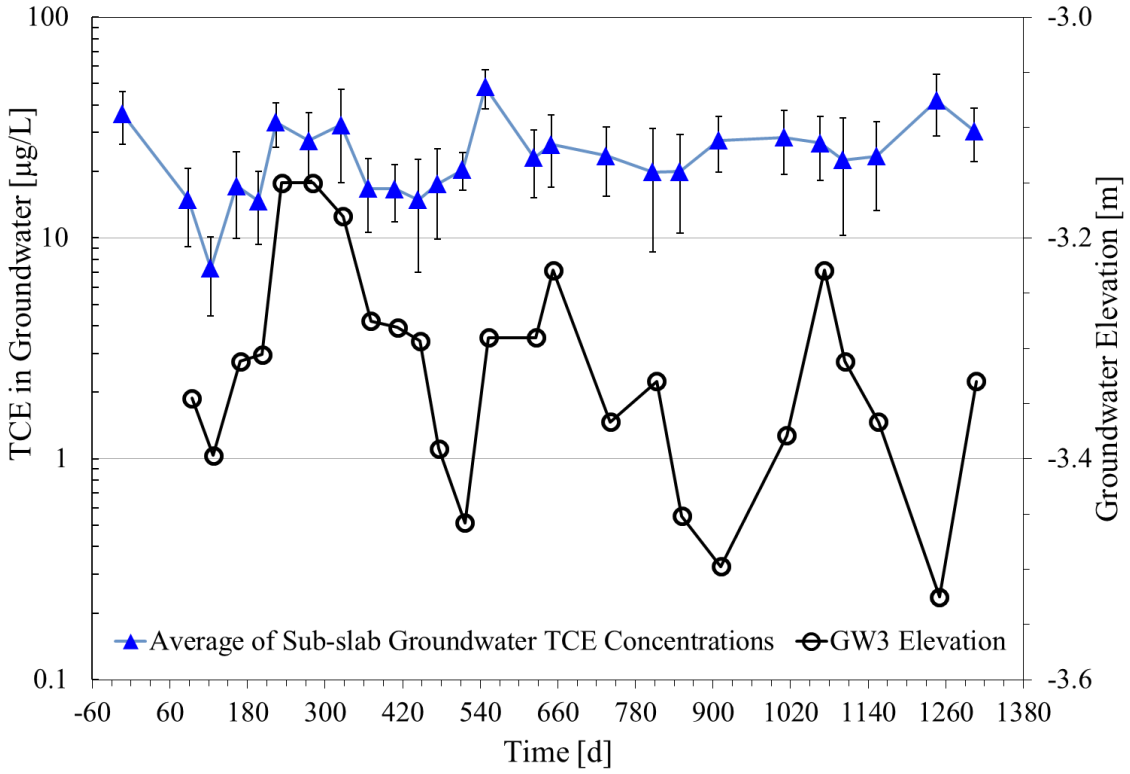

Figure A.7. Synoptic TCE concentrations in groundwater averaged across sampling locations below the foundation along with measured groundwater elevations from GW3 using time (t)= 0 day started on 08/15/2010 8:00 AM.

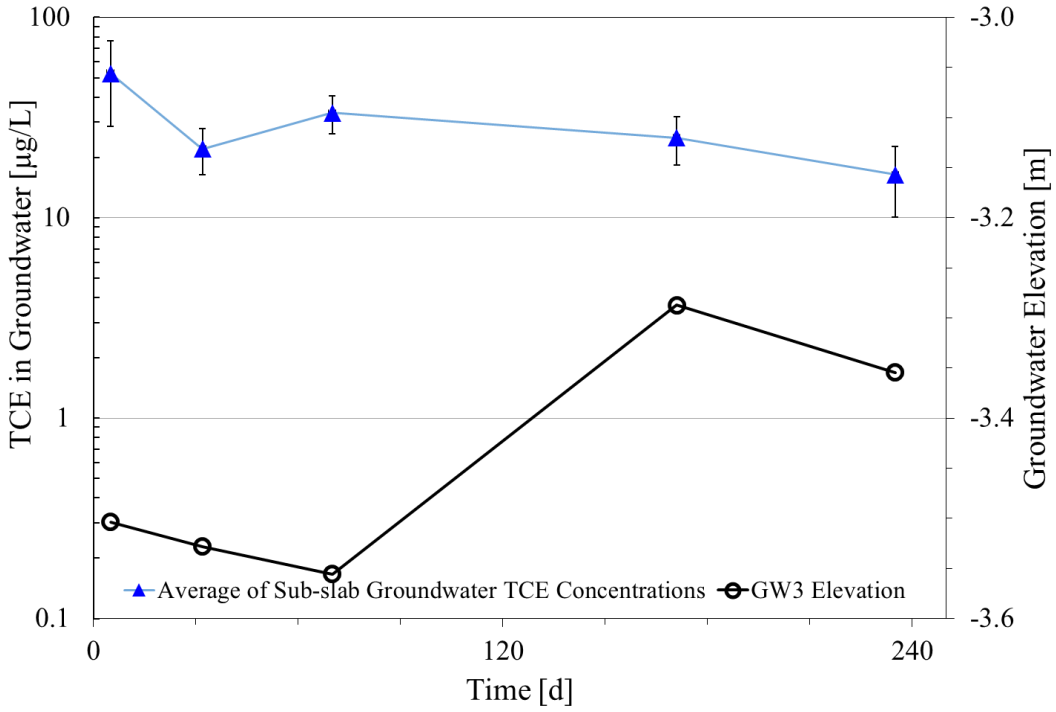

Figure A.8. Synoptic TCE concentrations in groundwater averaged across sampling locations below the foundation along with measured groundwater elevations from GW3 using time (t)= 0 day started on 01/11/2015 8:00 AM.

The soil beneath and adjacent to the house consists predominantly of fine sandy silt with fine sand stringers. Soil moisture content was determined from soil cores taken at the site in May 2011 at locations C, D, and F (see Figure 3 for locations). The results from the three soil core showed that soil moisture adjacent to the house was 0.20 ± 0.02 g-H_2O/g-soil within 0.6 m (2 ft) of ground surface and then increased and was relatively consistent with depth at 0.25 ± 0.01 g-H_2O/g-soil to 3.7 m (12 ft) below ground surface. The soil moisture content determined from three cores is shown in Figure A.9.

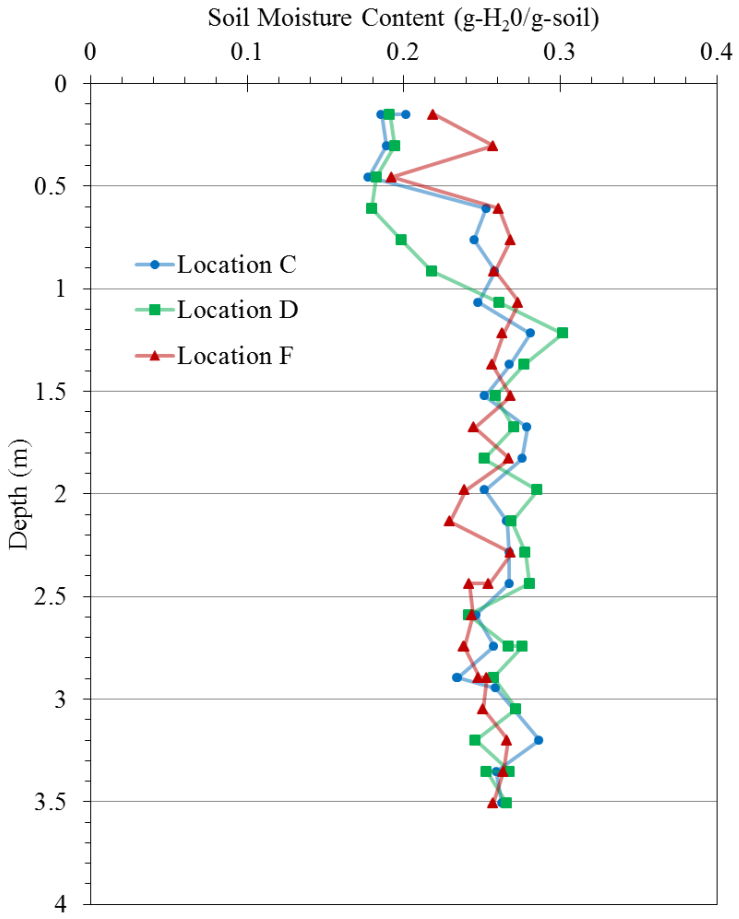

Figure A.9. Soil moisture content results from three soil cores collected and analyzed in May 2011.

No one lived in the house during the duration of the study, but there were study-related activities in and around the house approximately 20% of time. The following measures were taken to ensure that the house operated similarly to that of an occupied house:

- The indoor temperature was maintained at approximately 20.5°C using a central forced-air heating and cooling system
- Water was maintained in P-traps

- The lawn was watered 15-min daily by an automatic sprinkler system from late spring through early fall months

To avoid issues associated with indoor sources, all potential sources were removed from the site. The following measures were taken to reduce the possibility of interference by indoor sources:

- All chemicals were removed
- Groundwater analysis was performed at an analytical laboratory at ASU to avoid possible contamination of indoor air from chemical standards
- Furniture, with the exception of a few tables and chairs, was removed
- Activity/entry logs were recorded to ensure that potential sources were not introduced to the house

Visual inspections were conducted of the floors and walls and indicated the following:

- A gap between the building slab and stem wall is present below the stairwell (crawlspace) with an approximate size of 0.6 cm by 180 cm (width by length)
- There are flow drains located in the laundry room and bathroom on the lower level

An SSD system was installed the study house on December 20th 2006. Suction pit located at the south-east corner of the laundry room at the lower level of the house. A KT-150 turbine fan (Radon PDS, CO) was installed in the attic that draws air from the suction pit to atmosphere through 4-inch PVC pipes. A power supply/indicator box (KTA box) was used here to control the blower speed. The air flowrate through the vent pipe

was measured at about 35 cubic feet per minute (1 m^3/min) after the installation in 2006. Figure A.10 is a photo taken in February 2010 illustrating the suction port of this SSD system.

Figure A.10. Photo of sub-slab depressurization system, taken on February 2010.

I.3 REFERENCE

Holton, C. (2015). Evaluation of Vapor Intrusion Pathway Assessment through Long-Term Monitoring Studies. (Dissertation). Arizona State University, Tempe, AZ.

APPENDIX B

EXPERIMENTAL METHODS

B.1 SUMMARY OF METHODS USED

This integrated study involves numerous analytical methods focusing on volatile organic chemicals (VOC) and other environmental parameters. Table B.1 summarizes key measurements, sampling frequencies, analytical methods, quality assurance and quality control (QA/QC) measures for the data generated at the study site, as well as the related research topics. Again, all the measurements that were performed in the field used same technologies as reported by Holton (2015). The description of these technologies in this section were adapted from Holton's report (2015) with updated information.

Table B. 1.

Summary of key site measurements, analytical methods, and related research topics at the study site.

Key Site Measurements	Analytical Methods and Frequency	Sampling Media and/or Location	Data QA/QC	Related research topics
Real-time air sampling for analysis of chlorinated volatile organic compound concentrations	Collected on multi-bed thermal desorption tubes followed by desorption and analysis by Unity/GC/MS. 4 hour and 24 h time-averaged samples were collected	Indoor and outdoor air	Comparison with data from other methods, calibration and calibration verification, blanks, trip blanks, trip spikes, internal standards	Chapter 2: Evaluate VOCs emission vs groundwater fluctuation; Chapter 3: Identify alternative VI pathways; Chapter 4: Effectiveness of an SSD system.
	Collected by SRI 10-stream auto-sampler onto thermal desorption tube, followed by desorption and analysis using on-site GC/ECD. Sampling every 40 minutes.	Indoor, outdoor air and soil gas	Comparison with data from other methods, calibration and calibration verification, blanks	Chapter 3: Identify alternative VI pathways; Chapter 4: Effectiveness of an SSD system.
	Collected by SRI 10-stream auto-sampler onto thermal desorption tube, followed by desorption and analysis using GC/FID. Sampling every 60 min	Sweep gas of tank experiments	Calibration verification, blanks.	Chapter 2: Evaluate VOCs emission vs groundwater fluctuation
Real-time indoor air, outdoor air, and soil gas sampling for analysis of SF6 concentrations	Collected by SRI 10-stream auto-sampler and analyzed by GC/PDD. Sampling every 30 minutes	Indoor air, outdoor air, and selected soil gas locations	Standard gas sampling every 5 hours, calibration and calibration verification, blanks	Chapter 2: Evaluate VOCs emission vs groundwater fluctuation; Chapter 3: Identify alternative VI pathways.

Key Site Measurements	Analytical Methods and Frequency	Sampling Media and/or Location	Data QA/QC	Related research topics
Real-time indoor air sampling for analysis of radon concentrations	Collected and analyzed by Durridge RAD7 radon detector. 2 hour time-averaged sampling	Indoor air and SSD vent	Instrument calibrated annually by manufacturer	Chapter 4: Effectiveness of an SSD system.
Real-time differential pressure between outdoor and indoor air and soil gas and indoor air	Differential pressure transducers connected to data acquisition module; reading every 2 minutes	Outdoor air and all multi-depth soil gas locations	Transducers re-zeroed once every day; on site calibrations	Chapter 3: Identify alternative VI pathways; Chapter 4: Effectiveness of an SSD system.
Synoptic on-site measurements, including analysis of SF6, radon, and chlorinated compounds in soil gas, dissolved chlorinated compounds in groundwater, and groundwater table level	Soil gas samples collected using lung-sampler and Tedlar bags, and analyzed using, GC/DELCD, GC/PDD. Groundwater collected and preserved in 40 mL vials then shipped to ASU for analysis using GC/DELCD Water level data collected using Solinst water level sounder Soil gas radon analyzed with RAD7	Available soil gas and groundwater locations	Data checked using blanks, duplicates, replicates, calibration and calibration verification	Chapter 2: Evaluate VOCs emission vs groundwater fluctuation; Chapter 3: Identify alternative VI pathways; Chapter 4: Effectiveness of an SSD system.
Measurement of compounds in soil gas at a two-dimensional physical model	Soil samples were collected using gas-tight syringes and analyzed using GC/DELCD. Water samples collected and diluted in 40 mL vials and analyzed using GC/DELCD. Both soil gas and water samples were collected at the frequency of water table fluctuation	Available soil gas and groundwater ports	Data checked using blanks, duplicates, replicates, calibration and calibration verification	Chapter 2: Evaluate VOCs emission vs groundwater fluctuation

B.2 MEASUREMENT OF REAL-TIME VOCS IN GAS SAMPLES

Measurement of VOCs in air sample was performed using three separate methods: (a) 4 h/24 h time-averaged 12 L/72 L samples collected on a multi-bed sorbent tubes analyzed by thermal desorption and GC/MS, (b) 10 min time-averaged 100-500 mL samples collected every 40 min on a multi-bed sorbent tube and analyzed by a GC equipped with an electron capture detector (ECD), and (c) 15 min time-averaged 450 mL samples collected every 60 min on a multi-bed sorbent tube and analyzed by a GC equipped with a flame ionization detector (FID). Method (a) and (b) were used predominantly at field monitoring and method (c) were used for lab experiments.

B.2.1 Sorbent tubes. Multi-bed sorbent tube samples were collected using two customized SRI Instruments (SRI Instruments, Torrance, CA) 20-stream gas sampling valves, a vacuum pump (Rena 301 series, model BE-3012 vacuum/pressure pump), and a vacuum-configured, 0-100 mL/min mass flow controller (Alicat Scientific, Tucson, AZ). Sample collection was controlled by an SRI Instruments 6-channel data system and monitored using SRI PeakSimple software. The flowrate through the sorbent tubes was controlled at 50 mL/min. Two different types time averaged samples were collected, one was over a 4 h period for a total sample volume of 12 L and the other was 24 h averaged with the sample volume of 72 L. The first type of samples was collected during the tests performed in Chapter 2 and 3; and the second for Chapter 4. A schematic of this setup is shown in Figure B.1. The sorbent tubes (0.64 x 15.2 cm-long) were packed with Tenax-GR and Carboxen-569. During sample collection, sorbent tubes were capped with Difflock caps (Markes International, UK). After completion of a sampling set (38 sorbent tubes, approximately 6.3 days), sorbent tubes were capped using Swagelok brass caps

with Teflon ferrules, and shipped to an analytical laboratory at Arizona State University (ASU) for analysis.

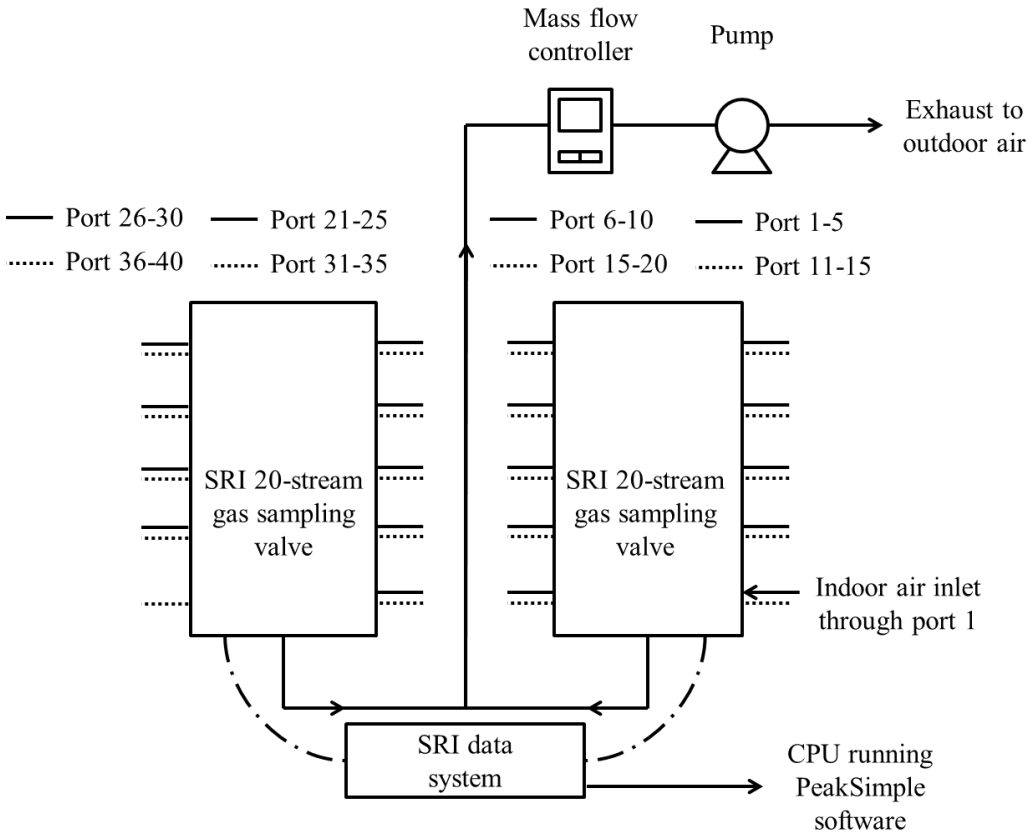

Figure B.1. Schematic of indoor and outdoor air sampling setup for multi-bed sorbent tubes used at study site.

Once at ASU, sorbent tubes were analyzed using a Markes Ultra autosampler and Markes Unity thermal desorber (Markes International, UK) attached to an HP5890 gas chromatograph (GC) with an HP5972 mass spectrometer (MS) for 4 h samples and to an HP7890A gas chromatograph with an HP5975C mass spectrometer for 24 h samples. The column used within the thermal desorber GC/MS configuration was a 60 m Restek RXI-5 capillary column. Analysis of samples on the GC/MS was performed using the selective-ion monitoring (SIM) mode. The MDLs were calculated as 0.008 ppbv and 0.00007 ppbv

for TCE for 4 h and 24 h samples respectively using USEPA's MDL procedure (USGS, 1999). The values used to calculate the MDL are shown in Table B.2.

Table B. 2

Spiked concentrations, responses, and calculated concentrations used to calculate the MDL for TCE using the sorbent tube method.

GC/MS 4 h average samples			
Sample	Spiked concentration [ppbv]	Response [area count]	Calculated concentration [ppbv]
1	0.05	21101	0.0515
2	0.05	21054	0.0514
3	0.05	19894	0.0487
4	0.05	19254	0.0472
5	0.05	20127	0.0492
6	0.05	18826	0.0461
7	0.05	21593	0.0526
		Average	0.0495
		Standard Deviation (s)	0.0024
		Student's t value (t)	3.142
		MDL [ppbv]	0.008
$MDL = s \times t_{(n-1,1-\alpha=0.99)}$			
GC/MS 24 h average samples			
Sample	Spiked concentration [ppbv]	Response [area count]	Calculated concentration [ppbv]
1	0.0005	5231	0.00049
2	0.0005	5307	0.00050
3	0.0005	5180	0.00049
4	0.0005	5270	0.00050
5	0.0005	5602	0.00053
6	0.0005	5699	0.00054
7	0.0005	5614	0.00053
		Average	0.00051
		Standard Deviation (s)	0.00002
		Student's t value (t)	3.142
		MDL [ppbv]	0.00007
$MDL = s \times t_{(n-1,1-\alpha=0.99)}$			

To reduce losses of sample mass, sorbent tubes were loaded for analysis as soon as possible upon delivery. Due to issues associated with maintenance of the analytical equipment, 1-3 day delays were not uncommon. In total, some sorbent tubes (i.e., tubes used earlier in sampling set), sat for up to 10 days before analysis (including sample set run time, shipping time, and analysis delays). In order to understand the potential losses that occurred during these periods, a 12 day holding test was performed using spiked sample tubes. In starting the test, 3 sorbent tubes were spiked with 0.1 ppb_v of a CHC mix (equivalent to 0.55 ng for TCE) and 3 other sorbent tubes were spiked 1.0 ppb_v of a CHC mix (equivalent to 5.46 for TCE). Additional sets of 6 spiked sorbent tubes were prepared 4, 8, and 11 days after with all of the tubes analyzed on the 12^{th} day. The results of this test for TCE mass are shown in Table B.3. In general, the results show that mass losses over the testing period were relatively low with similar losses observed between the shortest and longest holding times. The greatest percent difference between spiked mass and mean calculated mass was 13.5%. Another holding test was performed for 24 h samples, 1 sorbent tube was spiked with 0.01 ppbv of a CHC mix (equivalent to 3.87 ng for TCE) and 2 other sorbent tubes were spiked 0.05 ppb_v of a CHC mix (equivalent to 19.33 for TCE). The spiked samples were stored in a similar pattern as site collections for 30 days, all the samples showed over 90 % recovery rates.

Table B. 3

Results of sorbent tube holding tests for TCE mass.

	Spiked Mass, TCE [ng]		Spiked Mass, TCE [ng]	
	0.55		5.46	
Time since preparation [d]	Mean Calculated Mass [ng], n = 3	Perfecent Difference (%)	Mean Calculated Mass [ng], n = 3	Perfecent Difference (%)
1	0.51	7.3%	5.15	5.8%
4	0.59	7.7%	5.65	3.4%
8	0.60	9.3%	4.76	13.7%
12	0.61	9.5%	5.18	5.3%

B.2.2 GC/ECD. Air samples collected for analysis using the GC/ECD were pulled onto a multi-bed sorbent tube trap (0.64 x 15.2 cm) packed with Tenax-GR and Carboxen-569 by a vacuum pump (Rena 301 series, model BE-302 vacuum/pressure pump), and a vacuum-configured 0-100 mL/min mass flow controller (Alicat Scientific, Tucson, AZ) at 50 mL/min. Sample collection time was controlled using SRI's PeakSimple software. Once a sample was collected, the sorbent tube was heated to 240°C and helium carrier gas pushed the sample onto a 60 m MXT-5 capillary column held at 40°C. After a 2-min delay, to allow ample time for the trap heater to reach 240°C and for the sample to desorb from the trap, the column was heated from 40°C to 220°C at 10°C/min and the sample swept into the ECD cell.

10-steam gas sample valves, a Rena model BE-3012 vacuum pump and a vacuum-configured, 0-100 mL/min, vacuum configured, mass flow controller (Alicat Scientific, Tucson, AZ) were used here to collect real-time gas samples. These sample valves allow the GC/ECD pulling samples from varies locations, and the frequency and location sequences can be programed by Peaksimple software.

Calibration of the GC/ECD occurred every 1-3 months, during site visits, at the beginning and end of synoptic surveys, using gas standards prepared from a 1 ppmv commercial gas standard containing a suite of chlorinated VOCs. Replacement of the multi-bed sorbent trap occurred when calibration curves approached a 20% difference from the first calibration using the trap. On average, trap replacement occurred every 3 months. The MDL for TCE for this method was calculated as 0.009 ppbv (approximately 0.05 μg/m^3) using USEPA's MDL procedure (USGS, 1999). The results used to calculate the MDL are shown in Table B.4.

Table B.4

Spiked concentrations, responses, and calculated concentrations used to calculate the MDL for TCE using the GC/ECD method.

Sample	Spiked concentration [ppb_v]	Response [area count]	Calculated concentration [ppb_v]
1	0.04	578.054	0.0406
2	0.04	549.093	0.0385
3	0.04	586.832	0.0413
4	0.04	625.727	0.0442
5	0.04	552.682	0.0387
6	0.04	506.319	0.0353
7	0.04	599.79	0.0423
		Average:	0.0401
		Standard Deviation (s):	0.0029
		Student's t value (t):	3.14
		MDL [ppb_v]:	0.009

$$MDL = s \times t_{(n-1,1-\alpha=0.99)}$$

B.2.2 GC/FID. The sweep gas VOCs concentrations were qualified during the lab experiments. Sweep gas concentrations were continuously collected and measured by an

SRI GC equipped with a flame ionization detector (FID). Sweep gas samples of both tanks were collected alternatively by a 3-way solenoid valve (ASCO, NJ) controlled by SRI Peaksimple software in time sequence. Sweep gas samples collected for analysis using the GC/FID were pulled onto a multi-bed sorbent tube trap (0.64 x 15.2 cm) packed with Tenax-GR and Carboxen-569 by a vacuum pump (Rena 301 series, model B E-302 vacuum/pressure pump), and a vacuum-configured 0-100 mL/min mass flow controller (Alicat Scientific, Tucson, AZ) at 40 mL/min. Sample collection time was controlled using SRI's PeakSimple software. Once a sample was collected, the sorbent tube was heated to 230°C and helium carrier gas pushed the sample onto a 60 m MXT-5 capillary column held at 40°C. After a 2.5-min delay, to allow ample time for the trap heater to reach 240°C and for the sample to desorb from the trap, the column was heated from 40°C to 220°C at 12°C/min and the sample swept into the FID. Calibration checks were performed throughout the experiment. Less than 10 % differences between spiked samples and calculated concentrations using original calibration.

B.3 MEASUREMENT OF VOCS IN SOIL GAS GRAB SAMPLES

VOCs in soil gas was qualified in both field and lab works using grab samples. A GC with a dry electrolytic conductivity detector (DELCD) method was used both on site and in the lab. Concentration treatment was applied depending on the VOCs concentration level in the soil gas samples and instrument detection limit.

B.3.1 Collection of soil gas grab samples. Collection of soil gas samples for on-site synoptic surveys was done using a custom built vacuum box (lung sampler). The lung sampler utilizes negative pressure to collect soil gas samples in 1 L Tedlar vapor

bags (SKC 232-01). The box, shown in Figure B.2, is constructed from a Pelican case (Pelican, San Antonia, TX) and stainless steel Swagelok parts and is connected to a vacuum pump (Rena 301 series, model BE-3012 vacuum/pressure pump). The vacuum pump is located downstream of sampling to avoid cross contamination between soil gas samples.

The procedure for soil gas sampling was as follows:

- Tedlar bags were flushed with helium gas three times and then evacuated using a 60 mL syringe prior to use.
- The soil gas sampling port (network shown in Appendix I, Figure I.3) was opened and connected to the lung sampler (see Figure II.2 for photo).
- The lung sampler was opened and the Tedlar bag was connected to the internal sampling port. The valve on the Tedlar bag was then opened and the lung sampler was closed.
- The pump was then turned on and approximately 100 mL of soil gas was purged from sampling lines and exhausted to outdoor air to negate the effects from dilution from dead volume.
- The soil gas was then rerouted to flow into the Tedlar bag where an additional 100 mL of soil gas was collected. This volume was then flushed from the Tedlar bag and exhausted to outdoor air.
- The soil gas sample for analysis was then collected – roughly 500 to 800 mL of soil gas depending on anticipated concentration of sample.

- The vacuum pump was then turned off and the lung sampler was opened. The valve on the Tedlar bag was closed and the bag was removed from the sampler for analysis.
- The sampling port and lung sampler were then disconnected and the sampling port was resealed.

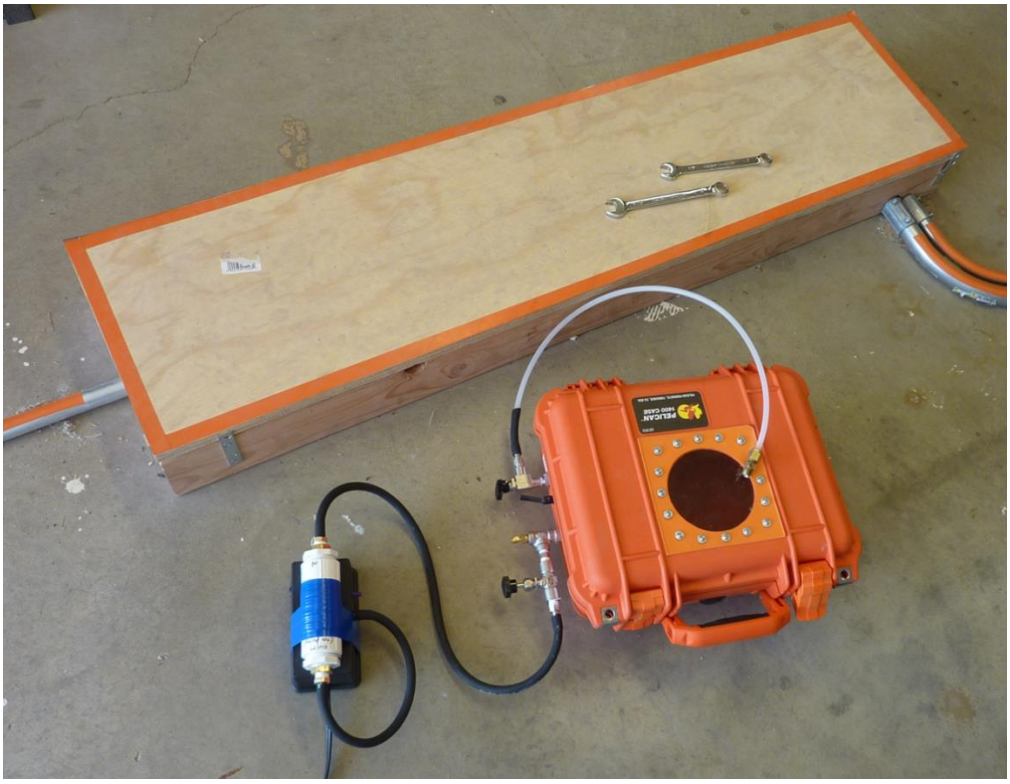

Figure B.2. Photo of lung sampler (orange box) next to a monitoring location in the garage of the study site.

Soil gas samples in the lab tanks experiments were collected using 500 µL gas tight syringes. In the front panels of the tanks, Swagelok® 1/4 in fittings were installed with Septa Thermolite® Shimadzu Plugs. These sampling port allowed one use syringes and needles to collect samples. Once a sample was pulled in a syringe, it would be

quickly injected to the analytical instrument which located within 3 m of tanks. Figure II. 3 shows the construction of sampling ports.

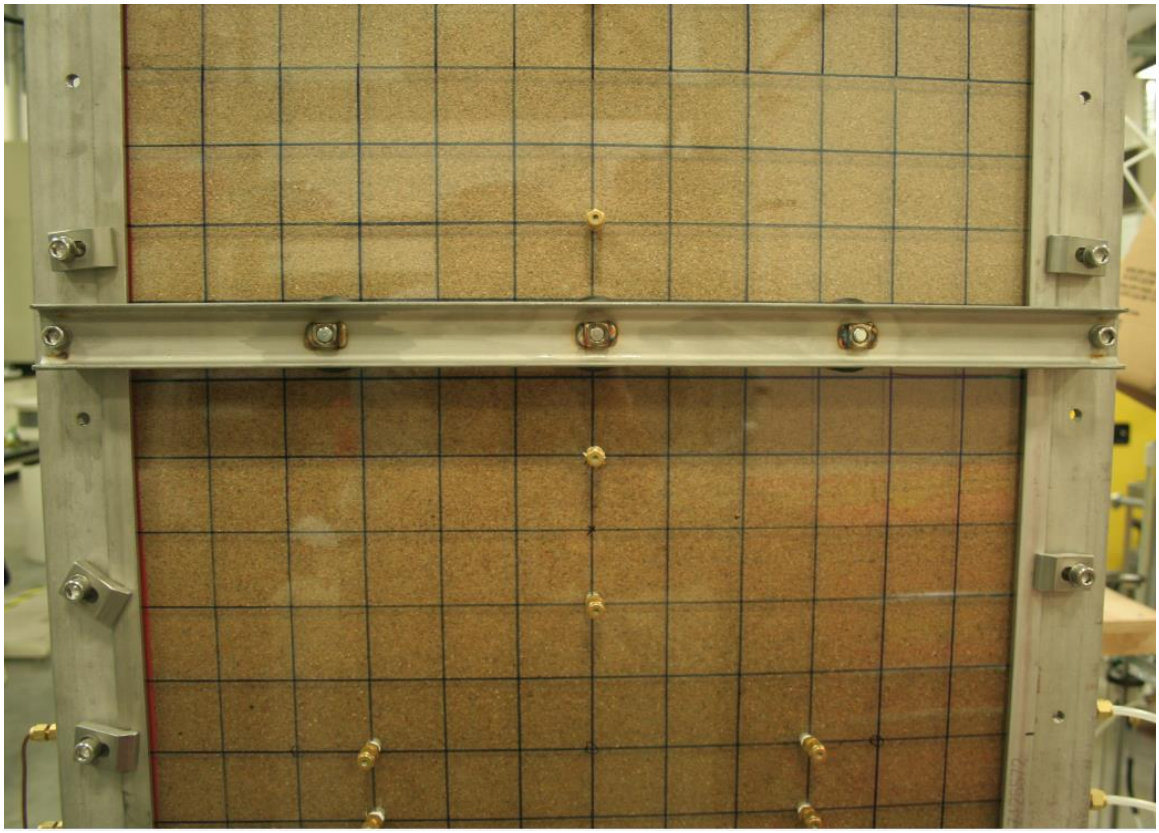

Figure B.3. Photo of soil gas and water sampling ports installed in the tanks.

B.3.2 Analysis of Soil Gas Grab Samples. Soil gas grab samples for analysis of chlorinated VOCs were analyzed by one of two methods: (a) on-column injection for samples >5 ppb_v and (b) concentration on a multi-bed sorbent trap and subsequent thermal desorption and injection for samples <5 ppb_v. The first method was applied in both synoptic field surveys and lab scale experiment, while the second was used for synoptic field surveys. For the first method, 500 μL of sample vapor was directly injected onto a 60m Restek MXT-1 column (Restek Corporation, Bellefonte, PA) held at 40°C in a SRI GC equipped with a dry electrolytic conductivity detector (DELCD). Following

injection, the GC oven was heated from 40°C to 220°C at 12°C/min and then held at 220°C for 3 min for sample release into the DELCD. The second method used a multi-bed sorbent trap (same packing as sorbent tubes above) for concentrating 500 mL of sample pulled from a 1-L Tedlar bag onto the sorbent tube using a vacuum pump (Rena 301 series, model BE-302 vacuum/pressure pump), and a vacuum-configured 0-100 mL/min mass flow controller (Alicat Scientific, Tucson, AZ) at 50 mL/min. After trapping the sample, the sorbent tube was heated to 240°C and held for 2 min to desorb the sample and allow helium carrier gas to sweep the sample onto the column. Similar to before, the column was then heated from 40°C to 220°C at 12°C/min and then held at 220°C for 3 min for release of the sample to the DELCD.

B.4 MEASUREMENT OF RADON IN INDOOR AIR AND SOIL GAS

A Durridge RAD7 (Durridge Company, Inc., Billerica, MA) was used to measure the concentration of radon in both indoor air and soil gas. The RAD7 radon detector is a portable solid state alpha detector with the ability to perform continuous real-time monitoring. When a gas sample enters the RAD7's internal sample cell, the radon contained in the sample decays and produces alpha particle emitting daughter products. The detector then produces an electrical signal based on the alpha particles energy to determine the radon concentration.

A schematic of the RAD7 sampling assembly is shown in Figure B.4. Prior to entering the detector, samples are pulled through a tube filled with desiccant to ensure that the relative humidity (RH) of the sample is low enough for the detector, followed by the inlet filter. The RAD7 manual states that the detector is more efficient and doesn't

require humidity correction when samples have 10% RH or less. The desiccant used with the RAD7 was Indicating DRIERITE (W. A. Hammond DRIERITE Co. LTD, Xenia, OH), which is anhydrous calcium sulfate impregnated with cobalt chloride. Indicating DRIERITE is blue in color, but turns pink when it absorbs moisture. Tubes of desiccant were changed out with new material when the majority of the Indicating DRIERITE appeared pink in color. As mentioned, following the desiccant tube is a fine inlet filter, which removes solids and desiccant dust from the sample. When sampling indoor air and soil gas within the building, the outlet of the RAD7 assembly was connected to an exhaust line to outdoor air.

The RAD7 instrument is calibrated by the manufacturer prior to use and once a year there after. The manufacturer uses a set of four control instruments as standards for the calibration of all RAD7s sold. The four control instruments are calibrated by inter-comparison with radon chambers designed by U.S. EPA (1). Using this method, the manufacturer claims the RAD7 accuracy to be ±5% or better. Each measurement from the RAD7 also includes a value for the uncertainty associated with the sample. The uncertainty value associated with each measurement is a 95% confidence interval based on the number of alpha particles the detector counts during the spectral analysis. The RAD7 is recalibrated annually based on the manufacturer's recommendation.

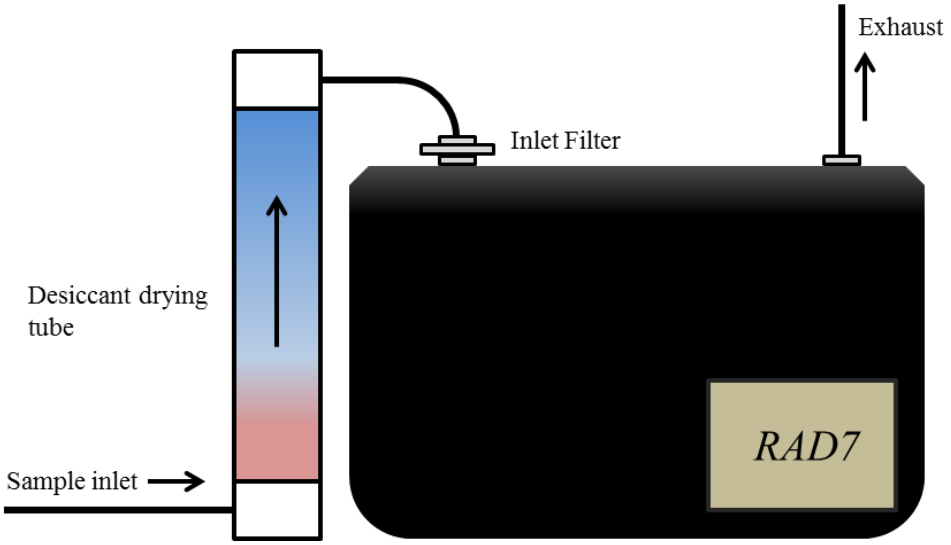

Figure B.4. Schematic of Durridge RAD7 sampling assembly used for analysis of indoor air and soil gas for radon.

Measurement of radon in indoor air and soil gas was conducted using two methods: (a) time-averaged samples collected over a 2-h period for real-time monitoring of indoor air and (b) an average of five 5-min cycles for synoptic soil gas sampling events. Real-time monitoring of radon concentration in indoor air was performed in the lower-level of the house at approximately 1 m above the floor. Synoptic soil gas sampling events were performed every 1-2 months at both indoor and outdoor locations.

Prior to initiating indoor air sampling and between each soil gas sample, the detector is purged using outdoor air. The purge function of the RAD7 turns on the internal pump and pulls in “clean” air to free the sample chamber from residual radon gas and moisture. For soil gas samples, the detector was purged for 5-min after each sample. The sampling protocol was to collect the shallowest soil gas first (SS), since its radon concentration is generally lower than deeper soil gas (0.9 m and 1.8 m BS). When sampling took place at soil gas depths of 0.9 m or 1.8 m BS the detector was purged for 15-min before returning to sample SS soil gas to ensure clearing of residual.

B.5 RELEASE OF SF_6 TRACER GAS

Sulfur hexafluoride (SF_6) was continuously released to indoor air at 5 mL/min in the study house during all phases of the project. The release of the gas was controlled by a 0-10 ml/min mass flow controller (Alicat Scientific, Tucson, AZ) and monitored using SRI PeakSimple software. SF_6 acted as a tracer for determining air exchange rate and for studying indoor source behavior.

B.6 MEASUREMENT OF SF_6 TRACER GAS

Two methods were used for analyzing SF_6 (tracer gas), one for continuous indoor air, outdoor air, and soil gas monitoring and one for synoptic soil gas surveys.

B.6.1 Continuous monitoring. For continuous monitoring, indoor air, outdoor air, soil gas, and standard gas samples were collected every 30-min using an SRI 10-stream gas sampling valve connected to an SRI 8610C Gas Chromatograph (GC) (SRI Instruments, Torrence, CA) equipped with a dual mode pulse discharge detector (PDD) (Model D-2, Valco Instruments Co. Inc., Houston, TX) run in electron capture (EC) mode. Samples were pulled through a 1-mL loop using a vacuum pump (Rena 301 series, model BE-3012 vacuum/pressure pump), and a vacuum-configured, 0-100 mL/min mass flow controller (Alicat Scientific, Tucson, AZ), before the loop volume was pushed onto a washed 0.6 m (2 ft) mol sieve 5A column, followed by a 5 cm (2 in) 0.25 mm ID bonded phase fused silica capillary column, by helium purified by a heated helium purifier (Model HP2, Valco Instruments Co. Inc., Houston, TX). Sample collection was setup to ensure the removal of dead space in sampling lines. The calculated MDL for this

instrument, as it is configured, is 0.97 ppb_v for SF_6 using USEPA's MDL procedure (USGS, 1999). The results used to calculate the MDL are shown in Table B.5.

Table B. 5

Spiked concentrations, responses, and calculated concentrations used to calculate the MDL for SF_6 using the GC/PDD method.

Sample	Spiked concentration [ppb_v]	Response [area count]	Calculated concentration [ppb_v]
1	10	408.37	10.03
2	10	422.17	10.46
3	10	405.16	9.94
4	10	430.42	10.72
5	10	410.23	10.09
6	10	419.46	10.38
7	10	427.88	10.64
		Average:	10.32
		Standard Deviation (s):	0.31
		Student's t value (t):	3.14
		MDL [ppb_v]:	0.97

$$MDL = s \times t_{(n-1,1-\alpha=0.99)}$$

Instrument calibration occurred every 1-2 months, during site visits, at the beginning and end of synoptic surveys. Due to changes in instrument sensitivity between site visits, starting May 24th, 2011, one port of the 10-stream gas sampling valve was dedicated to a standard gas of approximately 500 ppbv SF_6 held in a series of 10 L FlexFoil bags (SKC 262-10) to allow for calibration checks and modification. Standard gas bags were sampled once every 5 hours during continuous monitoring. Calibration curves were modified based on a ratio of the results from sampling of the standard bag

and the original standard bag concentration. For data collected prior to May 24th, 2011, data was modified based on the assumption that sensitivity change between instrument calibrations was linear.

B.6.2 Synoptic soil gas surveys. Multi-depth soil gas surveys were performed every 1-3 months. Soil gas samples were collected in 1-liter Tedlar bags (SKC 232-01) using the lung sampler. Reconfiguration of the GC/PDD setup described above allowed for 500 μL direct-injection of soil gas grab samples onto the mol sieve column. Samples were analyzed within 1 hour of collection.

B.7 DIFFERENTIAL PRESSURE MEASUREMENTS

Differential pressure transducers ((Model P300-0.4”-D, Pace Scientific Inc., Mooresville, NC) were used for monitoring differential pressures between soil gas and indoor air and between outdoor air and indoor air. The transducers have two ports, one high and one low. When the pressure of the high port is higher than that of the low port, a positive pressure response would be recorded. Readings from the transducers were taken every 2 min and were recorded by a data acquisition module (Model OMB-DAQ-56, Omega Engineering Inc., Stamford, CT). The transducers were calibrated on-site by applying a range of positive and negative pressures. Positive pressures were applied using nitrogen gas with specific pressures obtained by feed control and bypass valves. The applied pressures were recorded using a Magnahelic differential air pressure gauge (Dwyer Instruments, Inc., Michigan City, IN). At each pressure level measured, the differential pressure signal was monitored. To simulate negative pressures, the tubing to the high and low ports was reversed and the process repeated. Using the applied pressure

readings and the differential pressure signal, calibration curves were developed for each transducer used.

B.8 MEASURMENT OF VOCS IN GROUNDWATER

B.8.1 Collection of Groundwater Samples during Synoptic Survey. Prior to collection of groundwater samples, the depth to groundwater was measured to determine groundwater elevation and estimate well-volume. Groundwater wells were then purged three well-volumes using peristaltic pumps or polyethylene bailers. The use of bailers was necessary when a peristaltic pump was unable to collect a sample without vaporization.

Groundwater samples were collected 24 h after wells were purged using either a peristaltic pump with dedicated polyethylene tubing or a dedicated polyethylene bailer. Samples were collected in 40 mL volatile organic analysis (VOA) vials preserved with hydrochloric acid. All samples were collected with duplicates when enough groundwater was available. Additional samples were collected at 2-3 monitoring locations for additional QA/QC activities. After collection, the samples were placed on ice and shipped to ASU for analysis within 48 h after receipt.

B.8.1 Collection of Groundwater Samples in Lab-scale Tank Experiment. Groundwater samples in the tank were collected using a 1 mL gas tight syringe. 1 mL aqueous samples were pulled out of the tank through the sampling ports as described in Figure II.3, and diluted into 29 mL reverse osmosis (RO) treated water which was pre-filled in 40 mL VOA valves. Once the sample was collected, it was immediately transferred to water bath and analyzed within 120 min.

B.8.3 Analysis of Groundwater Samples. Groundwater samples were analyzed for dissolved CHCs by a 42° heated-headspace analysis and an SRI GC equipped with a DELCD. For every 10 samples analyzed, a duplicate sample was analyzed to assess variability and error in sampling and analysis.

B.9 SOIL MOISTURE CONTENT

B.9.1 Soil Moisture at study site. Soil moisture content was determined from soil samples taken using a hand-powered soil auger (AMS Inc., American Falls, ID). Starting at the surface, soil samples were collected at 0.15 m (6 in) increments to a depth of 3.81 m (150 in). Each sample was placed in an individual jar, sealed, and shipped back to ASU for analysis. To determine soil moisture content of each sample, the following procedure was used:

- Approximately 15 g of soil was taken from a sample jar and placed on a pre-weighed aluminum dish and the mass recorded using an analytical balance (Mettler-Toledo, LLC, Columbus, OH).
- The soil and aluminum dish were then dried in an oven at 105°C for 24 h.
- Following removal from the oven and a short cooling period, the dried soil and aluminum dish were reweighed.
- By subtracting the weight of the aluminum dish from the dried sample, the mass of dry soil was determined.
- Mass of water in the soil was then determined by taking the difference between the original mass measurement and the dried mass measurement.

- Soil moisture content was then calculated by taking the mass of water and dividing it by the mass of dry soil.

B.9.1 Soil Moisture in the study tanks. 10 ECH_2O EC-5 soil moisture sensors (Decagon Devices, WA) were installed in the back panels of lab tanks, as shown in Figure II.5. Soil moisture content for each data logger were read by an EM50 Digital/Analog data logger (Decagon Devices, WA) on 15-30 min intervals.

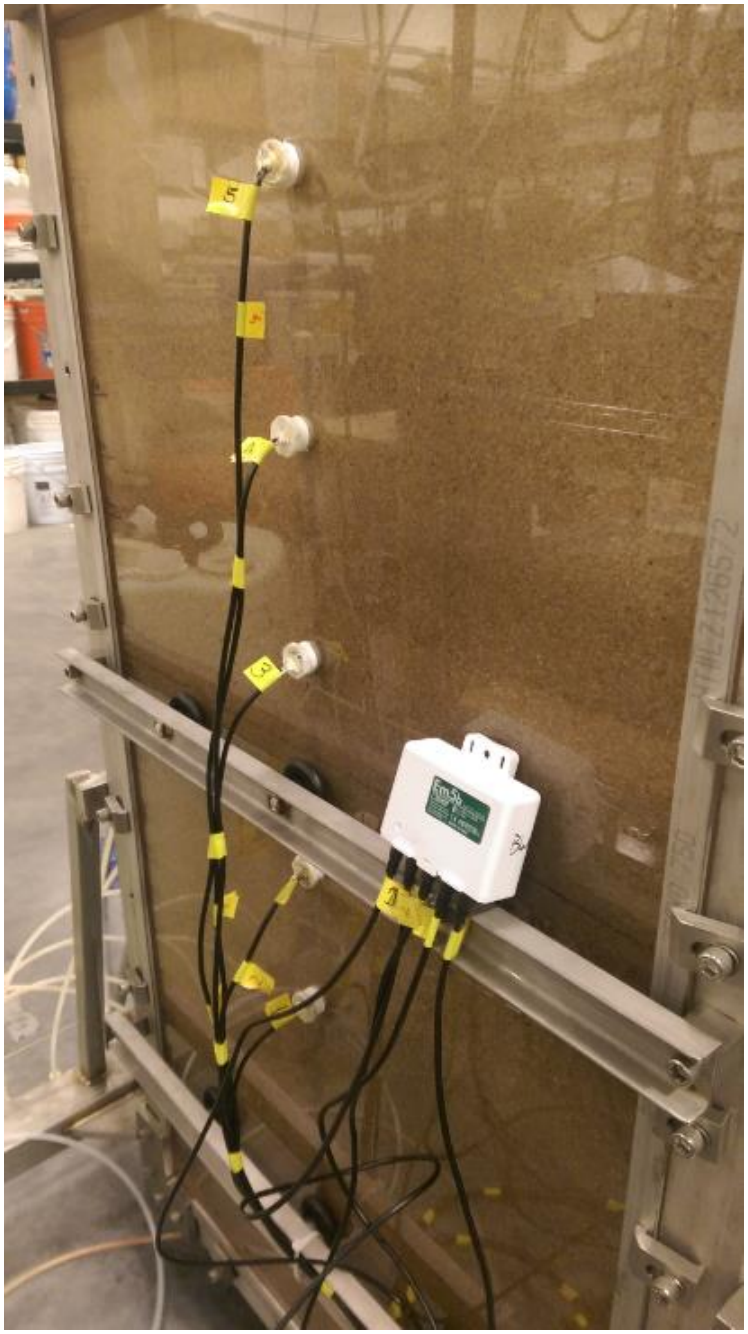

Figure B.5. Photo of soil moisture sensors and data logger.

APPENDIX C

SUPPLEMENTAL RESULTS FOR IMPACT OF GROUNDWATER TABLE FLUCTUATIONS ON CHLORINATED VOLATILE ORGANIC COMPOUND (VOC) EMISSIONS

C.1 OVERVIEW

The information presented below is supplemental to the Chapter 2. Data presented here was aimed to provide additional information that may help better understand the research work. Following sections include site observation, lab data and modeling results.

C.2 FIELD MEASUREMENTS

C.2.2 Real-time groundwater elevation. Real-time groundwater elevations were measured using water level transducers (Solinst Level-Logger) installed in three depth discrete screened intervals (4.2 m, 6.9 m and 9.3 m below ground surface (BGS)) at groundwater monitoring location GW3. The results are presented in Figure C.1.

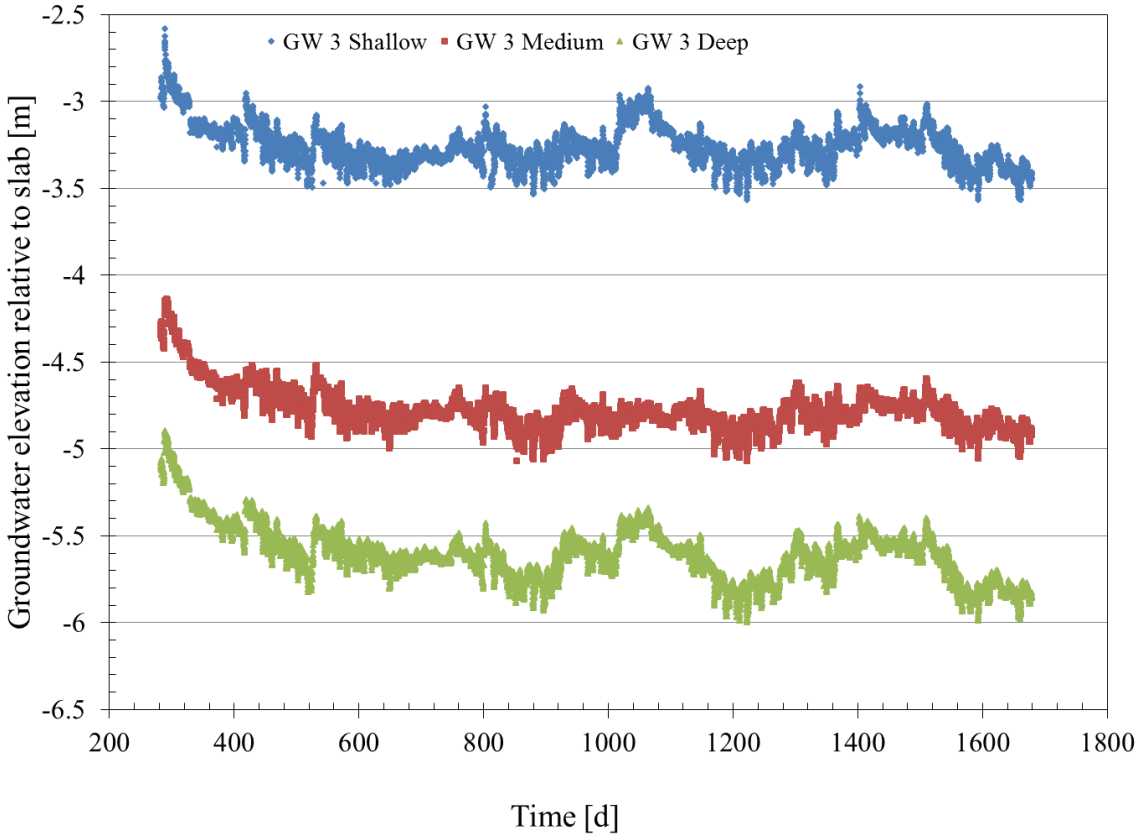

Figure C.1. Real-time groundwater elevations relative to study house slab.

C.2.1 Contaminant concentrations in groundwater. Analysis of groundwater was performed following field survey events. Table C.1 summarized all the TCE concentrations in groundwater from all the sampling wells.

Table C. 1

Summary table of groundwater concentrations from samples collected at study site.

Location	IGW[a] 1	IGW 2	IGW 3	IGW 4	IGW 5	IGW 6	1			2			3			4		
Depth	2.7 m BS[b]	2.7 m BS	2.7 m BS	2.7 m BS	2.7 m BS	2.7 m BS	4.9 m BS	10.2 m BS	12.9 m BS	4.9 m BS	10.2 m BS	12.9 m BS	4.3 m BS	7.1 m BS	9.5 m BS	3.4 m BS	6.5 m BS	9.2 m BS
Aug-10	24.0	NA[c]	40.1	NA	47.0	34.5	6.4	71.6	13.2	6.3	25.8	2.1	10.1	22.6	22.7	NA	24.1	40.9
Nov-10	6.7	NA	15.8	NA	20.2	17.1	5.6	23.4	10.1	4.0	19.6	3.5	16.5	28.1	12.6	7.3	9.2	27.5
Dec-10	5.1	11.2	7.3	3.4	9.6	7.1	5.8	30.4	12.4	2.8	26.7	4.4	13.1	12.4	16.9	5.5	17.8	NA
Jan-11	11.2	19.2	18.3	10.0	30.0	14.7	17.2	39.2	19.8	9.1	29.2	7.5	23.8	21.9	19.6	8.4	29.0	31.7
Feb-11	18.4	21.0	12.6	9.2	18.6	8.5	7.5	25.1	15.4	9.4	23.6	6.8	NA	27.5	32.6	10.0	22.2	21.6
Mar-11	25.2	43.8	30.5	38.4	37.4	25.3	15.2	18.2	7.8	14.5	28.6	10.7	20.3	36.9	39.4	16.5	43.5	42.2
May-11	20.2	32.3	30.9	13.1	39.2	29.7	12.0	41.9	11.4	9.4	29.0	3.2	17.0	25.8	29.9	12.9	40.4	44.9
Jul-11	16.0	53.8	38.2	16.2	39.8	31.0	12.5	42.8	22.1	8.0	32.4	4.3	13.0	20.3	26.0	10.1	33.9	70.3
Aug-11	9.7	24.5	20.6	NA	11.6	17.4	1.8	37.6	1.7	1.9	9.8	1.2	12.4	12.6	9.2	4.6	24.3	45.5
Sep-11	10.3	20.8	19.2	12.7	20.4	NS	7.5	45.8	3.6	4.4	34.1	4.8	14.0	23.0	33.2	9.7	25.9	52.6
Nov-11	9.2	26.1	19.7	8.9	19.2	6.3	7.1	24.6	9.2	6.7	37.9	5.7	13.8	15.5	21.9	8.8	13.9	22.8
Dec-11	9.2	23.3	23.0	7.8	25.8	16.2	7.4	42.6	10.3	NA	32.7	5.3	15.8	28.7	24.6	8.1	15.7	33.7
Jan-12	16.7	26.8	21.3	NA	19.1	17.9	NA	52.7	5.7	NA	43.7	5.8	14.8	26.9	21.4	6.4	42.8	44.4
Feb-12	54.7	59.4	34.5	NA	49.4	43.3	17.9	75.3	26.9	NA	52.1	9.1	49.3	48.8	43.3	28.4	105.6	81.5
Apr-12	14.0	29.4	27.4	13.7	32.0	22.1	12.1	41.5	11.8	NA	34.6	3.0	18.9	21.2	31.0	9.4	42.5	44.4
May-12	29.3	41.5	23.6	12.8	29.4	22.3	8.2	59.5	12.3	NA	66.9	4.3	16.2	24.1	31.5	11.2	50.9	56.2

Location	IGW[a] 1	IGW 2	IGW 3	IGW 4	IGW 5	IGW 6	1			2			3			4		
Depth	2.7 m BS[b]	2.7 m BS	2.7 m BS	2.7 m BS	2.7 m BS	2.7 m BS	4.9 m BS	10.2 m BS	12.9 m BS	4.9 m BS	10.2 m BS	12.9 m BS	4.3 m BS	7.1 m BS	9.5 m BS	3.4 m BS	6.5 m BS	9.2 m BS
Aug-12	12.4	32.5	30.4	NA	22.6	20.1	10.7	51.2	13.3	4.2	38.6	5.6	17.8	21.7	25.3	14.5	38.9	39.5
Nov-12	9.8	38.5	23.3	8.0	24.2	15.7	NA	49.8	18.9	NA	60.9	5.9	15.6	23.2	35.1	14.3	50.5	29.1
Dec-12	8.4	27.6	18.2	NA	31.5	14.3	NA	52.9	14.7	NA	44.6	4.9	46.9	13.6	46.8	10.5	19.6	28.6
Feb-13	19.0	37.8	31.8	NA	28.8	21.0	NA	49.4	15.6	NA	52.7	4.2	15.2	26.9	42.5	9.8	38.8	55.2
May-13	22.0	42.8	25.1	NA	32.6	20.5	9.9	33.9	17.2	7.9	36.0	4.8	NA	20.1	28.3	10.4	38.4	39.8
Jul-13	14.7	37.5	31.9	NA	27.6	22.8	10.2	50.3	24.4	2.5	53.3	6.6	18.3	27.7	29.5	27.6	48.0	50.0
Aug-13	6.9	41.4	20.9	NA	22.7	21.2	8.0	49.9	19.8	3.0	53.6	9.2	13.9	19.8	36.1	10.7	49.1	27.6
Oct-13	7.2	31.4	32.5	NA	24.1	22.1	7.3	39.3	32.1	1.7	44.7	7.4	17.5	24.3	38.8	14.9	54.5	28.6
Jan-14	52.7	59.1	33.5	NA	29.6	34.7	NA	78.1	40.4	NA	62.9	20.4	NA	28.6	40.2	14.4	79.4	52.6
Mar-14	25.6	44.8	31.0	NA	25.7	25.7	21.7	63.6	16.5	7.5	53.1	7.0	15.4	25.6	38.0	9.1	64.6	50.4
Jun-14	77.4	97.3	53.7	NA	52.0	126	22.2	45.6	52.9	31.6	71.9	37.8	104.7	126.5	140.1	115.8	181.0	127.6
Jan-15	NA	52.3	86.7	NA	34.2	37.2	NA	63.6	19.0	NA	99.3	101.1	84.7	68.9	134.2	27.8	72.2	38.6
Feb-15	14.9	26.5	29.0	NA	20.2	19.8	NA	67.2	21.3	NA	50.2	6.2	18.8	23.3	31.0	11.8	22.1	32.1
Mar-15	33.6	36.7	40.0	NA	35.0	21.4	NA	67.8	25.3	NA	49.3	16.8	22.8	33.4	39.6	11.2	61.3	47.4
Jun-15	18.5	36.7	26.5	18.0	25.2	25.6	13.1	40.1	9.9	7.6	46.9	2.6	14.7	25.1	36.6	14.2	43.0	38.5
Sep-15	10.1	27.6	17.1	10.7	17.5	15.3	8.2	53.0	19.9	0.8	40.0	4.2	10.4	18.3	21.8	8.7	40.7	33.6

a - Indoor groundwater wells.
b - Blow ground surface.
c - No data available.

C.3 LAB TESTS SUPPLIMENTAL INFORMATION

C.3.1 Soil organic fraction test. The soil organic fraction (f_{oc}) for both Play sand and Silico sand were tested with following procedure. Take 20-35 g of soil samples in aluminum tins and then dry them in the oven with temperature set at 105 °C for 24 h to obtain dry weights. Then the samples are heated back up to 450 °C for 24 h to obtain super-heated weights. f_{oc} can be calculated by divide the difference between the dry weight and super-heated weight to the dry weight. f_{oc} tests were performed three times for both soil types. The results are summarized in Table C.2.

Table C. 2

Summary of soil organic fraction test results.

Test time	Range of initial sample weight [g]	Sample numbers	foc measures				
			Mean	Max	Min	Standard deviation	% Standard deviation
Silica sand samples							
9/9/2014	12.4 - 39.6	6	0.0006	0.0010	-0.0004	0.0005	79.4
9/26/2015	38.2 - 47.7	5	0.0006	0.0010	0.0001	0.0003	47.9
10/6/2015	26.6 - 39.5	2	0.0009	0.0009	0.0008	-	-
Play sand samples							
8/15/2014	20 - 49.9	3	0.0029	0.0022	0.0016	0.0001	2.4
9/9/2014	11.1 - 26.3	4	0.0019	0.0022	0.0016	0.0003	15.3
9/26/2015	25.5 - 43.5	6	0.0035	0.0039	0.0032	0.0003	7.7

To evaluate the human factor error during the test, following tests were conducted: a) repeat heating samples at 100 °C and 450 °C and weigh them after each heating cycle and b) measure same samples 3 times in three days. Theoretically, no mass lost would be seen if the soil sample has already been super-heated at 450 °C before the replicated measures, however, the results of test a showed consistently weight reductions after the heating samples, results are show in Table C.3. This differences may be due to

1) mass loss in the process of transferring samples from oven to scale; 2) moisture in the atmosphere; 3) human operation; 4) decomposition of soil fractions (eg. particle fraction during the heating and cooling). Overall, this reduction reduced the confidence level of tested f_{oc} values, both of the soil types have minor soil organic fraction.

Table C. 3

Results of repeated heating test.

Sample	Heat cycles	(Dry weight-super heated weight)/Dry weight
1	1	0.00042
	2	0.00026
2	1	0.00045
	2	0.00035
3	1	0.00046
3	1	0.00009

C.2.2 Determine hydraulic conductivity. The hydraulic conductivity of both packed soils used was determined through a combination of the falling head and constant head procedure, and the average of these results was taken for the conductivity. The averaged hydraulic conductivity results for play sand is 0.083 cm/s and for silica sand is 0.186 cm/s.

C.2.3 Contaminant concentrations in feed water. During the tank experiment, horizontal flow fields were created and maintained stable contaminants concentration levels. Table C.4 summarized the characteristic of the measured feed water concentrations during the test. Overall, throughout these test the feed water concentrations varied less than 20 % of their mean measured values.

Table C. 4

The characteristics of VOCs concentrations in feeding water during the tank experiments.

Play sand tank	1,2-DCA			
concentration [mg/L]	Groundwater tablle drop at 4 inch/day	Groundwater tablle rise at 4 inch/day	Groundwater tablle fluctuation3 at 4 inch/day	Groundwater tablle fluctuation at 2 inch/day
Average	2.34	2.39	1.79	1.79
Max	2.87	2.84	2.25	2.02
Min	1.83	1.95	1.32	1.51
Standard deviation	0.43	0.45	0.23	0.21
	TCE			
Average	1.82	2.07	1.75	1.85
Max	2.41	2.74	2.22	2.60
Min	1.17	1.38	1.13	1.28
Standard deviation	0.45	0.68	0.30	0.46
	PCE			
Average	1.17	1.36	1.18	1.19
Max	1.63	1.62	2.61	2.00
Min	0.70	1.12	0.57	0.86
Standard deviation	0.31	0.25	0.49	0.43
Silica sand tank	1,2-DCA			
concentration [mg/L]	Groundwater tablle drop at 4 inch/day	Groundwater tablle rise at 4 inch/day	Groundwater tablle fluctuation3 at 4 inch/day	Groundwater tablle fluctuation at 2 inch/day
Average	2.34	2.39	1.76	1.83
Max	3.01	2.55	2.29	1.98
Min	1.61	2.30	1.50	1.61
Standard deviation	0.40	0.13	0.22	0.14
	TCE			
Average	1.93	2.18	1.63	1.75
Max	2.83	2.57	2.20	2.29
Min	1.17	1.97	1.08	1.43
Standard deviation	0.50	0.34	0.35	0.31
	PCE			
Average	1.10	1.26	1.05	1.08
Max	1.55	1.55	2.23	1.92
Min	0.61	0.95	0.51	0.71
Standard deviation	0.29	0.30	0.42	0.46

C.2.4 Soil moisture sensor data. Soil moisture sensor readings were logged throughout the experiment. The results are shown in Figure C.2 and C.3. For each tank sensors are installed at 51 cm, 63 cm, 76 cm, 91 cm and 101 cm above the bottom of the tank. Time t = 0 h in all the figures indicates the start of the water table movement. During the water table rising test, a tank leakage happened at about t = 110 h in Silica sand tank. For the water table fluctuation from bottom water boundary condition, a power outage was found during the period of – 85 h < t < 220 h for Silica tank data logger; and the soil moisture sensor installed at 63 cm above the bottom of the Play sand tank was found malfunction after t = 162 h.

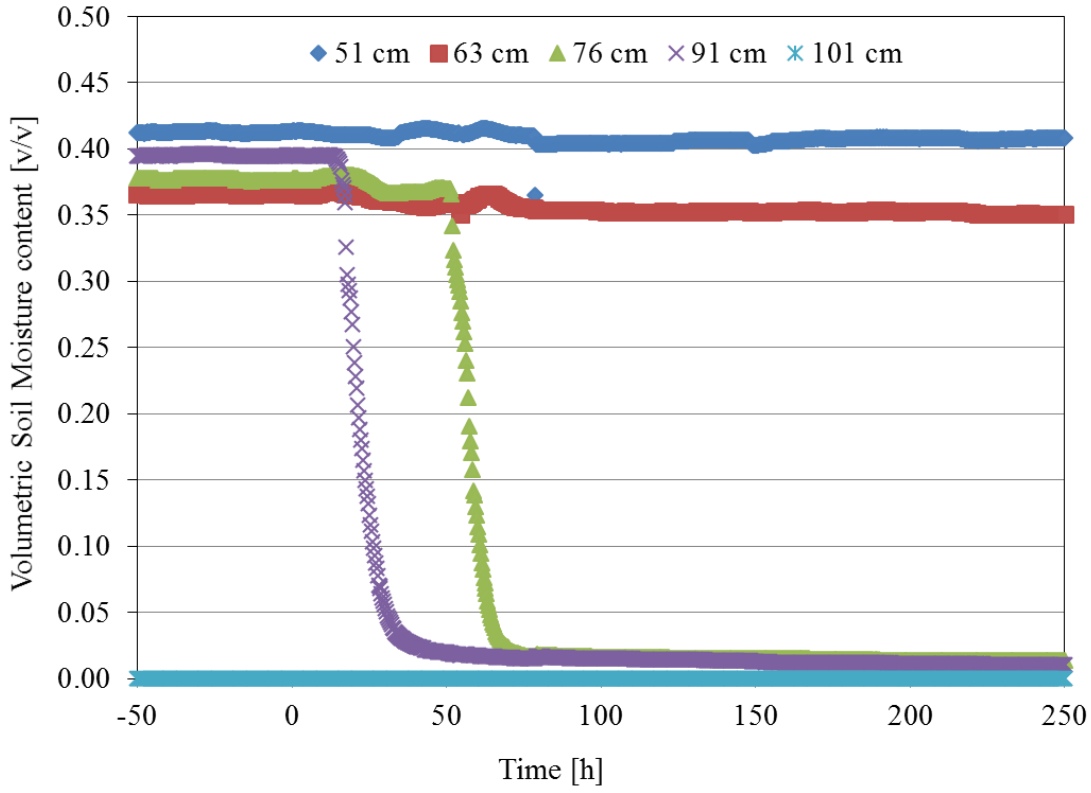
51 cm
63 cm
76 cm
91 cm
101 cm
Volumetric Soil Moisture content [v/v]
0.50
0.45
0.40
0.35
0.30
0.25
0.20
0.15
0.10
0.05
0.00
-50
0
50
100
150
200
250
Time [h]

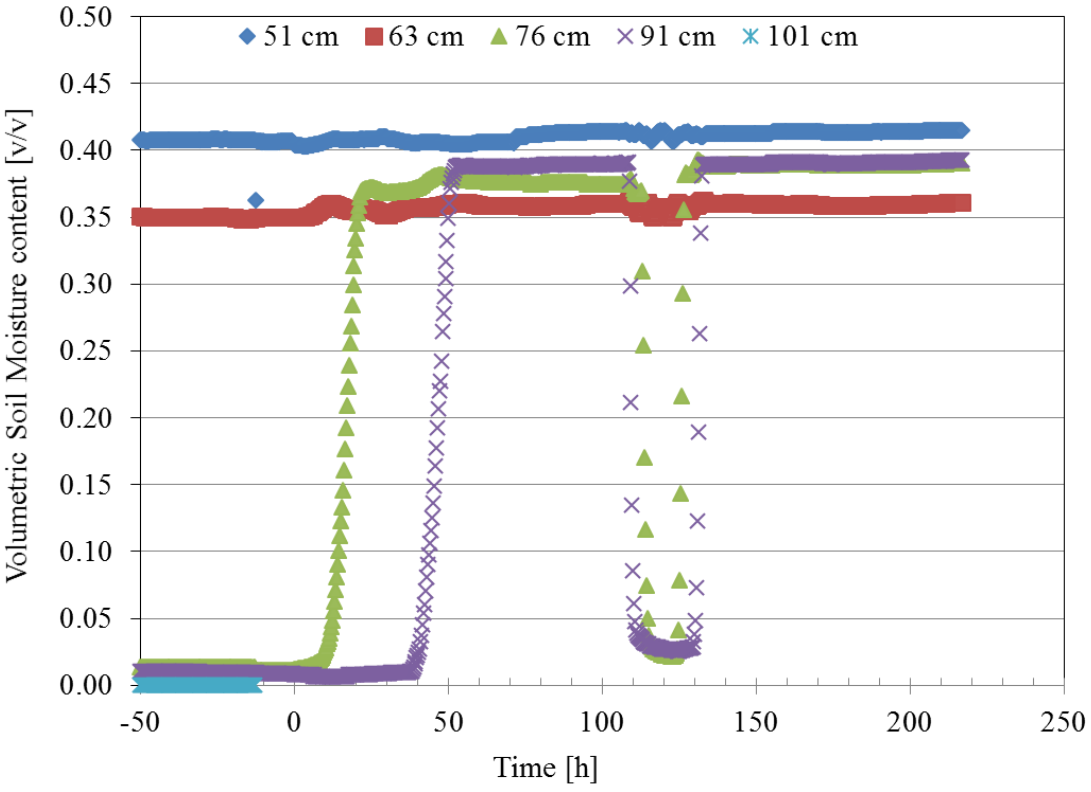
51 cm
63 cm
76 cm
91 cm
101 cm
Volumetric Soil Moisture content [v/v]
0.50
0.45
0.40
0.35
0.30
0.25
0.20
0.15
0.10
0.05
0.00
-50
0
50
100
150
200
250
Time [h]

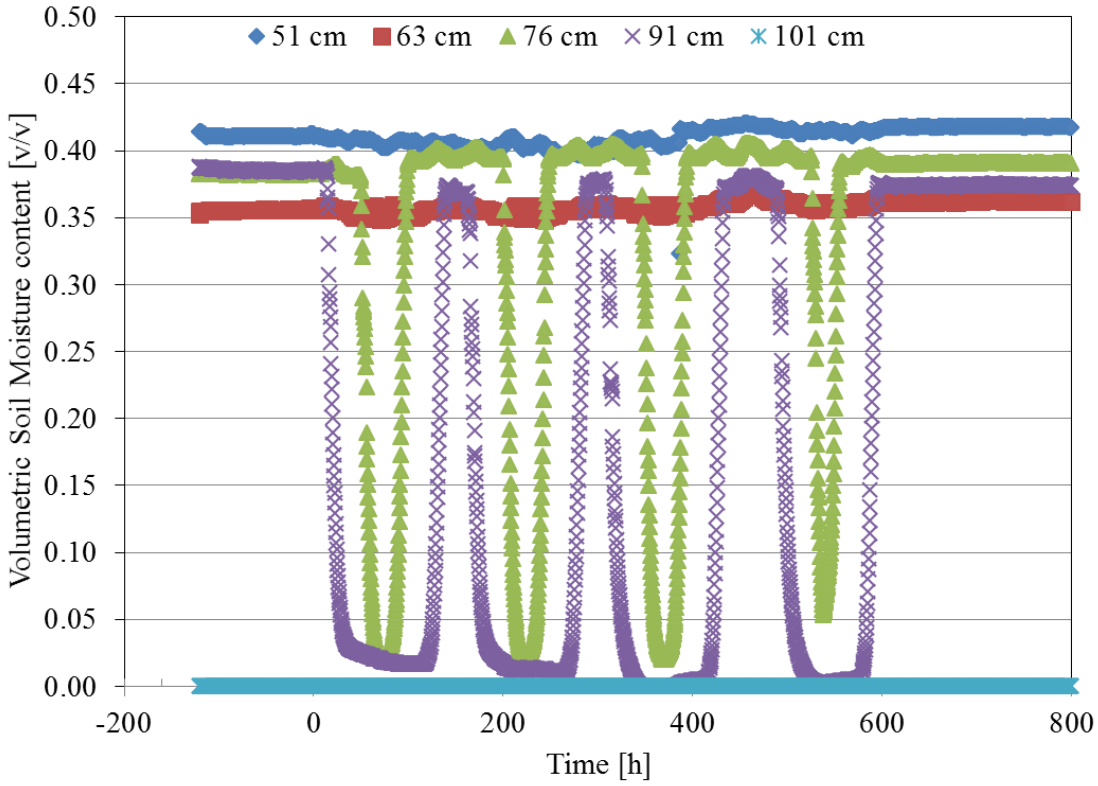
51 cm
63 cm
76 cm
91 cm
101 cm
Volumetric Soil Moisture content [v/v]
0.50
0.45
0.40
0.35
0.30
0.25
0.20
0.15
0.10
0.05
0.00
-200
0
200
400
600
800
Time [h]

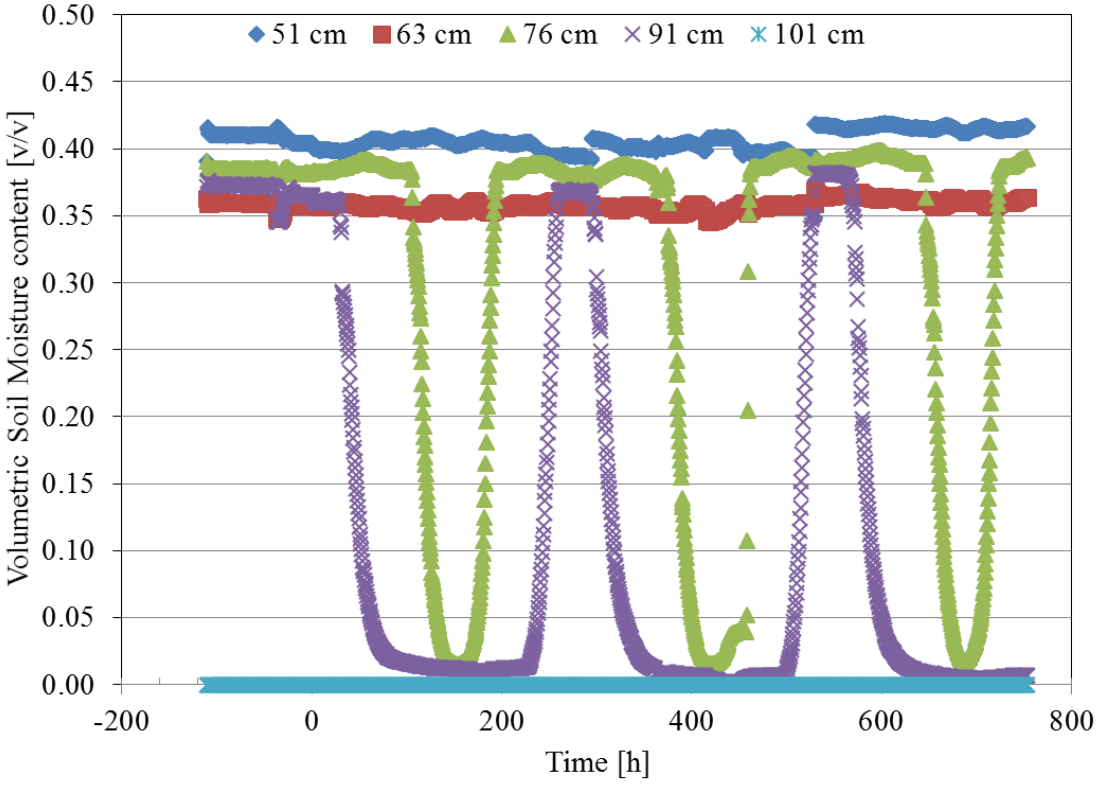
51 cm
63 cm
76 cm
91 cm
101 cm
Volumetric Soil Moisture content [v/v]
0.50
0.45
0.40
0.35
0.30
0.25
0.20
0.15
0.10
0.05
0.00
-200
0
200
400
600
800
Time [h]

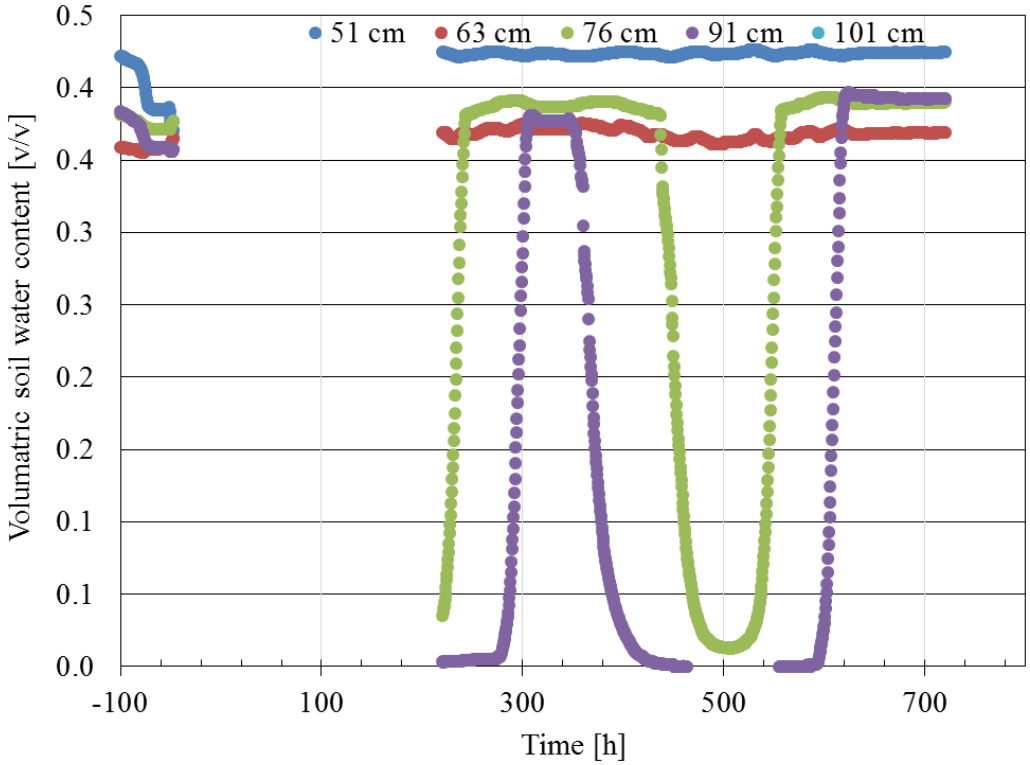

Figure C.2. Soil moisture sensor readings during water table fluctuation tests in Silica sand tank. From the beginning to end, the data presents the results for water table dropping test, rising test, 5 cm/day fluctuation test, 10 cm/day fluctuation test and the test of fluctuation from bottom boundary with the rate of 10 cm/day.

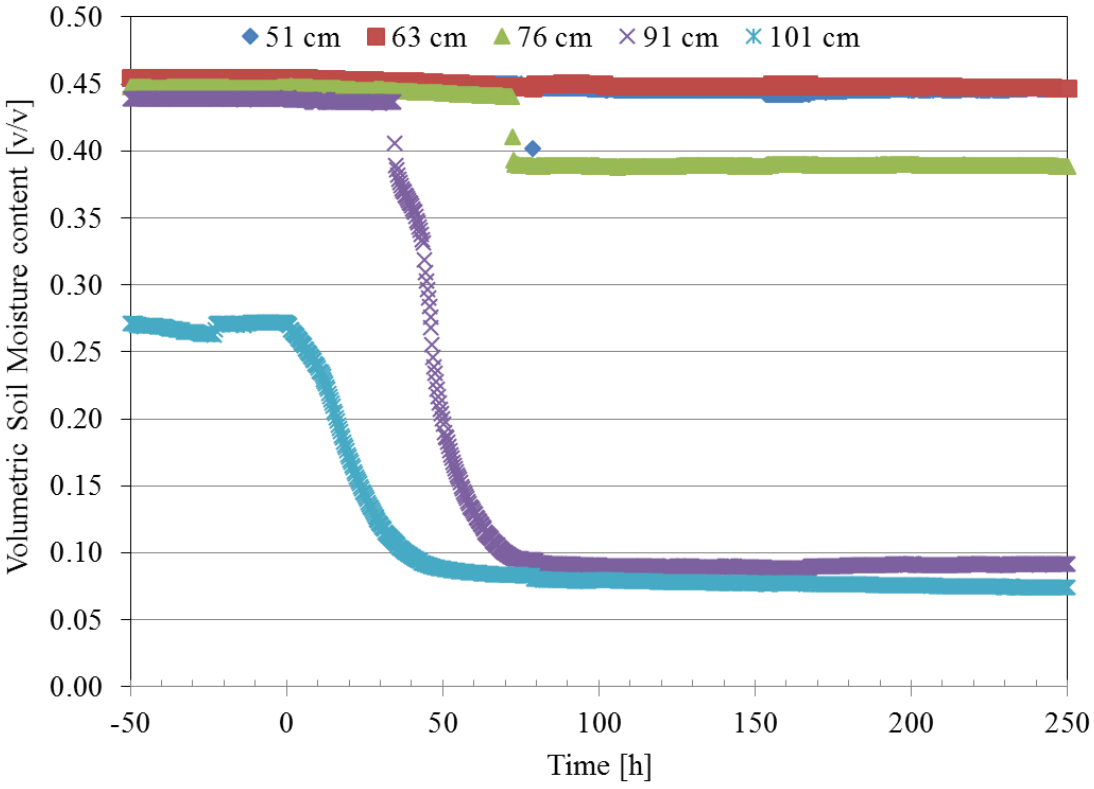
51 cm
63 cm
76 cm
91 cm
101 cm
Volumetric Soil Moisture content [v/v]
0.50
0.45
0.40
0.35
0.30
0.25
0.20
0.15
0.10
0.05
0.00
-50
0
50
100
150
200
250
Time [h]

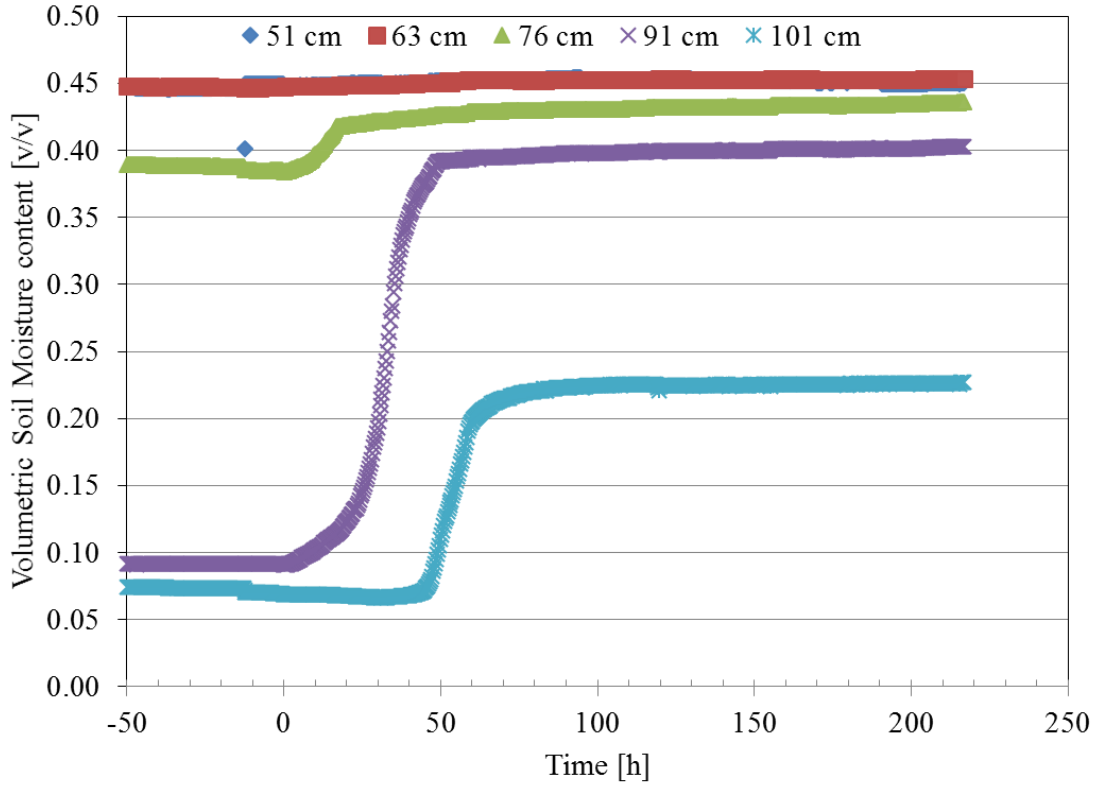
51 cm
63 cm
76 cm
91 cm
101 cm
Volumetric Soil Moisture content [v/v]
0.50
0.45
0.40
0.35
0.30
0.25
0.20
0.15
0.10
0.05
0.00
-50
0
50
100
150
200
250
Time [h]

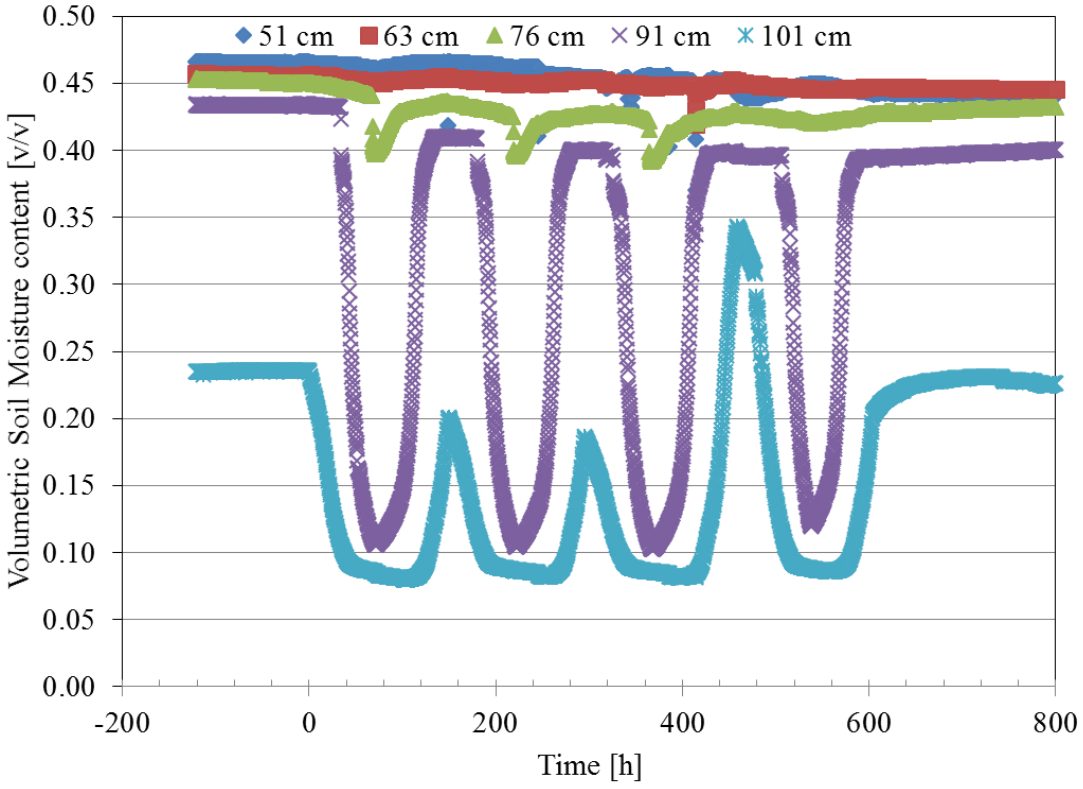
51 cm
63 cm
76 cm
91 cm
101 cm
Volumetric Soil Moisture content [v/v]
0.50
0.45
0.40
0.35
0.30
0.25
0.20
0.15
0.10
0.05
0.00
-200
0
200
400
600
800
Time [h]

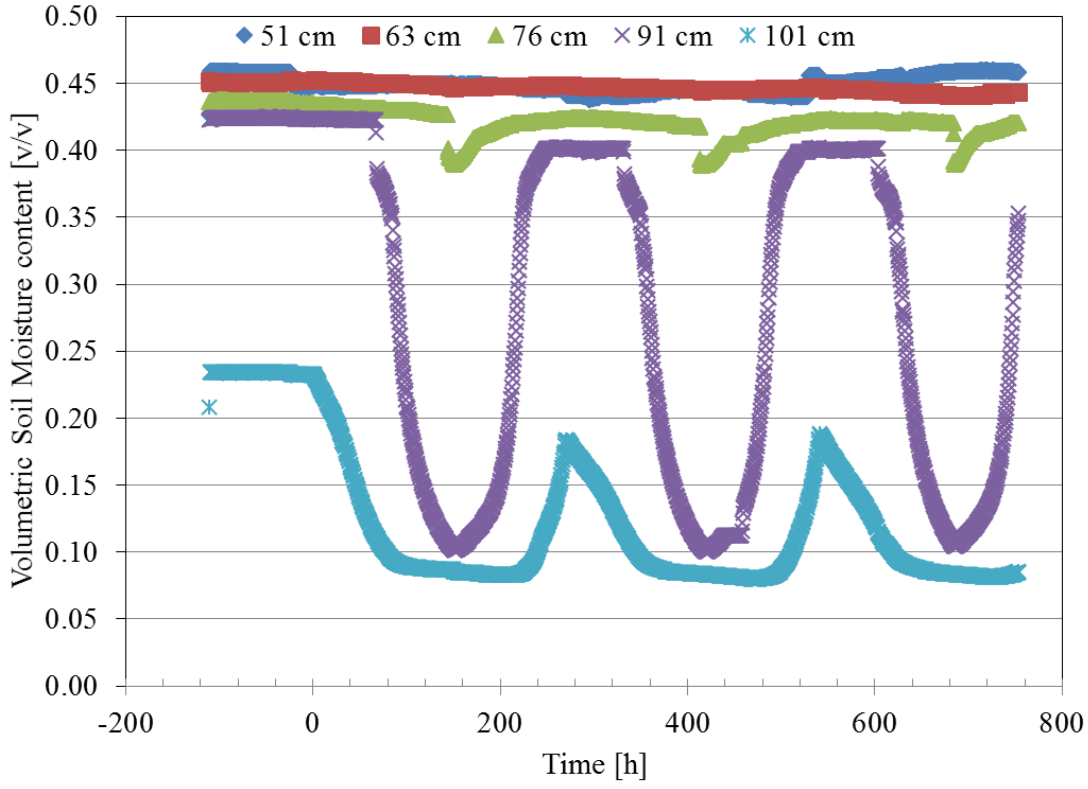
51 cm
63 cm
76 cm
91 cm
101 cm
Volumetric Soil Moisture content [v/v]
0.50
0.45
0.40
0.35
0.30
0.25
0.20
0.15
0.10
0.05
0.00
-200
0
200
400
600
800
Time [h]

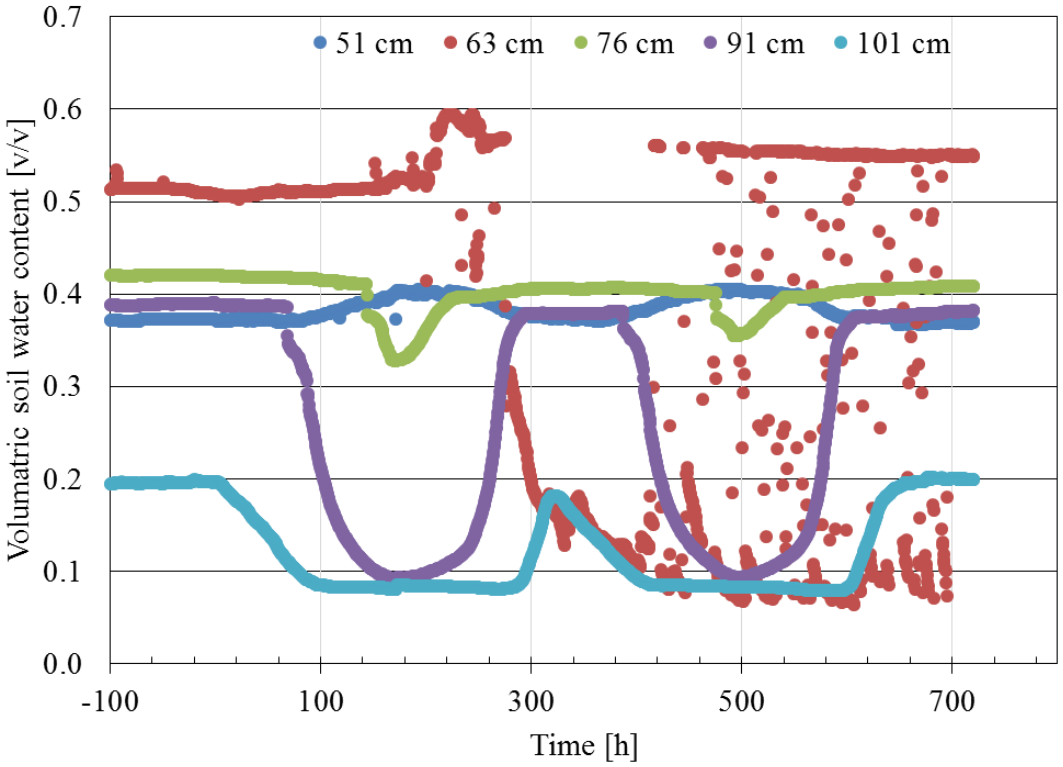

Figure C.3. Soil moisture sensor readings during water table fluctuation tests in Play sand tank. From the beginning to end, the data presents the results for water table dropping test, rising test, 5 cm/day fluctuation test, 10 cm/day fluctuation test and the test of fluctuation from bottom boundary with the rate of 10 cm/day.

C.2.5 Physical model layout and water table elevation control. Figure C.4 illustrates the photo of the physical model and water table control system. The physical models used in this study were two 182-cm tall, 61-cm wide and 10-cm thick stainless steel frame tanks. Plastic glasses at both sides allowed visual picture of packing as well as sample collections. Totally 36 brass Swagelok® 1/4 in fittings were installed with Septa Thermolite® Shimadzu Plugs through the window in the front side of each tank. The head spaces for both tanks were sealed and were continuous swept using compressed air

at stable flowrates. Samples can be pulled from the effluents of sweeping gas lines and be analyzed in GC/FID.

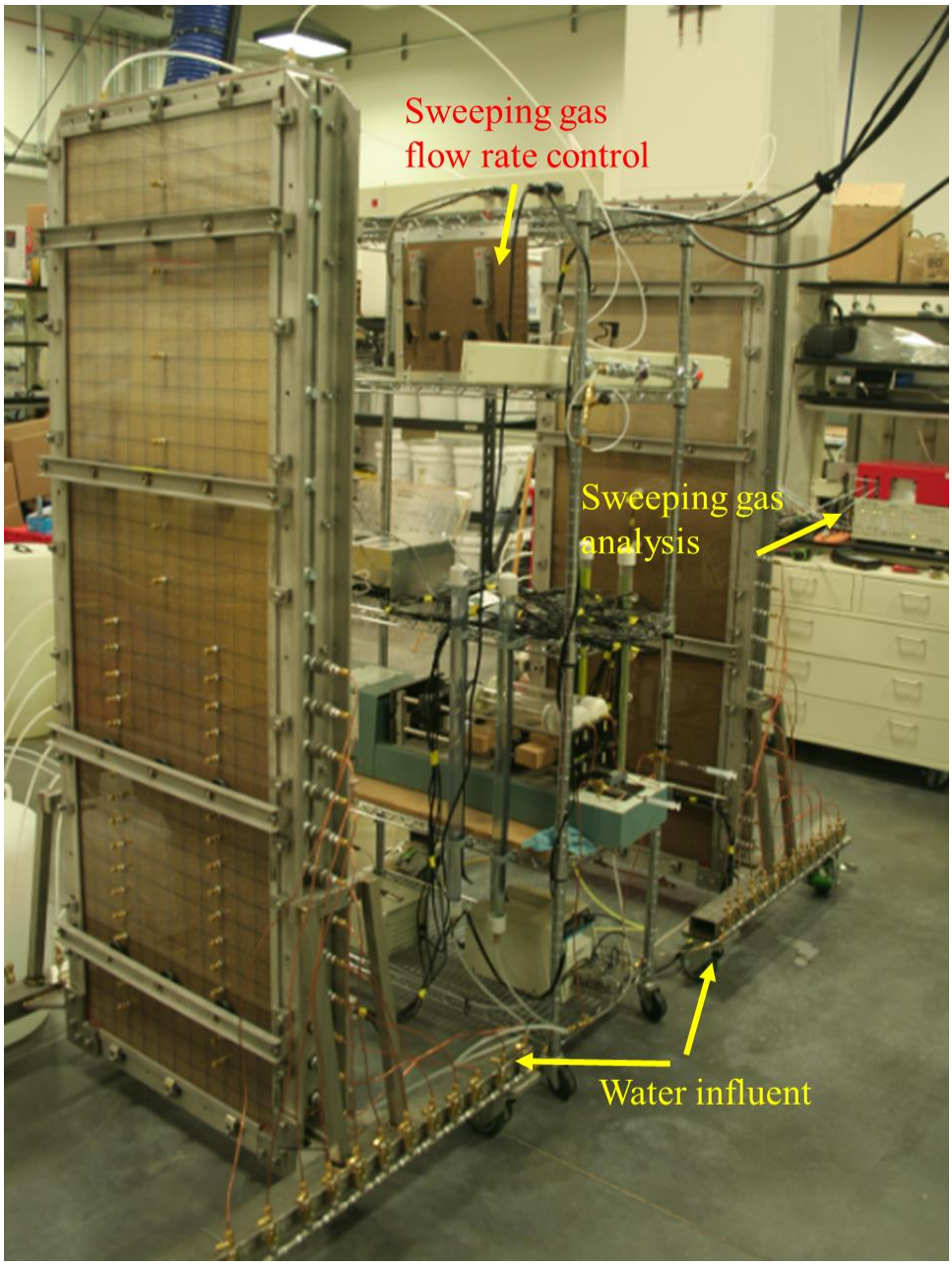

Figure C.4. Photo of physical model.

Figure C.5 shows an automatic position adjusting system was installed to allow groundwater table elevations in both tanks fluctuate at identical rates. This system was

composed by a STP-MTR-23079 stepper motor and a STP-DRV-6575 stepper drive (Automation Direct, GA) equipped with a pre-programmed D0-05DD PLC (Koyo, China).

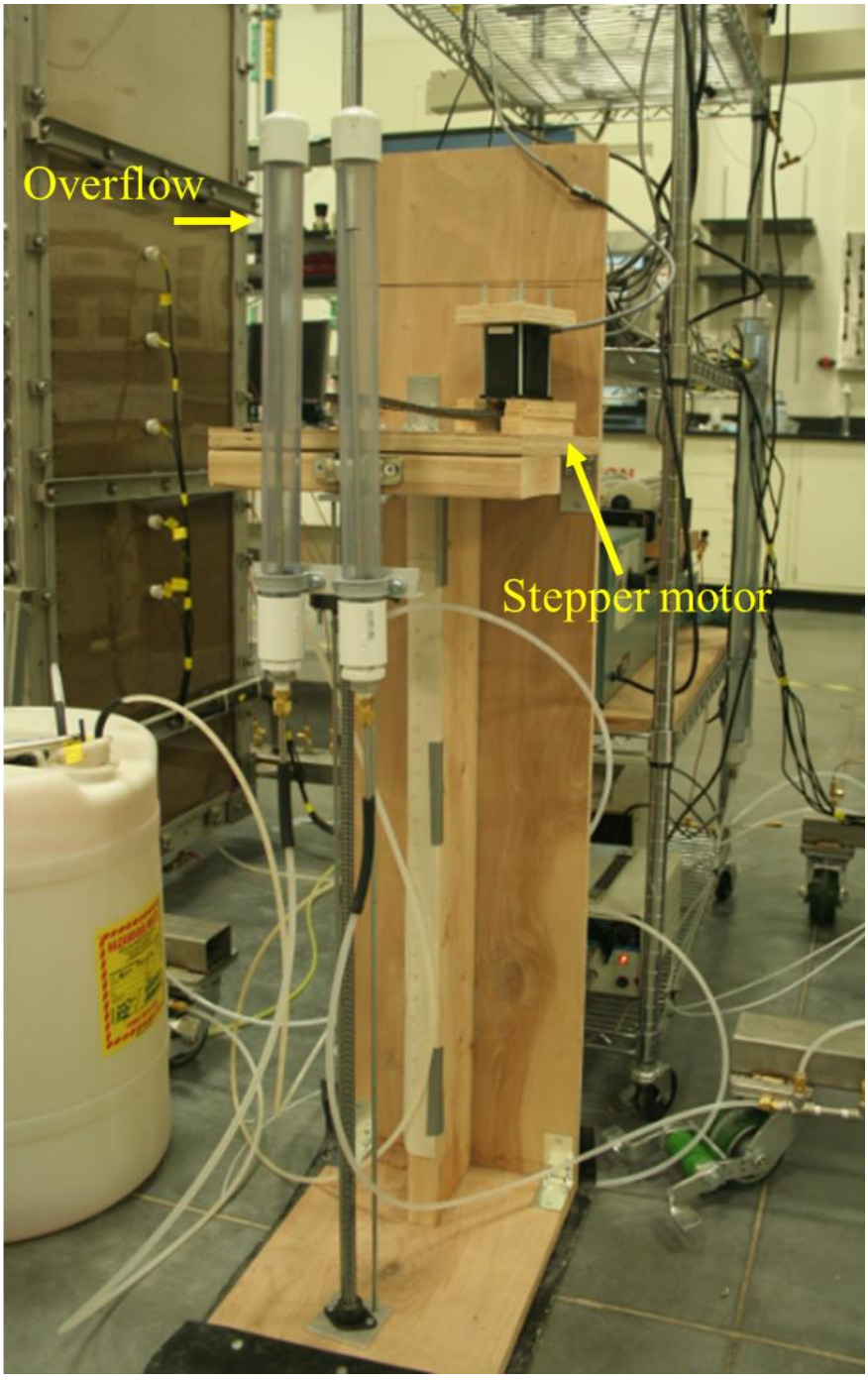

Figure C.5. Photo of water table elevation control system.

APPENDIX D

SUPPLEMENTAL INFORMATION FOR IDENTIFICATION OF ALTERNATIVE VAPOR INTRUSION PATHWAYS USING CONTROLLED PRESSURE TESTING, SOIL GAS MONITORING, AND SCREENING MODEL CALCULATIONS

Table D. 1

Effective TCE Diffusion Coefficients Survey Results.

	TCE Effective Diffusion Coefficients at the Sub-Slab Depth [cm^2/s]												
Survey time [d]	Outdoor Sampling Locations			Indoor Sampling Locations							Outdoor Sampling Locations		
	A	B	C	1	2	3	4	5	6	7	F	E	D
372- 373	N/A*	0.003	0.001	0.002	0.009	0.019	0.004	0.014	0.029	0.015	0.002	0.004	N/A
553- 554	0.002	0.002	0.002	0.003	0.020	0.013	0.005	0.014	0.032	0.019	0.002	0.004	N/A
627- 628	0.002	0.003	0.005	0.004	0.016	0.018	0.006	0.011	0.018	0.017	0.003	0.012	N/A
653- 654	0.004	0.007	0.008	0.008	0.013	0.016	0.007	0.016	0.018	0.023	0.009	0.014	N/A
741- 742	0.005	0.005	0.005	0.011	0.022	0.019	0.012	0.025	0.022	0.017	0.008	0.015	N/A
	Effective Diffusion Coefficients at the 0.9 m Below-Slab (BS) Depth [cm^2/s]												
372- 373	0.003	0.003	N/A	0.002	N/A	0.004	0.003	0.003	N/A	N/A	0.015	0.003	0.003
553- 554	0.003	0.002	0.001	N/A	0.001	0.001	0.001	0.003	0.001	N/A	0.002	0.002	0.002
627- 628	0.002	0.002	0.001	0.005	0.003	0.003	0.004	0.004	0.002	N/A	0.003	0.001	0.003
653- 654	0.004	0.004	0.004	0.005	0.005	0.007	0.006	0.007	0.006	N/A	0.007	0.007	0.006
741- 742	0.010	0.004	0.003	0.009	0.008	0.008	0.007	0.007	0.006	N/A	0.005	0.006	0.010
	TCE Effective Diffusion Coefficients at the 1.8 m Below-Slab (BS) Depth [cm^2/s]												
372- 373	N/A	N/A	0.002	0.003	0.003	0.002	0.001	0.004	0.002	N/A	0.003	0.005	0.003
553- 554	N/A	N/A	0.002	0.001	0.003	0.002	0.001	0.002	0.002	N/A	0.003	0.002	0.004
627- 628	N/A	N/A	0.002	0.004	0.007	0.004	0.002	0.004	0.002	N/A	0.002	0.002	0.001
653- 654	N/A	N/A	0.003	0.007	0.004	0.004	0.007	0.003	0.004	N/A	0.003	0.004	0.003
741- 742	N/A	N/A	0.004	0.006	0.006	0.003	0.006	0.006	0.005	N/A	0.010	0.005	0.005
	Average TCE Effective Diffusion Coefficients [cm^2/s]												
Depth	A	B	C	1	2	3	4	5	6	7	F	E	D
Sub-Slab	0.003	0.004	0.004	0.006	0.016	0.017	0.007	0.016	0.024	0.018	0.005	0.010	N/A
0.9 m BS	0.004	0.003	0.002	0.005	0.005	0.005	0.004	0.005	0.004	N/A	0.006	0.004	0.005
1.8 m BS	N/A	N/A	0.002	0.004	0.005	0.003	0.004	0.004	0.003	N/A	0.004	0.004	0.003
Equation (2) ($D_{i,j\ eff}$ /Li) [cm^2/s]				0.005	0.005	0.004	0.004	0.005	0.004				

* - No data available.

Table D. 2

TCE Soil Gas Concentrations.

TCE Soil Gas Concentration at the Sub-Slab Depth [µg/m^3]													
Event time [d]	Outdoor Sampling Locations						Indoor Sampling Locations						
	A	B	C	D	E	F	1	2	3	4	5	6	7
	Building pressure condition: Natural; lateral pipe valve: Open												
-10- -5	10.91	ND*	ND	N/A**	ND	ND	42.07	ND	ND	ND	ND	ND	0.24
90- 92	0.27	3.68	1.13	N/A	1.77	1.67	4.08	0.76	0.98	4.33	0.76	0.30	0.24
124- 127	0.35	3.49	0.98	N/A	0.81	0.92	12.46	1.81	2.25	10.70	2.79	0.69	0.78
201- 204	ND	2.66	0.39	N/A	ND	ND	8.65	0.82	1.67	7.59	2.26	12.58	0.46
227- 231	0.26	2.51	0.34	N/A	0.20	0.62	5.52	3.02	9.53	5.47	18.77	12.39	2.10
276- 278	0.50	0.77	0.67	N/A	0.50	1.31	1.08	ND	ND	1.03	0.68	0.59	0.40
326- 330	0.47	0.75	1.75	N/A	0.81	0.67	4.27	0.35	0.17	6.21	0.76	N/A	0.63
368- 370	1.31	3.05	2.12	N/A	0.37	1.61	5.57	0.05	0.07	6.87	0.12	0.18	0.11
409- 411	4.81	1.31	3.26	N/A	0.58	3.48	3.49	0.31	0.33	2.72	0.71	0.24	1.66
446- 447	11.81	0.56	0.61	N/A	3.09	8.24	3.44	1.28	0.83	1.53	2.71	0.93	1.10
475- 476	10.06	5.89	1.75	N/A	0.28	0.93	2.54	4.06	15.54	2.38	13.02	7.94	0.96
514- 516	12.11	0.87	1.77	N/A	0.65	8.07	3.24	1.01	10.80	2.16	9.52	ND	0.76
550- 551	6.30	0.92	1.86	N/A	2.16	6.14	4.37	1.31	1.29	2.47	1.84	0.88	1.69
624- 625	9.41	3.32	1.79	N/A	0.41	6.28	4.83	0.70	1.77	3.18	1.28	1.19	0.93
651- 652	10.25	1.37	1.15	N/A	0.39	5.91	3.44	2.67	0.71	2.23	0.86	0.42	2.55
736- 737	12.94	1.76	1.37	N/A	2.44	18.17	11.78	3.76	1.72	6.43	1.13	1.07	1.68
	Building pressure condition: Controlled under-pressurization; lateral pipe valve: Open												
808- 812	9.92	2.25	1.57	N/A	4.21	15.44	3.47	329.77	335.84	1.85	385.16	347.08	16.82
850- 851	4.64	0.97	0.35	N/A	4.55	8.54	2.95	514.32	567.62	1.93	429.55	514.89	3.64
910- 911	6.49	0.56	0.32	N/A	1.29	9.90	4.32	489.46	462.57	2.29	420.33	403.83	3.67
1010- 1011	12.42	1.28	0.11	N/A	0.18	6.24	5.95	330.39	432.10	2.31	383.33	409.91	1.17
	Building pressure condition: Controlled under-pressurization; lateral pipe valve: Closed												
1012- 1013	4.25	0.87	1.57	N/A	8.92	9.81	2.50	5.82	3.04	1.73	2.79	1.43	0.36
1154- 1155	22.17	7.33	6.82	N/A	7.52	13.07	1.81	3.40	1.22	1.58	1.04	0.90	0.71
	Building pressure condition: Natural; lateral pipe valve: Closed												
1247- 1248	1.83	3.94	1.93	N/A	9.35	4.84	5.16	1.29	0.80	3.18	1.73	0.49	1.49
1305- 1306	3.84	1.31	1.49	N/A	0.50	5.42	7.74	0.92	1.04	7.29	1.39	0.42	1.13
1394- 1395	7.78	1.34	1.52	N/A	0.32	8.70	3.84	1.49	0.55	5.60	1.09	0.43	0.28

TCE Soil Gas Concentration at the 0.9 m Below Slab Depth [µg/m^3]													
Event time [d]	Outdoor Sampling Locations						Indoor Sampling Locations						
	A	B	C	D	E	F	1	2	3	4	5	6	7
	Building pressure condition: Natural; lateral pipe valve: Open												
-10- -5	202.55	52.42	16.60	ND	10.52	46.17	273.28	238.96	63.40	215.58	260.45	ND	N/A
90- 92	213.52	38.79	20.74	0.82	1.05	156.44	134.92	29.88	20.08	118.43	39.57	5.67	N/A
124- 127	100.46	20.34	9.76	0.45	0.78	NA	81.96	14.68	17.76	91.98	23.59	7.27	N/A
201- 204	99.69	22.15	5.99	0.12	0.43	60.17	71.86	9.27	5.22	74.17	16.83	9.71	N/A
227- 231	85.85	27.59	5.37	0.12	0.26	15.72	70.08	10.83	13.45	42.30	28.11	2.95	N/A
276- 278	131.92	17.10	8.83	0.54	0.54	66.42	135.91	10.51	26.32	96.82	39.92	13.27	N/A
326- 330	101.96	21.16	16.00	0.50	0.94	57.99	73.81	10.07	19.12	42.75	18.32	41.22	N/A
368- 370	214.39	19.07	21.54	2.99	1.15	305.91	104.84	28.99	72.10	86.13	10.44	26.04	N/A
409- 411	253.54	53.74	41.09	1.66	4.67	419.40	144.14	7.53	55.27	117.15	14.41	17.59	N/A
446- 447	129.37	13.62	8.69	0.44	1.36	369.29	124.61	13.64	9.51	46.80	6.89	1.78	N/A
475- 476	116.21	19.63	26.92	1.13	1.27	307.33	65.03	23.74	14.01	33.57	22.04	4.16	N/A
514- 516	165.25	11.12	26.44	0.62	1.40	143.92	60.45	32.49	22.50	37.31	ND	12.43	N/A
550- 551	110.87	19.51	12.74	0.71	1.45	144.73	113.47	38.97	16.53	31.70	ND	4.96	N/A
624- 625	187.44	48.08	18.42	3.81	1.28	195.30	134.03	92.03	23.68	33.58	35.69	12.44	N/A
651- 652	186.10	50.16	36.05	0.97	3.56	332.53	226.04	42.42	30.55	76.75	92.24	ND	N/A
736- 737	294.36	46.11	35.57	2.63	7.20	332.53	344.73	57.61	24.60	59.05	48.68	ND	N/A
	Building pressure condition: Controlled under-pressurization; lateral pipe valve: Open												
808- 812	168.13	17.70	21.16	2.42	6.61	684.29	357.14	60.62	58.05	51.83	51.77	14.92	N/A
850- 851	181.42	49.26	34.94	0.42	2.41	995.23	223.64	63.15	57.80	51.57	47.55	9.33	N/A
910- 911	132.52	13.68	12.06	0.21	4.41	605.95	199.60	35.53	53.63	46.36	67.60	12.82	N/A
1010- 1011	128.91	14.55	0.54	0.18	1.33	446.52	194.73	95.92	57.59	135.20	95.16	7.27	N/A
	Building pressure condition: Controlled under-pressurization; lateral pipe valve: Closed												
1012- 1013	39.41	16.86	4.47	2.02	5.52	639.26	180.37	26.26	25.03	95.11	79.25	3.28	N/A
1154- 1155	38.03	16.30	ND	9.99	14.34	560.63	127.89	5.07	22.77	38.84	29.76	22.99	N/A
	Building pressure condition: Natural; lateral pipe valve: Closed												
1247- 1248	81.35	6.23	6.24	2.66	3.63	360.80	116.25	3.85	4.18	34.75	6.64	2.42	N/A
1305- 1306	69.27	6.66	5.38	1.75	0.82	588.27	40.07	3.85	4.43	104.93	7.45	ND	N/A
1394- 1395	124.44	13.00	6.08	0.40	1.32	515.54	139.12	5.77	10.72	66.38	4.81	3.01	N/A

TCE Soil Gas Concentration at the 1.8 m Below Slab Depth [µg/m^3]													
Event time [d]	Outdoor Sampling Locations						Indoor Sampling Locations						
	A	B	C	D	E	F	1	2	3	4	5	6	7
	Building pressure condition: Natural; lateral pipe valve: Open												
-10- -5	N/A	N/A	352.72	45.89	67.50	1579.58	627.53	2066.42	1211.09	491.34	1107.78	417.83	N/A
90- 92	N/A	N/A	636.69	9.80	153.85	2913.62	1092.78	788.97	721.62	573.03	404.03	238.58	N/A
124- 127	N/A	N/A	N/A	10.25	62.05	N/A	497.10	N/A	N/A	278.96	191.18	130.02	N/A
201- 204	N/A	N/A	158.73	5.27	8.51	1585.23	481.49	423.05	225.07	1069.40	309.48	189.88	N/A
227- 231	N/A	N/A	243.12	4.31	10.44	N/A	468.71	488.24	N/A	403.54	253.15	241.33	N/A
276- 278	N/A	N/A	197.05	9.96	7.61	2202.11	730.65	2317.31	N/A	195.10	160.82	N/A	N/A
326- 330	N/A	N/A	498.17	6.54	13.85	2263.68	627.78	1094.21	N/A	477.70	200.37	224.71	N/A
368- 370	N/A	N/A	464.93	4.25	338.98	2191.08	902.78	871.68	769.72	435.48	203.50	213.19	N/A
409- 411	N/A	N/A	359.23	2.88	551.42	2150.04	944.69	670.74	779.17	477.97	196.03	327.12	N/A
446- 447	N/A	N/A	322.39	2.47	304.97	2019.20	1282.91	842.57	455.04	477.97	126.39	187.78	N/A
475- 476	N/A	N/A	212.31	6.38	262.87	1561.09	628.23	366.32	444.59	308.62	148.52	222.39	N/A
514- 516	N/A	N/A	173.44	4.41	146.90	893.52	474.91	430.27	446.37	231.50	114.16	190.88	N/A
550- 551	N/A	N/A	243.90	2.32	99.61	1150.84	533.66	406.82	340.25	273.95	202.14	150.87	N/A
624- 625	N/A	N/A	243.90	7.29	184.48	1279.28	560.03	808.46	417.92	319.71	422.86	191.28	N/A
651- 652	N/A	N/A	299.20	8.15	307.71	1738.56	680.53	1137.26	603.56	467.38	741.64	395.29	N/A
736- 737	N/A	N/A	361.21	5.47	1298.80	1756.64	1190.63	1205.83	701.19	503.57	751.24	420.26	N/A
	Building pressure condition: Controlled under-pressurization; lateral pipe valve: Open												
808- 812	N/A	N/A	265.25	4.35	1048.32	1089.74	844.90	613.86	382.86	178.36	273.23	142.51	N/A
850- 851	N/A	N/A	287.57	1.46	484.41	1428.21	826.35	489.69	532.12	407.43	202.19	332.84	N/A
910- 911	N/A	N/A	245.68	0.97	211.45	1244.07	758.64	232.34	291.29	400.72	182.84	163.22	N/A
1010- 1011	N/A	N/A	334.41	4.70	308.24	1232.32	529.36	233.43	195.26	414.57	140.49	169.67	N/A
	Building pressure condition: Controlled under-pressurization; lateral pipe valve: Closed												
1012- 1013	N/A	N/A	164.49	3.75	578.73	1372.48	626.05	72.35	72.52	418.45	109.71	101.12	N/A
1154- 1155	N/A	N/A	222.68	15.41	501.84	1763.00	634.65	30.65	45.86	298.68	47.35	86.65	N/A
	Building pressure condition: Natural; lateral pipe valve: Closed												
1247- 1248	N/A	N/A	147.79	4.30	230.78	1141.27	296.07	124.94	149.74	176.10	58.85	130.03	N/A
1305- 1306	N/A	N/A	112.03	4.22	134.33	1186.54	151.30	46.24	44.54	104.93	36.49	57.14	N/A
1394- 1395	N/A	N/A	183.22	4.49	253.80	1554.38	291.83	316.80	60.10	66.38	203.06	30.05	N/A

* - None detected.

** - No data available.

Table D. 3.

Screening Model TCE Emission Calculation Results.

Event Time [d]	Estimated TCE Emission Rates using Equations (1) and (2) [g/d]					Estimated TCE Emission Rates using USEPA Johnson and Ettinger Model Spreadsheet [g/d]				
	High Resolution Estimates	Low Resolution Estimates				High Resolution Estimates	Low Resolution Estimates			
		C	F	E	D		C	F	E	D
-10- -5	1.9×10^{-3}	3.5×10^{-4}	5.9×10^{-5}	9.6×10^{-5}	2.5×10^{-3}	6.2×10^{-4}	2.9×10^{-4}	2.6×10^{-5}	3.9×10^{-5}	9.5×10^{-4}
90- 92	1.2×10^{-3}	6.3×10^{-4}	1.3×10^{-5}	2.2×10^{-4}	4.6×10^{-3}	4.0×10^{-4}	5.3×10^{-4}	5.5×10^{-6}	8.9×10^{-5}	1.7×10^{-3}
124- 127	N/A*	N/A	1.3×10^{-5}	8.9×10^{-5}	N/A	N/A	N/A	5.7×10^{-6}	3.6×10^{-5}	N/A
201- 204	8.2×10^{-4}	1.6×10^{-4}	6.8×10^{-5}	1.2×10^{-5}	2.5×10^{-3}	2.8×10^{-4}	1.3×10^{-4}	2.9×10^{-6}	4.9×10^{-6}	9.5×10^{-4}
227- 231	N/A	2.4×10^{-4}	5.6×10^{-5}	1.5×10^{-5}	N/A	N/A	2.0×10^{-4}	2.4×10^{-6}	6.0×10^{-6}	N/A
276- 278	N/A	1.9×10^{-4}	1.3×10^{-5}	1.1×10^{-5}	3.5×10^{-3}	N/A	1.6×10^{-4}	5.6×10^{-6}	4.4×10^{-6}	1.3×10^{-3}
326- 330	N/A	4.9×10^{-4}	8.4E-06	2.0×10^{-5}	3.6×10^{-3}	N/A	4.1×10^{-4}	3.6×10^{-6}	8.0×10^{-6}	1.4×10^{-3}
368- 370	1.1×10^{-3}	4.6×10^{-4}	5.5E-06	4.8×10^{-4}	3.5×10^{-3}	3.6×10^{-4}	3.8×10^{-4}	2.4×10^{-6}	2.0×10^{-4}	1.3×10^{-3}
409- 411	1.0×10^{-3}	3.5×10^{-4}	3.7E-06	7.9×10^{-4}	3.4×10^{-3}	3.6×10^{-4}	3.0×10^{-4}	1.6×10^{-6}	3.2×10^{-4}	1.3×10^{-3}
446- 447	1.1×10^{-3}	3.2×10^{-4}	3.2E-06	4.4×10^{-4}	3.2×10^{-3}	3.6×10^{-4}	2.7×10^{-4}	1.4×10^{-6}	1.8×10^{-4}	1.2×10^{-3}
475- 476	6.5×10^{-4}	2.1×10^{-4}	8.2E-06	3.8×10^{-4}	2.5×10^{-3}	2.2×10^{-4}	1.8×10^{-4}	3.6×10^{-6}	1.5×10^{-4}	9.4×10^{-4}
514- 516	5.9×10^{-4}	1.7×10^{-4}	5.7×10^{-6}	2.1×10^{-4}	1.4×10^{-3}	2.0×10^{-4}	1.4×10^{-4}	2.5×10^{-6}	8.5×10^{-5}	5.4×10^{-4}
550- 551	5.9×10^{-4}	2.4×10^{-4}	3.0×10^{-6}	1.4×10^{-4}	1.8×10^{-3}	2.0×10^{-4}	2.0×10^{-4}	1.3×10^{-6}	5.8×10^{-5}	6.9×10^{-4}
624- 625	8.6×10^{-4}	2.4×10^{-4}	9.4×10^{-6}	2.6×10^{-4}	2.0×10^{-3}	2.9×10^{-4}	2.0×10^{-4}	4.1×10^{-6}	1.1×10^{-4}	7.7×10^{-4}
651- 652	1.3×10^{-3}	3.0×10^{-4}	1.1×10^{-5}	4.4×10^{-4}	2.7×10^{-3}	4.2×10^{-4}	2.5×10^{-4}	4.5×10^{-6}	1.8×10^{-4}	1.0×10^{-3}
736- 737	1.5×10^{-3}	3.6×10^{-4}	7.1×10^{-6}	1.9×10^{-3}	2.8×10^{-3}	5.0×10^{-4}	3.0×10^{-4}	3.0×10^{-6}	7.5×10^{-4}	1.1×10^{-3}
808- 812	7.8×10^{-4}	2.6×10^{-4}	5.6×10^{-6}	1.5×10^{-3}	1.7×10^{-3}	2.6×10^{-4}	2.2×10^{-4}	2.4×10^{-6}	6.1×10^{-4}	6.5×10^{-4}
850- 851	8.6×10^{-4}	2.8×10^{-4}	1.9×10^{-6}	6.9×10^{-4}	2.3×10^{-3}	2.9×10^{-4}	2.4×10^{-4}	8.1×10^{-7}	2.8×10^{-4}	8.6×10^{-4}

Event Time [d]	Estimated TCE Emission Rates using Equations (1) and (2) [g/d]					Estimated TCE Emission Rates using USEPA Johnson and Ettinger Model Spreadsheet [g/d]				
	High Resolution Estimates	Low Resolution Estimates				High Resolution Estimates	Low Resolution Estimates			
		C	F	E	D		C	F	E	D
910- 911	6.2×10^{-4}	2.4×10^{-4}	1.3×10^{-6}	3.0×10^{-4}	2.0×10^{-3}	2.1×10^{-4}	2.0×10^{-4}	5.4×10^{-7}	1.2×10^{-4}	7.5×10^{-4}
1010-	5.2×10^{-4}	3.3×10^{-4}	6.1×10^{-6}	4.4×10^{-4}	1.9×10^{-3}	1.8×10^{-4}	2.8×10^{-4}	2.6×10^{-6}	1.8×10^{-4}	7.4×10^{-4}
1012-	4.3×10^{-4}	1.6×10^{-4}	4.8×10^{-6}	8.3×10^{-4}	2.2×10^{-3}	1.5×10^{-4}	1.4×10^{-4}	2.1×10^{-6}	3.3×10^{-4}	8.2×10^{-4}
1154-	3.5×10^{-4}	2.2×10^{-4}	2.0×10^{-5}	7.2×10^{-4}	2.8×10^{-3}	1.2×10^{-4}	1.8×10^{-4}	8.6×10^{-6}	2.9×10^{-4}	1.1×10^{-3}
1247-	2.8×10^{-4}	1.5×10^{-4}	5.5×10^{-6}	3.3×10^{-4}	1.8×10^{-3}	9.9×10^{-5}	1.2×10^{-4}	2.4×10^{-6}	1.3×10^{-4}	6.8×10^{-4}
1305-	1.3×10^{-4}	1.1×10^{-4}	5.4×10^{-6}	1.9×10^{-4}	1.9×10^{-3}	4.6×10^{-5}	9.3×10^{-5}	2.4×10^{-6}	7.8×10^{-5}	7.1×10^{-4}
1394-	3.2×10^{-4}	1.8×10^{-4}	5.8×10^{-6}	3.6×10^{-4}	2.5×10^{-3}	1.0×10^{-4}	1.5×10^{-4}	2.5×10^{-6}	1.5×10^{-4}	9.3×10^{-4}

* - No data available

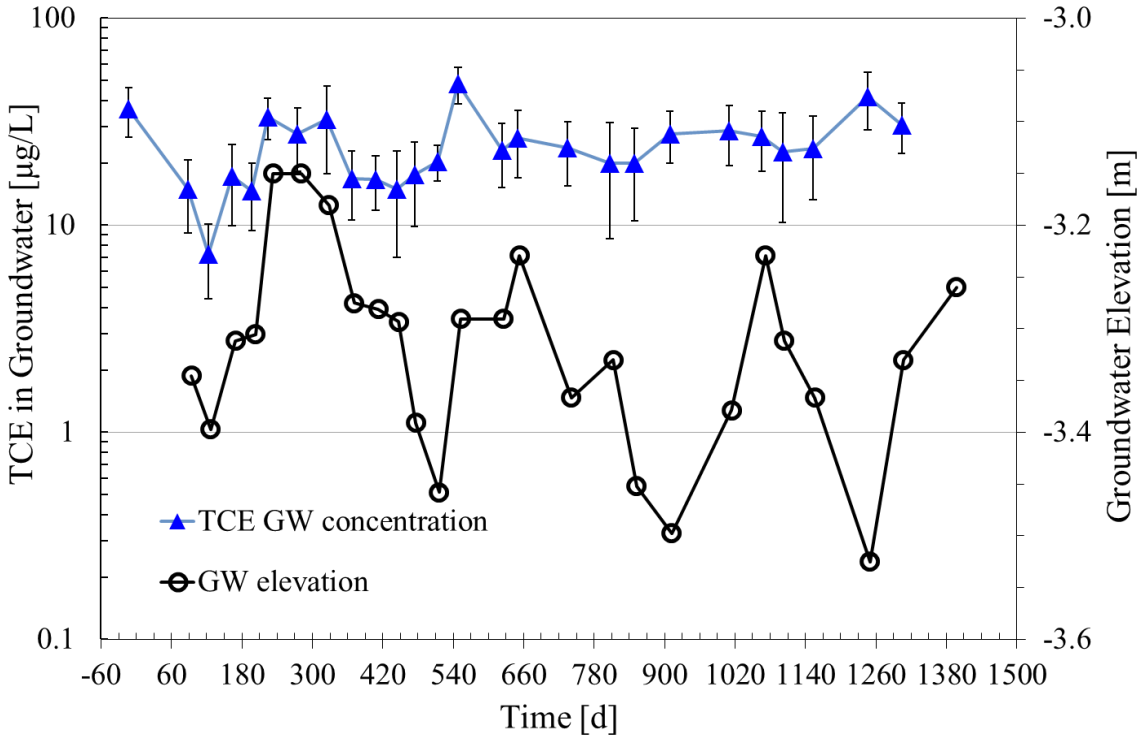

Figure D.1. Average TCE groundwater concentration for samples collected below the building foundation at 2.7 m (9 ft) below-slab (BS) and groundwater elevation measurements at GW3. Error bars represent the standard deviation of GW concentrations from each sampling event.

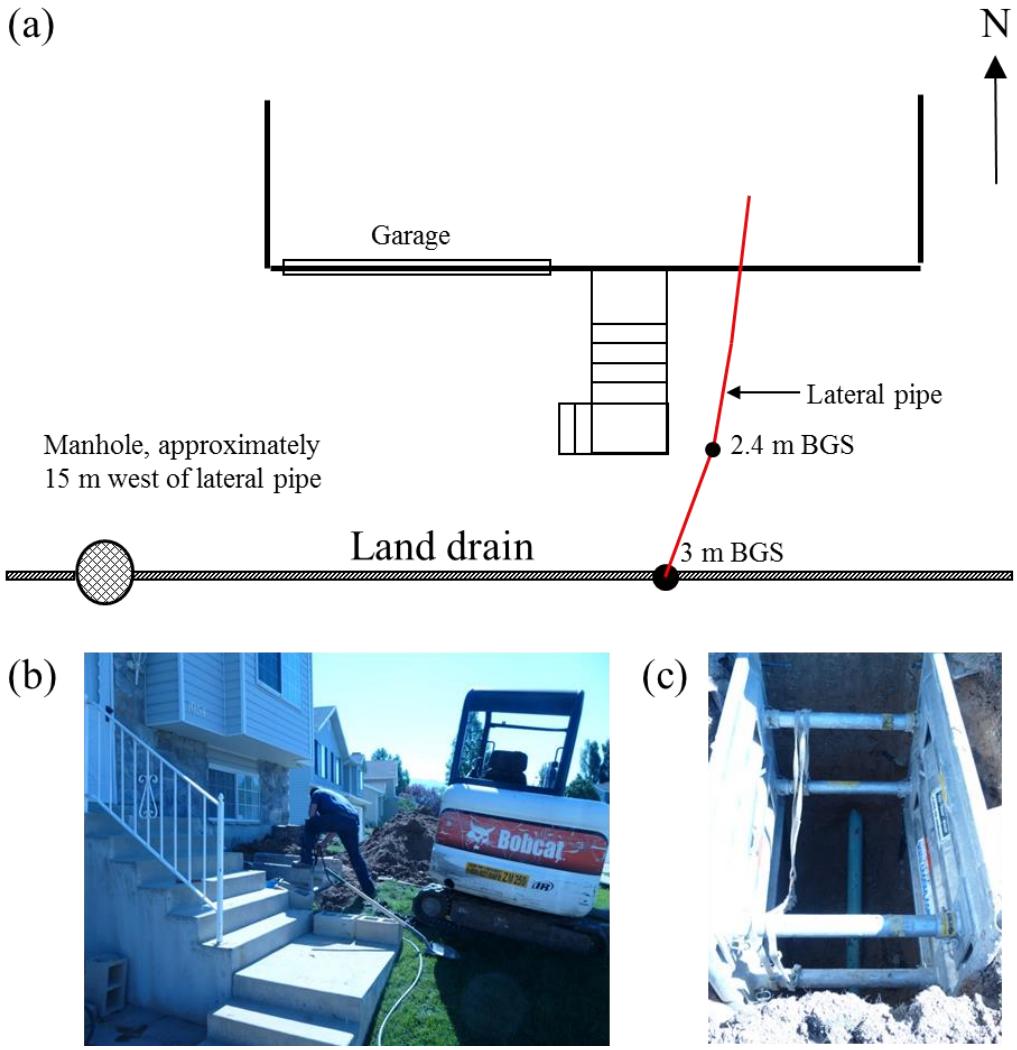

Figure D.2. Schematic of land drain location and butterfly valve installation photos.

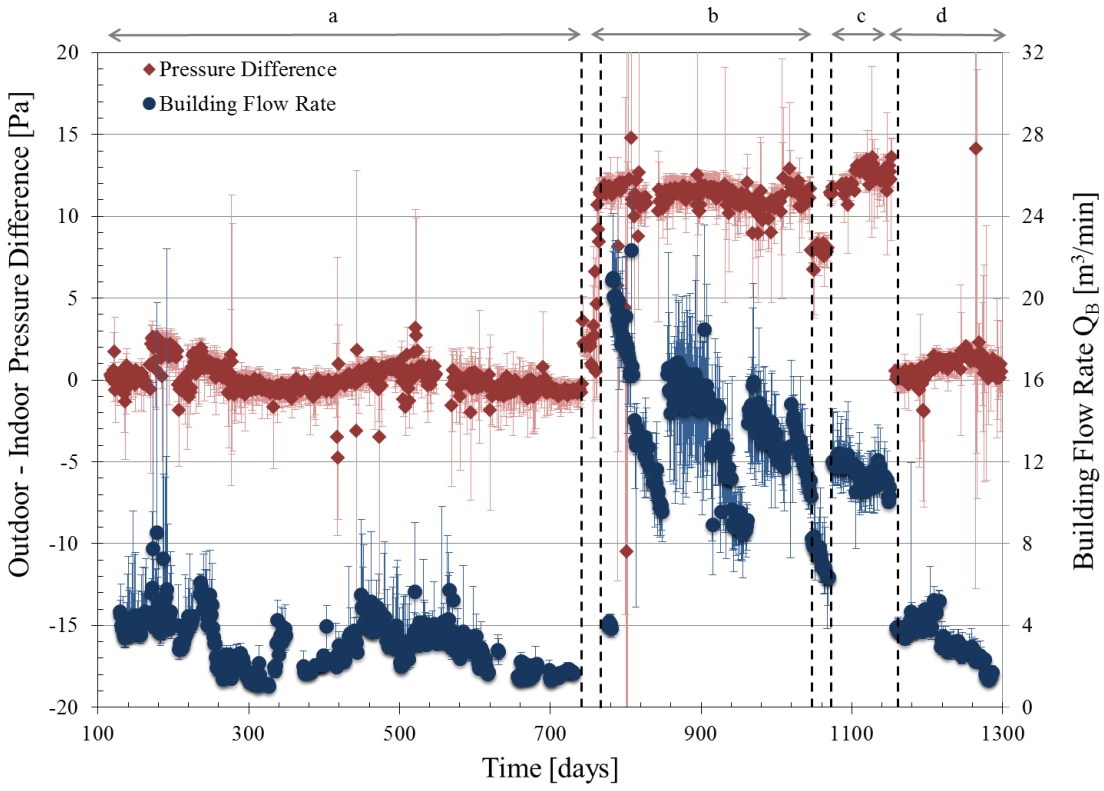

Figure D.3. 24-h average outdoor to indoor pressure differentials and building air exchange flow rates for the four building operation conditions: a) natural condition with lateral pipe connected; b) CPM condition with lateral pipe connected; c) CPM condition with lateral valve closed and d) natural condition with lateral pipe closed. Error bars indicate the daily minimum and maximum values.

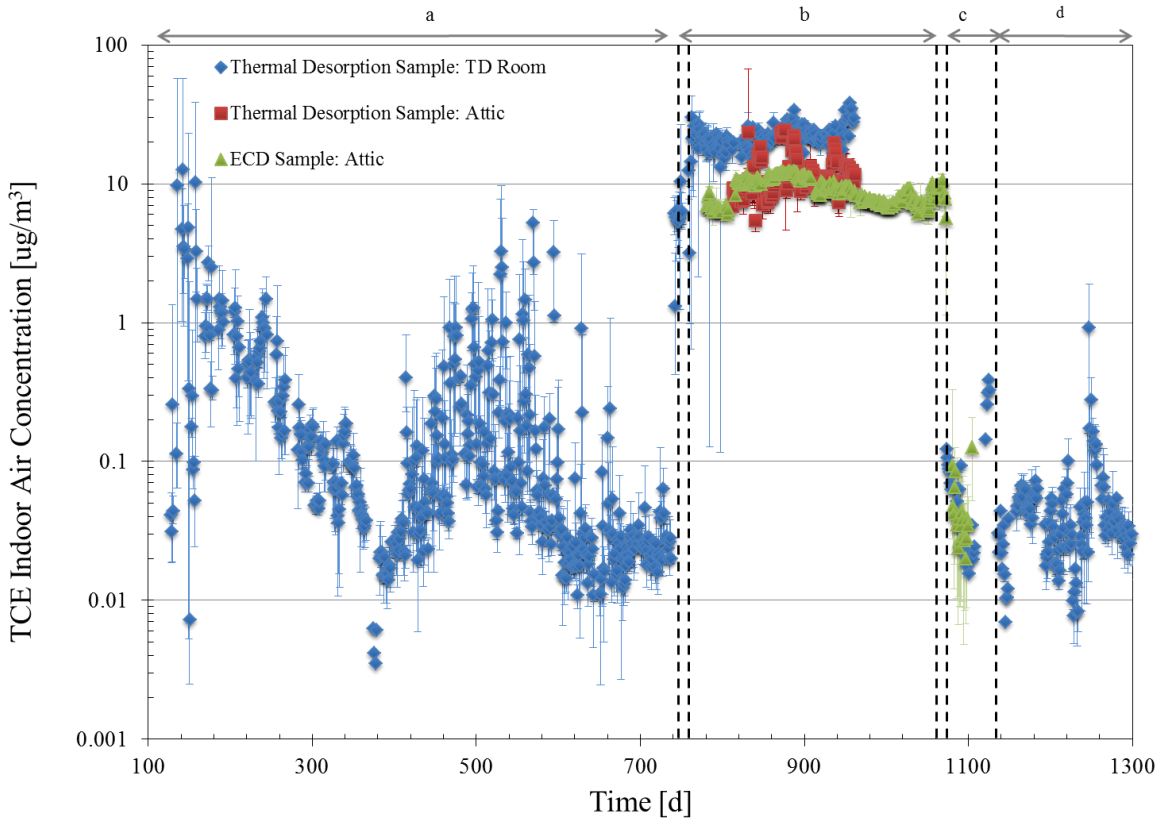

Figure D.4. 24-h average indoor air TCE concentrations for the four building operation conditions: a) natural condition with lateral pipe connected; b) CPM condition with lateral pipe connected; c) CPM condition with lateral valve closed and d) natural condition with lateral pipe closed. Error bars indicate the daily minimum and maximum values.

APPENDIX E

SUPPLEMENTAL INFORMATION FOR EFFECTIVENESS OF A SUB-SLAB DEPRESSURIZATION SYSTEM AT AN ALTERNATIVE VI VAPOR INTRUSION PATHWAY PRESENTING SITE

E.1. AIR FLOW IN VENT PIPE MEASUREMENT

Helium tracer test. The air flowrate in the vent pipe (Q_{vent}, (m^3/min)) can be determined by releasing and measuring tracer (helium) at the suction inlet and vent exhaust. The air flowrate can be qualified using following calculation:

$$Q_{vent} = \frac{Q_{tracer}}{C_{out}} \times 1000$$

where Q_{tracer} is helium releasing rate, [L/min]; C_{out} is helium volumetric concentration at the vent exhaust, [ppmv]. In this case, multiple helium releasing rates were applied using a positive configured 0-1.2 L/min mass flow controller (Alicat Scientific, Tucson, AZ). The helium volumetric concentrations at the vent exhaust were qualified using a MGD-2002 Multi-Gas Leak Detector for helium (Radiodetection, ME, USA). The results are shown in Figure E.1. Averaged vent flowrate can be obtained by calculating the slope of the data set, the results is 2.1 m^3/min.

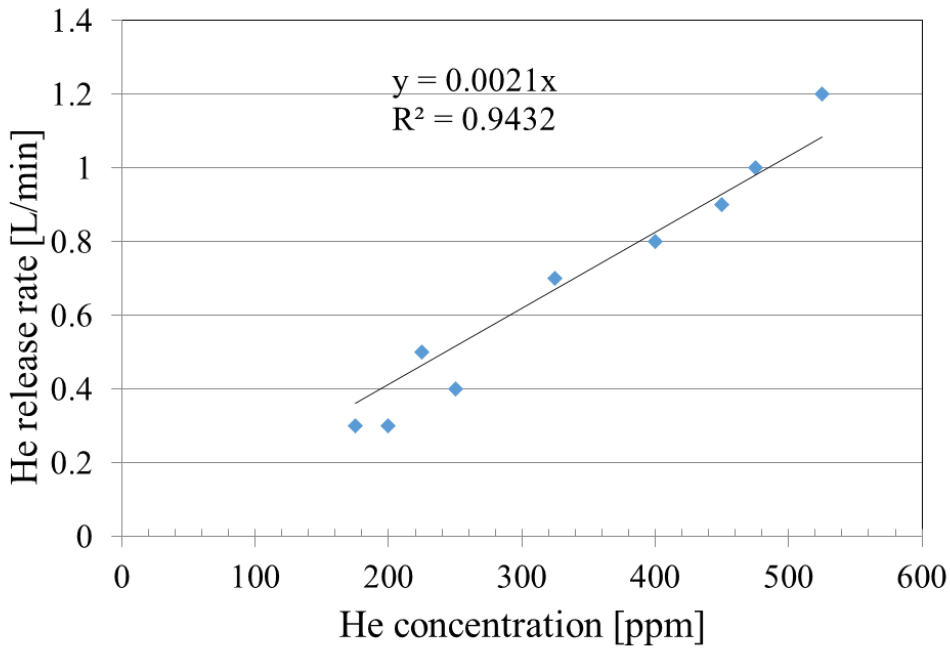

Figure E.1. Vent flowrate measurements using helium as tracer.

In-line flow meter. A Series 641 Air Velocity Transmitter (Dwyer Instruments, IN, USA) was install about 1.8 m above the foundation at the sub-slab depressurization (SSD) system vent pipe. The resolution of this transmitter is 1 foot per minute (FPM) with accuracy of 3% under the temperature environment range of 0 – 50 C. The flow rates can be read from a LED screen, based on the observation at site, the flow rate stabilized around 870 to 890 FPM (2.0 – 2.1 m^3/min).

Pitot tube calculation. A Pitot tube was also installed in the vent pipe, pressure differential between the stagnation pressure and the static pressure was monitored every 2 min using an electronic differential pressure transducers (Model P300-0.4”-D, Pace Scientific Inc., Mooresville, NC). The volumetric velocity then can be calculated using following equation:

$$Q_{vent} = A \times \sqrt{\frac{2\Delta P}{\rho}}$$

where A is the cross-section area of the vent pipe, 0.00785 m^2; ΔP is the pressure differential between the stagnation pressure and the static pressure [Pa]; and ρ is air density at 25 C, 1.225 kg/m^3. Figure E.2 presents the calculated real-time Q_{vent} using hourly averaged pressure differentials between the stagnation pressure and the static pressure. The averaged calculated flow rates are 2.4 ± 0.01 m^3/min for the lateral valve closed condition; and 2.3 ± 0.04 m^3/min for the lateral valve closed condition.

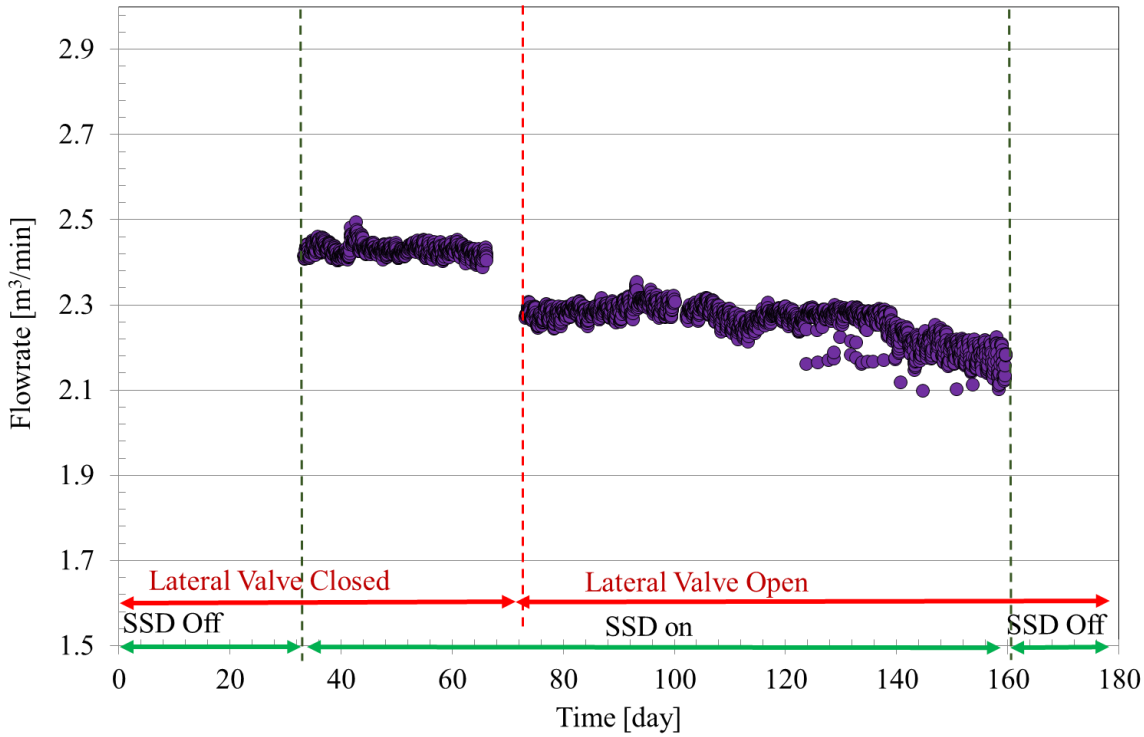

Figure E.2. Air flow rate in SSD vent pipe calculated using hourly averaged pressure differentials between the stagnation pressure and the static pressure of a Pitot tube.

E.2. GROUNDWATER CONCENTRATIONS

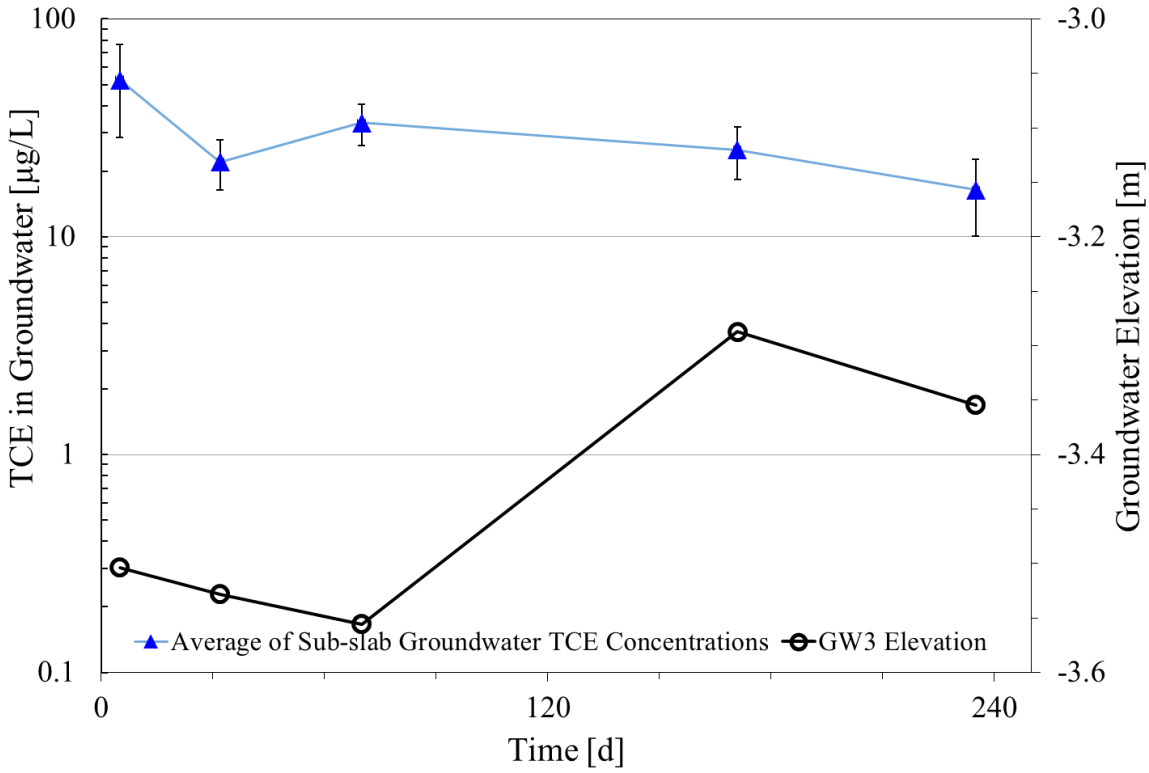

Figure E.3. Average TCE concentration of groundwater samples collected below the building foundation at 2.7 m (9 ft) below-slab (BS) and groundwater depth below slab at GW3.

E.3 REAL-TIME INDOOR AIR TO OUTDOOR AIR PRESSURE DIFFERENTIALS

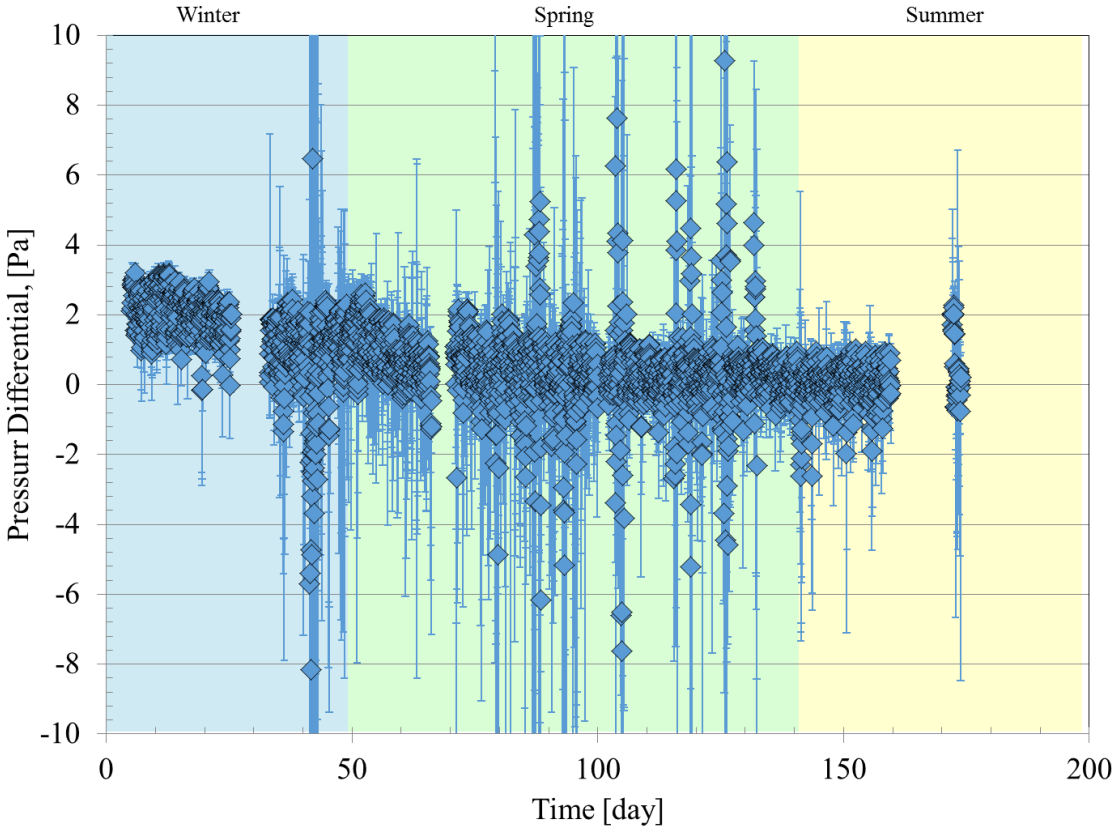

Figure E.4. Hourly average differential pressure values between indoor air and outdoor air, with error bars spanning the 90th and 10th percentile of the daily data sets.

E.4 WEATHER DATA

The precipitation, wind speed and daily maximum/minimum atmosphere temperature data in the vicinity of this study site were obtained from a ground weather station, which locates about 10 miles northern away from the study house. Figure E.5 to 7 shows the daily values.

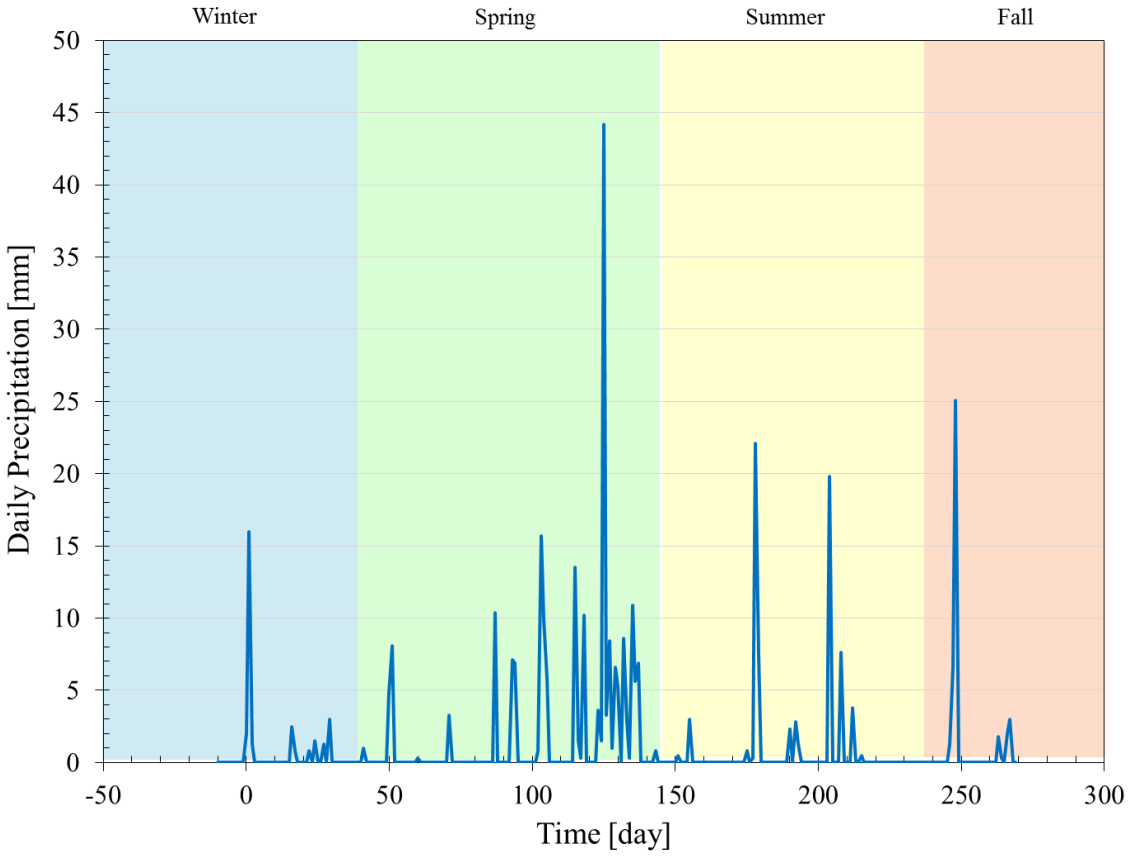

Figure E.5. Daily precipitation values from the Ogden-Hinckley Airport weather station obtained from the National Oceanic and Atmospheric Administration's National Climatic Data Center.

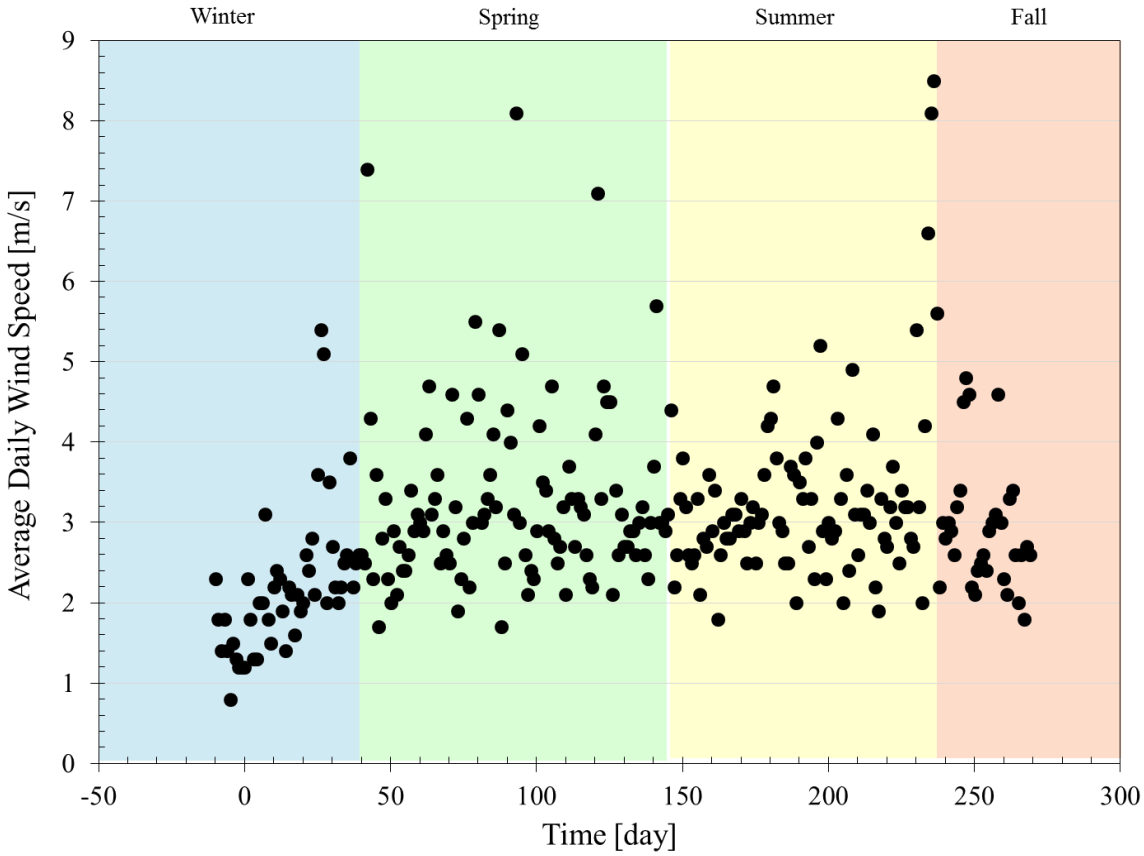

Figure E.6. Average daily wind speed from the Ogden-Hinckley Airport weather station obtained from the National Oceanic and Atmospheric Administration's National Climatic Data Center.

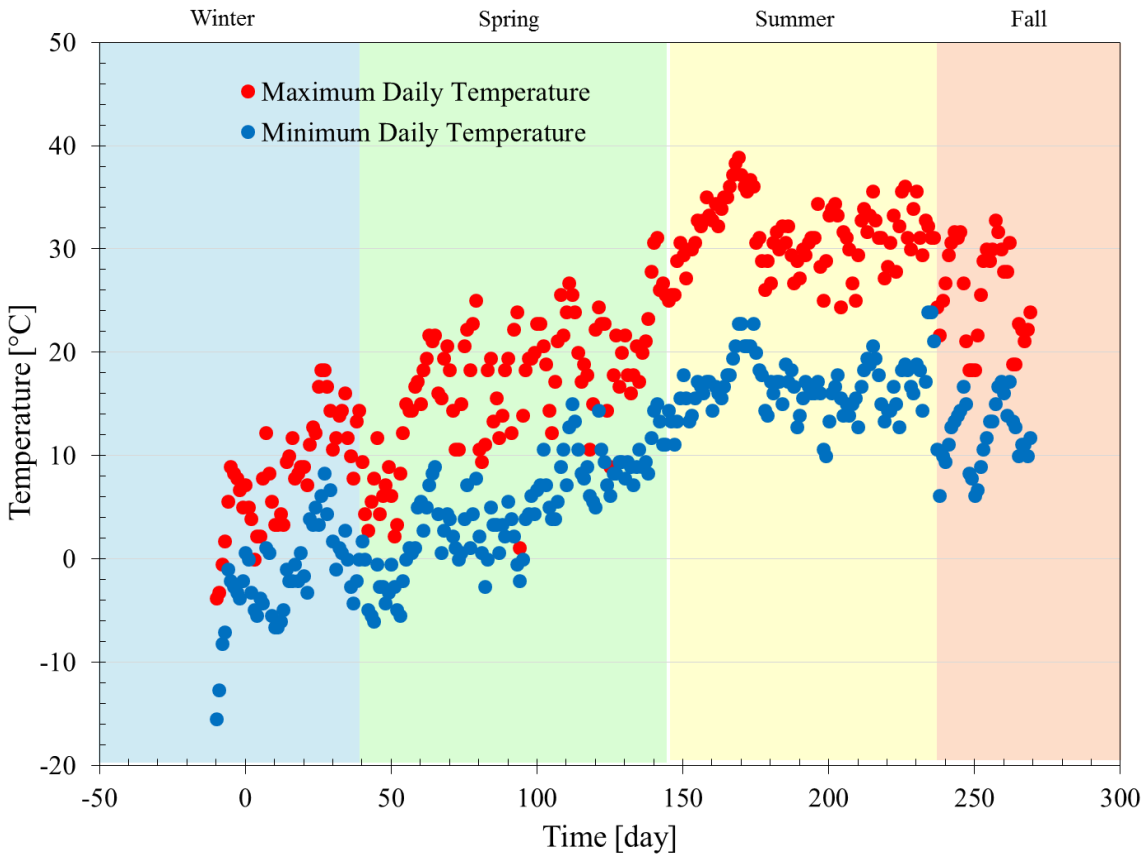

Figure E.7. Maximum and minimum daily temperature values from the Ogden-Hinckley Airport weather station obtained from the National Oceanic and Atmospheric Administration's National Climatic Data Center.

APPENDIX F

ON SITE INVESTIGATIONS OF VOLATILE ORGANIC CHEMICALS IN LAND DRAIN SYSTEM

F.1 OVERVIEW

This section shows the investigation results of volatile organic chemicals (VOCs) concentrations in the land drain system in the vicinity of the study house. Both gas and aqueous samples were collected and qualified.

F.2 SAMPLE COLLECTION

Both water and gas samples were collected from the manhole in the land drain system following the procedures as described below:

- Before manhole cover removal, use water level meter determine the depth from water table to manhole cover;
- Cut a piece of ¼ inch diameter Teflon tubing to 30 cm less than the depth measured from last step;
- Collect gas samples into Tedler gas sample bags using prepared tubing and a box gas sampler, the gas samples were then collected about 30 cm above water table in the manhole;
- Remove manhole and quickly collect water samples into 40 mL volatile organic analysis (VOA) vials using a peristaltic pump.
- Gas samples were analyzed on site within 60 min, and water samples were placed on ice and shipped to ASU for analysis within 48 h.

F.3 RESULTS

The results of this investigation are presented in Figure F.1 in trichloroethene (TCE) concentrations.

ND: None detectable.

Figure F.1. TCE concentrations in manhole gas and water samples. The red numbers are water samples and the green numbers are TCE concentrations in manhole gas samples.